ABILITY OF BIOELECTRIC SIGNALS TO INSTRUCT REGENERATION AND CANCER-ASSOCIATED BEHAVIORS

A thesis

submitted by

Amy E. Thurber

In partial fulfillment of the requirements

for the degree of

Doctor of Philosophy

In

Cell, Molecular, and Developmental Biology

TUFTS UNIVERSITY

Sackler School of Graduate Biomedical Sciences

February 2016

Advisor: David L. Kaplan

Thesis Committee Chair: Grace Gill
Thesis Committee:
Mark E. Ewen
Mike Levin
Jim E. Schwob

ABILITY OF BIOELECTRIC SIGNALS TO INSTRUCT REGENERATION AND CANCER-ASSOCIATED BEHAVIORS

By Amy E. Thurber

A dissertation submitted in partial fulfillment of the requirements for the degree of Doctor of Philosophy in Cell, Molecular, and Developmental Biology

ABSTRACT

In many ways cancer is regeneration gone awry. Both processes involve many of the same behaviors and molecular pathways. However, regeneration occurs with impeccable coordination while in cancer many control mechanisms are lost leading to vastly different outcomes. Discovering the key factors responsible for the bifurcation between a path of regulated healing or unrestricted growth will provide valuable insight into new clinical strategies to both cure cancer and to improve healing after injury or disease. The determining factor is often thought to be mutations in DNA, however only a small percentage of cells carrying cancer causing mutations ever go on to form a tumor suggesting additional factors are at play. One mechanism with an early involvement in both regeneration and cancer is bioelectric signaling; changes in ion flows and the electric potential across a cell membrane. The purpose of this work was to explore this understudied signaling mechanism, specifically investigating whether changes in the electric membrane potential (V_{mem}) are sufficient to instruct regeneration and

cancer-associated behaviors. Ostoegenic differentiation of human adult mesenchymal stem cells (hMSC) was used as a model of healthy regeneration. I utilized expression of specific ion channels, culture in different extracellular ion concentrations and inhibition or activation of ion channels with pharmacological agents to modulate V_{mem} of hMSC during differentiation. None of the conditions tested increased differentiation as determined by quantitative analysis of osteogenic markers. Differences in membrane potential have also been reported between healthy and cancerous cells. In order to test whether V_{mem} plays an instructive role in cancer, similar methods were used to modulate the V_{mem} of two breast epithelial cell lines. One of the cell lines was highly metastatic and thus modeled the highly diseased state and the other was a spontaneously immortalized non-tumorigenic cell line with a lower threshold of transformation than primary healthy cells, providing a model to investigate disease onset. While some of the treatments did lead to changes in cancer-related behaviors, overall the effects did not correlate with membrane potential suggesting they were enacted by V_{mem}-independent mechanisms. Together, these results are not supportive of an instructive role for V_{mem}, but instead suggest V_{mem} is a critical part of the cell machinery that is beneficial to most cell behaviors.

ACKNOWLEDGMENTS

I would first like to thank my advisor, David Kaplan, for providing support and guidance through years of research in his lab and for allowing me the freedom to pursue my own ideas. I would also like to thank Will Brackenbury, who agreed to collaborate, mentor me through the process of learning electrophysiology, and invited me to spend 6 months in his lab, all after meeting once at a conference. Working in his lab was an incredibly enriching experience and I would like to thank all of his lab members for their patience teaching me and help with my project. I would like to thank Mike Levin, who was present at nearly every lab meeting and provided much insight and feedback on the projects. I am very grateful to Grace Gill, Jim Schwob, and Mark Ewen who have kindly served on my committee offering their time and insights to help guide not only my research but also by path through the graduate program. I would like to especially thank Grace for the most helpful criticism of written reports and for sharing many lab resources.

I would like to thank many people from within David's lab, the Sackler community, and outside of Tufts who have donated their time to mentor and teach me in the lab. I am grateful to Barry Trimmer, Alenka Lovy, Allen Parmellee, and Stephen Kwok for help with

laboratory equipment training and experiments. I would like to thank Sarah Sundelacruz for training me when I first joined the lab and for countless discussions of the true meaning of bioelectricity. I would like to especially thank my long-time officemates and team of helpful post-docs Kelly Burke, Tessa DesRochers and Jelena Rnjak-Kovacina, first of all for their patience, and also for their constant support. I am indebted to Milva Ricci, who has an invisible hand in every experiment in the BME department and whose hard work and dedication keeps the department running without a hitch.

I would like to thank all of the members of the Tufts University and Sackler scientific community for creating an, energetic, engaging, and welcoming environment. It has truly been an honor and a privilege to work here. I would especially like to thank my fellow classmates and labmates who are always there to keep things fun.

Finally, I would like to thank my friends and family for being incredibly supportive for all these years. Thank you for pretending to pay attention when I talked about my project and keeping my social calendar booked when I got lost in lab.

TABLE OF CONTENTS

LIST OF TABLES

LIST OF FIGURES

LIST OF EQUATIONS

List of Abbreviations

1-EBIO – 1- Ethylbenzimidazolinone
ACL – anterior cruciate ligament
ADP – adenosine diphosphate
ALP – alkaline phosphatase
ATP – adenosine triphosphate
bFGF – basic fibroblast growth factor
BGLAP – bone gamma-carboxyglutamate protein
BK – large conductance calcium-activated potassium channel
BMP – bone morphogenetic protein
$[Ca]_I$ – intracellular calcium concentration
$[Ca]_o$ – extracellular (outer) calcium concentration
CapZ – capsazepine
Cpn – capsaicin
DMSO – dimethyl sulfoxide
ECM – extracellular matrix
EGF – epidermal growth factor
EGTA – ethylene glycol-bis(2-aminoethylether)-*N-N-N'-N'*-tetraacitic acid
EMT – epithelial to mesenchymal transitions
E_{Rev} – reversal potential
FACS – fluorescence activated cell sorting
FBGC – foreign body giant cell
FBS – fetal bovine serum
FGF – fibroblast growth factor
FP – fluorescent protein
FRET – fluorescence resonance energy transfer
GAPDH – glyceraldenhyde 3-phosphate dehydrogenase
GFP – green fluorescent protein
GlyR – glycine receptor chloride channel
HEPES – 4-(2-Hydroxyethyl)piperazine-1-ethanesulfonic acid
HFIP – hexafluoro-2-propanol
hMSC – human mesenchymal stem cell
IK – intermediate conductance calcium-activated potassium channel
IL-4 – interleukin-4
IL-13 – interleukin-13
K_{ATP} – ATP-sensitive potassium channels

Kir2.1 – inward rectifier potassium channel member 2.1
MNGC – Multinuclear giant cell
MSC – mesenchymal stem cell
NHE1 – sodium hydrogen exchanger 1
NMDG – N-methyl-D-glucamine
PBS – phosphate-buffered saline
PET – poly(ethyleneterephthalate)
PGA – poly glycolic acid
PHB – Poly (3-hydroxybutyrate)
P_I – inorganic phosphate
PIP – phosophoinositide phosphatase
PLA – poly lactic acid
PLGA – poly(lactic-co-glycolic acid)
PPARγ – peroxisome proliferator-activated receptor gamma
PRR – pattern recognition receptors
PS – phosphoserine
PTFE – polytetrafluoroethylene
RFP – red fluorescent protein
RPI – region of interest
Shh – sonic hedgehog
SK – small conductance calcium-activated potassium channels
TCP – tricalcium phosphate
TRPC4 – transient receptor potential cation channel, member 4
TRPV1 – transient receptor potential cation channel subfamily V, member 1
TRPV6 – transient receptor potential cation channel subfamily V, member 6
TSPC – tendon stem/progenitor cells
TTX – tetrodotoxin
VEGF – vascular endothelial growth factor
VGSC – voltage gated sodium channel
V_{mem} – membrane potential

CHAPTER I:
INTRODUCTION

I.1 Endogenous Healing and Regeneration

Throughout life, organisms face insults from the environment that result in cell and tissue damage. The better an organism can recover from these insults, the greater its chances at survival. Organisms have therefore developed wound healing mechanisms that are capable of repairing minor damage. During healing, nearby cells of the same type that were injured proliferate and migrate to repair the wound. Some species are capable of recovering from more significant damage that requires the formation of new tissues made up of multiple cell types through the process of regeneration. In regeneration, numerous processes must be coordinated to create replacement tissue with the correct size, shape, and functionality. Importantly, this must be completed with careful regulation to prevent unrestricted growth associated with cancer. Loss, damage, or lack of function of the damaged tissue must first be recognized. Next, signaling must instruct the proliferation, migration, differentiation, and organization of replacement cells. Finally, completion of regrowth must be detected and all of the regenerative pathways must be turned off.

Humans, and most mammals, have very limited regenerative abilities and are therefore unable to regain complete health after major damage inflicted by injury or disease (Forbes and Rosenthal,

2014). However, certain species have significantly enhanced regeneration indicating recovery from major insults is possible in higher order organisms. It is hoped that a better understanding of the molecular mechanisms driving native healing in humans and regeneration in other species will allow for biomedical interventions able to restore healthy tissue under all circumstances. Much progress has been made understanding signaling pathways governing single cell behavior, but how individual cells are coordinated to enact tissue and organ-level remodeling and growth remains unclear (King and Newmark, 2012). Many fundamental questions remain unanswered including how organisms detect injured tissue, how they recognize when healing is complete, what cell types are responsible for producing replacement cells, and whether regeneration utilizes the same or independent pathways from embryonic development.

In general, regenerative abilities inversely correlate with organism complexity such that lower organisms, such as planaria, are able to completely regenerate after loss of sometimes over half their body while higher organisms are unable to regenerate from significant loss of a single tissue. However, there are notable exceptions of higher organisms that have extraordinary regenerative capabilities as compared to closely related species. For example, the African spiny mouse (*Acomys kempi*) can regrow full thickness dermal tissue

including hair follicles, sweat glands, and cartilage (Jenkins et al., 1996; Seifert et al., 2012). Investigation of regeneration in super-regenerative species has identified mechanisms that potentially could be used clinically to improve human healing.

Large differences exist in the ability of amphibian species to regenerate with some species capable of regenerating adult limbs and others having minimal re-growth after limb loss. Interestingly, regenerative species have different bioelectrical properties just after amputation as compared to non-regenerative species (Jenkins et al., 1996). At first, both exhibit a positive current exiting the wound. In non-regenerative species this current decreases slowly as epithelial cells are replaced in a wound healing process. However, in regenerative species, the current switches polarity and reaches a peak negative current at the time of maximal cell proliferation. Disruption of the endogenous currents causes incomplete or inappropriate regeneration demonstrating the significance of the electrical current. Furthermore, addition of exogenous currents was sufficient to increase regeneration in a poorly regenerative species (Tseng et al., 2010). The addition of proton efflux induced regenerated tissue with normal patterning including organized innervation and pigmentation (Adams et al., 2007).

It remains unclear whether signaling pathways utilized by especially regenerative species could be induced to function similarly in other organisms. Do some species contain special stem cell pools or signaling pathways? Or, are these capabilities available in all species but simply not initiated?

I.2 Clinical need for improved tissue engineering strategies

Tissue engineering presents a potential means to repair or replace tissue unable to heal on its own. The ultimate goal of the field is to be able to restore normal function and appearance to any tissue in the body. In principle, this can be accomplished by fabricating functional tissues *ex vivo* and/or by stimulating improved healing and regeneration in the body.

Creating artificial tissues *ex vivo* requires a suitable scaffolding material to provide an underlying structure, incorporation of appropriate cell types, assembly of the scaffold and cells to generate proper spatial patterning, and culture conditions that promote required functionalities. The scaffold is analogous to the extracellular matrix (ECM) and in addition to providing structural support it provides a surface for cells to attach and migrate and can influence cell behavior through mechanical and biochemical signaling. The choice of

scaffolding material must also take into account how it will behave once implanted in the body. An ideal material interacts favorably with surrounding cells and tissue to prevent an excessive immune or inflammatory response and possible host rejection. The degradation rate should also be designed such that the material can maintain necessary mechanical properties until newly formed tissue is able to accommodate the load. Scaffolds are fabricated using synthetic materials such as polylactic acid and polyglycolic acid or natural materials including silk, alginate, or ECM proteins like collagen. In general, synthetic materials are stronger and degrade more slowly while natural materials have better interactions with cells and induce less of an inflammatory response (Thurber et al., 2015).

Cells make up the other major functional component of a tissue engineered structure. The gold standard is to use autologous cells in order to avoid host rejection and disease transmission. Often, mature cells are either too challenging to extract or not available in sufficient numbers, and instead stem cells are propagated and differentiated to the needed cell types. A major obstacle facing tissue engineering is determining culture conditions that can promote formation of functional tissues. Induction of stem cell differentiation with biochemical factors has proven to be a successful means to produce tissue constructs of one particular cell type. However, due to

difficulties in controlling growth factor diffusion, or in physically placing multiple constructs together, the utility of biochemical signaling for developing more complicated structures is limited. Additional means of controlling differentiation are needed to allow for patterned tissue regeneration of complex anatomical structures.

Investigation and characterization of signaling mechanisms driving differentiation apart from biochemical growth factors that could be used for patterning are an active area of research. Bioelectric signaling is beginning to emerge as an important new tool in stem cell biology with the potential to enable better spatial control of differentiation (Levin, 2007). Major advances in the ability to precisely control bioelectric signaling, the flow of ions across the cell membrane, make it an ideal candidate. Development of light-activated ion channels in conjunction with site-directed lasers allows for precise spatial and temporal regulation of specific ion currents. The light-activated channels were derived from the channel rhodopsin family in archea and initially developed to control individual neuron activity (Boyden et al., 2005). A library of channels now exists encompassing a range of ion flows activated by different wavelengths of light, which in combination with specialized lasers that have micrometer resolution, allows for stimulation of individual cells. With a better understanding of its role in differentiation and integration within signaling pathways,

bioelectricity is a promising mechanism that could be used to drive differentiation to specific cell types with precise spatial resolution.

I.3 Bioelectric regulation and integration with other signaling pathways

Bioelectric regulation refers to signaling that occurs through changes in ion flows or the electrical potential across the cell membrane. These properties are most commonly associated with their role in neuronal firing and contraction of cardiac cells. However, increasing evidence points towards bioelectricity in non-excitable cells as a fundamental component of the signaling milieu in much the same way as biochemical signaling factors or mechanical tension cues (Levin, 2007, 2009). Recent studies support a role for bioelectric signaling in numerous cell behaviors including proliferation, differentiation, and migration (Lang et al., 2005; Prevarskaya et al., 2007; Schwab et al., 2012). Loss of appropriate regulation of ion fluxes is associated with numerous diseases such as epilepsy, developmental abnormalities, and cancer. Even with the recent renewed interest in biophysics, the extent of the influence of non-excitatory bioelectric signaling as a master regulator of cell behavior is only beginning to be appreciated.

Ion channels, pumps, and transporters produce ion currents across the cell membrane that create an electrical potential difference between the inside and the outside of the cell. The lipid bilayer making up the cell membrane is impermeable to charged molecules including ions and ions are only able to cross the membrane through specific channels, pumps, and transporters. Channels do not utilize energy and are passive, such that when the channel opens ions move according to the forces exerted by the electric potential across the membrane and the concentration gradient. In contrast, pumps and transporters do utilize energy, often by hydrolyzing adenosine triphosphate (ATP) to adenosine diphosphate (ADP) and inorganic phosphate (P_I), and are able to move ions against the electrochemical gradient allowing cells to preferentially exclude or concentrate specific ions. The typical intracellular and extracellular concentrations in mammalian cells of the predominant ion species and the electric and chemical gradient forces acting upon them are depicted in figure 1 (Lodish et al., 2000).

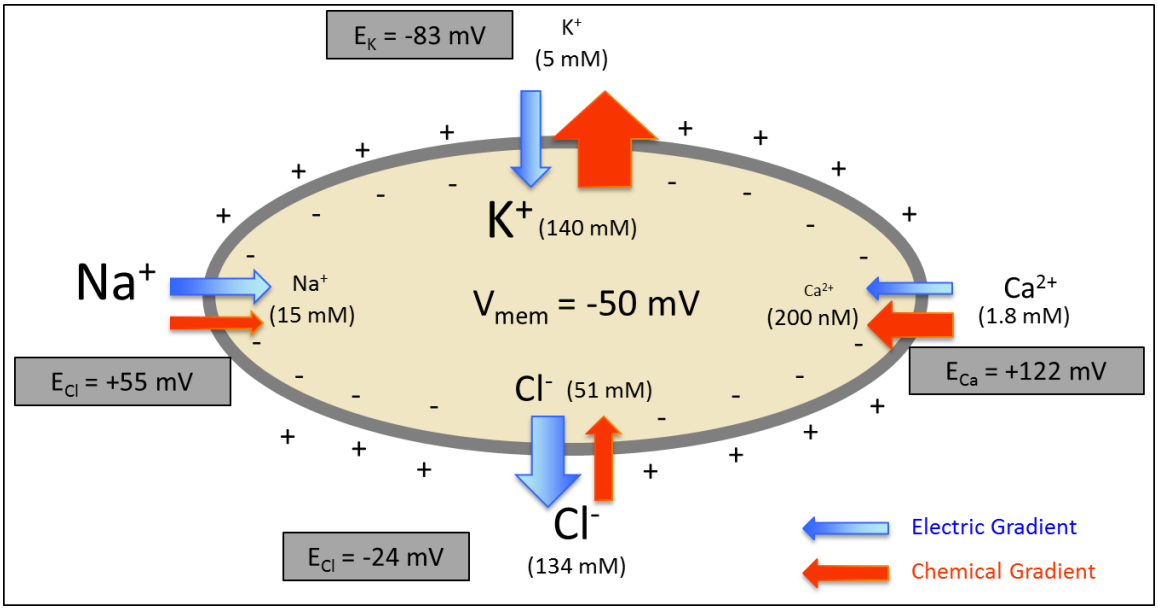

Figure I-1: Typical intracellular and extracellular ion concentrations and ion reversal potentials for mammalian cells. Blue and red arrows indicate direction of electric gradient and chemical gradient forces respectively with size indicative of relative strength (not to scale).

The electric potential across the cell membrane, the resting membrane potential (V_{mem}), is determined by the difference in the intracellular and extracellular ion concentrations as well as the relative permeability of the cell to each ion species as described by the Goldman equation (Equation 1). For each ion X, there is an electrical potential at which there is no net flow into or out of the cell known as the reversal potential (E_{RevX}). This is the point where the electrical force is exactly equal and opposite to the force of the concentration gradient and is described by the Nernst equation (Equation 2), which shows that E_{RevX} is dependent upon the intra- and extra-cellular

concentration and ion charge. If V_{mem} is not equal to E_{RevX} and channels for ion X open, the X ions will flow so that the V_{mem} moves towards E_{RevX}. As more X ion channels open and the cell becomes more permeable to X, V_{mem} moves closer to E_{RevX}. The overall V_{mem} is dependent upon E_{Rev} for each ion as well as the relative permeability to each ion. Thus, V_{mem} changes when the relative permeability to ions changes through the opening and closing of ion channels, or when the intra- and extra-cellular ion concentrations change causing E_{Rev} to shift.

$$V_{mem} = \frac{RT}{F} \ln\left(\frac{P_K[K]_O + P_{Na}[Na]_O + P_{Cl}[Cl]_I}{P_K[K]_I + P_{Na}[Na]_I + P_{Cl}[Cl]_O}\right)$$

Equation I-1: The Goldman equation. In which T is temperature, F is Faraday's constant, R is the universal gas constant, and *P* is the relative permeability.

$$E_{RevX} = \frac{RT}{zF} \ln\left(\frac{[X]_O}{[X]_I}\right)$$

Equation I-2: The Nernst equation. In which variables are as above and z is the charge of the ion.

In order for bioelectricity to exert regulation over cell behaviors, changes in the bioelectric state must be sensed by proteins within the

cell and transduced to modulate protein activity including possibly the activity of transcription factors. To detect the biophysical state, a protein must be responsive to either V_{mem} or to ion concentrations. Indeed, numerous proteins contain voltage-sensing domains or ion binding sites.

A homologous voltage-sensing domain that activates the opening of channels has been found in sodium, potassium, calcium, and hydrogen channels. The voltage-sensing domain consists of 4 transmembrane domains (S1-S4), one of which contains a series of positively charged residues (Figure 2A). Changes in V_{mem} exert a physical force on the charges that induces a conformational change to activate the channel (Borjesson and Elinder, 2008). Thus, sodium, potassium, calcium, and hydrogen currents through their respective voltage-gated channels are V_{mem} dependent.

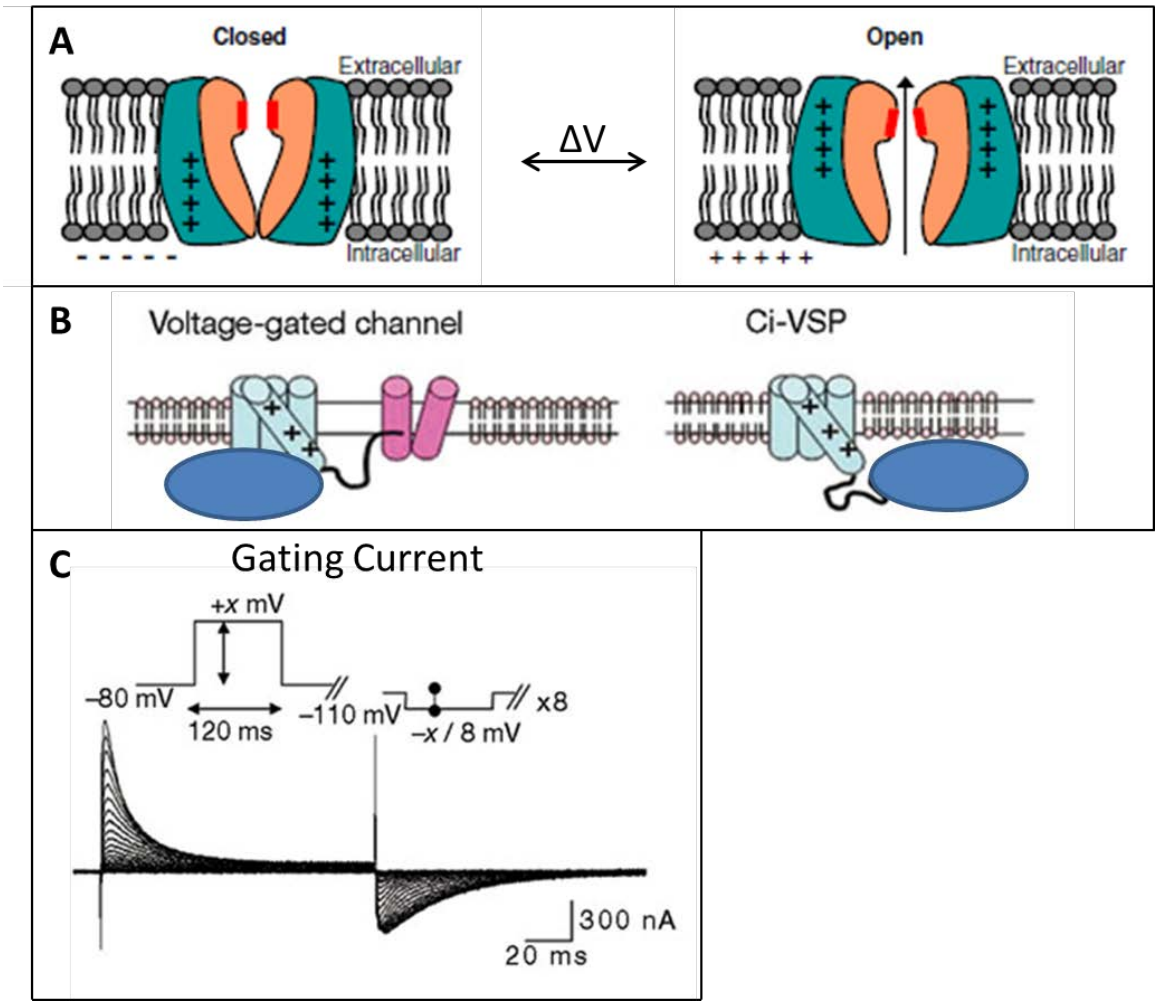

Figure I-2: Voltage sensing domain structure, interaction with associated proteins or enzymatic domain, and gating current. **(A)** The S1-S4 voltage sensing domain contains positively charged residues that respond to a change in membrane potential with a conformational change that opens the ion channel. **(B)** Movement of the S1-S4 domain in response to voltage can effect the activity of closely associated proteins (left) or covalently linked enzymatic domains such as is found in the *Ciona* voltage sensitive PIP protein(right). **(C)** Characteristic current created by the movement of the positive charges within the S1-S4 domain in response to a voltage step. A pulse was applied ranging from -80 to 160 mV in 10-mV steps. Linear and symmetrical currents were subtracted (inset). ((A) Reproduced from Borjesson and Elinder, 2008; (B-C) reproduced from Murata, Iwasaki et al. 2005 with permission)

In addition to regulating the opening of channels, the S1-S4 voltage-gated domain can enact signaling via non-conducting mechanism. Ion channels physically interact with numerous other proteins at the cell membrane. When the S1-S4 domain responds to V_{mem} with a conformational change, it can alter the physical interactions with other proteins increasing or decreasing their activity (Figure 2B). The voltage-gated potassium channel $K_V10.1$, also known as ether-à-go-go K+ channel, increases proliferation of NIH 3T3 fibroblasts via a non-conducting mechanism (Hegle et al., 2006). A mutant of $K_V10.1$ with a point mutation in the pore forming domain has a gating current but no potassium current indicating the S1-S4 domain can move in response to V_{mem} but that potassium ions are blocked from passing through the channel. Fibroblasts transfected with wild type or non-conducting $K_V10.1$ had a similar increase in proliferation. The increased proliferation was dependent on p38 MAP kinase activation and both channels increased p38 phosphorylation to a similar degree. Further investigation of the dependence of proliferation on V_{mem} revealed proliferation was dependent on S1-S4 in the open conformation. Depolarization, which holds $K_V10.1$ in the closed conformation, abolished the proliferative phenotype, while mutant $K_V10.1$ channels that remained open despite alterations in

V_{mem} retained proliferation similar to wild type $K_V10.1$ in standard conditions.

Voltage-gated channels physically interact with proteins on the cell membrane including kinases and adhesion molecules providing a direct mechanism to activate intracellular signaling pathways. For example, the beta-subunit of voltage-gated sodium channels (VGSC) is a cell adhesion molecule and also a substrate for alpha, beta, and gamma secretases (Patel and Brackenbury, 2015). Cleavage by a secretase releases the intracellular domain which translocates to the nucleus and alters mRNA expression suggesting it functions as a transcriptional regulator by a similar mechanism as Notch signaling (Kim et al., 2007a). Additionally, VGSCs are required for migration in many cell types and data supports a mechanism involving beta-subunit mediated adhesion. Many of the functions of beta subunits, including their role in forming cell adhesions, are dependent on sodium current suggesting their downstream signaling is directly linked to VGSC activity (Brackenbury and Isom, 2011). Interactions between voltage-gated channels and membrane-associated proteins are highly specific making differences in channel expression and activity a highly sensitive mechanism to regulate cell response.

After the initial discovery of S1-S4 domains, it was long thought that they were only found in voltage-gated ion channels. However, an

S1-S4 domain was discovered in a phosphoinositide phosphatase (PIP) protein from *Ciona intestinalis* (Murata et al., 2005). Expression of the protein induced a small current in the absence of ion flow across the cell membrane, which is characteristic of the S1-S4 gating current (Figure 2C), suggesting its structure and function were truly homologous to ion channel S1-S4 domains. Furthermore, PIP activity directly correlated with V_{mem} making it the first non-ion channel protein whose function was directly induced by V_{mem}. A similar domain was found within a mammalian PIP protein, but its activity has not yet been shown to be V_{mem} dependent. Even so, this discovery opens a new possibility for linking well-known signaling mechanisms to V_{mem}. Non-conducting proteins may contain S1-S4 domains with less structural similarity or perhaps even unrelated voltage-sensing domains that have yet to be discovered.

Very recently the activity of the potent oncogene Ras was linked to V_{mem} by interactions between Ras and lipids whose localization was V_{mem} dependent (Zhou et al., 2015). Accumulation of Ras proteins in nanoclusters in close association with the plasma membrane is an essential step in their activation. Nanoclustering is mediated by interactions between the Ras lipid anchor and local phospholipids in the plasma membrane. Phospholipids are charged and electric fields with magnitudes on the order of V_{mem} are sufficient to alter their

localization. Depolarization induced nanoclustering of phosphoserine (PS) and was demonstrated to correlate with nanoclustering of Ras molecules. The activity of Ras, as measured by MAPK activation, was also increased by depolarization. The data provides clear proof of principle that changes in the electric field induced by physiologically relevant fluctuations in V_{mem} are sufficient to shift localization of charged lipid residues which in turn effect localization and activity of plasma membrane associated proteins. It is interesting to note that while nanoclustering occurred through a V_{mem} range of -45 to 5 mV, Ras activation only occurred from -10 to 5 mV. Recordings from non-excitatory cells are typically below -15 mV but are found at more depolarized levels in cancer cells and when sodium channels are highly active which may suggest that this mechanism is highly selective.

In addition to sensing V_{mem}, cells can also respond to fluctuations in intracellular ion concentrations. The most studied ion-responsive proteins are calcium activated proteins. Calcium is a unique ion in that it is excluded to a very high degree from inside the cell and therefore relatively small calcium currents can increase the intracellular calcium concentration ($[Ca]_I$) by many fold. Cells contain numerous calcium-binding proteins that are inactive at low $[Ca]_I$ and bind calcium to become active at high $[Ca]_I$. Once bound to calcium, the active calcium-binding protein can in turn activate various downstream

effectors (Berridge, 2000). The mechanism by which $[Ca]_I$ is propagated and transduced into cell behaviors is highly sensitive to the speed, amplitude, and spatio-temporal patterning of calcium influx. This allows calcium signaling to regulate an incredibly versatile range of processes on the cellular and organismal level such as proliferation, fertilization, and memory. Importantly, calcium dynamics are inextricably linked to V_{mem}. The flux of calcium depends on both the quantity of open calcium channels and also the current density of ions flowing through the channels. The current density is dependent on the electrical driving force created by V_{mem} with more hyperpolarized V_{mem} creating a larger driving force on calcium ions and increasing the current density. Thus, calcium signaling provides an indirect mechanism by which numerous signaling pathways may be V_{mem} responsive.

The role of ion channels and V_{mem}, outside of calcium signaling which may itself be regulated by V_{mem}, is often assumed to be purely mechanical. However, the diverse mechanisms by which cells are responsive to bioelectric signals enables the degree of sensitivity required to direct differentiation and other cell behaviors.

I.4 Evidence of bioelectric properties regulating cell behaviors

An increasing number of diseases and developmental defects have been linked to impaired channel function, so called channelopathies, demonstrating the fundamental importance of bioelectric signaling to cell behavior. These abnormalities provide clues to the connections between ion channel activity and changes in cell behavior helping to improve our understanding of the signaling mechanisms.

Changes in ion flows have long been associated with many developmental and regenerative processes, including left-right patterning and epithelial wound healing (Levin, 2007). Membrane potential specifically is involved in proliferation, differentiation, and migration, all of which are required in tissue regeneration. Evidence from work in *Xenopus laevis* has shown that membrane potential and pH play extremely important roles in regulating craniofacial development (Vandenberg et al., 2011). Changes in V_{mem} during development were detected by soaking entire embryos in V_{mem} sensitive fluorescent dyes. Multiple 'waves' of hyperpolarization were observed, one of which corresponded with the locations and gene expression patterns of craniofacial structures. Disruption of the hyperpolarized wave by injection of a dominant negative H^+-V-ATPase subunit mRNA caused an array of craniofacial abnormalities, including morphological changes in the jaw, branchial arches, otocysts, otoliths,

olfactory pits, and eyes. Expression patterns of several genes critical to early craniofacial development including slug, sox9, and pax8 were disrupted, and correlated with morphological deformities. Changes in bioelectric signaling are also sufficient to induce superfluous organ formation as shown by the growth of ectopic eyes in *Xenopus* tadpole tails and guts upon hyperpolarization of the region. The ectopic eyes were well organized as shown by innervation and expression of structure specific markers for rods and cones, Xap2 and Calbindin respectively (Blackiston and Levin, 2013). The ability of exogenous bioelectric events to induce the development of well organized structures demonstrates bioelectricity can act as an upstream initiator with the ability to coordinate complicated signaling pathways.

In many of the examples of bioelectric regulation, the specific ion channel responsible for inducing the change in current has been identified using pharmacological and genetic techniques. For example, in planaria, determination of anterior polarity during both development and regeneration requires depolarization which was determined via a pharmacological screen to be endogenously mediated by the H^+, K^+ - ATPase (Beane et al., 2011). In the case of *Xenopus* tail regeneration, the necessary current was mediated by the voltage sensitive sodium channel $Na_v1.2$, identified by a pharmacological inhibitor and gene expression analysis (Tseng et al., 2010). Identification of the precise

current flow has led to further understanding of the mechanism both regulating the initial change in current as well as transduction of the ion flow to downstream signals. Some of the mechanisms involved include electrophoresis of charged signaling molecules, such as calcium and seratonin, voltage regulation of membrane proteins such as integrins, and activation of voltage sensitive phosphatases (Levin, 2012).

While much of the seminal work understanding bioelectric signaling was performed in lower organisms, its importance to mammalian cell biology is also well established with clear consistencies across species. In much the same way V_{mem} is critical to *Xenopus* development, it is also required in mammalian differentiation. In our previously published results, our group has demonstrated the ability of V_{mem} to regulate stem cell differentiation (Sundelacruz et al., 2008). The membrane potential of human mesenchymal stem cells (hMSC) hyperpolarized during differentiation by 56 mV and 74 mV during osteogenic and adipogenic differentiation respectively. hMSCs grown in osteogenic media and depolarizing conditions exhibited decreased osteogenic marker expression, including decreased alkaline phosphatase activity and mineralization. Conversely, when grown in osteogenic media and hyperpolarizing conditions, hMSC osteogenic gene expression increased. The results are consistent with other

studies that have shown a close correlation between hyperpolarized membrane potential and differentiation (Levin, 2007).

Currently it is not known whether V_{mem} modulation induces a stepwise response in which cells behave differently depending on the strength of the induced potential. Preliminary results in *Xenopus* suggest that the response is highly dependent on the $V_{mem,}$ implying a sophisticated system of regulation capable of promoting specific differentiation pathways (Vandenberg et al., 2011). Such a mechanism suggests bioelectric signaling would be a valuable clinical target because relatively simple cues induce intricate organizational cascades. The ability of bioelectric signaling to increase regeneration in lower organisms, in combination with results showing V_{mem} modulation can regulate mammalian stem cell differentiation, suggests that modulation of ion flows will likely be sufficient to induce increased regenerative capabilities in human tissues naturally lacking regenerative potential (Jenkins et al., 1996; Zhao et al., 2006).

Our previous results modulating V_{mem} in hMSCs demonstrated correlations between differentiation and V_{mem}. We are now interested in further characterizing the ability of V_{mem} signaling to direct differentiation to determine whether modulating V_{mem} to different degrees, ie. hyperpolarizing by 10 mV versus 30 mV, leads to induction of different pathways or differences in the degree of

induction of the same pathways. We aimed to determine if varying the strength of V_{mem} modulation leads to differential effects in adult stem cell differentiation and whether the effects are cell type specific and results are presented in chapter 2.

I.5 Yin yang relationship between regeneration and cancer

Cancer has been called a developmental disorder because it is a dysregulated form of many embryonic processes. The idea arose centuries ago with the proposal that cancer perhaps originated from retained embryonic stem cells and the observation that tumors are remarkably similar to the trophoblast cells responsible for implantation within the uterine wall (Ferretti et al., 2007). In both cancer and embryonic development, cells are reprogrammed, proliferate, migrate, induce vascular growth, undergo epithelial to mesenchymal transitions (EMT), self-renew, and differentiate (Ma et al., 2010). Research over the past century has determined that along with having similar behaviors, cancer and development are also similar at a molecular level, including possibly bioelectric regulated pathways.

Many embryonic signaling pathways and developmentally restricted proteins are reactivated in cancer, much like in regeneration but in the case of cancer are responsible for imparting aggressive

behaviors (Harris et al., 2012). Tumors with less differentiated genetic profiles, particularly with high expression of the genes involved in maintaining embryonic stem cells, are associated with the most aggressive phenotypes (Ben-Porath et al., 2008). Hedgehog, Wnt, fibroblast growth factor (FGF), Notch, and bone morphogenetic protein (BMP) signaling are essential to normal development and are responsible for coordinating proliferation, differentiation, migration and invasion. Their signaling is context dependent and involves extensive cross-talk between pathways allowing unique and highly regulated roles in different stages of development. These pathways are also reactivated in regeneration where the signaling remains under control and maintains appropriate contextual response. For reasons that remain unclear, they are reactivated in cancer, but seemingly without all of the controls that exist during normal development.

As a specific example, hedgehog signaling regulates proliferation and patterning of differentiation during development including of the limb, neural tube, and heart. During regeneration of the limb in *Urodeles*, the signaling factor sonic hedgehog (Shh) is expressed within the blastemal directing limb growth in a similar pattern to its expression in the limb bud during development (Imokawa and Yoshizato, 1997). Exogenous expression of Shh in anterior regions during development and regeneration results in digit duplication. This

demonstrates not only similarities in the signaling pathways but also the importance of precise spatial control of signaling. Hedgehog signaling is over-active compared to healthy tissue in nearly every cancer type, but in this setting, it seems the respective regulatory mechanisms are not reciprocally activated causing the pathway to unleash havoc (Harris et al., 2012).

Interestingly, species with heightened regenerative abilities are also resistant to cancer formation (Brockes, 1998). When the limbs of regenerative and non-regenerative newt species were treated with chemical carcinogens, fewer tumors formed in the regenerative limbs suggesting the plasticity of regenerative environments may protect against cancer initiation (Tsonis, 1983). Further evidence for a link between plasticity and cancer protection arises from studies investigating the ability of embryonic environments to revert cancer phenotypes (Bizzarri et al., 2011). Embryonic carcinoma cells injected into a mouse blastocyst formed a chimeric mouse with no tumor formation indicating the cells were reprogrammed to respond to developmental programs and were integrated into multiple tissues (Brinster, 1974). The ability to reprogram cancer cells is spatially restricted to the blastocoel and cells injected between the *zona pellicula* and trophectoderm remained malignant (Pierce et al., 1979). This suggests precise and highly specific signaling from the

morphogenetic field is required for cancer reversion much as it is essential for proper development. Additional studies indicate only early embryonic environments have sufficiently strong signaling fields to induce cancer reversion. Human melanoma cells injected into chick embryonic neural tubes migrated along neural crest migration pathways but did not form tumors (Kulesa et al., 2006). In contrast, when injected into chick neural crest, the cells formed invasive tumors (Hendrix et al., 2007). The importance of the microenvironment has long been appreciated but more often for its role in promoting cancer progression. However, these studies suggest the ability of highly plastic microenvironments in development and regeneration to promote normalization of malignant cells even in the presence of oncogenic mutations.

Little is known about the mechanism by which plastic environments induce reversion of cancer cells and it is hoped that a better understanding could lead to novel clinical treatments. One of the most interesting aspects of the mechanism is that it overrides genetic mutations since the reverted cells contain the same oncogenic mutations as the parental malignant cells. The mechanism therefore must rely on microenvironmental factors with the ability to precisely re-induce appropriate regulatory pathways. Given its important role in development, regeneration, and cancer, bioelectric signaling may be a

fundamental component of this mechanism. It is conceivable that embryonic and regenerative environments, which are known to experience waves of shifts in V_{mem} and additional bioelectric events, stimulate bioelectric-responsive pathways in cancer cells leading to normalized behavior.

Significant evidence exists demonstrating the importance of bioelectric signaling in regeneration making ion channels and other bioelectric modulators an exciting potential target for clinical therapies aimed at improving healing. However, development, regeneration, and cancer share numerous behaviors and molecular signaling pathways in which bioelectric signaling is required. Thus, a clear obstacle to developing clinical treatments to improve healing through regenerative processes is the risk of inducing malignancies. Further studies are needed to understand the subtle differences in regulatory mechanisms to ensure treatments do not induce harmful cell behaviors.

I.6 Bioelectricity and breast cancer

Cancer is defined as abnormal cell growth with the ability to invade other parts of the body. Typically it is not the growth of the primary tumor that causes severe health concerns, but rather metastasis, the spread and growth of cancer in additional locations in

the body. Tumors compete for space, oxygen, and nutrients with surrounding healthy tissue inhibiting the ability of the tissue it invades to perform its normal function. When this occurs within important organs such as the brain, bone marrow, or kidneys, critical functions are compromised eventually leading to death.

Breast cancer is one of the most common forms of cancer with roughly 230,000 new cases per year and is responsible for 40,000 deaths in the United States alone (National Cancer Institute Statistics). About 1 in every 8 women will be diagnosed with breast cancer at some point in her lifetime. Women diagnosed with localized breast cancer have an excellent prognosis with over 98% 5 year survival. Unfortunately, patients with metastases have only a 25.9% 5 year survival highlighting the need for treatments aimed at metastasis.

A major hindrance to the development of better breast cancer treatments is a lack of understanding of what drives disease progression to metastasis. For decades it has been known that some cancers remain in a benign state for long time periods while others quickly progress to malignancy. Although many metastasis-specific pathways have been described, the upstream signals that activate these pathways remain largely unknown. The initiators are likely to be the most effective therapeutic targets as they affect multiple molecular cascades and may completely inhibit metastatic behaviors.

Another obstacle in cancer treatment design is developing therapeutics that act specifically on cancer cells. Behaviors characteristic of cancer are also performed by healthy cells but in a regulated form. Most chemotherapeutics used clinically target the cell cycle killing any actively proliferating cell. This includes not only cancer cells but also dividing cells in the intestine, skin, and bone marrow causing severe nausea and immune suppression. During the treatment of advanced cancers, the dosage of cancer drugs is sometimes limited by the side effects that the patient can withstand. In the 1960's during trials for some of the first chemotherapies, oncologist William Maloney said "If we did not kill the tumor, we killed the patients." Oncologists today continue to face the same dilemma and must weigh the risks of tumor progression with the risks of aggressive treatment. Thus, a major goal of cancer research is to elucidate targets that are unique to cancer cells and would result in less severe side effects. There has been a limited degree of success pursuing specific treatments, with one of the first examples being the treatment of Her2 positive breast cancers. A subtype of breast cancer expresses high levels of the tyrosine kinase receptor Her2, which is expressed only at much lower levels in healthy cells (Press et al., 1990). Treatment of patients with Her2 inhibitors kill cancer cells that depend on Her2 activity for survival without killing healthy cells. However, this example is not the

norm and many cancers remain where no specific targets are known. Identifying unique targets that could be used to develop novel anti-cancer therapeutics to replace current treatments with life threatening toxicities is a major goal of current cancer research.

A better understanding of bioelectric signaling has the potential to elucidate new, highly specific cancer drug targets. Studies have demonstrated that changes in proliferation, invasion, and other cancer-associated behaviors are often accompanied by predictable changes in ion channel expression (Huber, 2013). Furthermore, a number of the channels with increased expression are expressed as neonatal variants in cancer or are not expressed in the healthy adult tissue making them highly specific targets (Fraser et al., 2005). Currently, our understanding of the functional role of these channels in cancer onset and metastasis is in its infancy.

Interestingly, numerous cancer types are more depolarized than their healthy counterparts suggesting dysregulation of V_{mem} may be a pivotal factor in cell transformation (Yang and Brackenbury, 2013). However, it remains unclear whether shifts in V_{mem} are simply a secondary effect of changes in ion channel activity, particularly those associated with proliferation, or if depolarization has an instructive role in which it drives aggressive cell behaviors. If V_{mem} is found to drive cancer progression, its mechanism of action could provide a vast new

array of anti-cancer targets. As described previously, V_{mem} fluctuates during the cell cycle and altering V_{mem} induces corresponding changes in proliferation. It is challenging to conceptualize how cells could differentially respond to fluctuations in the cell cycle and to the generalized depolarization described in cancer. However, similar complexities are found in calcium signaling and research has clearly demonstrated signaling mechanisms capable of maintaining a 'memory' of basal states, the amplitude and frequency of signaling, and relative changes in signal intensity (Berridge et al., 2000). V_{mem} may utilize analogously networked signaling mechanisms to allow equal complexity in signal response. Additionally, it is possible that much of V_{mem} signaling occurs via its effect on intracellular calcium. Hyperpolarization increases calcium influx via voltage-independent calcium channels while depolarization may activate voltage-gated channels. Activation of potassium channels during migration increases calcium influx via a voltage-dependent mechanism (Schwab et al., 2008). Importantly, V_{mem} also signals through calcium-independent pathways. Depolarization of kidney epithelial cells activates the Rho-Rho kinase pathway and induces dephosphorylation of myosin light chain even in calcium-free conditions (Szaszi et al., 2005). Further characterization of V_{mem} dynamics in healthy and cancerous cells is needed to determine the importance of V_{mem} signaling in driving

cancer progression and to gauge the potential of using V_{mem} as a cancer specific therapeutic target.

Bioelectric signaling in cancer may alternatively depend on specific ion channels and ion currents rather than on the induced V_{mem} shift, making individual channels potential therapeutic targets. As changes in ion currents are known to be involved in cell proliferation and migration, it is thought that they may be important to these processes in cancer. A common trend in many cancer types is an increase in conductance of potassium, sodium, and chloride (Kunzelman, 2005). Characterization of the roles of each of these currents in proliferation, migration and metastasis is an active area of research and many links between specific ion channels upregulated in cancer and aggressive behaviors have been identified.

Increased voltage-gated sodium channel (VGSC) expression and activity has been found in numerous cancer types including lung, prostate and breast (Huber, 2013). The level of VGSC expression correlates with disease severity such that more aggressive cancers have higher VGSC expression (Onkal and Djamgoz, 2009). Inhibition of these channels, by siRNA knock down or pharmacological inhibition, significantly decreases invasion typically to similar levels as non-metastatic cells (Bennett et al., 2004). Interestingly, each type of cancer with VGSC over-expression predominantly over-expresses a

single VGSC family member and this member is different between cancer types. Breast cancer frequently over-expresses the neonatal variant of $Na_V1.5$ with expression levels correlating with disease severity (Fraser et al., 2005). In the metastatic cell line MDA-MB-231, inhibition of VGSC channels or siRNA knock-down of $nNa_V1.5$ significantly reduced invasion and migration but had no effect on proliferation (Onkal and Djamgoz, 2009). *In vivo*, treatment with a $Na_V1.5$ inhibitor significantly reduced tumor growth and metastasis in mice further supporting $Na_V1.5$ as a clinically viable target (Nelson et al., 2015). One outstanding question in the field is whether the mechanism by which VGSCs allows invasion is dependent on sodium influx and therefore conserved between cancer types, or if the mechanism depends on specific attributes of individual VGSC family members. A further and more important question is whether over-expression of VGSCs is sufficient to induce invasive capabilities, and if this is so, whether they have a similar affect in healthy cells as this would have important implications regarding VGSC channel mechanisms of action and clinical utility.

Significant evidence exists in the literature suggesting VGSC over-expression is sufficient to drive invasion in otherwise non-invasive cells. Bennett et al. (2004) investigated the effect of VGSC in a series of prostate cancer cell lines that included one non-metastatic

and two metastatic cancer lines. The metastatic lines had significantly increased expression of VGSCs and increased invasion as compared to the non-metastatic line. The invasive ability of the metastatic cells decreased to the same level as the non-metastatic line by treatment with the VGSC-specific inhibitor tetrodotoxin (TTX) demonstrating the requirement for VGSC in invasion. More interestingly, transient over-expression of $Na_V1.4$ significantly increased invasion in all three cell lines demonstrating that VGSC over-expression is sufficient to drive invasion even in non-metastatic cancer cells. Additional evidence for the importance of VGSCs comes from a probabilistic modeling loss-of-function screen that found $Na_V1.5$ was a high level regulator of colon cancer invasion (House et al., 2010). In the study, siRNA was first used to knock down expression of $Na_V1.5$ or one of 21 genes reportedly linked to invasion and the effect on invasion was assessed. Next, microarray data from the 22 individual gene knock downs was used to perform probabilistic modeling to predict the hierarchy of gene regulation. The results of the modeling placed $Na_V1.5$ as the most upstream regulator in the network with high confidence and its downstream targets included Wnt signaling, the MAPK pathway, and calcium signaling. The work strongly suggested $Na_V1.5$ could be an initiator of invasive pathways and directly demonstrated that $Na_V1.5$ is capable of signaling changes in transcriptional regulation. If VGSCs are

initiators of invasive signaling cascades, inhibition could provide a highly effective mechanism to prevent metastasis.

Numerous potassium currents including calcium-sensitive, voltage gated, and ATP sensitive potassium channel currents are increased in certain cancer types and may also have important roles driving cancer progression. Most studies investigating potassium channels and cancer have focused on proliferation because potassium channels are needed for progression through checkpoints of the cell cycle (Wonderlin et al., 1995). Proliferating cells undergo a cyclical change in V_{mem} with a brief hyperpolarization during G1 and S phase that is mediated by increased potassium channel opening (Figure 3A) (Huang et al., 2014). Inhibition of these channels generally leads to a decrease in proliferation (Kunzelmann, 2005). Particular families of potassium channels are associated with cell cycle arrest at certain points. For example, inhibition of EAG potassium channels causes cells to accumulate in the early G1 phase while inhibition of the large conductance calcium-activated potassium channels (BK) causes accumulation in the S phase (Day et al., 2001; Ouadid-Ahidouch et al., 2004a). Much work has focused on calcium activated potassium channels which are over-expressed in numerous cancer types including breast, prostate, uterus, stomach, colorectal, pancreas, pituitary gland, and brain cancers (Kunzelmann, 2005). Inhibition of the

intermediate conductance calcium-activated potassium channel (IK) in prostate cancer cell lines as well as primary prostate cancer cells inhibits proliferation (Lallet-Daher et al., 2009; Parihar et al., 2003). Treatment of breast cancer cells with an IK inhibitor similarly decreased proliferation (Furtado et al., 2012; Ouadid-Ahidouch et al., 2004b). Interestingly, IK mRNA expression is increased by activation of the Ras/Raf pathway indicating a direct link between important cancer signaling pathways and IK (Huang and Rane, 1994).

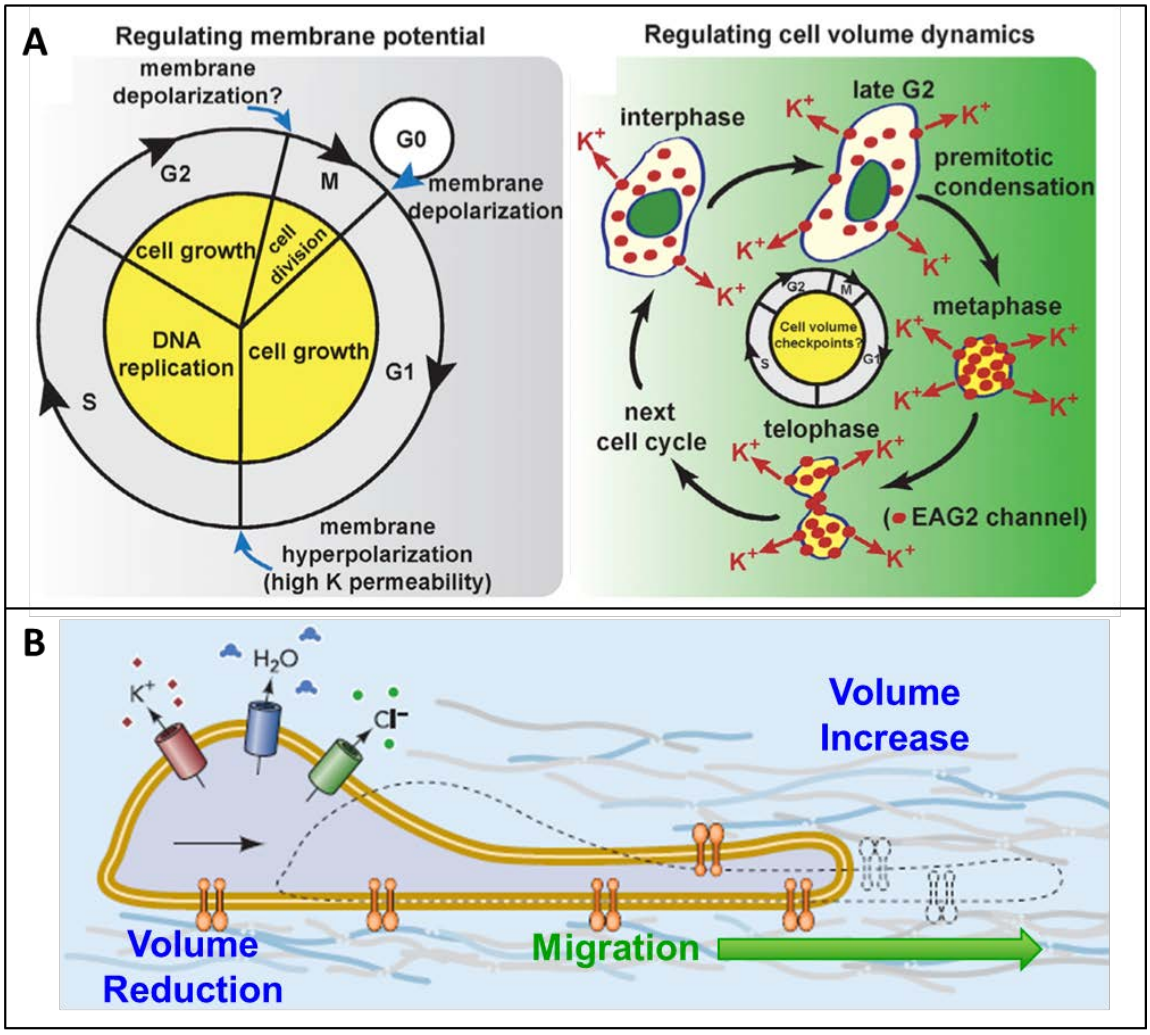

Figure I-3: Involvement of potassium channels in cell proliferation and migration. (A) Potassium channel activity is responsible for changes in V_{mem} (left) and volume (right) during the cell cycle. **(B)** Potassium channel mediated volume decrease during migration is spatially restricted to the lagging edge. ((A) Reproduced from (Huang and Jan, 2014) and (B) (Schwab et al., 2008) with permission)

In addition to being required for proliferation, activation of IK with pharmacological agonists increased proliferation of prostate cancer cells demonstrating it is sufficient to promote proliferation

(Lallet-Daher et al., 2009; Parihar et al., 2003). While current data strongly suggest a conserved requirement for potassium channels in proliferation and especially highly proliferative cancer cells, more studies are needed to determine if the sufficiency of potassium currents to promote proliferation is similarly conserved. Furthermore, additional studies are needed to determine whether the sufficiency of potassium channels to increase proliferation is specific to particular potassium channel families or to increased potassium currents generally.

Potassium channels, and specifically IK, are also important in migration suggesting they may have a broad role in promoting cancer progression (Huang et al., 2014). Formation of metastases relies on cell migration, making the migration machinery an important potential cancer therapy target. During migration, cells become polarized and must extend a leading edge while simultaneously retracting a lagging edge. This process requires coordinated differential regulation of cell membrane trafficking, actin dynamics, and cell volume changes.

Potassium channels are most likely involved in migration primarily by their requirement for cell volume shrinkage, although the channels may have additional regulatory roles as well. Cell volume is regulated indirectly by using intracellular ion concentrations to alter osmotic forces and induce the flow of water molecules into or out of

the cell. Cells do not actively transport water molecules and instead water diffuses through aquaporin channels in the cell membrane that are constitutively open (Okada, 2004). Regulated opening of ion channels and activation of ion pumps is used to control ion concentrations and induce osmotic pressures. Ion flow into or out of the cell disrupts the osmotic equilibrium and creates a driving force that carries water molecules in the same direction and in proportion to the net flow of ions. It is the flow of water molecules that causes the change in cell volume.

Potassium channels are utilized to induce an efflux of ions and therefore cell volume shrinkage. Typically cells have about a 10-fold higher concentration of potassium ions intracellularly compared with the extracellular environment. Thus, when potassium channels open the ions flow out of the cell creating osmotic pressure that also drives water out of the cell causing cell shrinkage (Figure 3B). It is important to note that chloride channels must also open to allow efflux of negatively charged chloride ions to counteract the electrical potential created by the exiting positively charged potassium ions (Pedersen et al., 2013). Activation of ion channels and pumps involved in cell volume regulation is tightly spatially regulated within a cell so that the cell can experience volume increases and decreases simultaneously in

different locations. Migrating cells require volume increases at the leading edge with concurrent volume decreases at the lagging edge.

As with proliferation, the families of calcium-activated potassium channels have been shown to be important in migration. During normal development IK activity is required for appropriate migration of neuroblast cells (Turner and Sontheimer, 2014) and inhibition of BK in glioma cells decreased migration (Yang et al., 2013). Due to the polarized nature of migration, it would be expected that potassium channels involved in migration would respond differently on the leading verses lagging edge. Indeed, this was found to be the case in transformed renal epithelial cells in which IK inhibition on the leading edge had no effect but IK inhibition on the lagging edge decreased migration similarly to pan-IK inhibition (Schwab et al., 1995). The requirement for potassium channels in migration is well established with different channels being utilized depending on the cell type. The channels are traditionally thought to simply be an indispensable component of the migratory machinery. However, it remains unclear whether potassium channels may also be sufficient to initiate or increase migration. One potential mechanism is that higher potassium channel expression increases the ability of a cell to induce potassium efflux and improves the speed with which a cell can perform cell volume shrinkage. Alternatively, potassium channels may have a more

instructive role in which they initiate the migratory machinery. If potassium channels are initiators inhibiting their action could provide a potent mechanism to prevent metastasis.

As chloride channels are similarly required for volume decrease, it is not surprising that they are also up-regulated in some cancers, and may be similarly effective therapeutic targets (Huber, 2013). Glioblastoma express high levels of the $Na^+/K^+/2Cl^-$ transporter and ClC-3 chloride channel and inhibition of either decreases migration (Haas and Sontheimer, 2010; Lui et al., 2010). Under normal conditions the glioblastoma cells have an unusually high intracellular chloride concentration which is likely used as an osmolyte when volume reduction is needed during migration. ClC-3 is being tested clinically as a specific glioblastoma target because it is expressed on the plasma membrane of glioblastoma cells whereas it is only found intracellularly in healthy cells (Hockaday et al., 2005).

Much work to date has identified bioelectric signaling and changes in cell ion flux as being required for metastatic behaviors. Numerous ion channels and currents are associated and even required for cancer progression, however a major question in the field is whether bioelectric signaling is sufficient to promote aggressive phenotypes. The greater the role as an instructor of cancer progression the more likely inhibition will be a highly effective clinical

treatment. Proliferation, migration, and invasion clearly require ion flux as part of the cellular machinery. However, little work has focused on the ability of bioelectric signaling to promote metastatic behaviors in otherwise non-metastatic cells. Recent work demonstrating the ability of ion channels to induce transcriptional changes suggests the potential for bioelectric signaling to function as an initiator of metastasis. Proposed mechanisms illustrate pathways that bioelectric events are integrated with cell signaling networks. As ion channels are known to be responsive to many microenvironmental factors, they provide an appealing mechanism that could explain why cells with the same genetic background develop and display different behaviors. Further studies are needed to determine whether modulation of ion channel activity is sufficient to drive aggressive cancer behaviors, transformation, and metastasis and to better understand interactions between bioelectricity and downstream signaling pathways. Detailed characterization may identify unique properties in cancer that can be used to develop highly specific and effective anti-cancer therapies. Results from studies investigating the effect of modulating bioelectric properties in mammary epithelial and breast cancer cell lines are reported in chapters 3, 4, and 5.

I.7 Experimental approaches to investigate bioelectric signaling

A critical obstacle to improving our understanding of bioelectric signaling is the ability to accurately measure V_{mem} and ion currents across the cell membrane. Unlike many cellular processes, bioelectricity can only be measured in real time with live cells. The measurement techniques fall into two categories, electrophysiological recordings and fluorescent dye imaging.

Electrophysiological recordings create an electrical circuit in which the current or electric potential across the cell membrane can be measured. One electrode is placed such that it has direct access to the intracellular space and a second electrode is placed in the solution surrounding the cell. An amplifier is then used to measure the electrical current required to hold a specific electrical potential, the voltage clamp configuration, or to measure the membrane potential while holding a specific current (typically current = 0 to measure V_{mem}), the current-clamp configuration. In the voltage and current clamp configurations the electrical current or potential between the two electrodes is exactly equal and opposite to that of the cell membrane.

In order for the recordings to be accurate, the electrode must gain access to the cell cytoplasm without disrupting the integrity of the

cell membrane. This method was originally developed using extremely small and sharp glass electrodes that puncture the cell membrane and is referred to as intracellular recording. Intracellular recording is effective in the current clamp configuration and is utilized to measure V_{mem} but is ineffective in the voltage clamp configuration. The size of the electrode opening is limited to less than 1 μm to avoid damaging the cell membrane, which also limits the current that can pass through the electrode. The maximum current is insufficient to create and hold the electrical potential needed for voltage-clamp recordings. Thus, the patch clamping method was developed. In this method, the tip of a glass electrode is gently pressed to the outside of the cell membrane to form an extremely high resistance seal, a gigaseal, with the extracellular leaflet of the cell membrane. The cell membrane within the electrode is termed the patch and the solution surrounding the cell the bath. One of several common variations is then applied for recording (1) cell attached: the electrode is left in place and electrical activity through any channels within the patch can be recorded (2) inside-out patch: the electrode is pulled away from the cell and the patch of membrane remains attached to the electrode with the intracellular leaflet of the cell membrane exposed to the bath (3) whole cell: negative pressure inside the electrode is increased to rupture the patch causing the electrode to now be in direct contact

with the cytoplasm allowing recording from the entire cell (4) negative pressure is used to burst the patch as in whole cell configuration and then the electrode is pulled away from the cell causing the membrane around the electrode to fold inward and re-seal the tip of the electrode, now with the extracellular surface of the membrane facing the bath (Figure 4). Each method has advantages and drawbacks relating to the ability to modulate ligand or other signaling molecule concentrations, sensitivity for small currents, and maintenance of the endogenous cell state.

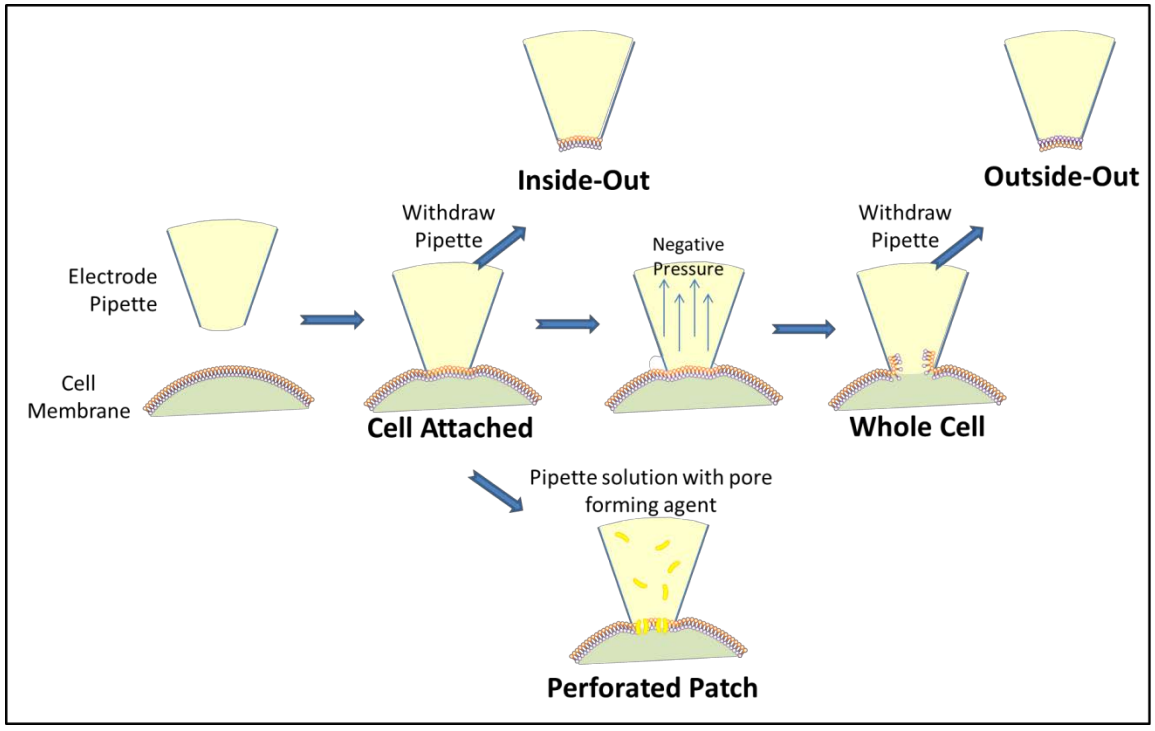

Figure I-4: Electrophysiology patch-clamp configurations. The electrode is pushed against the cell membrane to create a seal with giga-ohm resistance. This results in the cell attached configuration. Withdrawing the electrode separates the patch within the electrode

from the rest of the cell with the intracellular leaflet of the membrane facing the bath. Alternatively, negative pressure can be added to rupture the patch resulting in the whole cell configuration. If the pipette is withdrawn after bursting the patch, hydrostatic forces cause the inner leaflet of the cell membrane to come together re-sealing the pipette tip now with the outer leaflet exposed to the bath. Finally, the cell attached configuration with a pore forming agent in the electrode solution will lead to a perforated patch where the electrode has electrical access to the whole cell without the need to rupture the membrane.

Of the patch-clamp methods only the whole cell configuration permits recording of V_{mem}. The large size of the electrode opening provides enhanced electrical access as compared to intracellular recording. However, the large size also allows molecules from within the cell to diffuse more easily into the electrode depleting the cell of its contents, which can alter the endogenous bioelectric properties. A minor variation to the whole-cell configuration is the perforated-patch in which a pore forming chemical is used to gain access to the cytoplasm. The pore forming chemical is added to the electrode solution and forms pores within the patch after the gigaseal is formed. The pores are selective for monovalent ions providing electrical access to the cytoplasm while simultaneously preserving levels of signaling molecules such as Ca^{2+} and cAMP. Thus, the perforated patch clamp method gives the most accurate recordings of endogenous V_{mem} while also allowing for current recordings.

Electrophysiology recordings provide extremely sensitive measurements, but are extremely time consuming and labor intensive. More recently, fluorescent dyes that are sensitive to specific ion concentrations or the local electric potential have been developed. The dyes can be used to measure electrical properties in a field of cells giving a more accurate representation of a cell population. Measurements from a field of cells can also be used to investigate the effect of electrical dynamics between neighboring cells. Dyes have been developed that are sensitive to calcium concentration, sodium concentration, pH, or V_{mem}. However, the dyes have a lower signal to noise ratio than electrophysiology recordings and many have a slow or irreversible response. It is also challenging to develop standards needed for quantitative data and often only relative comparisons can be made.

Investigating bioelectric signaling also requires tools to modulate bioelectric events. Pharmacological agents, genetic engineering, and extracellular ion conditions can be utilized to induce or inhibit specific bioelectric properties.

Numerous pharmacological agents exist targeting ion channels to increase or decrease the open probability. Hierarchical screens utilizing first less-specific followed by more specific reagents are useful in channel identification. Inhibitory molecules are most advantageous for

channels with high endogenous activity, although there is a risk that other channels may become active to compensate. Channel activators have the most predictable effect, particularly if the goal is to modulate V_{mem}. However, with fewer known agonists, it may be challenging to enact desired modulation with endogenously expressed channels.

Genetic engineering can be used to increase or decrease expression of specific ion channels. Similarly to pharmacological agents, the addition of currents and channels is often more effective than knocking out channels because of compensation. Viruses such as lentivirus and retroviruses provide a means to enact stable expression levels required for long-term experiments. Genetic engineering can also be used to add mutations to the channel sequence to make the channel more or less active, change the ion selectivity, or alter its response to signaling pathways.

Altering the extracellular environment also has predictable effects on bioelectric properties. As described previously, modulating the extracellular ion concentration will shift the ion's equilibrium potential and thereby change V_{mem} and the current density through open channels. Combining genetic engineering, pharmacological agents, and extracellular ion conditions provides a powerful toolkit to specifically modulate bioelectricity with appropriate conditions to control for off-target effects.

It is expected that if V_{mem} is an instructive regulator of cell behavior, channels that induce similar absolute V_{mem} will cause similar changes in cell behavior. To investigate the instructive role of changes in absolute V_{mem}, a set of ionic conditions should be chosen such that V_{mem} can be induced to different ranges throughout the physiologically relevant spectrum. Ideally, multiple sets of conditions utilizing different ion currents would be developed for each range in V_{mem} to control for ion-specific effects.

Experiments performed in *Xenopus* have identified ion channels that allow for easy manipulation of V_{mem}. One of the most versatile channels is the glycine receptor chloride channel (GlyR). GlyR is active transiently in the presence of glycine but can also be stably inhibited or activated by strychnine and ivermectin respectively. It is selective only to chloride ions and therefore increasing GlyR activity shifts V_{mem} towards the chloride reversal potential. For most mammalian cells, the endogenous chloride E_{Rev} is around -50 mV, which is also close to the resting potential of many mature cell types. Thus, addition of GlyR activity has little effect on V_{mem} in standard conditions for most cell types. However, the E_{Rev} of chloride can be altered by changing the extracellular chloride concentrations with increased chloride making E_{Rev} more negative and decreased chloride making it more positive. Therefore increasing GlyR activity in altered chloride conditions causes

hyperpolarization and depolarization respectively. The ability to use one channel to modulate V_{mem} in both directions enables experiments to test for specificity to changes in V_{mem} rather than non-conducting channel effects. Furthermore, the ability to control GlyR activity with pharmacological agents allows temporal control of activity and investigation of time-sensitive responses. Imaging with voltage-sensitive dyes in *Xenopus* has demonstrated the ability to use extracellular chloride concentration in combination with exogenous GlyR expression to induce differential changes in V_{mem}.

Addition of exogenous potassium currents provides a mechanism to induce hyperpolarization. Mammalian cells are primarily permeable to potassium and also have limited permeability to sodium and chloride making the V_{mem} close but depolarized in comparison to the potassium E_{Rev}. Increasing potassium currents increases the relative permeability of potassium and therefore hyperpolarizes V_{mem} to be closer to E_{RevK}. ATP-sensitive potassium channels (K_{ATP}) are expressed by most cell types and can be targeted with pharmacological agonists to increase their endogenous activity. Genetic engineering can also be used to increase potassium currents by adding potassium channels with either high constitutive activity or known agonists. A mutant version of Kir2.1 in which an inhibitory phosphorylation site is deleted has a high open probability and has been used for hyperpolarization in

Xenopus (Adams and Levin, 2013). The intermediate conductance calcium-activated potassium channel is also a good candidate as it has stable activation in response to the agonist 1-EBIO.

Potassium can also be used to induce depolarization by increasing the extracellular potassium concentration and shifting E_{RevK} more positive. Importantly, the effect on V_{mem} of changing extracellular ion concentrations is larger in cells with a higher relative permeability to the ion because they are more responsive to the change in E_{Rev}. This can lead to counterintuitive effects on V_{mem}. For example, cells genetically engineered to have increased potassium channel expression will be hyperpolarized compared to wild type cells in standard extracellular potassium in which E_{RevK} is very negative. But in high concentrations of extracellular potassium where E_{RevK} is shifted positively, the genetically engineered cells are more sensitive to the shift due to a higher dependence on E_{RevK} and will be more depolarized than parental cells cultured in the same potassium concentration.

Ion channels whose expression correlates with differentiation or cancer progression also present excellent candidates to investigate bioelectric induced behaviors. Signaling may require the precise activity pattern of the channel or channel specific protein-protein interactions.

The V-ATPase proton pump is over-expressed and over-active in metastatic cancer. Inhibiting its activity significantly decreases invasion in the metastatic breast cancer cell line MDA-MB-231 (Sennoune et al., 2004). An unanswered question is whether V-ATPase over-activity is sufficient to induce metastatic behaviors and if the behavioral changes are caused directly by proton efflux or by some other mechanism of V-ATPase signaling. Over-expressing the V-ATPase a3 subunit increases localization of the pump to the plasma membrane and induces a significant increase in proton efflux (Capecci and Forgac, 2013). The yeast proton pump PMA has also previously been expressed and demonstrated to function in mammalian cells. Expression of either a3 or PMA has the potential to induce the pH gradient inversion found in cancer and could be used to investigate the sufficiency of increased extracellular acidity to promote specific cell behaviors such as migration and invasion.

While the importance of VGSCs for invasion has been clearly demonstrated in many cancer types, little is known about the molecular mechanisms by which invasion is promoted and particularly how VGSCs function as a transcriptional regulator. A few mechanisms have been suggested, one of which was discussed previously and involved translocation of the beta subunit intracellular domain to the nucleus where it regulates transcription. Alternatively, a mechanism

involving the effect of VGSC activity on calcium signaling has been suggested. Calcium functions as a secondary messenger to activate numerous signaling pathways by activating calcium sensitive kinases and phosphatases (Berridge et al., 2000). Typically, calcium signaling is initiated by extracellular initiators that lead to calcium release from ER stores and/or calcium influx from activation of calcium channels in the plasma membrane (Cullen and Lockyer, 2002). The activity of VGSCs is likely to affect the amount of calcium entering cells through channels by increasingly depolarizing the V_{mem} via the increased sodium influx. Both the activity of calcium channels and the amount of calcium flux through the channels is affected by V_{mem}. The open-probability of many calcium channels is increased by depolarization leading to increased calcium influx for a given stimulatory signal (Pietrobon and Hess, 1990). Interestingly, many cancers express neuron-specific ion channels and some cancer cells are able to produce action potentials suggesting they are highly responsive to depolarization (Onkal and Djamgoz, 2009). Furthermore, V_{mem} effects the driving force on calcium ions such that the number of calcium ions passing through a calcium channel in a given time period will change depending on V_{mem} (Huber, 2013). Thus, in this model VGSC activity directly regulates intracellular calcium levels and downstream calcium signaling pathways thereby modulating transcriptional activity of many

genes. Identification of the molecular mechanism linking sodium currents to transcriptional regulation would provide the strongest evidence to date of sodium currents as an important regulator of oncogenic signaling and demonstrate the utility of sodium channels as an anti-cancer therapeutic target.

1.8 Significance of the Project

Bioelectric signaling has critical roles in tissue repair and also cancer behaviors, but the extent of its regulatory influence is poorly characterized. Proteins sensitive to changes in ion currents and V_{mem} modulation are integrated with major signaling pathways creating potential mechanisms by which bioelectric cues could be sufficient to drive and coordinate complicated behaviors. Interestingly, certain bioelectric properties that are typically restricted to developmental processes are re-activated in cancer in much the same way as many molecular signaling pathways. This brings up important questions relating to how bioelectricity signaling differs in the healthy and diseased state to lead to divergent cell behavior.

The influence of bioelectricity over many signaling pathways and cell behaviors makes it an exciting potential target for new clinical therapies. However, first a better understanding of endogenous

bioelectric signaling and knowledge of molecular mechanisms of action are needed. The goal of this project is to enhance our knowledge of bioelectric signaling related to cell behaviors involved in regeneration and cancer in order to move towards viable clinical strategies. V_{mem} signaling during hMSC differentiation was investigated to determine if V_{mem} modulation could be used to direct differentiation in chapter 2. The effect of V_{mem} modulation was also studied in cancer cells to investigate how it affects cancer-associated behaviors in chapters 3 and 4. Finally, the ability of IK, a channel highly expressed in many cancer types, to induce aggressive cancer behaviors was characterized in chapter 5. The results of these studies increase our knowledge of the scope of bioelectric signaling and help to elucidate important differences between signaling in the healthy and diseased state.

CHAPTER II: REGULATION OF HUMAN MESENCHYMAL STEM CELL DIFFERENTIATION BY RESTING MEMBRANE POTENTIAL

II.1 Abstract

Previous studies from our lab demonstrated that depolarization decreased osteogenic and adipogenic differentiation and that hyperpolarization increased osteogenic differentiation of human mesenchymal stem cells (hMSCs). Better understanding of V_{mem} signaling in differentiation would allow V_{mem} modulation to be used as an alternative to biochemical induction of differentiation. We hypothesized that distinct ranges of membrane potential (V_{mem}) would have a more pronounced effect on differentiation and that effects would be pathway specific increasing differentiation of one pathway while having little effect on the other. We were particularly interested to identify V_{mem} conditions that specifically increased osteogenic differentiation over adipogenic differentiation. To test our hypothesis, hMSCs were differentiated in conditions predicted to modulate the V_{mem} throughout the physiologically relevant range during osteogenic differentiation and differentiation markers were assessed. There was significant variability in the hMSC response to V_{mem} modulation in cells derived from different patients and none of the hyperpolarizing or depolarizing conditions tested induced a reproducible increase in osteogenic differentiation.

II.2 Rationale

Previous results from our lab demonstrated that modulating V_{mem} induced changes in adipogenic and osteogenic hMSC differentiation. Depolarization using either increased extracellular potassium or treatment with the sodium/potassium ATPase inhibitor ouabain decreased expression of differentiation markers of cells cultured in both osteogenic and adipogenic differentiation media. Hyperpolarization using potassium channel activators induced increased osteogenic but not adipogenic markers in differentiation media. The eventual goal is to determine bioelectric cues to induce differentiation of a specific pathway without the need for the biochemical factors used in differentiation media. The bioelectric signals could be administered through optogenetic channels allowing for patterning of differentiation to multiple cell types.

In order for bioelectricity to be sufficient to induce specific differentiation pathways, each pathway must be activated by a unique set of bioelectric signals. Currently, very little is known about differences in bioelectric properties between different mature cell types. One potential mechanism of signaling is that particular ranges of V_{mem} may instruct cells to differentiate towards specific cell types. Osteogenic and adipogenic differentiated hMSCs have significantly

different membrane potentials throughout 4 weeks of differentiation demonstrating that V_{mem} is a distinguishing feature between these two cell types (Sundelacruz et al., 2008). We were next interested in characterizing differentiation after modulation of V_{mem} to a specific range. It was hypothesized that certain ranges of V_{mem} would increase differentiation of one lineage while having little or no effect on the other. A challenging aspect of testing this hypothesis is the ability to specifically modulate V_{mem}. A combination of genetic engineering to add exogenous ion channel expression, pharmacological activation and inhibition of channels, and changes in extracellular ion concentrations was used to alter V_{mem}. The extent of differentiation in osteogenic or adipogenic media was then characterized.

II.3 Methods

All reagents were purchased from Thermo Fisher Scientific unless otherwise noted.

hMSC Cultivation - Cells were isolated from bone marrow aspirate from a 25 yo male purchased from Lonza as previously described (Sundelacruz et al., 2008). Cells were expanded in control media, DMEM supplemented with 10% fetal bovine serum (FBS), 0.1 mM non-essential amino acids,1 ng/mL basic fibroblast growth factor (bFGF),

100 U/mL penicillin, and 100 μg/mL streptomycin. To maintain stemness, cells were grown in low oxygen (5%) in a humidified incubator at 37° C with 5% CO_2. Media was changed every 3-4 days and cells were trypsinized at 90% confluence with 0.25% Trypsin-EDTA and split 1:5. For osteogenic differentiation, hMSCs were plated at 5,000 cells/cm2 and cultured in control media supplemented with 10 mM β-glycerophosphate, 0.05 mM L-ascorbic acid-2-phosphate, and 100 nM dexamethasone. For adipogenic differentiation cells were plated at 10,000 cells/cm2 and cultured in control media supplemented with 0.5 mM 3-isobutyl-1-methyl-xanthine, 1 mM dexamethasone, 5 mg/mL insulin, and 50 mM indomethacin. During differentiation cells were grown in ambient oxygen in a 37° C humidified incubator with 5% CO_2.

Modulating V_{mem} of hMSCs – Cells were cultured in media with altered ion concentrations or were treated with ion channel agonists or antagonists to modulate V_{mem}. Extracellular potassium was increased by adding potassium-gluconate. Addition of N-methyl-D-glucamine (NMDG) was used as an osmotic control. Custom DMEM media lacking sodium chloride (NaCl) was used to culture cells in decreased extracellular chloride. NaCl was used to add the desired concentration of chloride and supplemented with sodium-gluconate to increase the sodium concentration to that found in DMEM. ATP-sensitive potassium

channels (K_{ATP}) were activated by addition of 10 μM diazoxide or 10 μM pinacidil. To modulate transient potential cation channel subfamily V member 1 (TRPV1) activity, cells were treated with 10 μM capsaicin (Cpn) or 10 μM capsazepine (CapZ).

RNA isolation, purification and quantitative RT-PCR - Total RNA was isolated using Trizol reagent with chloroform extraction and RNA was purified using the RNEasy mini kit (Qiagen) per manufacturer instructions. RNA was quantified with a Nanodrop 2000. Reverse transcriptase reactions were performed with 1 μg RNA in a 20 μL reaction using the High Capacity Reverse Transcriptase kit with random primers. Taqman gene expression assay fluorescent primer-probe sets were purchased for osteogenic differentiation markers runt related transcription factor 2 (Runx2), alkaline phosphatase (ALP), bone gamma-carboxyglutamate protein (BGLAP), and osteocalcin, for adipogenic differentiation markers peroxisome proliferator-activated receptor gamma (PPARγ) and perilipin, and the housekeeping gene glyceraldenhyde 3-phosphate dehydrogenase (GAPDH) (Applied Biosystems). Quantitative RT-PCR was performed with 100 ng cDNA in a 20 μL using an ABI Prism 7000 Real Time PCR System (Applied Biosystems) with the following cycling conditions: 95° C for 3min, and 40 cycles of 95° C 15 sec, 60° C 30 sec. The delta delta Ct method was used to calculate relative mRNA expression.

Generation of Glycine Receptor Chloride Channel (GlyR) Expression Plasmid – *E. coli* carrying the pLenti CMV Blast DEST expression plasmid was purchased from Addgene (#17451). Mike Levin kindly provided a plasmid containing the GlyR coding sequence. Primers were designed to amplify the full GlyR coding sequence with flanking attB sequences as per manufacturer's instructions for Gateway cloning (forward primer – GGGGACAAGTTTGTACAAAAAAGCAGGCTTCACCATGTACAGCTTCAATACT CTTCGACTC reverse primer - GGGGACCACTTTGTACAAGAAAGCTGGGTTTCACTGGTTGTGGACGTCC). The channel was cloned into pDonr221 and the resulting plasmid was used to transform Dhα E. coli following manufacturer instructions for Gateway cloning. Bacteria clones were screened by kanamycin selection and sequenced to verify channel insertion. LR reactions were performed using 150 ng of the GlyR-pDonr221 plasmid and 150 ng of plenty CMV Blast DEST and transformed into Stbl3 *E. coli.*

Fluorescent Protein Reporters - Transcriptional reporter lentivirus plasmids for BGLAP and perilipin and transcription factor activity reporters for Runx2 and PPARγ were purchased from Systems Biosciences. These constructs had not been validated for appropriate reporter activation.

Lentivirus Production – Two days prior to transfection, 15 x 10^6 293 FT cells were seeded in a triple flask. Transfection was performed with 260 μL of lipofectamine 2000, 8 μg of the REV, RRE, and VSV third generation packaging plasmids, and 16 μg of the reporter plasmid following manufacturer's instructions. Cells were incubated in the DNA:liposome complex overnight in a final volume of 30 mL. At 72 hours post-transfection, the virus media was collected and filtered through a 45 μm filter. The virus media was spun in an Optima LE-80K ultracentrifuge using an SW-28 swinging bucket rotor (Beckman Coulter) at 5 x 10^4 g for 90 minutes at 4° C. The supernatant was discarded and the remaining viral pellet was re-suspended in 300 μL DMEM overnight resulting in a 1:100 concentration.

Virus Transduction and Titration – Cells were transduced by incubating 50% confluent cells with virus in media supplemented with 6 μg/mL polybrene for 24 hours. Virus titration was performed using 293 FT cells. 72 hours after transduction cells were lysed and and the Global Ultra Rapid Titering kit (Systems Biosciences) was used to quantify viral DNA integration by RT-PCR. hMSCs were transduced with an MOI of 10.

ALP Staining – Cells were rinsed in PBS and fixed in 10% formalin for 1 hr. The Leukocyte Alkaline Phosphatase kit (Sigma Aldrich) was used to stain sites of ALP activity per manufacturer instructions.

Calcium Staining – Alizarin red, which binds to all forms of calcium, was used to stain calcium deposits. Cells stained for ALP were incubated in 200 mg/mL alizarin red pH 4.2 for 30 minutes. Samples were rinsed with water and bright field images were acquired as above.

ALP enzyme activity assay – Cells were lysed with 0.2% v/v Triton-X in 5 mM $MgCl_2$. Cell lysate was incubated with p-nitrophenyl phosphate substrate, which is hydrolyzed to the colored product p-nitrophenol by ALP. The reaction was stopped with 0.2M NaOH and the absorbance was read at 405 nm with a VersaMax microplate reader (Molecular Devices) to detect the colored end product.

Calcium Quantification – Total calcium content was determined using a Calcium Liquicolor Test (StanBio Laboratory) per manufacturer instructions.

Cell Viability – Cells were incubated in 10% Alamar Blue reagent for 1 hr and fluorescence was measured on a VersaMax microplate reader (Molecular Devices) with excitation 560 nm, emission 590 nm.

Statistics – Statistics were calculated with Prism 5 using a two-sample T test or one-way ANOVA with Tukey or Dunnett post-test for significance with alpha = .05.

II.4 Results

II.4.1 Characterization of hMSC Differentiation Marker Expression for Higher Throughput Differentiation Screen

In order to enable higher throughput assessment of osteogenic and adipogenic differentiation, a fluorescent protein (FP) reporter based screen was designed. The molecular pathways involved in osteogenic and adipogenic differentiation have been well characterized with known early and late markers for each pathway. One marker each for early and late adipogenic and osteogenic differentiation were chosen to use for FP reporter constructs. FP reporter constructs enable real-time and non-destructive assessment of either transcription factor activity or promoter activity of specific genes.

Commercially available green fluorescent protein (GFP) reporters for the osteogenic genes Runx2 and BGLAP and red fluorescent protein (RFP) reporters for the adipogenic genes PPARγ and perilipin were chosen for the screen to provide early and late markers for each differentiation pathway. These markers were selected due to their reported large and pathway specific increase in expression during differentiation. The reporters for the transcription factors Runx2 and PPARγ provide a read-out of their transcription factor activity while the

reporters for the differentiation markers BGLAP and perilipin evaluate mRNA transcription levels. Using markers corresponding to early and late stages of differentiation will provide insight into the mechanism linking V_{mem} and differentiation. The dual colors were also chosen to allow for investigation of the possibility of trans-differentiation or simultaneous activation of both pathways.

hMSCs derived from different patient donors have variable differentiation capabilities. We first wanted to establish that hMSCs used in this study were capable of robust osteogenic and adipogenic differentiation. We also wanted to confirm that expression of the chosen differentiation markers was similar to previous reports. Low passage hMSCs were cultured in control, adipogenic, or osteogenic media for three weeks. Bright field images at the end of three weeks show clear lipid accumulation in adipogenic samples and mineralization in osteogenic samples (Figure 1A). Total RNA was isolated every 7 days and analyzed for marker mRNA levels by RT-PCR (Figure 1B). Runx2 expression was increased throughout the time course in every media condition. Expression was most highly increased in osteogenic media and had the lowest expression in adipogenic media. PPARγ expression also increased in every condition throughout the time course with much greater expression in adipogenic media. PPARγ expression peaked in adipogenic media on day 14 with 60 fold increase

in expression as compared to only a 12 fold increase in osteogenic media. Expression of perilipin was highly specific with no detectable expression in control or osteogenic media and high expression in adipogenic media at all time points. BGLAP expression was only analyzed at day 7 due to technical difficulties. Interestingly, expression was similar across all samples.

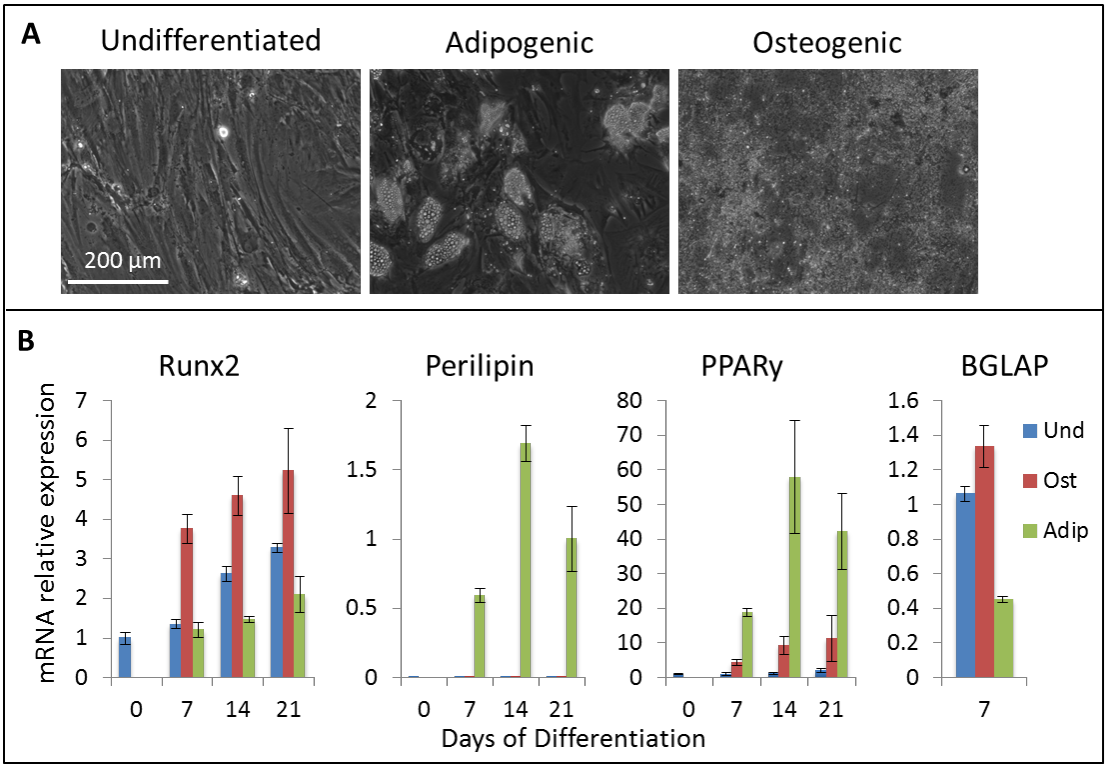

Figure II-1: hMSCs Express Fat and Bone Markers in Response to Differentiation Media. (A) Phase contrast images of hMSCs cultured in control undifferentiated, adipogenic differentiation, or osteogenic differentiation media for 21 days. Cells grown in adipogenic and osteogenic media have lipid accumulation and mineralization respectively. **(B)** Total RNA was isolated from hMSCs grown in control undifferentiated (Und), osteogenic (Ost), or

adipogenic (Adip) media during 3 weeks of culture. mRNA expression levels of indicated bone and fat differentiation markers were quantified by RT-PCR using GAPDH as the housekeeping gene and normalized to day 0 control (Perilipin shown as expression relative to GAPDH). Data are presented as mean with standard deviation of 3 replicates.

II.4.2 Pilot Study of Fluorescent Protein Reporters

The FP reporters first needed to be validated to show that FP expression accurately reflected marker levels during differentiation. Runx2, BGLAP, PPARγ, and perilipin FP reporter virus was produced and used to infect low passage hMSCs. Cells were cultured in control, adipogenic, or osteogenic differentiation media and fluorescence was monitored by fluorescent microscopy twice weekly for 3 weeks.

It was expected that FP reporter cell fluorescence would mimic endogenous expression levels. However, three out of the four reporters had no detectable fluorescent signal with only BGLAP having increased fluorescence over negative control in any condition (Figure 2A). BGLAP had similar levels of fluorescence in both the control and osteogenic conditions with less fluorescence in adipogenic media. However, fluorescence was observed in cells containing lipid droplets.

One possible explanation for the lack of reporter activity is that lentivirus infection may inhibit hMSC differentiation. Lipid accumulation in adipogenic differentiated and mineralization in osteogenic

differentiated hMSCs was similar in cells infected with lentivirus prior to differentiation as compared to un-infected cells (Figure 2B, compare to 1A). Furthermore, infection with reporter lentivirus did not significantly alter expression levels of bone or fat markers as compared to uninfected cells (Figure 2C). Alternatively, there may have been issues with virus infection efficiency of hMSCs. The reporter constructs did not contain a marker and thus it was not possible to directly quantify the percentage of infected cells. However, infection was assessed for a control vector with constitutive GFP expression. All viruses were produced simultaneously and titrated by quantifying viral DNA integration into genomic DNA of 293 cells. hMSCs infected with an equivalent multiplicity of infection of the control virus as reporter infected cells had greater than 50% GFP positive cells indicating successful incorporation of viral DNA in a significant portion of cells (Figure 2D).

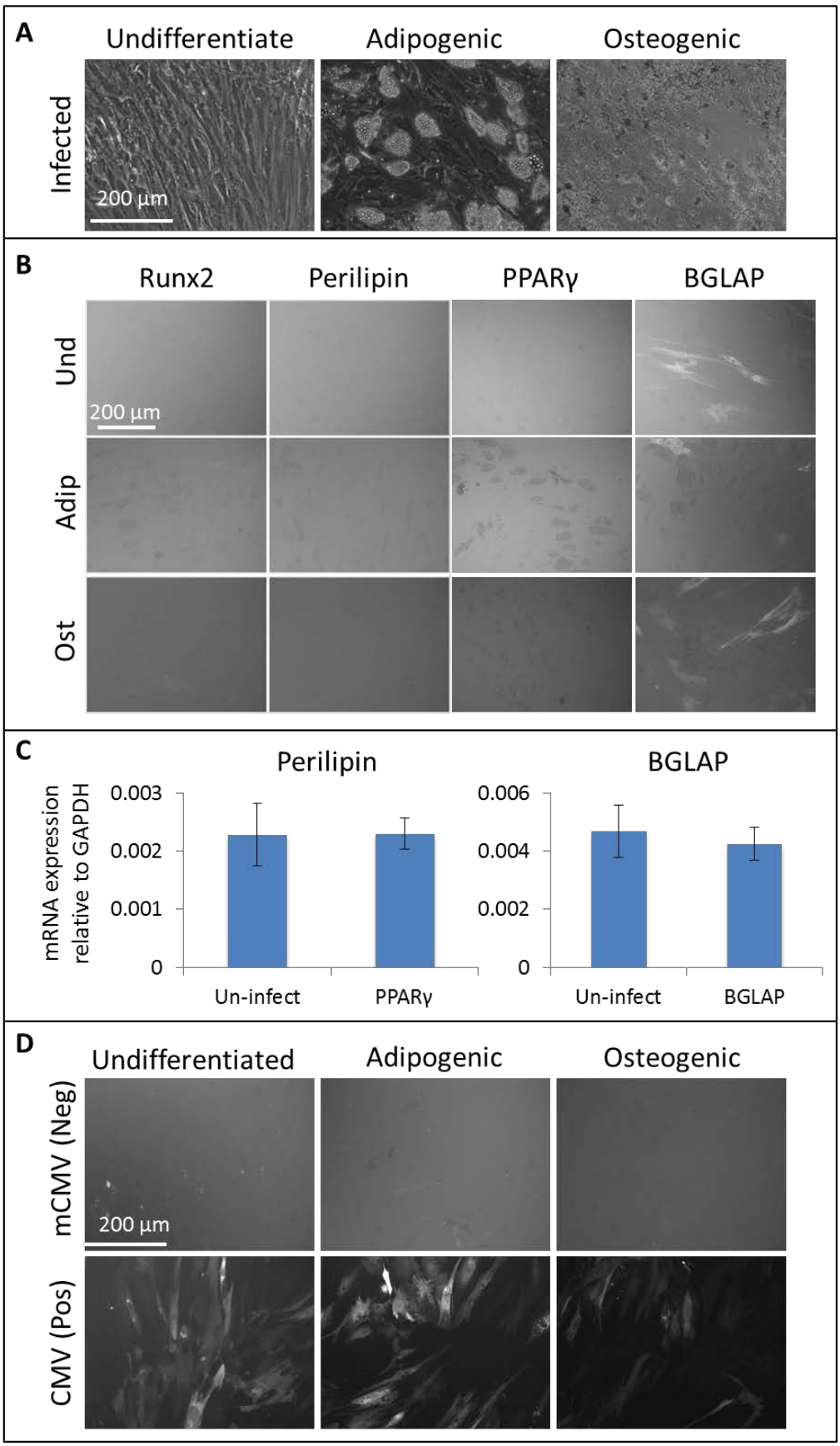
A
Undifferentiate
Adipogenic
Osteogenic
Infected
200 µm
B
Runx2
Perilipin
PPARγ
BGLAP
Und
Adip
Ost
200 µm
C
Perilipin
BGLAP
mRNA expression relative to GAPDH
0.003
0.002
0.001
0
Un-infect
PPARγ
0.006
0.004
0.002
0
Un-infect
BGLAP
D
Undifferentiated
Adipogenic
Osteogenic
mCMV (Neg)
CMV (Pos)
200 µm

Figure II-2: Osteogenic and adipogenic FP reporters do not match mRNA expression. (A) Phase contrast images of lentivirus infected hMSCs cultured in control undifferentiated, adipogenic, or osteogenic differentiation media for 21 days have similar lipid accumulation and mineral deposition as un-infected cells (compare to figure 1A). **(B)** Fluorescent images were taken of hMSCs infected with indicated FP reporter virus at MOI = 10 and cultured in undifferentiated control, adipogenic, or osteogenic media. Runx2 and perilipin images were acquired on day 10 of culture and PPAR γ and BGLAP images were acquired on day 14. **(C)** mRNA expression levels of the adipogenic marker PPARγ and the osteogenic marker BGLAP in uninfected control and FP reporter infected hMSCs cultured in adipogenic media (PPARγ) or osteogenic media (BGLAP) for 14 days. **(D)** Fluorescent images taken 7 days after infection of hMSCs with negative and positive GFP expression control vectors at MOI = 10.

II.4.3 Increased extracellular potassium decreases hMSC osteogenic differentiation.

Previously, it was shown that extreme depolarization conditions, in which 80 mM potassium was added to the media, inhibited osteogenic differentiation of hMSCs (Sundelacruz et al., 2008). We were next interested to see if inducing a lesser degree of depolarization by culturing hMSCs in lower concentrations of extracellular potassium, also inhibited differentiation, and if certain levels of depolarization were more effective at inhibiting osteogenesis. The effect of increasing extracellular potassium concentrations on V_{mem} was predicted using the Goldman-Hodgkins-Katz equation (Table 1). hMSCs were cultured in differentiation media supplemented with potassium for 3 weeks.

Staining with alizarin red demonstrated decreased mineralization in potassium treated samples (Figure 3). Cells were culture in osteogenic media supplemented with equivalent concentrations of NMDG and no significant difference in calcium content was observed, ruling out effects of osmotic pressure on osteogenic differentiation (Figure 3). Quantification of calcium content revealed a concentration dependent decrease in potassium treated but not NMDG treated cells (Figure 4A-B). The relationship between mineralization and potassium concentration was best characterized with the exponential decay line of best fit $y = 0.3879e^{-0.11x}$ which had an R^2 value of 0.95 (Figure 4C). In addition to a change in mineralization, high potassium also caused a decrease in mRNA expression of ALP but this effect did not correlate with concentration (4E).

Table II-1: Predicated V_{mem} induced by addition of potassium to cell media. Table lists potassium added in addition to 4 mM potassium contained in media.

K^+ added (mM)	Predicted V_{mem} (mV)
0	-68
5	-61
10	-55
15	-51
20	-47
30	-40
40	-35

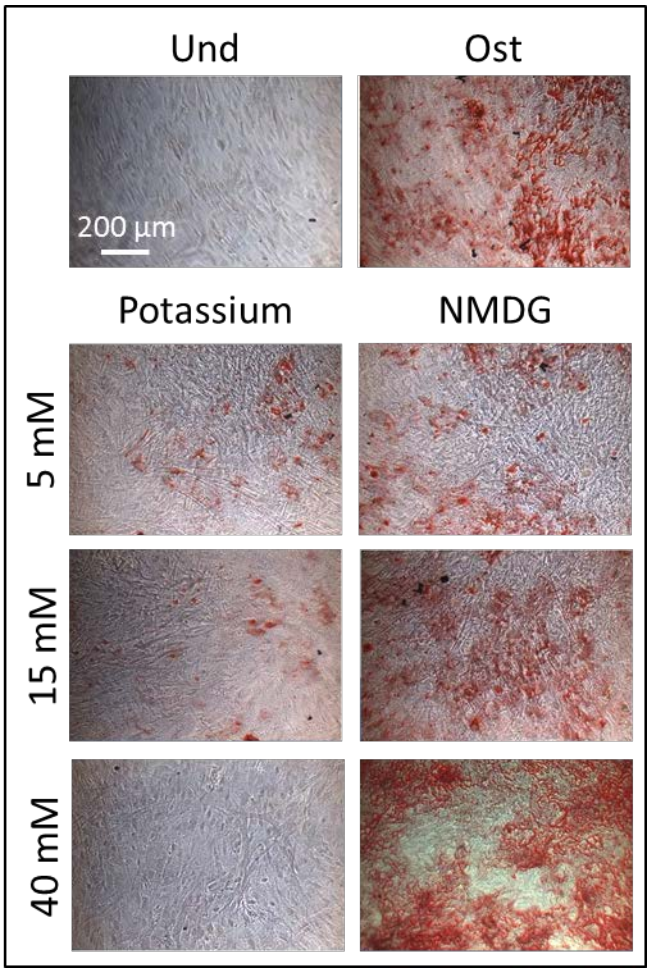

Figure II-3: Increased potassium but not NMDG decreases mineralization in osteogenic differentiated hMSCs. Bright field images of hMSC cultured for 21 days in osteogenic media (Ost) or osteogenic media supplemented with indicated concentration of potassium-gluconate or NMDG as osmolarity control and stained with alizarin red to show mineralization. Und shows undifferentiated cells cultured in control media for comparison.

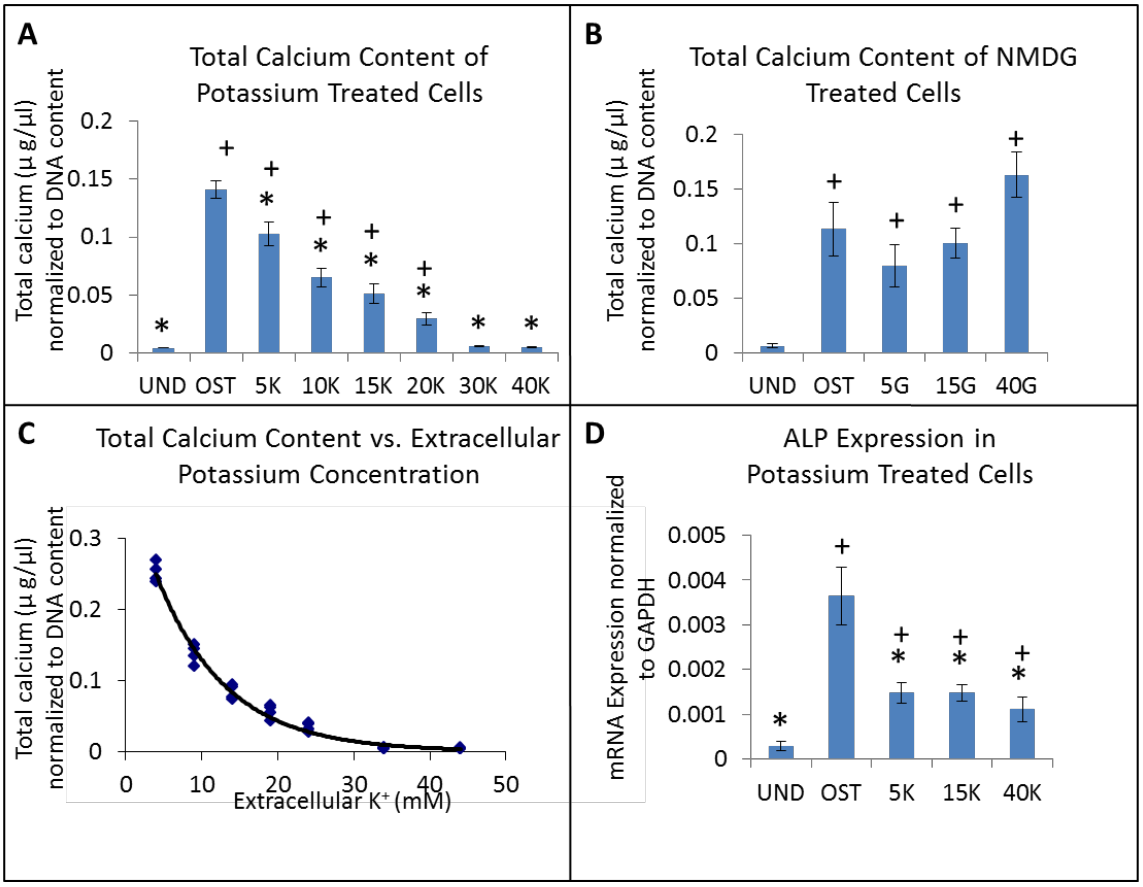

Figure II-4: Extracellular potassium decreases calcium content and ALP Expression in hMSC osteogenic differentiated cells. (A-B) Quantification of total calcium in hMSCs cultures grown for 21 days in undifferentiated control media (Und), osteogenic media (Ost), or osteogenic media supplemented with potassium (A) or NMDG (B) and normalized to DNA content. (C) Total calcium content of potassium treated cells plotted vs extracellular potassium concentration (mM) with exponential decay line of best fit $y = 0.3879e^{-0.11x}$ which had an R^2 value of 0.95. (D) Total RNA was extracted from 14 day osteogenic differentiated hMSCs treated with indicated extracellular potassium

and analyzed for ALP mRNA expression levels by RT-PCR. UND shows cells cultured in undifferentiated control media for comparison. Data points are mean with standard deviation calculated from 4 replicates in a single experiment, A was repeated in 3 independent experiments. + indicates significantly different from Und, * indicates significantly different from Ost (one-way ANOVA, Tukey's post hoc test $p<.05$)

II.4.4 Activation of K_{ATP} Channels Inhibits Osteogenic Differentiation

We were also interested to further investigate our previous finding that hyperpolarization increased osteogenic differentiation to determine whether a specific range of V_{mem} was particularly effective at increasing differentiation. In the previous study, diazoxide and pinacidil were used to activate K_{ATP} and hyperpolarize hMSCs resulting in increased osteogenic differentiation (Sundelacruz et al., 2008). We first wanted to detect which K_{ATP} members were expressed in undifferentiated and osteogenic hMSCs. Primers were designed to specifically amplify regions of the coding sequence of the two K_{ATP} members Kir6.1 and Kir6.2. PCR was used to detect Kir6.1 and Kir6.2 transcripts in cDNA reverse transcribed from total RNA isolated from undifferentiated and 3 week osteogenic differentiated hMSCs. Bands of

the expected PCR product size were observed for both channels in undifferentiated and osteogenic differentiated samples (Figure 5A). We next wanted to compare the increase in osteogenic markers of hMSCs hyperpolarized with diazoxide and pinicidil to hMSCs hyperpolarized by different methods to identify modulations to V_{mem} that maximized osteogenic differentiation. However, hMSCs cultured in osteogenic media with 10 μM diazoxide or 10 μM pinacidil for two weeks had ALP staining that resembled undifferentiated control more than osteogenic control cells (Figure 5B). mRNA expression of the bone differentiation markers Runx2, ALP, and BSP were also more similar to undifferentiated than osteogenic cells (Figure 5C).

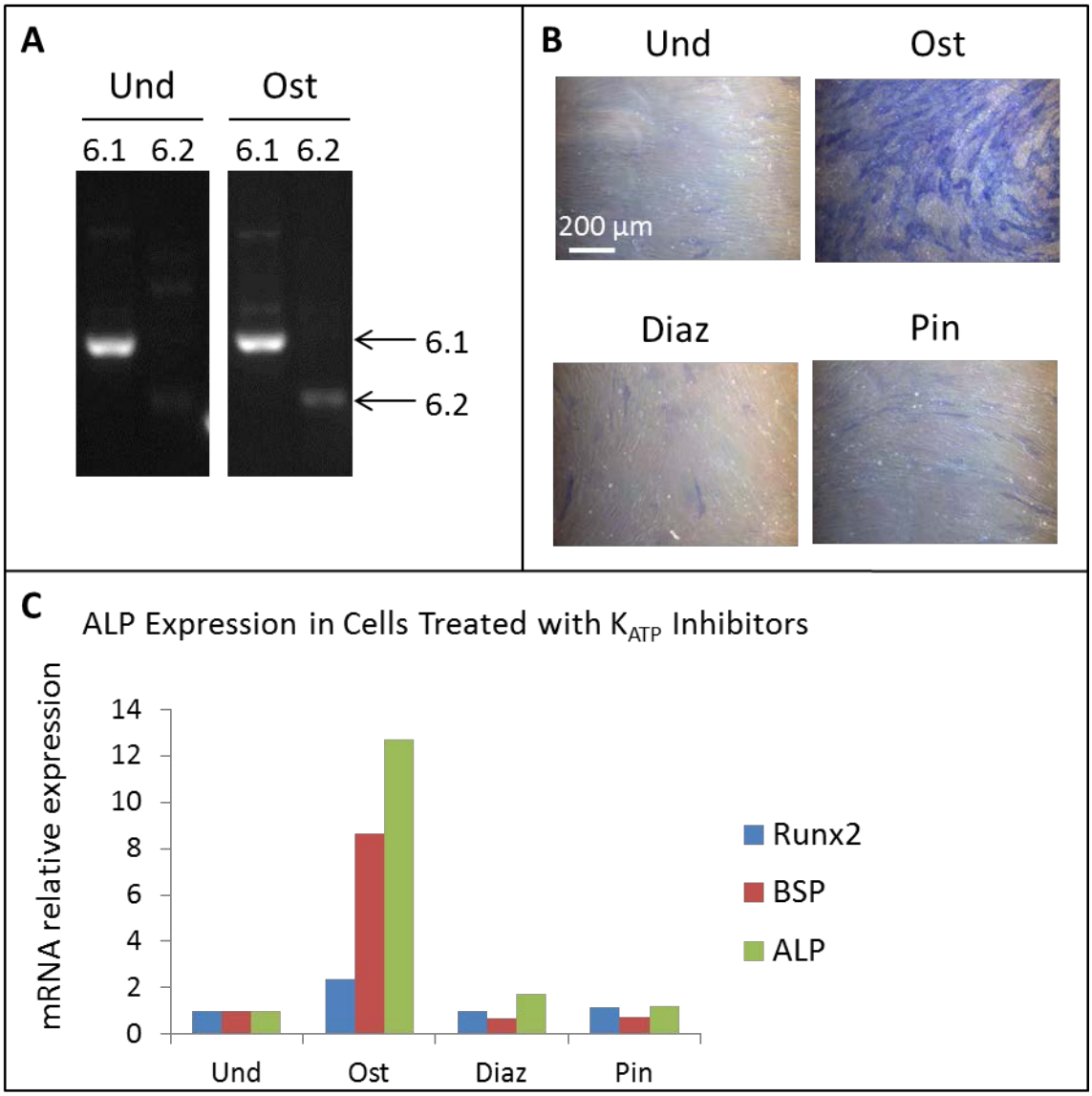

Figure II-5: KATP activators decrease osteogenic differentiation of hMSCs. (A) Expression of the two K_{ATP} family members Kir6.1 and Kir6.2 in undifferentiated (Und) and 3 week osteogenic differentiated (Ost) hMSCs. Total RNA was isolated and converted to cDNA in a reverse transcriptase reaction. cDNA was used as template in a PCR reaction with primers specific to coding regions of each channel and the resulting products were separated on a DNA gel. Arrows mark expected DNA band for Kir6.1 and Kir6.2. (B) Bright field images of hMSCs cultured in undifferentiated control (Und), osteogenic control (Ost), or osteogenic media supplemented with 10 µM diazoxide (Diaz) or 10 µM pinacidil (Pin) for 14 days and stained for ALP. (C) mRNA expression levels normalized to undifferentiated control using

GAPDH as a housekeeping gene of bone markers in total RNA isolated from cells cultured for 21 days, same conditions as C. Data points are mean expression from four replicates.

II.4.5 The TRPV1 antagonist capsazepine induces donor-specific increase in mineralization of osteogenic differentiated hMSCs

TRPV1 is a non-specific cation channel and is primarily responsible for maintaining body temperature. Interestingly, activation of TRPV1 has been reported to increase mineralization of primary osteoblasts (Lee et al., 2010). Activation of TRPV1 allows influx of sodium and calcium ions and thus induces depolarization. TRPV1 provided an alternative means to modulate V_{mem} and we wanted to investigate whether altering V_{mem} via TRPV1 induced similar responses as the methods of V_{mem} modulation discussed above. Furthermore, We wanted to determine whether the increased mineralization induced by TRPV1 activity was dependent on the change in V_{mem}.

We first wanted to determine if TRPV1 activation increased mineralization in hMSCs. To more closely mimic the study by Lee et al., which was performed with primary osteoblasts, hMSCs were differentiated in osteogenic media for 3 weeks prior to experiments. Osteogenic markers were then assessed after 3 weeks of culture in

osteogenic media supplemented with the TRPV1 agonist capsaicin (Cpn) or the antagonist capsazepine (CapZ) (Figure 6A). Contrary to expectations, cells treated for 3 weeks with CapZ had a dramatic increase in calcium but not ALP staining while Cpn treated cells were similar to controls (Figure 6B). These results were confirmed by ALP enzyme activity and calcium accumulation quantitative assays in which CapZ treated cells had significantly increased total calcium as compared to osteogenic control (6C).

Total RNA was isolated from the same samples and mRNA levels of osteogenic markers were analyzed with quantitative RT-PCR. As compared to osteogenic control, CapZ treated cells had significantly less ALP and BSP expression and significantly higher osteocalcin expression. Cpn treated cell expression levels were similar to osteogenic control for all markers.

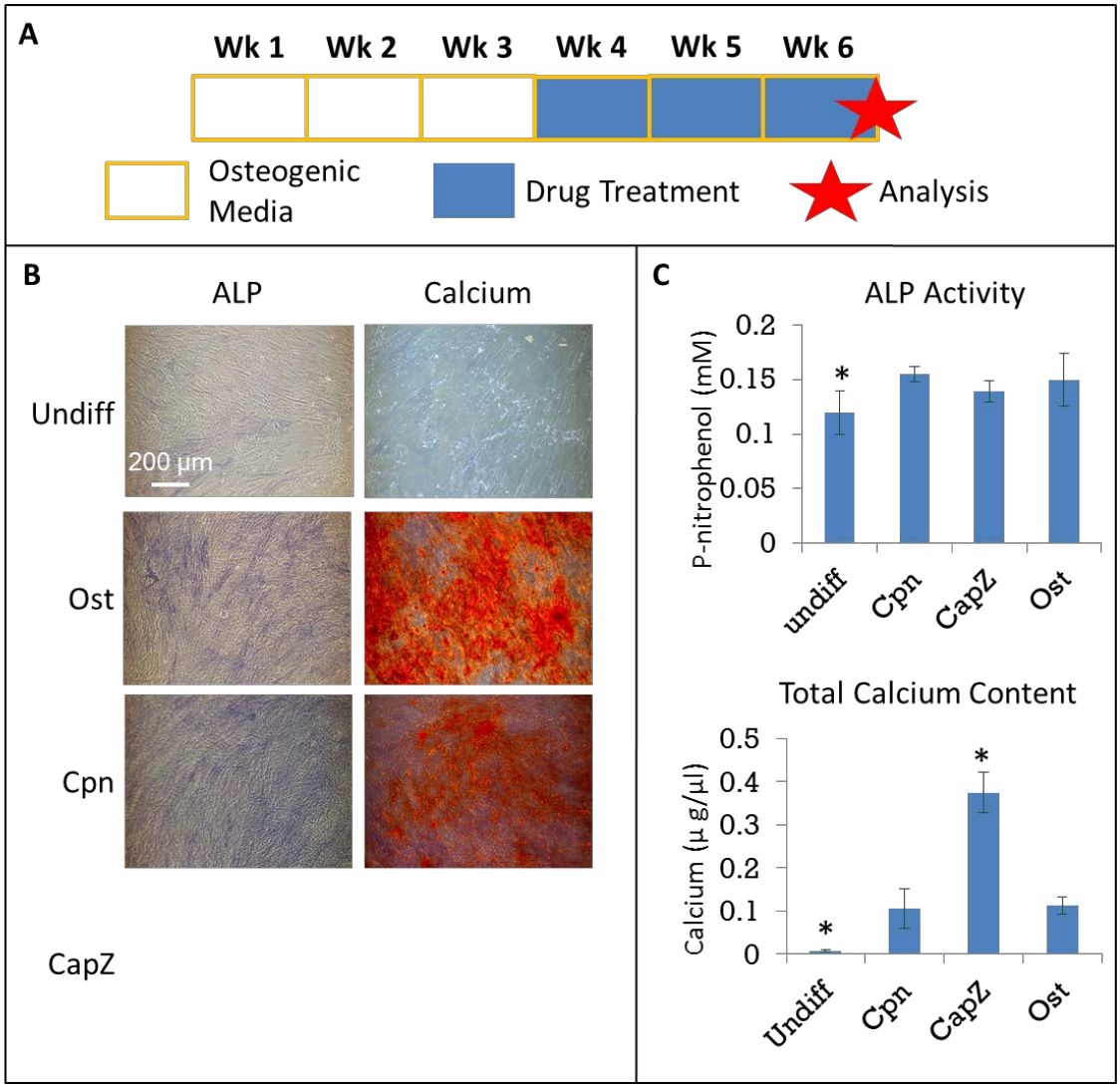

Figure II-6: CapZ treatment of Donor 1 osteogenic differentiated hMSCs increases mineralization. (A) Schematic of culture conditions. hMSCs were first cultured in osteogenic media for 3 weeks. Cells were then cultured in osteogenic media (Ost) or osteogenic media supplemented with 10 µM capsaicin (Cpn) or 10 µM capsazepine (CapZ) for an additional 3 weeks. Undifferentiated controls (Undiff) were cultured in control media for 6 weeks. All analysis was performed on samples collected at the end of 6 weeks of culture. (B) Bright field images of ALP and calcium staining. (C) Quantification of ALP activity and total calcium content. Data are mean and standard deviation of 6 replicates from a single experiment.* indicates significantly different from Ost (one-way ANOVA, Tukey's post hoc test $p<.05$)

We wanted to assess if Cpn or CapZ treatment induced cell toxicity. hMSCs were cultured for 5 days in the presence of 1, 10, and 50 μM Cpn or CapZ and analyzed for Ki67 and TUNEL staining to mark proliferating and apoptotic cells respectively. Cpn treated cells were similar to untreated control at all concentrations, while CapZ 10 μM and 50 μM treatment significantly decreased the percentage of Ki67 positive cells (Figure 7A). None of the conditions, including control, had any apoptotic cells as determined by TUNEL staining (Figure 7B).

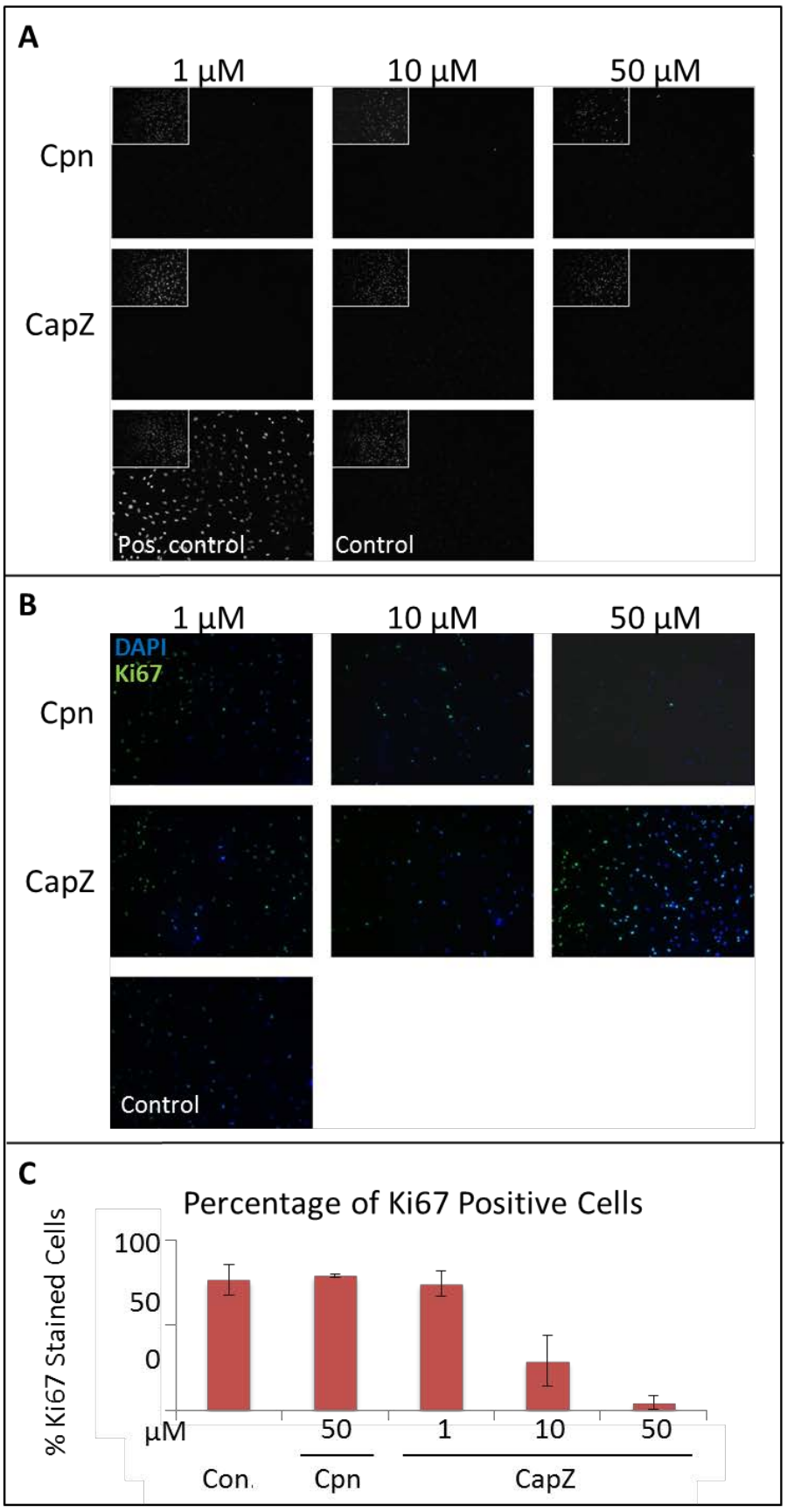
A
1 µM
10 µM
50 µM
Cpn
CapZ
Pos. control
Control
B
1 µM
10 µM
50 µM
DAPI
Ki67
Cpn
CapZ
Control
C
Percentage of Ki67 Positive Cells
% Ki67 Stained Cells
100
50
0
µM
50
1
10
50
Con.
Cpn
CapZ

Figure II-7: CapZ but not Cpn treatment decreases proliferating cells. (A) TUNEL staining of hMSCs treated for 5 days in the indicated concentration of Cpn or CapZ. Positive control cells were treated with DNAse I, control cells were left untreated. **(B)** Immunofluorescent staining with anti-Ki67 of samples from A counterstained with DAPI. **(C)** The number of Ki67 positive cells was counted in 4 fields of view of 3 replicates for each condition. Data presented as mean with standard deviation, * indicates significantly different from control (one-way ANOVA, Tukey's post hoc test $p<.05$).

We wanted to ensure that the increased mineralization induced by CapZ treatment was not a donor specific effect and repeated experiments using hMSCs isolated from a second donor. The control osteogenic differentiated cells from donor 2 had increased mineralization as compared to cells from donor 1 (Figure 8A). However, there was no significant increase in calcium content of CapZ treated cells as compared to osteogenic control. It is possible that the higher overall mineralization masked any effect of CapZ treatment. To test the effect of CapZ treatment before accumulation of significant mineralization, cells from donor 2 were treated with CapZ during the first three weeks of growth in osteogenic media and analyzed for mineralization (Figure 9A). There was no significant difference in calcium accumulation or ALP activity between cells treated during the first three weeks of culture with CapZ and osteogenic control (9B). These results suggest the effect of CapZ treatment is not reproducible

between hMSCs from different donors and therefore TRPV1 modulation to study differentiation is of questionable utility.

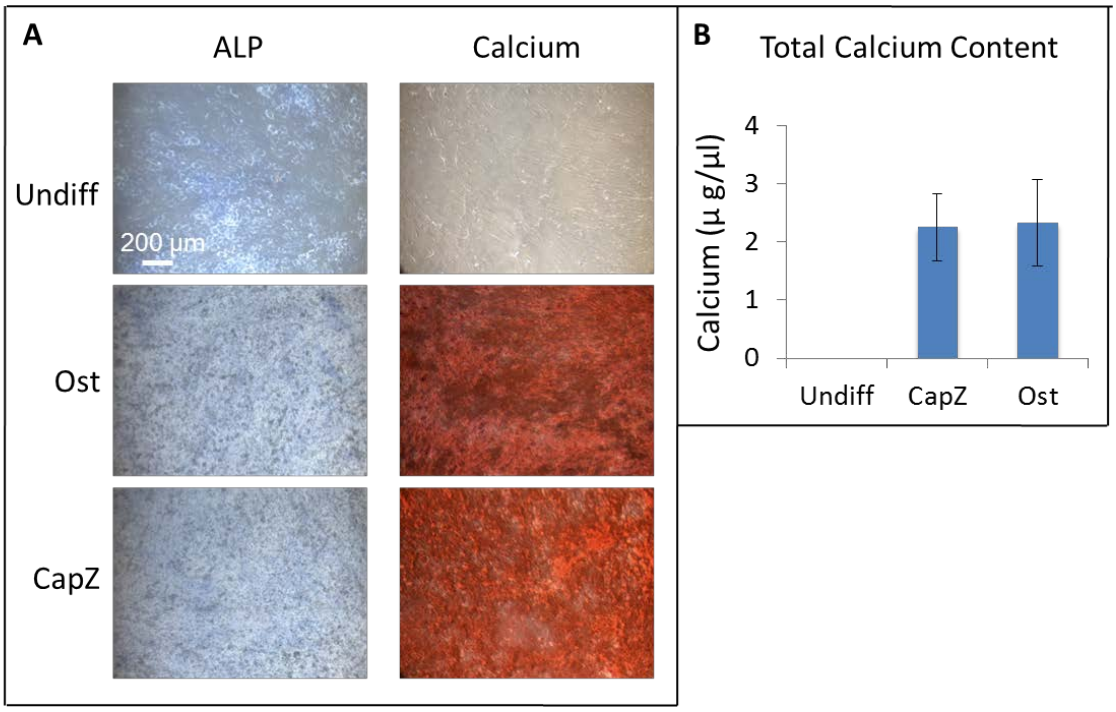

Figure II-8: CapZ treatment of osteogenic differentiated hMSCs from donor 2 did not increase mineralization. hMSCs from donor 2 were first cultured in osteogenic media for 3 weeks. Cells were then cultured in osteogenic media (Ost) or osteogenic media supplemented with 10 µM capsazepine (CapZ) for an additional 3 weeks. Undifferentiated controls (Undiff) were cultured in control media for 6 weeks. **(A)** Bright field images of ALP and calcium staining after 6 weeks of culture. **(B)** Quantification of total calcium content. Data are mean and standard deviation of 6 replicates from a single experiment. No significant difference between CapZ and Ost samples (one-way ANOVA, Tukey's post hoc test $p<.05$).

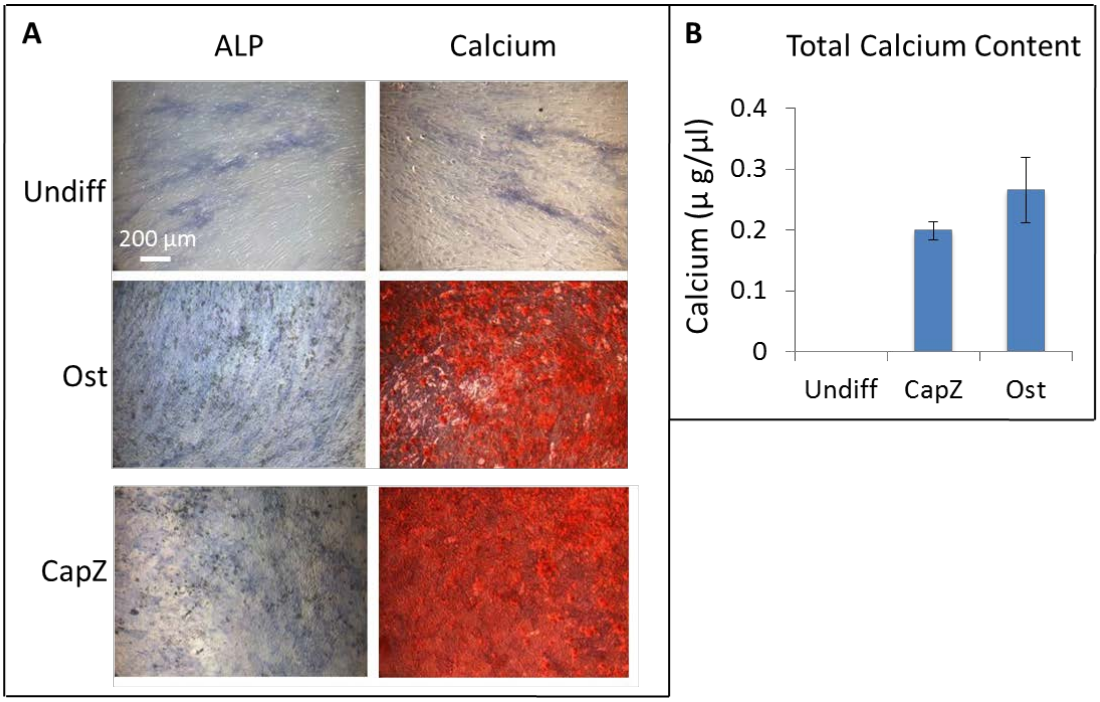

Figure II-9: CapZ treatment did not increase mineralization during osteogenic differentiation of hMSCs from donor 2. (A) hMSCs from donor 2 cultured in osteogenic media (Ost) or osteogenic media supplemented with 10 µM capsazepine (CapZ) for 3 weeks and stained for ALP and calcium. Undifferentiated controls (Undiff) were cultured in control media for 3 weeks. **(B)** Quantification of total calcium content. Data are mean and standard deviation of 6 replicates from a single experiment. No significant difference between CapZ and Ost samples (one-way ANOVA, Tukey's post hoc test $p<.05$).

II.4.6 Ion channel expression to modulate hMSC V_{mem}

Over-expression of ion channels is an additional mechanism of modulating V_{mem}. GlyR, which has low endogenous expression, was chosen to be highly over-expressed in order to enable both depolarization and hyperpolarization by modulation of extracellular

chloride concentration. GlyR has high endogenous activity because it is activated by glycine in the media. It is expected to be slightly depolarizing in standard 110 mM extracellular chloride and the depolarization can be increased by culturing cells in low extracellular chloride.

GlyR was expressed in hMSCs by infection with lentivirus and over-expression was confirmed by mRNA quantification and western blot (data not shown). We first wanted to determine if GlyR expression or culture in low chloride conditions caused cell toxicity. hMSCs infected with GlyR lentivirus or GFP control were cultured for 14 days in 15 mM to 110 mM extracellular chloride with or without glycine. Control cells had a similar morphology in all culture conditions (10A-B). GlyR expressing cells grown in standard 110 mM chloride developed large intracellular vesicles in the presence but not absence of glycine (10A-B). Fewer vesicles were observed in 70 mM chloride with no vesicles at lower chloride concentrations. GlyR expressing cells had significantly reduced metabolic activity as measured by alamar blue reduction capacity in comparison to control in all conditions (10C). Both control and GlyR cells exhibited a concentration dependent decrease in reduction capacity in low chloride conditions. The reduction capacity was not affected by the presence or absence of glycine. Quantitative cell number analysis is needed to determine if

decreased metabolic readout is from a decreased metabolic rate or individual cells or reduced proliferation.

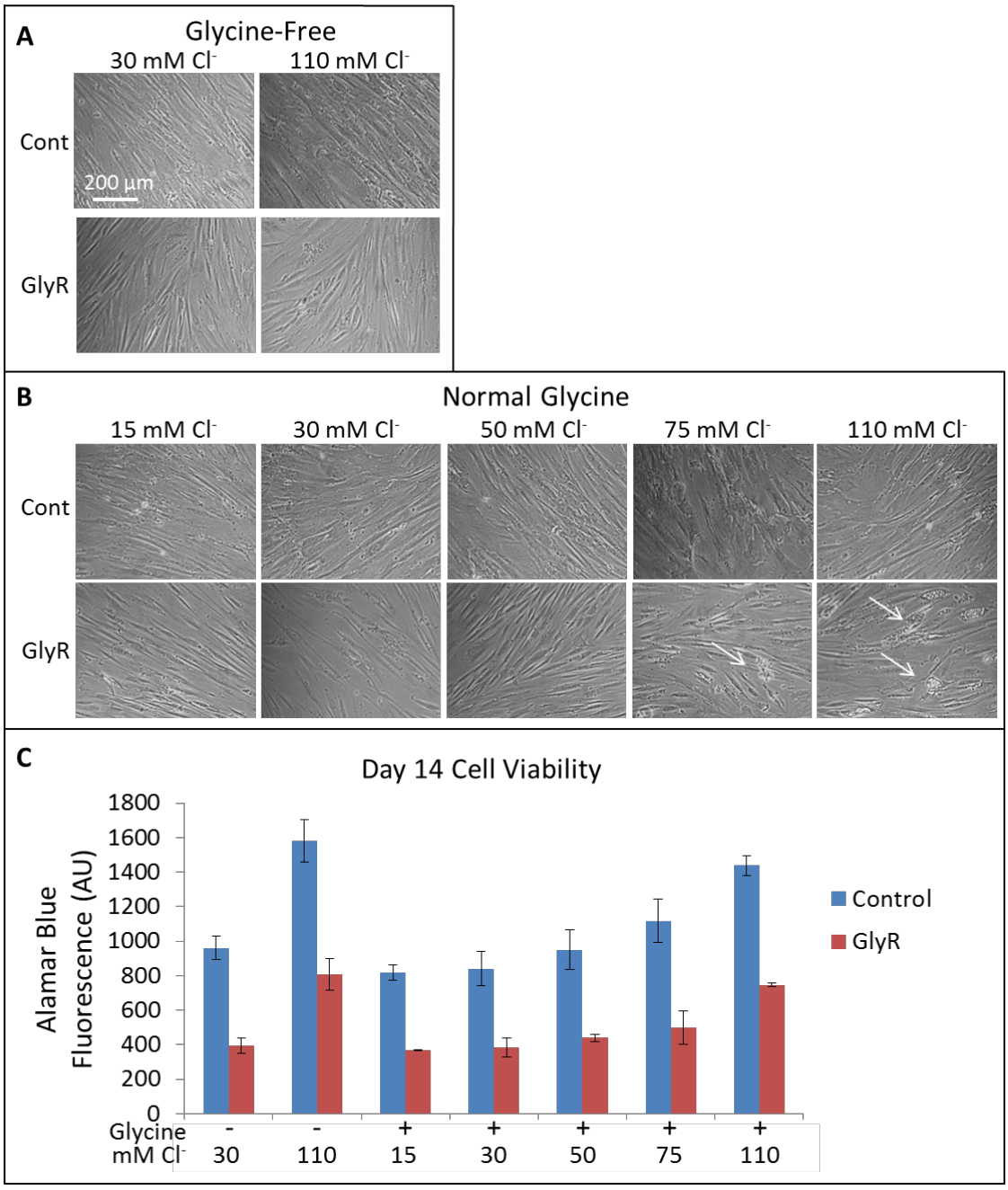

Figure II-10: hMSCs expressing GlyR and grown in low extracellular chloride have decreased viability. (A-B) Phase contrast images of hMSCs infected with control or GlyR vector and cultured for 14 days in indicated extracellular chloride concentration in

glycine-free (A) or normal media with 0.4 mM glycine (B). Arrows mark cells with vesicles. **(C)** Alamar blue reduction of cells from A-B incubated in reagent for 1 hr. Data are mean and standard deviation of 6 replicates from a single experiment. Control and GlyR are significantly different for every condition (one-way ANOVA, Tukey's post hoc test $p<.05$).

Attempts to use patch-clamping and voltage-sensitive fluorescent dyes to assess the change in V_{mem} induced by GlyR expression or changes to extracellular ion concentrations proved unsuccessful.

II.5 Analysis

II.5.1 Effect of V_{mem} Modulation on Osteogenic Differentiation

Previously, it was reported that depolarization inhibited and hyperpolarization enhanced osteogenic differentiation of hMSCs. We wanted to investigate if specific ranges of V_{mem} were more effective at inhibition or enhancement of differentiation to specific lineages. Increasing extracellular potassium is predicted to depolarize the V_{mem}. Treating hMSCs with increased extracellular potassium induced a concentration dependent decrease in mineralization. This may suggest that inhibition of osteogenic differentiation correlates with depolarization and that maximum inhibition occurs with maximum

depolarization. However, while high potassium decreased ALP expression, the effect was similar across all potassium treatments. Further characterization of osteogenic differentiation is needed to confirm that maximum inhibition occurs with maximum depolarization. Alternative methods of depolarization also need to be investigated in order to assess whether the decreased osteogenic differentiation is dependent on V_{mem} and not another aspect of high extracellular potassium.

In contrast to what was previously reported, hMSCs cultured in osteogenic differentiation media with K_{ATP} agonists had a significant decrease in early and late osteogenic markers Runx2, ALP, and BSP as well as decreased ALP staining. A possible explanation for the discrepancy is variability across donors. Primary hMSCs are derived from individual donors and harbor characteristics specific to the individual as well as attributes that may have been induced during the cell isolation process. It is therefore critical to repeat findings in cells isolated from multiple donors.

A similar issue with donor variability was observed with hMSC response to TRPV1 activation and inhibition. hMSCs from donor 1 pre-differentiated down the osteogenic lineage and treated with the TRPV1 antagonist CapZ had significantly increased mineralization and osteocalcin gene expression. Other markers of osteogenic

differentiation, ALP activity and BSP and ALP gene expression, were not increased. These results suggest treatment with CapZ may induce mineralization without inducing the entire osteogenic differentiation pathway in donor 1 hMSCs. However, CapZ treatment of cells isolated from donor 2 did not have increased mineralization or osteocalcin expression. Interestingly, osteogenic controls for donor 2 had increased mineralization compared to donor 1. Little is known about the factors that cause donor to donor variability of hMSCs differentiation from age and gender matched donors. One contributing factor may be culture differences during hMSC isolation. hMSCs are highly sensitive to conditions including confluence and oxygen levels and it is possible that unavoidable differences during isolation, such as increased oxygen levels caused by opening the incubator door more frequently, might affect cell behavior. These results highlight the importance of performing experiments in multiple donors to confirm important findings.

High chloride permeability in low extracellular chloride conditions provides an alternative method to depolarize V_{mem} independently of potassium. The chloride channel GlyR was expressed in hMSCs and cells were cultured in low chloride with or without the GlyR agonist glycine. GlyR cells had significantly decreased reduction of alamar blue reagent as compared to control in all chloride conditions. Furthermore,

GlyR expressing cells cultured in normal 110 mM chloride with glycine developed large vesicles. These results suggest the GlyR channel is functional but also suggest culture in low chloride and GlyR expression is detrimental to cell viability and therefore do not provide optimal tools to study V_{mem} effects on differentiation.

hMSCs are a challenging cell type to study due to high variability in behavioral response and also high sensitivity to culture conditions. In order to combat these issues, high throughput methods to analyze many replicates from multiple donors are needed. Investigation of modulation to V_{mem} also requires quantitative measurement of V_{mem}. In this study, the Goldman-Hodgkins-Katz equation was used to predict V_{mem} but this equation is a simplification of actual ion dynamics and may not be accurate for all cell types. Further studies using hMSCs derived from multiple donors and accurate quantification of the V_{mem} are needed before concrete conclusions about the relationship between V_{mem} and differentiation of hMSCs can be determined. However, the results of this study do not support V_{mem} as an instructor of differentiation and suggest V_{mem} modulation is unlikely to be a viable clinical strategy to induce differentiation for tissue engineering or regeneration applications.

II.5.2 Fluorescent Protein Reporters to Monitor Adipogenic and Osteogenic Differentiation

Because the fluorescent reporter constructs tested for this study did not reflect endogenous expression levels, the high-throughput non-destructive method of differentiation screening could not be used. Runx2 is a transcription factor that is active during early and mid-osteogenic differentiation and induces expression of many bone markers. However, the Runx2 activity reporter construct did not give a fluorescent signal in control, osteogenic, or adipogenic differentiation media. The adipogenic reporters perilipin, a late differentiation marker, and PPARy, an important transcription factor active throughout differentiation, also did not show any fluorescence in any of the media conditions. BGLAP is a marker of late bone differentiation and was expected to have high expression in osteogenic media at late time points, although this was not confirmed. However, fluorescence from the BGLAP reporter was equal in osteogenic and undifferentiated cells and was also observed in adipogenic cells containing fat droplets. The adipogenic and osteogenic pathways negatively regulate one another making it unlikely that a cell containing lipid droplets would also be expressing high levels of BGLAP.

Positive control vectors induced robust GFP expression demonstrating virus successfully infected cells and integrated within active areas of the genome in a significant percentage of cells. Thus, the results indicate the target-specific DNA sequence driving fluorescent protein expression for each reporter is either not the appropriate promoter for the differentiation marker, or not the correct response element sequence for the transcription factor. Modification of the target sequence is needed for fluorescent protein expression to accurately correlate with marker expression and transcription factor activity. Due to the failure of these constructs, traditional means of monitoring differentiation including assaying for ALP activity, mineralization, and mRNA transcript levels were used to assess differentiation status.

Chapter III: High Extracellular Potassium During 3D Embedded Matrigel Culture of Spontaneously Immortalized Breast Epithelial Cell Line Induces Branched Morphology and Increased Proliferation

III.1 Abstract

Potassium currents are altered in cancer and may be partially responsible for cancer onset and progression. In this study, a breast epithelial cell line MCF-10A was cultured in high potassium media to decrease potassium efflux. Cells grown in 3D had a striking change in morphology with a concentration dependent increase in branched morphology. The structures had irregular borders and cellular projections reminiscent of invasive cells. After 14 days in 3D culture a higher percentage of cells grown in high potassium were proliferating, suggesting the cells may not be responsive to growth inhibitory signaling. These results suggest changes in potassium dynamics are sufficient to induce malignant phenotypes. A mechanistic screen failed to identify signaling pathways involved in the altered morphology. The mechanism may be related to potassium currents specifically, possible changes in the matrix stiffness, or to depolarization of the membrane potential. Further studies are needed to distinguish between these potential mechanisms. Investigation of high extracellular potassium during 3D matrigel culture in additional non-cancerous breast epithelial cell lines is needed to confirm the phenotype seen in MCF-10A is representative of healthy mammary epithelial cells.

III.2 Rationale

Bioelectric properties are important regulators of many cell behaviors associated with cancer including proliferation, migration, and differentiation. Cancer cells often have increased potassium currents as compared to healthy cells and expression of certain potassium channels correlates with cancer aggression. However, the role of potassium currents in cancer progression is poorly understood. Increased potassium conductance is thought to increase the speed at which cells are able to proliferate and migrate. It remains unknown whether potassium currents are also involved in signaling changes that cause the loss of organization and uncontrolled proliferation found in cancer. The purpose of this study was to investigate how changes in the dynamics of potassium flux affect cell response to regulatory signaling involved in growth inhibition and apical basal cell polarity.

Healthy mammary glands contain highly organized breast epithelial cell ductal and acinar structures. The epithelial cells surround a hollow lumen and are polarized with differential protein localization to the apical and basal surfaces. The cells maintain tight junctions with one another and specific attachments to the basement membrane. Disruption of the organized structure is found early in carcinogenesis

and is thought to contribute to loss of regulatory mechanisms including those involved in proliferation.

Formation of breast epithelial structures and loss of organization associated with cancer can be modeled *in vitro* by culturing breast epithelial cells within a basement membrane protein gel (Debnath et al., 2002). The spontaneously immortalized non-tumorigenic breast epithelial cell line MCF-10A form growth arrested spheroids with hollow lumens and appropriate expression of polarization markers when cultured in the extracellular protein gel matrigel. Activation of oncogenic signaling pathways such as receptor tyrosine-protein kinase erbB-2 causes changes in spheroid morphology with filling of the inner lumen (Debnath et al., 2003). Induced expression of oncogenes also causes loss of apical-basal polarity. Differences in spheroid morphology are sometimes detected in cells that have no significant difference in proliferation or migration in 2D making the spheroid assay a more sensitive assay for early carcinogenesis.

To test the effect of modulating potassium current on early cancer behaviors, cells were cultured in high potassium media which both decreases the flow of potassium out of cells and depolarizes the V_{mem}. We hypothesized that disrupting normal potassium flux would cause deregulation of potassium sensitive signaling and lead to aberrations in acinar structures.

III.3 Methods

Cell Cultivation – MCF-10A cells (ATCC) and mammary fibroblasts (Lonza) were maintained and propagated according to ATCC and Lonza recommendations respectively.

MCF-10A Spheroid Formation Assay- For spheroid formation assays, cells were cultured in 90% matrigel (BD Bioscience) in the upper chamber of transwells (BD Biosciences) with a 12 mm diameter and 0.4 μm pores. Transwells were coated with 150 μL of acellular 90% matrigel diluted in PBS and incubated for 30 minutes at 37° C to allow the solution to gel. MCF-10A cells were diluted to 2.5 x 10^5 cells/mL in 90% matrigel and 400 μL were added on top of the coated transwells. For co-culture experiments, mammary fibroblasts were diluted to 1.25 x 10^5 cells/mL in the matrigel mixture. Transwells were incubated at 37° C for 1 hr to allow gelation followed by addition of MCF-10A media to the upper and lower chamber. For samples with modulated extracellular ion conditions, the media was changed to media supplemented with potassium-gluconate to increase potassium concentrations or N-methyl-D-glucamine (NMDG) as an osmolarity

control 24 hours after plating. Cells remained in altered ion conditions throughout the durations of culture with media changes every 4 days.

Spheroid Histology - At the end of the culture period, samples were fixed in 10% formalin for 24 hours. For carmine staining, samples were rinsed in PBS 2 x 10 minutes and incubated in carmine stain solution for 24 hours. After removing excess staining solution by washing in PBS, bright field images were acquired using an Olympus IX71 inverted microscope and Olympus DP70 digital camera with associated software. For histological staining and immunofluorescence, samples were embedded in paraffin and sectioned at 5 μm thickness. Sections were stained with hematoxylin and eosin (H&E) following the Cold Springs Harbor protocol and bright field images were acquired as above.

Cell Proliferation – Cells were incubated in altered potassium conditions for 48 hrs and cells were lysed in 0.2% v/v Triton-X, 5 mM $MgCl_2$. Double stranded DNA was quantified with a Quant-iT Picogreen dsDNA assay kit per manufacturer instructions using a SpectraMax M5 (Molecular Devices) plate reader to detect fluorescence.

Cell Toxicity – Culture media from cells incubated in altered potassium conditions for 48 hrs was analyzed for lactate dehydrogenase (LDH)

activity using an LDH cytotoxicity assay kit (Thermo Scientific) according to manufacturer instructions.

Immunofluorescence – Spheroid 5 μm thickness sections were deparaffinized and re-hydrated by incubating in 100% xylene 2 x 4 min, 100% EtOH 2 min, fresh 100% EtOH 3 min, 95% EtOH 1 min, fresh 95% EtOH 1 min, 70% EtOH 1 min, DIH_2O 2 min. Antigen retrieval was performed by incubating in citrate buffer (10 mM citric acid, 0.05% v/v Tween 20, pH 6.0) in a steamer for 20 min. Sections were blocked in 5% goat serum diluted in PBS for 1 hr and incubated in primary antibody overnight at 4° C at the following dilution in 2% goat serum: 1:300 Ki67 (abCam), 1:100 beta-1-integrin (Cell Signaling), 1:25 laminin V (AbCam), 1:100 GM130 (BD Biosciences). Samples were incubated in the appropriate secondary antibody conjugated to alexafluor-488 or alexafluor-594 diluted 1:200 in 2% goat serum for 1 hr. Coverslips were mounted with vectashield containing DAPI (Vector Laboratories) and fluorescent images were acquired on an Eclipse 80i (Nikon) fluorescent microscope equipped with an Orca-ER (Hammamatsu) digital camera and Velocity 6.0.1 software.

TUNEL Staining – Spheroid sections were stained following manufacturer instructions with the Dead End Colorimetric TUNEL Staining kit (Promega). Images were acquired as above.

Statistics – Statistics were calculated with Prism 5 using a two-sample T test or one-way ANOVA with Tukey or Dunnett post-test for significance with alpha = .05.

III.4 Results

III.4.1 Gross Morphology

MCF-10A cells were cultured embedded in matrigel in increasing concentrations of extracellular potassium for 14 days. Extracellular potassium induced a striking concentration dependent change to a more branched and invasive morphology (Figure 1A). Control cells formed round spheroids with well-defined smooth borders. Increasing extracellular potassium by adding 20 mM to 80 mM potassium-gluconate induced an increase in branched, more ductal-like structures. The structures had irregular borders with cell extensions resembling more invasive cell types (Figure 1B). Cells remained in contact with one another and did not migrate away from structural

units as is found for metastatic cells. Culturing cells in media supplemented with equivalent concentrations of NMDG did not induce changes in spheroid morphology indicating the phenotypes are not a result of changes in osmotic pressure.

Structure morphology was assessed throughout the time course of 3D culture. Cell projections formed within 48 hours of 80 mM potassium treatment and persisted throughout the 14 days of culture (Figure 1C). Both control and high potassium samples cultured for 28 days had a similar morphology as 14 day samples (data not shown).

Proliferation and cell toxicity was assessed in 2D after treatment with high potassium for 48 hrs. Cell proliferation was measured by quantifying total DNA from lysed cells. Proliferation of MCF-10A cells was not significantly altered by treatment with 20 mM or 40 mM potassium but was decreased by 32 % with 80 mM and 87 % with 120 mM treatment (Figure 1D). Cell toxicity was measured by quantifying lactate dehydrogenase (LDH) activity in the cell media. LDH is a cytosolic enzyme that is released into the media when there is significant damage to the cell membrane. Thus, quantifying LDH activity in cell media by measuring production of a colored enzymatic product is used as a measure of cell toxicity. Treatment of MCF-10A cells with 20 mM, 40 mM, or 80 mM potassium did not significantly increase LDH activity in comparison to untreated control while

treatment with 120 mM potassium increased LDH activity by 59 %. Further analysis of the spheroid phenotype was performed only with 80 mM potassium where the phenotype was most prominent and toxicity was minimal.

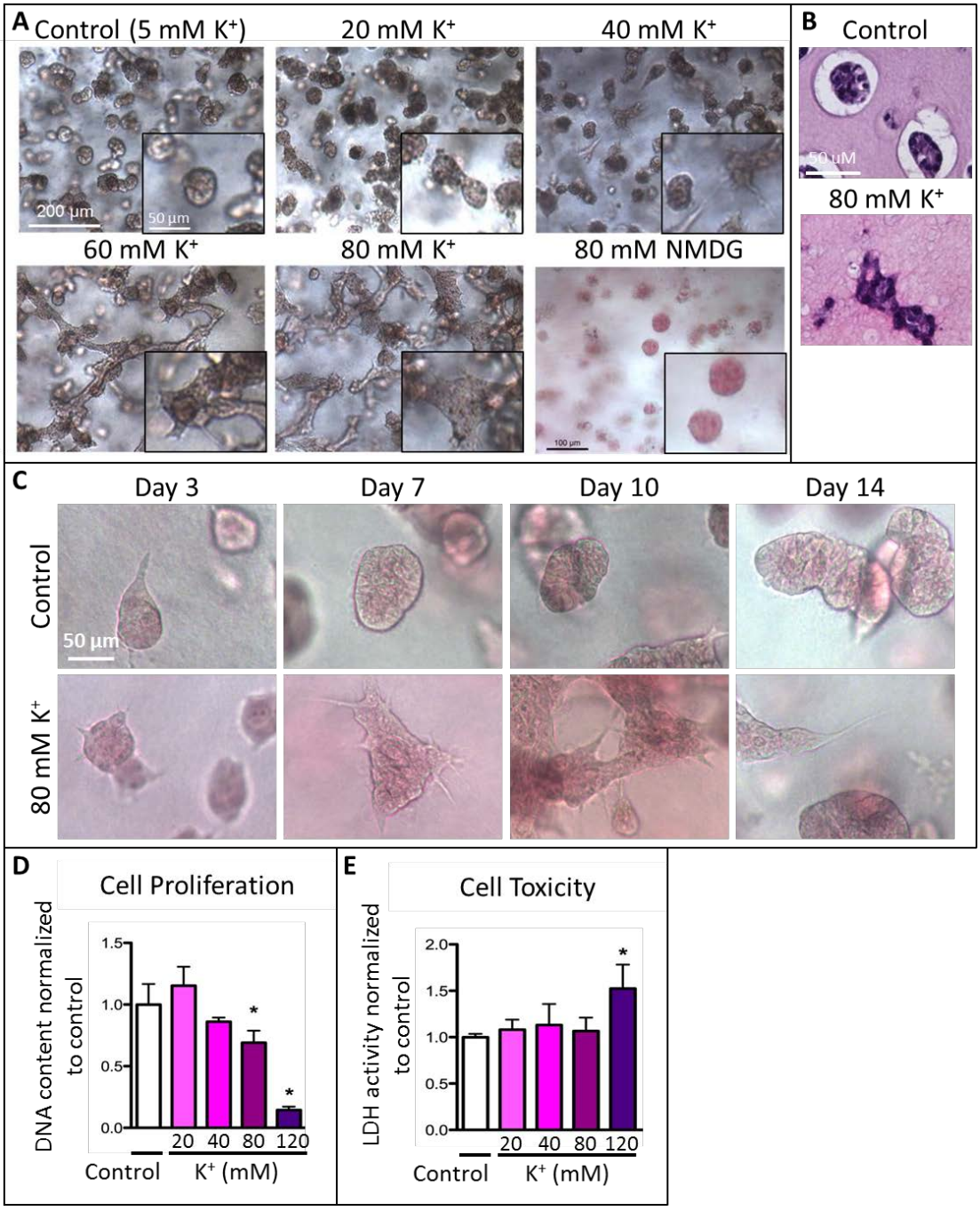

Figure III-1: High potassium induces branching and cell

projections in MCF-10A cells cultured in matrigel. (A) Bright field images of whole mount carmine staining of MCF-10A cells cultured embedded in matrigel for 14 days in control media or media supplemented with indicated concentration of potassium or NMDG. Inset shows higher magnification image. **(B)** Hematoxylin and eosin staining of samples from A. Images are representative of 3 independent experiments. **(C)** Time course images of whole mount carmine stained matrigel cultures. **(D)** Total DNA content as measure of cell number of MCF-10A cells cultured for 48 hrs in control media or media supplemented with indicated concentration of potassium in 2D on tissue culture plastic. **(E)** LDH activity in media from samples in D. Data presented as mean with standard deviation from 3 replicates, * indicates significantly different from control (one-way ANOVA, Dunett's post hoc test $p<.05$).

Co-culture of MCF-10A cells with fibroblasts also induces increased branching. We were interested to compare the high potassium phenotype to the morphology induced by co-culture. We also wanted to investigate whether high potassium had a similar effect in the presence of fibroblasts. MCF-10A cells and primary fibroblasts derived from the mammary gland were cultured embedded in matrigel for 14 days in normal media or media supplemented with 80 mM potassium. Co-culture with fibroblasts induced branching in MCF-10A cells but structures retained clear borders lacking cellular projections (Figure 2A-B). In high potassium treated co-cultures, MCF-10A cells had a similar morphology as high potassium monoculture with both branching and irregular borders with cell projections.

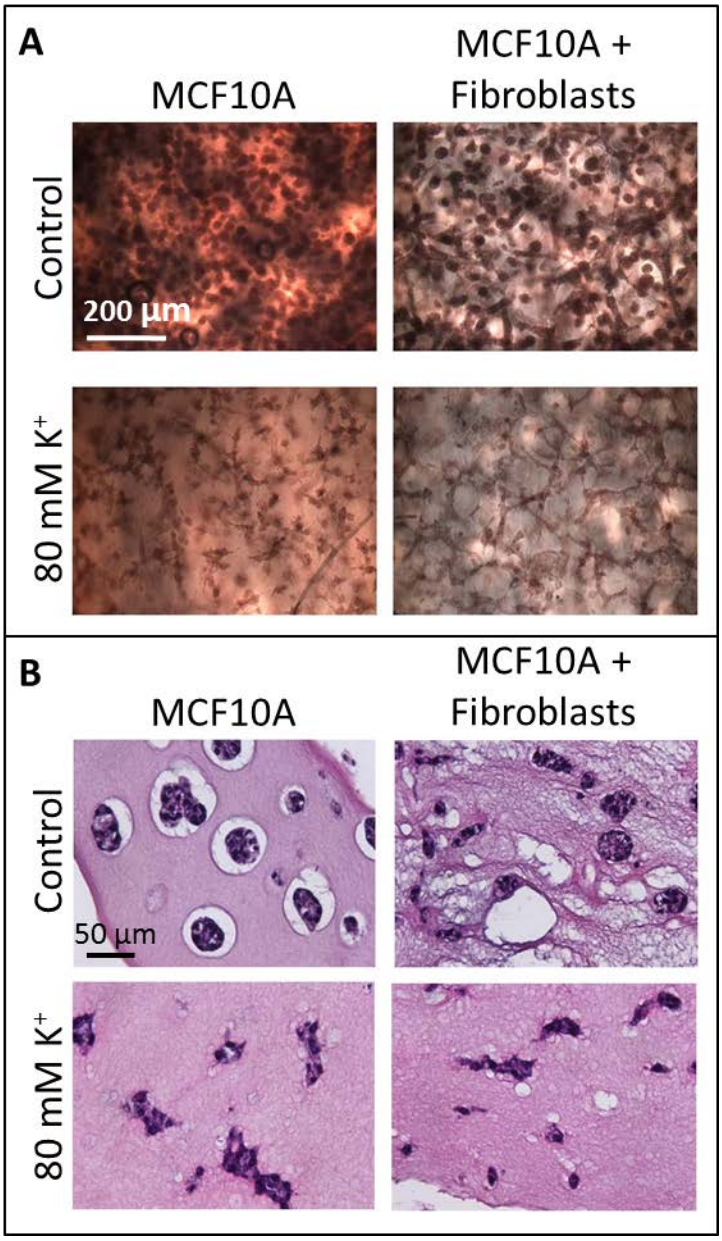

Figure III-2: Fibroblast co-culture induces branching but not cell projections of MCF-10A cells. (A) Bright field images of whole mount carmine staining of MCF-10A cells cultured embedded in matrigel for 14 days with or without mammary fibroblasts in control media or media supplemented with 80 mM potassium. **(B)** Hematoxylin and eosin staining of samples from A.

III.4.2 High Potassium Increased Proliferation and Had No Effect on Apoptosis In Spheroids

In the spheroid assay, MCF-10A cells undergo highly regulated changes in proliferation and apoptosis (Debnath et al., 2003). During the first 6-8 days of culture cells are highly proliferative with little apoptosis. Around day 8, cells in the lumen lacking contact with the basement membrane begin to undergo apoptosis creating a hollow lumen by days 12-14. Around day 10, proliferation of the outer cells begins to decrease so that by day 14 the spheroid is growth arrested with minimal proliferating cells. Cells cultured embedded in matrigel and treated with high potassium media had no significant difference in apoptotic cells as compared to control (Figure 3A). However, there was a significant increase in the percentage of Ki67 positive proliferating cells in potassium treated samples (Figure 3B).

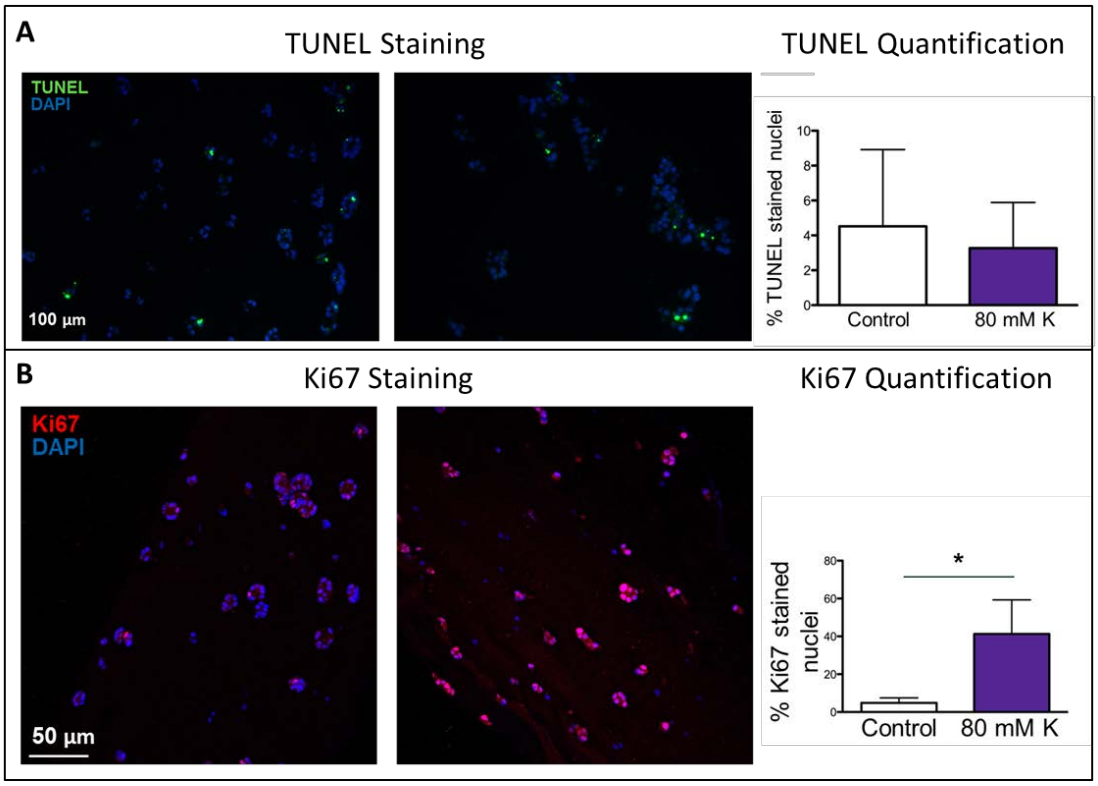

Figure III-3: High Potassium Increases Proliferation But Does Not Alter Apoptosis in MCF-10A Embedded Matrigel Culture. (A) Fluorescent images (left) and quantification (right) of MCF-10A cells cultured embedded in matrigel for 14 days in control media or media supplemented with 80 mM potassium and labeled with TUNEL stain. **(B)** Ki67 labeling (left) and quantification (right) of samples from A. Data presented as mean with standard deviation from 4 fields of view in 2 replicates, * indicates significantly different from control (2-sample T test $p<.05$)

III.4.3 Golgi Matrix Loses Apical Localization in High Potassium Culture

MCF-10A cells grown in matrigel typically show clear apical-basal polarity with basal deposition of the extracellular matrix proteins laminin V and beta-1 integrin and apical localization of the Golgi

matrix. Control MCF-10A cells did not display normal polarity of basal extracellular matrix proteins. Beta-1 integrin was found at the cell membrane of cell-cell junctions and laminin V was expressed throughout the cell membrane (Figure 4). The Golgi matrix, identified by staining of the Golgi matrix protein GM130, was appropriately localized to the apical side of the nucleus in control cells. MCF-10A cells grown in high potassium did not show any clear differences in Beta-1-integrin or laminin V expression. There were changes to Golgi matrix localization, which was no longer as clearly on the apical side of the nucleus (Figure 4 arrows).

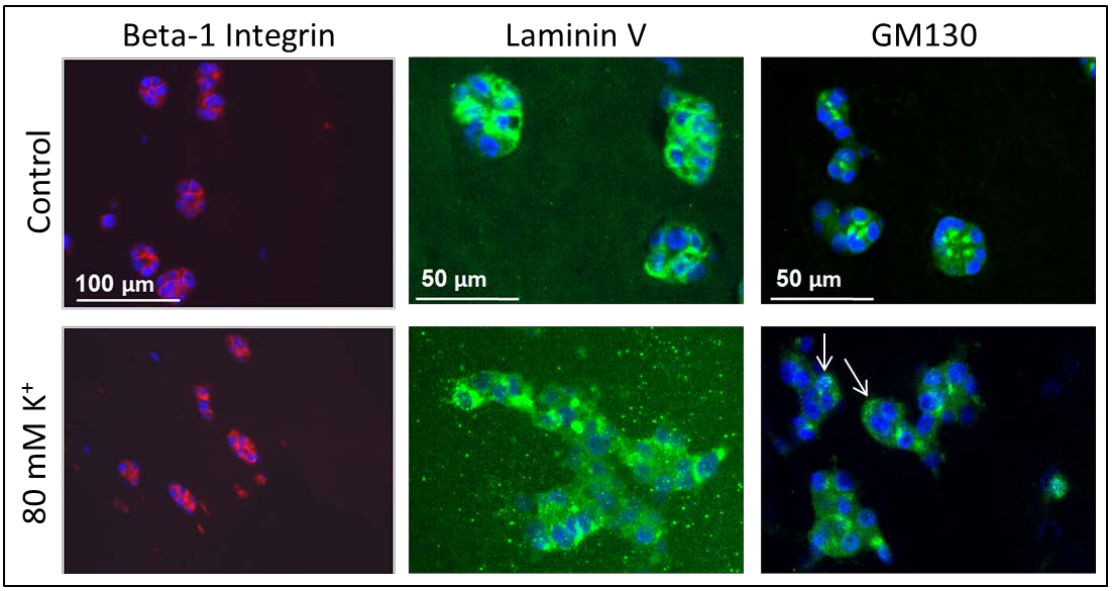

Figure III-4: High Potassium Alters Golgi Matrix But Not Basal Protein Apical-basal Polarity. Fluorescent images of MCF-10A cells cultured embedded in matrigel for 14 days in control media or media supplemented with 80 mM potassium and labeled with indicated

antibodies and DAPI (blue) nuclear stain. Arrows mark cells with GM130 on the basal side of the nucleus.

III.4.4 Mechanistic Screen

A drug screen was performed in order to identify signaling pathways involved in the change in morphology induced by high extracellular potassium. Cells were grown in control or high potassium media and treated with inhibitors of molecules involved in signaling mechanisms previously shown to be responsive to bioelectric signaling. Inhibition of signaling molecules required for the high potassium phenotype were expected to induce a reduction of the branched and invasive phenotype. Treatment of MCF-10A cells with lindane to block gap junctions, fluoxetine to block serotonin transporters, or cadmium chloride to block voltage-gated calcium channels did not affect the morphology of cells grown in control or high potassium conditions (Figure 5). Control and high potassium cells treated with concanamycin a to inhibit the V-ATPase were unable to proliferate in matrigel culture.

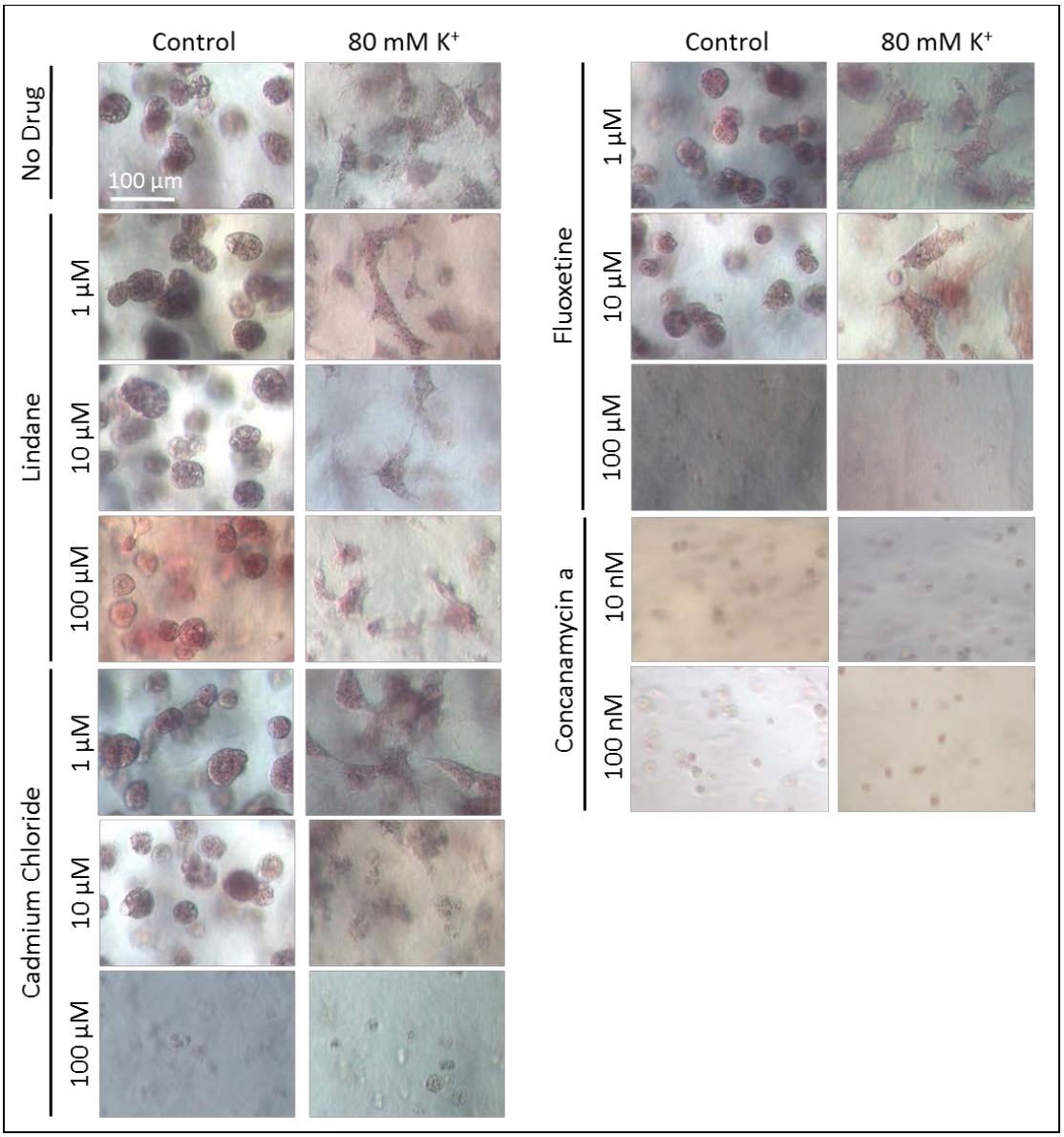

Figure III-5: Mechanistic drug screen of high potassium phenotype. Bright field images of whole mount carmine staining in MCF-10A cells cultured embedded in matrigel for 14 days in control or 80 mM potassium media and treated with the indicated pharmacological inhibitors.

III.5 Analysis

Changes in bioelectric properties are required for cancer progression, most likely due to their obligatory role in the mechanics of proliferation and migration, but also possibly due to additional regulatory functions. Little is known about the requirement for appropriate potassium currents to maintain normal cell growth and organization. It was expected that alteration of potassium dynamics would cause a loss of responsiveness to regulatory mechanisms that maintain normal tissue form and function.

Spheroid culture of MCF-10A in high potassium, which decreases normal potassium efflux through open potassium channels and depolarizes the V_{mem}, induces a dramatic increase in branched morphology including invasive-like cellular projections. The change in morphology was accompanied by an increase in cell proliferation and no change in the percentage of apoptotic cells. These results suggest cells grown in high potassium maintain a requirement for basal membrane contact but no longer respond to growth inhibitory signaling. Interestingly, while there was an increase in proliferation in 3D, cells cultured in 2D on tissue culture plastic and treated with high potassium had decreased proliferation. The difference in response could be due to signaling mechanisms that are activated in 3D growth or by interactions with the ECM proteins found in matrigel. Alternatively, the increased proliferation seen after 14 days in 3D

could be an artifact of decreased proliferation at earlier time points resulting in ‘immature’ spheroids at day 14.

Unfortunately, appropriate apical-basal polarity in the spheroid assay, an additional indicator of tissue organization, could not be analyzed because apical basal polarity had already been disrupted in the cell line. The loss of appropriate basal expression might be due to extensive and improper culturing in 2D prior to the spheroid assay. MCF-10A cells are highly sensitive to culture conditions and mistreating the cells including culturing to super-confluence can cause them to undergo an epithelial to mesenchymal transition (Valerie Weaver personal correspondence).

In the mammary gland, breast epithelial cells form both ducts and acinar structures. MCF-10A cells can be induced to form branched structures that are more similar to the native mammary gland architecture by a variety of factors including the mechanical stiffness of the microenvironment and co-culture with fibroblasts. Thus, branching alone does not indicate a loss of organization or progression to carcinogenesis. However, high potassium also induced irregular structure borders and cell projections that are not found in healthy tissue and are considered an invasive behavior. The results of this study suggest potassium dynamics may be sufficient to induce dysregulation associated with early cancer. However, further

characterization is needed in order to definitively classify the potassium phenotype as indicative of carcinoma.

We were interested to identify signaling molecules downstream of high potassium that are involved in the change in morphology. The initial mechanistic screen, in which cells were treated with inhibitors to signaling mechanisms that are responsive to bioelectricity in *Xenopus*, failed to identify any hits. The efficacy of drug inhibitors was not tested leaving the possibility that the drugs may not have truly inhibited their targets. However, the inhibitors were tested using a range of concentrations that covered previously reported effective concentrations and thus were likely functional in at least one concentration. Thus, the mechanisms targeted by the screen, which included gap junctions, serotonin transport, voltage-gated calcium, and action of the V-ATPase, are likely not involved in the high potassium phenotype.

As an alternative to direct effects of changes in potassium flux, the induced morphological phenotype may be caused by depolarization of the V_{mem} or by alterations in the gel matrix composition. V_{mem} is known to have important roles in many cell processes. If the phenotype is dependant on a V_{mem} sensitive signaling mechanism, modulation of V_{mem} using alteration to different ion flows would induce a similar effect. Alternatively, the phenotype may be an indirect effect

of changes to the gel matrix that are caused by high potassium. Increasing the matrix stiffness is sufficient to induce increased branching and cellular projections similar to those seen in high potassium (Chaudhuri et al., 2014). In order to elucidate the mechanism, future studies should aim to first determine whether it is dependent on potassium currents, V_{mem} , and/or alterations to the gel matrix.

MCF-10A cells are often used to represent 'normal' breast epithelial cells. But due to genetic alterations and other effects of prolonged culture the cells are no longer truly indicative of normal breast epithelial cells. Investigation of the effect of high potassium on primary breast epithelial cells or additional 'normal' cell lines is needed to ensure the induced phenotypes are not an artifact of alterations to MCF-10A cells that occurred in culture.

In sum, the results of this study support an integral role for potassium currents in maintaining breast epithelial cell structure and organization. Abolishing endogenous currents by culturing cells in high extracellular potassium media caused irregular structure formation in 3D growth and loss of polarized Golgi matrix localization. Further analysis is needed to determine whether the loss of organization also coincides with a loss of function, such as a decreased ability to produce

milk, and whether additional characteristics associated with cancer are induced.

Chapter IV: Expression of Ion Channels to Modulate Resting Membrane Potential Does Not Alter MCF-10A Behavior

IV.1 Abstract

Cancer cells are depolarized compared to their healthy counterparts raising the question of whether depolarization is an initiating event sufficient to induce properties associated with tumorigenesis including unregulated cell growth. In order to investigate this possibility, ion channels were over-expressed, extracellular ion concentrations were altered, and/or cells were treated with channel activators or inhibitors to modulate the membrane potential (V_{mem}) of the breast epithelial cell line MCF-10A. Multiple conditions utilizing changes in different ion flows to induce both depolarization and hyperpolarization were tested in order to determine the dependence on V_{mem} verses specific ion flows. Cells were then characterized for changes in cancer-associated behaviors. Expression of ion channels and changes to extracellular ion concentrations did not affect migration, invasion, or spheroid growth of cells cultured in matrigel, an assay that can identify hyperplasia forming cells. The results do not provide support for the hypothesis that altering V_{mem} is sufficient to induce cancer-associated properties.

IV.2 Rationale

Depolarization of V_{mem} correlates with advancing stages of cancer. The importance and specific requirement for depolarization in driving disease progression remains poorly characterized. Inhibition of channels responsible for inducing depolarization has been shown to decrease cancer-associated behaviors such as proliferation and migration. However, the relationship between V_{mem} and changes in behavior has not been fully characterized. It remains unknown whether changes in behavior are due to altered V_{mem} or if they are more specifically related to inhibition of particular channels. Similarly, it is unknown whether V_{mem} dependent effects are sensitive to which ion currents cause the shift in V_{mem}; that is, whether a cell depolarized by inhibition of potassium currents would have the same behavioral response as cells depolarized by increased sodium currents.

The aim of this study was to investigate the V_{mem} dependence of cancer-associated behaviors and the sensitivity to changes in particular ion currents. A combination of both pharmacological and genetic engineering techniques was employed to depolarize or hyperpolarize the V_{mem}. A set of channels was chosen for expression based on a predicted large effect on V_{mem}, ease of modulating channel activity, and specificity towards different ions.

Experiments were performed using the spontaneously immortalized non-tumorigenic breast epithelial cell line MCF-10A. This

cell line presents an excellent model for cancer onset because it is sensitive to growth inhibitory signaling but can be converted to unrestricted growth more easily than non-immortalized cells. The ability of cells to respond to growth inhibitory signaling can be tested by culturing cells embedded in matrigel. Cells responding appropriately to signaling require physical interaction with laminin in order to proliferate while those lacking contact undergo apoptosis. In matrigel, this requirement causes the cells to form small spheroids in which interior cells lacking contact to the matrigel undergo apoptosis (Shaw et al., 2004). The size of the spheroid is also restricted and typically reaches a final diameter of 50-100 μm (Debnath et al., 2003). MCF-10A cells expressing oncogenes form larger spheroids with a filled lumen because cells are less responsive to apoptotic and growth inhibitory signaling (Debnath et al., 2002; Hoenerhoff et al., 2009). This change in growth pattern is reflective of *in situ* hyperplasia, an early stage of cancer. To test for more aggressive phenotypes *in vitro,* cell migration and invasion was assessed.

Alteration of MCF-10A V_{mem} was expected to cause changes in cancer-associated behaviors with depolarization causing the cells to behave more cancer-like. A list of the over-expressed channels with a description of endogenous activity and the predicted effect on V_{mem} in different extracellular ion conditions is provided in table 1. Under

standard extracellular ion conditions expression of the glycine receptor chloride channel (GlyR), the inward rectifying potassium channel member 2.1 (Kir2.1), the V-ATPase subunit a3, and the yeast plasma membrane proton pump 1 (PMA) induce hyperpolarization while the non-specific cation channel Exp-1 induces depolarization. Changing extracellular ion concentrations can modulate the effect of channel expression on V_{mem}. In particular, GlyR can be used to depolarize cells by decreasing the extracellular chloride concentration and to induce greater hyperpolarization by increasing the chloride concentration.

Table IV-1: List of ion channels expressed in MCF-10A with predicted V_{mem} shift. Shift in V_{mem} is as compared to wild type cells in standard extracellular ion conditions. GlyR – Glycine receptor chloride channel, Kir2.1 – inward rectifying potassium channel member 2.1, PMA-1 plasma membrane proton pump 1, EC ion- extracellular ion condition

Channel	Endogenous activity	Agonists	Antagonists	EC Ion	V_{mem} shift
GlyR	Chloride specific channel activated by glycine	Glycine, ivermectin	Strychnine	Normal	Small Hyperpol
				High Cl^-	Depol
				Low Cl^-	Hyperpol
Kir2.2	Potassium specific channel containing activating mutation and covalently linked to GFP on n-terminal		ML 133	Normal	Hyperpol
				High K^+	Depol
Exp-1	Non-specific cation channel, primarily allows sodium entry	GABA			Depol
PMA	Yeast proton pump				Hyperpol
a3	V-ATPase subunit that increases localization and activity of the V-ATPase to the plasma membrane		Concana-mycin A		Hyperpol

IV.3 Methods

Materials and reagents were purchased from Thermo Fisher Scientific unless otherwise specified.

Generation of pINDUCER20 Channel Expression Plasmids – The pINDUCER20 plasmid was kindly provided by Mark Ewen. Plasmids containing the GlyR, Kir2.1-GFP, and Exp-1 coding sequence were kindly provided by Mike Levin. Primers were designed to amplify the full coding sequence of each channel with flanking attB sequences as per manufacturer instructions for Gateway cloning (Table 2). Channels were cloned into pDonr221 and the resulting plasmids were used to transform Dhα *E. coli* following manufacturer instructions. Bacteria clones were screened by kanamycin selection and sequenced to verify channel insertion. LR reactions were performed using 150 ng of the channel-pDonr221 plasmid and 150 ng of pINDUCER20 and transformed into Stbl3 *E. coli*.

Table IV-2: Primers for cloning and RT-PCR.

Cloning Primers		
Transcript	Forward	Reverse
GlyR	GGGGACAAGTTTGTACAAAAAAGCAGGCTTCACCAT	GGGGACCACTTTGTACAAGAAAGCTGGGTTTCACTGGTTGTG

	GTACAGCTTCAATACTCTTCGACTC	GACGTCC
Kir2.1	GGGGACAAGTTTGTACAAAAAAGCAGGCTACCATGGTGAGCAAGGGCGAG	GGGGACCACTTTGTACAAGAAAGCTGGGTTCATATCTCCGACTCTCGCC
Exp-1	GGGGACAAGTTTGTACAAAAAAGCAGGCTACCATGTGGATTAAACTATTATTCTTTTTC	GGGGACCACTTTGTACAAGAAAGCTGGGTTTCAGAAGCTTGTCTCTTCGC
a3	GTCAAGAAGAGACGTTGGACCATGGGCTCCATGTTCCGG	TCTCCTGCTTGCTTTAACAGAGAGAAGTTCGTGGCTCCGGATCCGTCATCTGTGGCAGCGAAG
PMA	GTCAAGAAGAGACGTTGGACCATGACTGATACATCATCATCCTCTTCATCA	TCTCCTGCTTGCTTTAACAGAGAGAAGTTCGTGGCTCCGGATCCCGGTTTCCTTTTCGTGTTGAGTAGAGA
GFP	GGGGACAAGTTTGTACAAAAAAGCAGGCTTCGAAGGAGATAGAACCATGGTGAGCAAGGGCGAG	GGGGACCACTTTGTACAAGAAAGCTGGGTTCTTGTACAGCTCGTCCATGC
tagRFP	TCTCTCTGTTAAAGCAAGCAGGAGACGTGGAAGAAAACCCCGGTCCTGTGTCTAAGGGCGAAGAGCTGA	CCTACAGGTGGGGTCTCACTTGTACAGCTCGTCCATGCC
pMIG	GCCAAGCTTATCGATAAAATAAAAGA	AATTCCGGCGCCTAGAGA
RT-PCR Primers		
Target	Forward	Reverse
GAPDH	TTCGACAGTCAGCCGCATCTTCTT	ACCAAATCCGTTGACTCCGACCTT
GlyR	AGGGTCAACATCTTCCTGCG	TCCCATTCCGGGAGATCCTT
Kir2.1	TGCAAATGGCTTTGGGAACG	TGAAGCTGTTGACCTCGGAC
Exp-1	GGAGGCGTCGACTCTTATGG	GTCTCGCCACGATTCTCGAT
a3	CATGGTCCTTGCGGAGAACC	GCCGGTGTAGATGGAGAACAG

PMA	ATTTTGGCTGCCGGTTTGTC	ACGACTTCGTTGGCTGGAAT

Generation of pMIG Channel Expression Plasmids – Plasmids containing the V-ATPase a3 subunit and PMA were provided by Mike Forgac and Mike Levin respectively. The retroviral expression plasmid pMIG and a plasmid containing tagRFP (RFP- red fluorescent protein) were purchased from Addgene (#12282 and #37537). The channel coding sequence in tandem with P2A and tagRFP was inserted into pMIG to replace the IRES and gren fluorescent protein (GFP) sequence using the Gibson cloning method following manufacturer instructions (NEB). Briefly, primers were designed to amplify pMIG excluding the IRES-GFP sequence. Primers for the channels and tagRFP were designed with 25-40 bp overhanging sequences to match the adjacent DNA sequence of the final plasmid and to insert the P2A sequence (Table 2). All fragments were amplified by PCR and gel purified. A Gibson reaction was performed using three DNA fragments, the pMIG backbone, channel, and tagRFP, to create the final plasmid. A plasmid containing GFP instead of an ion channel was made as a control vector.

Lentivirus Production – Lentivirus was produced as described in chapter 2.

Retrovirus Production – Two days prior to transfection, 2 x 10^6 293 Plat GP cells (Cell Biolabs) were plated on a 10 cm dish. Transfection was performed with 60 μL of lipofectamine 2000, 6 μg of VSV packaging plasmid, and 12 μg of pMIG-Channel-P2A-RFP plasmid per manufacturer instructions. Cells were incubated in the DNA:liposome complex overnight in a final volume of 6 mL. At 72 hours post transfection, virus media was collected and filtered through a 45 μm filter.

Mammary Epithelial Cell Cultivation- MCF-10A were maintained and passaged as recommended by ATCC. All cells transduced with pINDUCER20 series were cultured in 1 μg/mL doxycycline (dox) beginning 4 days prior to plating and throughout behavioral assays unless otherwise stated.

Virus Transduction – Cells were transduced by incubating 50% confluent cells with virus in media supplemented with 6 μg/mL polybrene for 24 hours. At 72 hours post-transduction, lentivirus infected cells were placed in media containing 50 μg/mL G418 for selection. Retrovirus infected cells were expanded for later FACS sorting.

Cell sorting of Retrovirus Transduced cells – Cells were trypsonized to create a single cell suspension and sorted on a Legacy MoFlo (Cytomation) gating to collect cells with positive red fluorescence.

RNA Isolation, Purification, and Quantitative PCR – RNA was isolated from confluent cells in a 6-well plate. Cells were rinsed with PBS and 200 μL RNA-later (Ambion) was added before scraping and transferring cells to a 1.5 mL tube. RNA was purified using an RNeasy mini kit (Qiagen) per manufacturer instructions. The concentration of RNA was determined with a NanoDrop 2000 (Thermo Scientific). Reverse transcription reactions were performed with 1 μg of RNA in a 20 μl reaction using iScript Reverse Transcription Supermix (Bio-Rad) following manufacturer instructions. Transcript expression levels were quantified with a Bio-Rad CFX96 Real Time System. Reactions were performed in 20 μL using iQ SYBR Green Supermix (Bio-Rad) and 40 ng cDNA with the following reaction conditions: 95 ° C 10 min, 40 cycles of 95° C 30 sec, 58° C 1 minute, 72 C° 1 minute. Primers for each of the transcripts are listed in Table 1. Expression levels were calculated using the Pfaffl method (Pfaffl, 2001) normalizing to the housekeeping gene glyceraldehyde-3-phosphate dehydrogenase (GAPDH).

Western Blot Protein Analysis – Protein lysates were collected from confluent 6-well plates by rinsing cells in PBS and adding 200 μL RIPA buffer with 1X Halt protease and phosphatase inhibitor cocktail and incubating on ice for 5 minutes. Cells were scraped, transferred to a 1.5 mL tube and centrifuged at 1 x 10^4 g for 10 minutes at 4° C. Protein concentrations were determined using a BCA assay per manufacturer instructions. The NuPAGE system with 10 μg of protein loaded on a 10% bis-Tris gel was used to separate samples according to instructions. Proteins were transferred onto a PVDF membrane at 30 V for 1 hr in NuPAGE transfer buffer with 20% MeOH. Membranes were incubated with primary antibody for 1 hr at room temperature or at 4° C overnight at the following dilutions in 5% skim milk: GlyRα 1:2000 (AbCam), GFP 1:2000 (AbCam), β-actin 1:3000 (Cell Signaling). The appropriate horseradish peroxidase-conjugated secondary antibody (AbCam) diluted 1:10000 in 5% skim milk was incubated with membranes for 1 hr and signal was visualized with ECL Select (GE Healthcare).

MCF-10A Spheroid Formation Assay- The basement membrane gel (BMG) consisted of 50% matrigel (BD Bioscience), 1 mg/mL collagen type I from rat tail (BD Biosciences), and 23 mM NaOH. Transwells

with a 12 mm diameter and 0.4 μm pores (BD Biosciences) were coated with 150 μL of acellular BMG and incubated for 30 minutes at 37° C to allow the solution to gel. MCF-10A cells were diluted to 2.5 x 10^5 cells/mL in BMG and 400 μL were added on top of the coated transwells. Transwells were incubated at 37° C for 1 hr to allow gelation followed by addition of 3D media to the upper and lower chamber. 3D media contained the same supplements as normal MCF-10A media except with only 2% horse serum and 5 ng/mL EGF. To modulate the effect of GlyR channels on V_{mem}, GlyR cells were cultured in normal media or with the addition of 50 mM choline chloride with either 1 μM ivermectin agonist or 1 μM strychnine antagonist. Media was exchanged every 4 days and samples were collected after 14 days. Samples were cut in half and fixed in 10% formalin for 24 hours. One half was rinsed in PBS 2 x 10 minutes and incubated in carmine stain solution for 24 hours. Samples were rinsed in PBS 2 x 10 minutes and bright field images were acquired using an Olympus IX71 inverted microscope and Olympus DP70 digital camera with associated software. The other half of the sample was embedded in paraffin and sectioned at 5 μm thickness. Sections were stained with hematoxylin and eosin (H&E) following the Cold Springs Harbor protocol and bright field images were acquired as above.

Migration and Invasion Assays- For migration assays, 3.75 x 10^5 cells/cm^2 were plated in a 24-well plate. Cells were incubated in MCF-10A low serum media (0.5 % horse serum, 2 ng/mL EGF) overnight to serum starve cells. A yellow tip was used to make a scratch through the confluent cell layer and media was exchanged to fresh low serum media. Bright field images were acquired as described above at 0 hrs and 12 hrs after scratching. The area of the scratch wound was measured using ImageJ. The day prior to invasion assays, cells were placed in low serum media to serum starve. Basement membrane coated transwells with 6.5 mm diameter and 8 μm pore size (BD Biosciences) were pre-incubated with 500 μL DMEM in the upper chamber for 2 hours. MCF-10A cells were diluted to 5 x 10^5 cells/mL in low serum media and 200 μL of the cell suspension was placed in the upper chamber giving 1 x 10^5 cells per well. The bottom chamber was filled with 600 μL of normal full serum media as a chemoattractant. After 24 hours, transwells were rinsed in PBS and cells were scraped off of the upper chamber. Remaining cells were fixed in 4% PFA for 10 minutes. Transwells were rinsed in PBS and stained with 1 μg/mL 4', 6-Diamidino-2-Phenylindole Dihydrochloride (DAPI) for 10 minutes. The number of invading cells was counted in 4 fields of view for each sample.

Cell Viability – Cell health was determined using either an alamar blue cell viability assay or a lactate dehydrogenase (LDH) toxicity assay. MCF-10A cells were plated in 96 well plates and allowed to grow to 75% confluence. For the alamar blue cell viability assay, cells were incubated in 10% alamar blue solution for 1 hr and fluorescence was measured on a SpectraMax M5 (Molecular Devices) plate reader with excitation 560 nm, emission 590 nm. Alternatively, cell viability was quantified using an LDH cytotoxicity assay kit (Thermo Scientific) according to manufacturer instructions.

Statistics – Statistics were calculated with Prism 5 using a two-sample T test or one-way ANOVA with Tukey or Dunnett post-test for significance with alpha = .05.

IV.4 Results

IV.4.1 Expression of ion channels

Channels with high endogenous activity and different ion specificity were cloned into expression vectors and expressed in MCF-10A. Channels for which cell toxicity was not a concern, PMA and a3,

were cloned into the pMIG retroviral expression vector which induces high expression in breast epithelial cells. The channel sequences were cloned in tandem with the P2A peptide bond-skip sequence and tagRFP (Figure 1A). This system causes the channel and tagRFP peptide chains to be translated by the same ribosome, but due to the peptide-skip sequence, form two separate proteins. Thus, production of the two proteins precisely correlates so that RFP fluorescence can be used as an accurate indicator of channel protein levels. The variant of RFP, tagRFP, was chosen because its excitation and emission spectrum is shifted to longer wavelengths and has less interference with green fluorescent molecules such as calcium indicator dyes. A control vector was constructed containing GFP linked to tagRFP by P2A.

MCF-10A retrovirus infected cells were sorted for RFP positive cells using fluorescence activated cell sorting (FACS). Virus treated cells had higher RFP fluorescence than uninfected cells, with a higher RFP signal in pMIG-a3-RFP than pMIG-PMA-RFP infected cells (Figure 1B). mRNA expression levels were quantified by RT-PCR. Expression of both channels was strongly induced with higher levels of a3 than PMA, as expected based on the RFP fluorescence (Figure 2A). Increased protein expression of a3 was confirmed by western blot, but not for PMA due to a lack of commercially available antibody (Figure 2B).

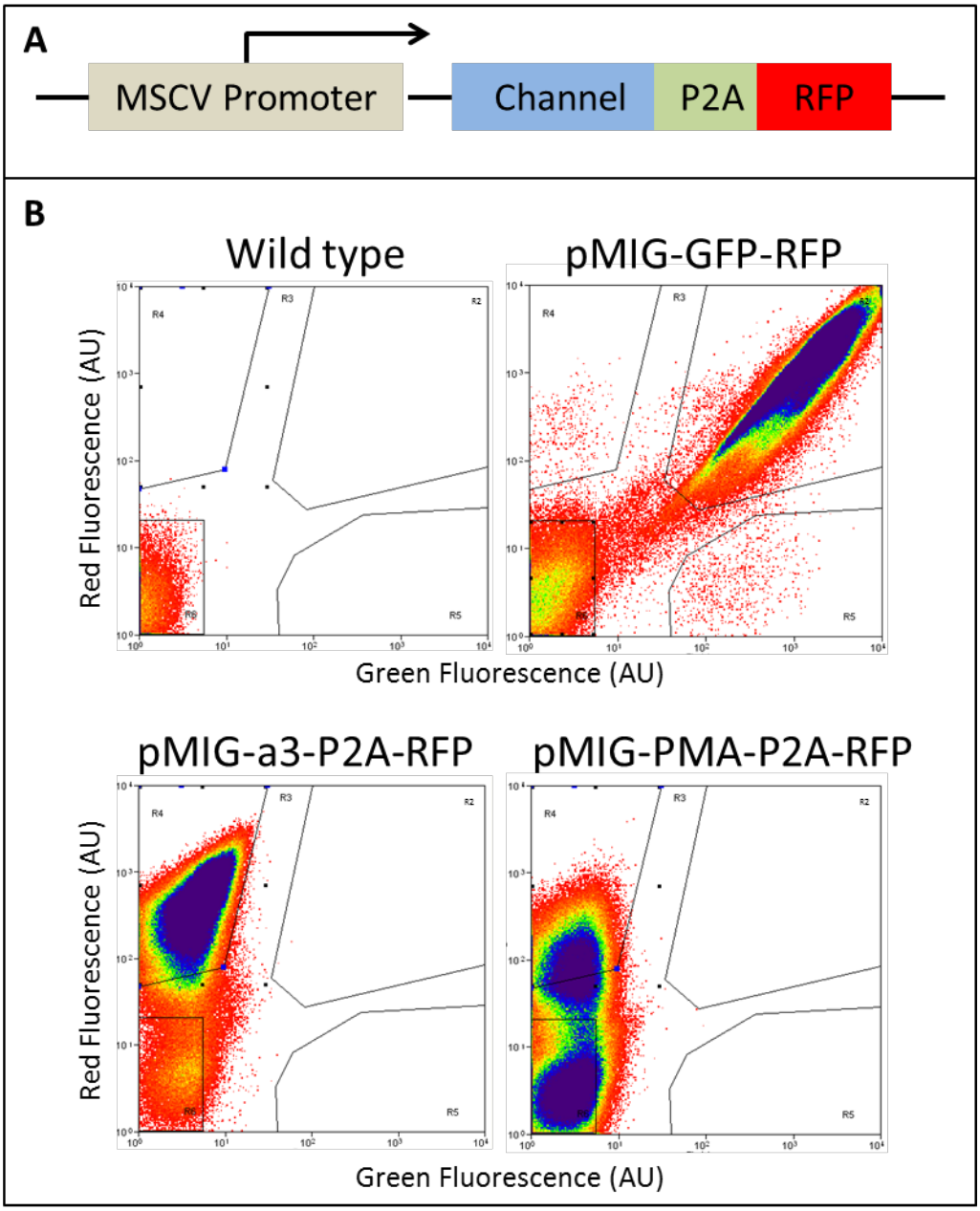

Figure IV-1: Selection of a3 and PMA expressing MCF-10A cells. **(A)** Schematic of expression plasmid. **(B)** Plot of FACS sort showing individual cell green and red fluorescence. Control GFP cells were selected with gate R2 for dual red and green fluorescent cells. Channel expressing cells were selected with gate R4 for only red fluorescence.

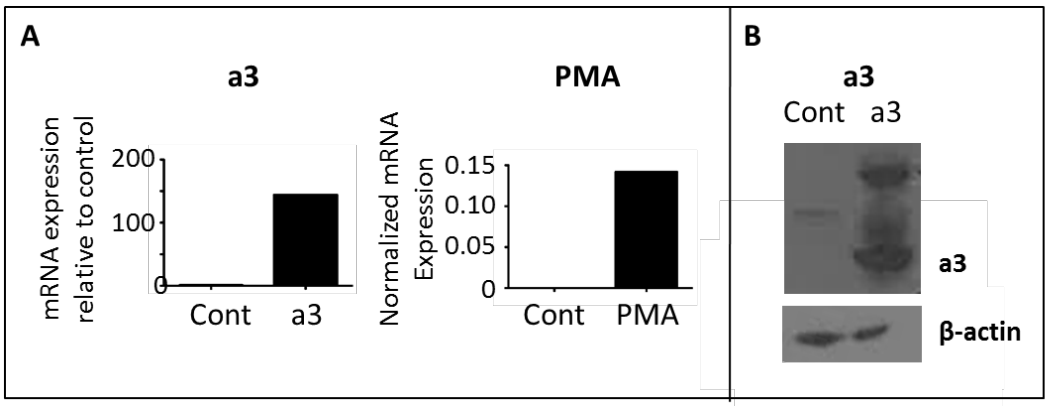

Figure IV-2: pMIG-Channel-P2A-RFP expression in MCF-10A. **(A)** RT-PCR analysis of mRNA transcript levels in FACS sorted populations normalized to GAPDH. **(B)** Western blot of total protein lysates prepared from control and a3 expressing MCF-10A cells probed with anti-a3 and anti-β-actin as loading control.

Channels with especially high endogenous activity have the potential to cause cell toxicity. These channels, which included GlyR, Kir2.1, and Exp-1, were therefore cloned into the doxycycline inducible pINDUCER20 lentivirus expression plasmid (Figure 3A) (Meerbrey et al., 2011).(Lerchner et al., 2007)(Lerchner et al., 2007)(Lerchner et al., 2007) The Kir2.1 sequence contained a mutation that deleted an inhibitory phosphorylation site causing increased activity and was also covalently linked to GFP on the N-terminal end (Hinard et al., 2008).

MCF-10A cells were infected with lentivirus and selected by antibiotic resistance. Cells were cultured in 0 µg/mL to 5 µg/mL doxycycline for 4 days prior to RNA collection and analyzed for channel expression by RT-PCR. Expression of all three channels was dose-dependent with doxycycline treatment and high concentrations

induced robust expression levels (Figure 3B). GlyR and Kir2.1 expression was also confirmed at the protein level by western blot and was similarly dose dependent on doxycycline treatment (Figure 3C). Exp-1 protein levels were not analyzed because of a lack of specific antibody. Imaging of the GFP fusion tag demonstrated Kir2.1 was primarily localized to the plasma membrane (Figure 3D).

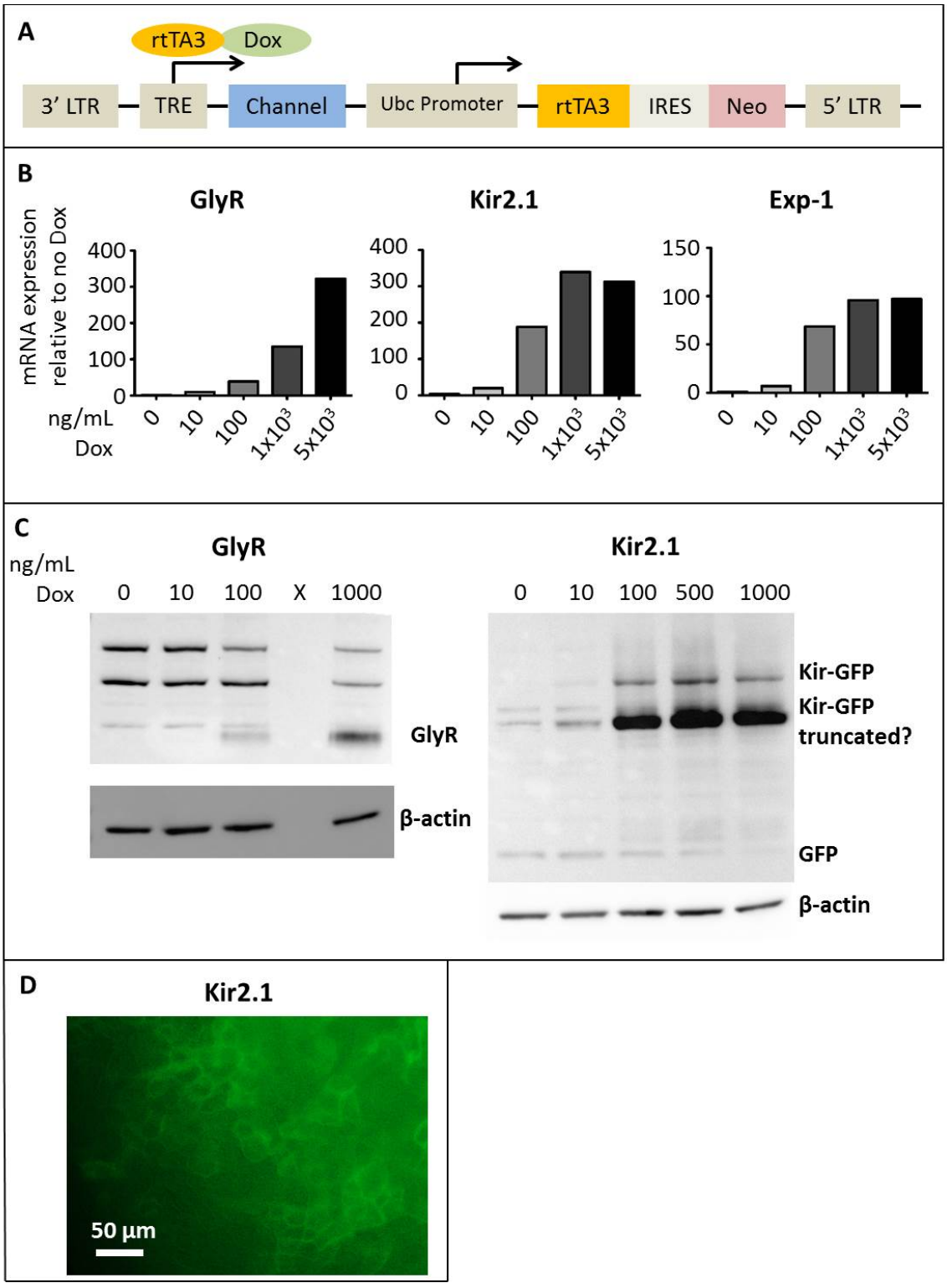

Figure IV-3: pINUCER20-Channel expression in MCF-10A. (A) Schematic of pINDUCER20 expression plasmid. **(B)** Cells were treated with doxycycline for 4 days prior to total RNA isolation and RT-PCR

analysis of mRNA transcript levels normalized to GAPDH. **(C)** Western blot of total protein lysates from the same samples probed with anti-GlyRα, anti-GFP, and anti-β-actin as loading control. **(D)** Fluorescent image of Kir2.1 expressing cells pre-treated with 1 µg/mL dox for four days showing plasma membrane localization of Kir2.1 channels tagged with GFP.

MCF-10A cells were also infected with pMIG retrovirus encoding Ras or Myc expression as a positive control.

IV.4.2 Effect of channel expression on 3D morphology and invasive behaviors.

Expression of ion channels did not induce changes in MCF-10A growth in the spheroid formation assay. MCF-10A wild type cells formed circular shaped spheroids with clearly defined smooth borders. Transformed MCF-10A cells form larger and more irregularly shaped structures as can be seen in the Myc, Ras, and Myc and Ras co-expressing cell lines (Figure 4A). Channel expressing cells resembled control cells with clearly defined borders and no significant change in size (Figure 4A-B). This included GlyR cells grown in normal and high chloride media with the agonist ivermectin to increase GlyR activity and hyperpolarization.

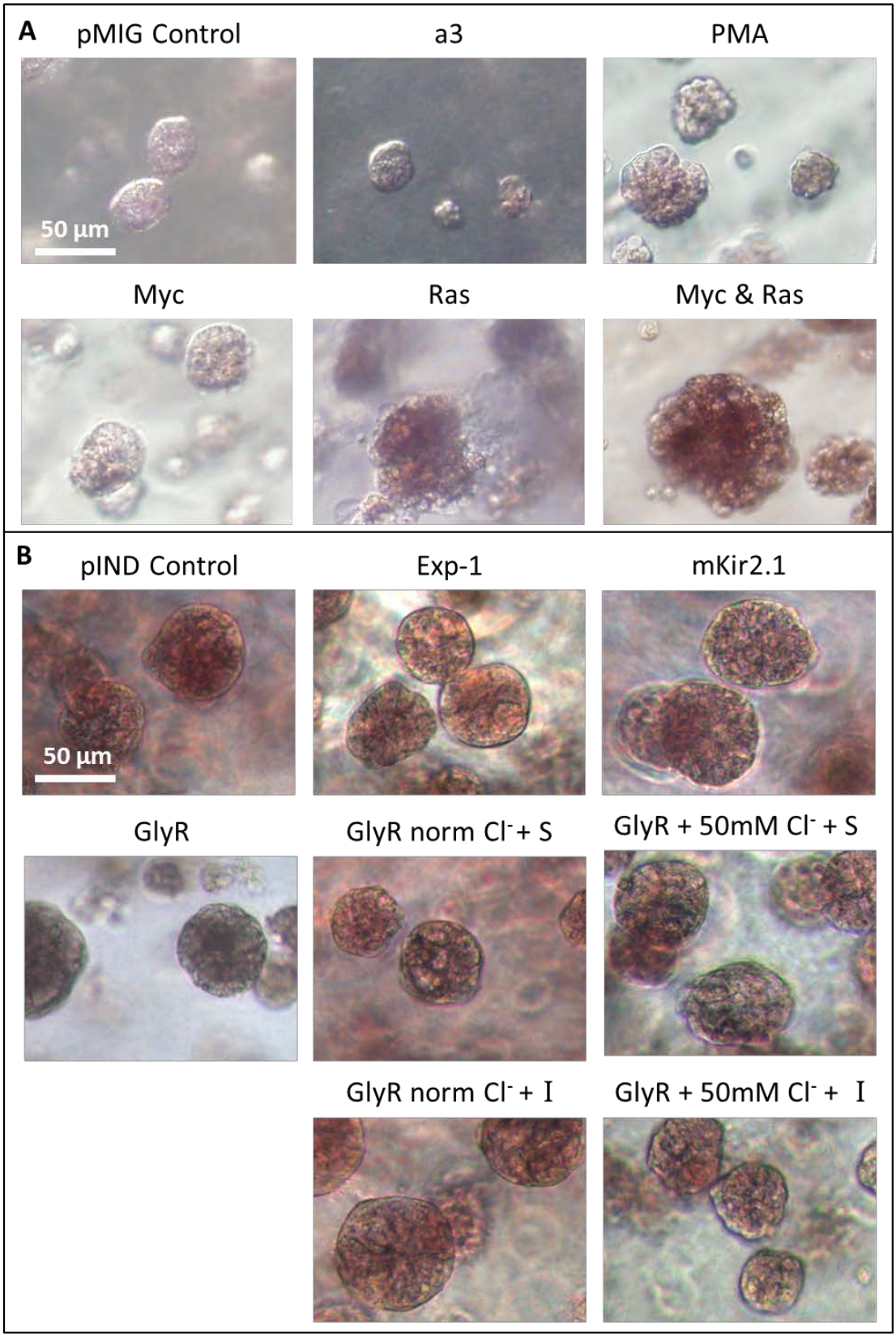
A
pMIG Control
a3
PMA
50 µm
Myc
Ras
Myc & Ras
B
pIND Control
Exp-1
mKir2.1
50 µm
GlyR
GlyR norm Cl- + S
GlyR + 50mM Cl- + S
GlyR norm Cl- + I
GlyR + 50mM Cl- + I

Figure IV-4: Spheroid growth of channel-expressing MCF-10A. Bright field images of whole mount carmine stained cells grown embedded in matrigel for 14 days. **(A)** MCF-10A cells infected with the indicated pMIG backbone expression plasmids. **(B)** pINDUCER lentiviral infected MCF-10A cells expressing the indicated channels. GlyR expressing cells were grown in normal media (norm Cl^-) containing 118 mM Cl^- or high extracellular chloride media (+ 50 mM Cl^-) supplemented with 50 mM choline chloride with the GlyR agonist ivermectin (I, 1 µM) or antagonist strychnine (S, 1 µM).

As an additional method to assay for increased cancer-associated behaviors, cells were also tested for migration and invasion in 2D. Invasion through matrigel was assessed in PMA and a3 expressing cells. Neither PMA nor a3 expression caused a significant change in invasion while both Myc and Ras increased invasion (Figure 5A-B). Similarly, no significant change in migration was found in Exp-1, GlyR or mKir2.1 expressing cells (Figure 5C-E). Channel expression did not induce cell toxicity as measured by alamar blue reduction or LDH activity in the cell media (Figure 5B,E).

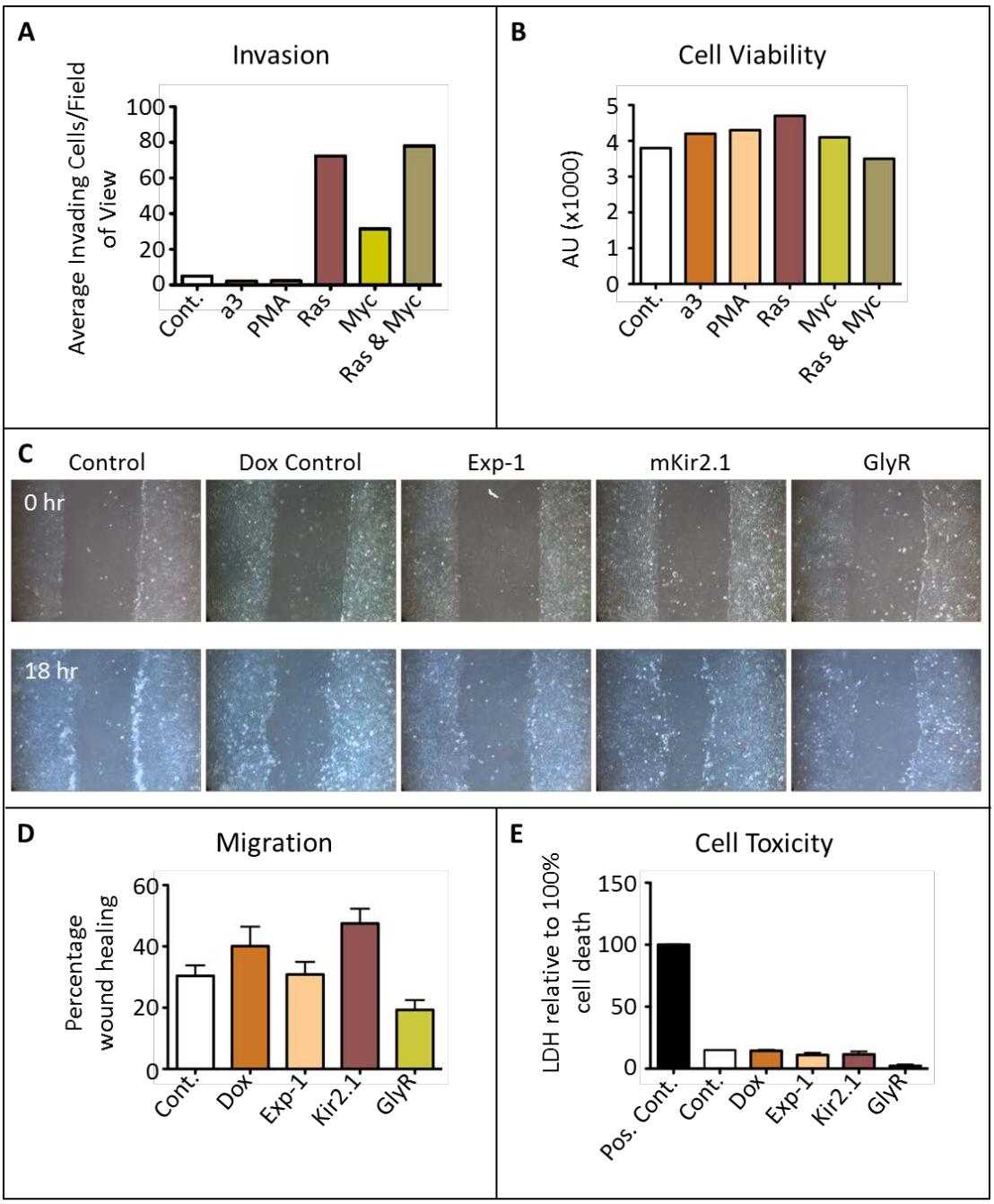

Figure IV-5: Invasion and migration of channel expressing MCF-10A. (A) pMIG MCF-10A cells invasion through matrigel coated transwell membrane for 24 hours using horse serum and EGF as chemoattractants. Average number of invading cells per field of view from 4 fields of view per transwell and 4 replicates for each cell type. **(B)** Quantification of cell viability by reduction of alamar blue reagent for 1 hr of cell lines from A. **(C)** Bright field images of migration into a

scratch wound of serum starved pINDUCER cells pre-incubated with 1 μg/ mL dox for 4 days at 0 hr and 18 hrs post scratch. **(D)** Quantification of wound healing from C. **(E)** Cell toxicity of dox treatment and channel expression in cells from C measured by LDH activity in media incubated with cells for 24 hours. Data presented as mean with standard deviation of 4 replicates from a single experiment.

IV.5 Analysis

Ion channels selective for different ions were successfully expressed in MCF-10A cells as demonstrated by increased mRNA and protein levels. Cells were cultured embedded in matrigel, as this method can distinguish between healthy and early cancer stage cells that form hyperplasia *in vivo*. However, expression of the channels did not affect MCF-10A growth in 3D matrigel culture as no change was observed in the size or shape of the spheroids. This was in contrast to expression of the oncogenes Ras and Myc which caused an increase in size of spheroids as well as irregular spheroid borders. Given that channel expression and culture conditions were expected to induce both depolarization and hyperpolarization, these data suggest modulation of V_{mem} is insufficient to drive cancer behaviors associated with the progression to hyperplasia. Furthermore, it suggests the phenotype associated with high extracellular potassium (Chapter 3) is not related to depolarization as alternative methods of depolarization were unable to induce a similar phenotype. Channel expression also

had no effect on cell migration or invasion in pilot studies. V_{mem} might be insufficient to drive aggressive behaviors in healthy cells but may have a more pronounced effect in transformed cells. In future studies, the effect of V_{mem} modulation could be investigated in tumorigenic and metastatic cell lines in which some of the regulatory mechanisms are lost.

A major caveat to the interpretation of these results is that predicted effects of ion channel expression on ion currents and V_{mem} were not verified. GlyR, Kir2.1, and a3 have been over-expressed and demonstrated to increase current density in mammalian cells in prior studies suggesting the channels are likely active in this study (Blackiston et al., 2011; Capecci and Forgac, 2013; Hinard et al., 2008). However, the previous studies utilized different expression systems and cell types leaving the possibility that the channels were not functional in MCF-10A. Even if the channels were active, it is possible other channels were activated to compensate, potentially causing the V_{mem} to be different than predicted. In order to definitively link changes in V_{mem} to cell behaviors, the effect of V_{mem} modulation must be quantified.

The original model predicting a direct correlation between absolute V_{mem} and cancer-associated behaviors is likely overly simplistic. V_{mem} signaling may involve more complicated fluctuations

with important instructions embedded in the temporal dynamics. Currently, little is known about the temporal variation in V_{mem} during cancer progression outside of the cyclical fluctuation associated with the cell cycle. Further characterization of V_{mem} dynamics that occur during migration and invasion as well as those associated with increasing cancer grade is needed. Most of the methods to measure V_{mem} only allow measurement for short time periods due to cell toxicity or photobleaching of fluorescent probes. However, recently developed voltage-sensitive fluorescence resonance energy transfer (FRET) protein reporters may enable longer time scale studies to study V_{mem} in these processes (Tsutsui et al., 2008). V_{mem} signaling may also require interactions with surrounding stromal cell types. Studies from *Xenopus* suggest differences in V_{mem} between neighboring cells might be more instructive than absolute V_{mem} (Blackiston et al., 2015). Towards the goal of investigating V_{mem} signaling in an experimental setting that reflects native epithelial-stromal cell interactions, tissue engineering strategies that better replicate *in vivo* breast tissue are explored in appendix I. Investigation of endogenous V_{mem} dynamics during cancer-associated behaviors and response to V_{mem} modulation in a culture system that more accurately reflects the *in vivo* environment will enable a better understanding of the role of V_{mem} in cancer progression.

CHAPTER V:

SUFFICIENCY OF INTERMEDIATE CONDUCTANCE CALCIUM-ACTIVATED POTASSIUM CHANNEL (IK) TO PROMOTE CANCER-ASSOCIATED BEHAVIORS

V.1 Abstract

Many potassium channel families are over-expressed in cancer, but their mechanistic role in disease progression is poorly understood. Potassium channels modulate membrane potential (V_{mem}) and thereby influence calcium ion dynamics and other voltage-sensitive signaling mechanisms, potentially acting as transcriptional regulators. This study investigated the differential response to over-expression and activation of a cancer-associated potassium channel, the intermediate conductance calcium-activated potassium channel (IK), on aggressive behaviors in healthy and breast cancer cell lines. IK was over-expressed in the spontaneously immortalized breast epithelial cell line MCF-10A and the highly metastatic breast cancer cell line MDA-MB-231, and the effect on cancer-associated behaviors was assessed. IK over-expression and treatment with the IK agonist 1-Ethylbenzimidazolinone (1-EBIO) increased potassium current density and hyperpolarized V_{mem} in both cell lines demonstrating the channel was functional. IK decreased MCF-10A proliferation and invasion through matrigel but had no effect on migration in a scratch-wound assay while MDA-MB-231 proliferation, invasion, and migration were all unaffected. Interestingly, colony formation of MDA-MB-231 cells was decreased by IK expression and further decreased by treatment

with 1-EBIO. In contrast, IK over-expression increased primary tumor growth of MDA-MB-231 in orthotopic xenografts. To our knowledge, this study is the first to characterize differential behavior response to bioelectric signaling between healthy and cancerous cells. Changes in potassium current signaling networks during cancer progression could provide targets to create more specific cancer therapies.

V.2 Rationale

Potassium channel expression is altered in many cancers with expression of certain channels correlating with disease progression. Potassium channels play important mechanical roles in proliferation and migration in part due to their requirement in regulation if cell volume (Kunzelmann, 2005; Urrego et al., 2014). The flow of potassium ions across the cell membrane also alters the V_{mem} and therefore the driving force on calcium ions. Through this mechanism, potassium channels may play an important role regulating cancer-associated behaviors.

IK is over-expressed in numerous cancer types and inhibition of IK decreases proliferation and migration while activation by treatment with an agonist lead to increased proliferation in prostate cancer cells (Ouadid-Ahidouch et al., 2004b; Schwab et al., 2012). IK activity has

also been directly linked to intracellular calcium levels in prostate cancer cells with IK agonist treatment leading to an immediate increase in intracellular calcium (Lallet-Daher et al., 2009). Calcium entry was inhibited by knock down of calcium channel transient receptor potential cation channel subfamily V, member 6 (TRPV6), which was shown to physically interact with IK by co-immunoprecipitation. Interestingly, IK activity is associated with calcium entry through a different TRP calcium channel family member, TRPC4, in alveolar epithelial cells (Girault et al., 2015). Association with different TRP members may function as a mechanism to enable unique responses to IK activation in different cell types. The ability of IK activation to increase prostate cancer proliferation is currently the only example of potassium currents being sufficient to increase cancer-associated behaviors.

High IK expression is associated with the highly aggressive triple negative breast cancer subtype but its role in cancer aggression is not known (Oncomine cancer subtype analysis, www.oncomine.org). I hypothesized that the ability to increase proliferation is conserved across cancer types and that IK activation would similarly increase breast cancer cell proliferation. I also wanted to determine whether increasing IK activation in non-cancerous cells leads to a similar increase in proliferation as in cancer cells. Additionally, due to the

influence of IK activity on intracellular calcium levels, I also hypothesized that IK activation is sufficient to increase additional cancer-associated behaviors and primary tumor growth and metastasis *in vivo*. In order to test these hypotheses, IK was over-expressed in the metastatic breast cancer cell line MDA-MB-231 and the non-tumorigenic spontaneously immortalized breast epithelial cell line MCF-10A. IK is activated in response to high intracellular calcium concentrations making its activity highly spatially and temporally regulated. Increased IK expression is expected to induce larger potassium currents but still under the regulation of endogenous calcium signaling. IK can also be activated with the agonist 1-ethyl-2-benzimidazolinone (1-EBIO). Both control and IK expressing cells were treated with 1-EBIO to investigate the effect of different levels of pan-IK activation. Proliferation, migration, and invasion were then assessed *in vitro* in control and IK-expressing cells treated or untreated with 1-EBIO. Primary tumor growth and metastasis of MDA-MB-231 IK expressing cells was also characterized *in vivo*.

V.3 Methods

Generation of pMIG Expression Plasmid – A plasmid containing the IK complete coding sequence was purchased from Genecopoeia (GC-

0G00902). IK was cloned into the pMIG plasmid in tandem with the P2A peptide bond-skip sequence and tagRFP (pMIG-IK) as described in Chapter 4. The primers used to amplify IK were forward primer 5' CTAGGCGCCGGAATTACCATGGGCGGGGATCTGG, and reverse primer 5' TCTCCTGCTTGCTTTAACAGAGAGAAGTTCGTGGCTCCGGATCCCTTGGACT GCTGGCTGGG. A plasmid with only tagRFP inserted was generated as a control (pMIG-RFP).

Lentivirus Production and Transduction – Virus was produced in 293FT cells and used to transduce MCF-10A and MDA-MB-231 cells as described in Chapter 2.

Cell Cultivation and Spheroid Assay – MCF-10A and MDA-MB-231 cells were maintained following ATCC recommendations. The spheroid assay was performed essentially as described in Chapter 3, the only difference being that cells were seeded at 2.5 x 10^4 cells per well. Sphere size was calculated by manually outlining spheres in ImageJ.

IK activation – Cells were treated with 200 µM 1-EBIO diluted from a 400 mM 1-EBIO stock solution in dimethyl sulfoxide (DMSO) resulting in a final concentration of .05% DMSO in the cell media. Control

samples were treated with an equivalent concentration of DMSO as vehicle control.

Electrophysiology – Patch clamp recordings were performed in the cell attached perforated patch configuration and data was recorded with an Axon DigiData 1550 (Axon Instruments) data acquisition system and an Axopatch 200B (Molecular Devices) amplifier. Data was low pass filtered at 5 kHz, sampled at 50 kHz, and analyzed using pClamp 10 software (Axon Instruments). Patch pipettes were pulled from thin-wall borosilicate glass with a P-97 micropipette puller (Sutter Instruments) and fire polished resulting in 4-7 MΩ resistance pipettes. Pipettes were filled with intracellular electrode solution (5 mM NaCl, 145 mM KCl, 2 mM $MgCl_2$, 1 mM $CaCl_2$, 1.57 mM ethylene glycol-bis(2-aminoethylether)-*N-N-N'-N'*-tetraacitic acid (EGTA), 10 mM 4-(2-Hydroxyethyl)piperazine-1-ethanesulfonic acid (HEPES), pH adjusted to 7.4 with 1 M KOH) supplemented with 150 ng/mL Nystatin to induce pore formation. Prior to recording, cells plated on glass coverslips were perfused with external bath solution (144 mM NaCl, 5.4 mM KCl, 1 mM $MgCl_2$, 2.5 mM $CaCl_2$, 5.6 mM Glucose, 5mM HEPES, adjusted to pH 7.2 with 1 M NaOH). After initial seal formation, with a minimal seal resistance cut off of 1.0 GΩ, perforation was assayed by monitoring the capacitive current transient to a 2.5 mV step with -30 mV holding

potential. Recordings were acquired once the series resistance was below 75 MΩ. V_{mem} recordings were taken for 30 seconds in control extracellular solution supplemented with 0.05% vehicle control with no fluid-flow, during 30 seconds of bath exchange with the same solution, during 30 seconds of bath exchange with bath solution containing 200 uM 1-EBIO, and for 30 seconds in 200uM 1-EBIO with no fluid flow. The reported V_{mem} values are the average from the last 20 seconds recorded in static fluid from each condition. For the current-voltage protocol, cells were held at -30 mV holding potential with 50 ms test pulses between -120 mV and 80 mV in 40 mV steps. Current density was calculated by dividing the average current during the voltage step without leak subtraction by the whole cell capacitance.

RNA Isolation, Purification, and Quantitative PCR - All steps were performed as described in Chapter 4 and RT-PCR primers for IK were forward primer 5' CTGCTGCGTCTCTACCTGG and reverse primer 5' AGGGTGCGTGTTCATGTAAAG.

Proliferation Assay – MCF-10A cells were plated at 7.5 x 10^3 cells/cm^2 and MDA-MB-231 cells were plated at 1 x 10^4 cells/cm^2 in 6 well plates. Cells were allowed to attach in normal media for 3 hrs followed by exchange to media supplemented with drug treatment. Cells were

trypsonized and counted with a TC 10 automated cell counter (BioRad) daily for 4 days with a media change after 2 days.

Apoptosis, Cell Death, and Cell Cycle Analysis – Cells were plated at 5 x 10^4 cells/cm^2 and allowed to attach for 3 hours. Media was exchanged to media supplemented with vehicle or 200 μM 1-EBIO and cells were incubated for 24 hrs. To quantify the percentage of apoptotic and dead cells, cells were trypsonized, washed in PBS, and incubated in 0.1% Live/Dead Fixable Violet Dead Cell stain for 30 min. Cells were washed in Annexin V Binding Buffer and incubated in anti-Annexin V antibody conjugated to Alexa Fluor 488 diluted 1:125 in Annexin V Binding Buffer. For cell cycle analysis, cells were fixed in 70% EtOH and washed in phosphate-buffered saline (PBS). Cells were incubated in 50 ng/mL propidium iodide, 250 ng/mL RNase diluted in PBS for 1hr. Cell fluorescence was detected using an LSR II (Becton Dickenson) fluorescent cell analyzer and data was analyzed with FlowJo software.

Migration Assay – Migration assays with MCF-10A cells were performed as described in Chapter 4. MDA-MB-231 cells were plated at 2.5 x 10^5 cells/cm^2 in a 24 well plate and were serum starved in 1% FBS media overnight. A scratch was made with a yellow tip and media was

exchanged with low serum media containing drug treatment. Phase contrast images were acquired of the initial scratch. 10 hrs post scratch, cells were incubated in 0.5 µg/mL calcein AM for 15 minutes and fluorescent images were acquired. ImageJ was used to calculate wound healing by first manually outlining the wound at time 0 hr to create a region of interest (ROI). The fluorescent 10 hr image of calcein AM stained cells was converted to a binary image such that white pixels corresponded to the surface area covered by cells. The percentage of white pixels within the initial wound ROI was quantified to measure wound healing.

Invasion Assay – MCF-10A invasion assays were performed as described in Chapter 4. MDA-MD-231 invasion assays were performed similarly except with 5 x 10^4 cells per transwell and incubation for 16 hrs. Drug treatment was added to the media of both the upper and lower chambers at the time of seeding.

Colony Formation Assay – MCF-10A cells were plated at 3 x 10^4 cells per well and MDA-MB-231 were plated at 5 x 10^3 cells per well of a six well plate. The wells were first coated in 1.5 mL of 0.8% agarose diluted in normal culture media. Cells were plated in 1.5 mL of 0.4% agarose diluted in normal culture media and the agarose was allowed

to set at room temperature for 1 hr. Samples were cultured for 4 weeks with 0.5 mL culture media added on top of the culture media with media exchanges every 2-3 days. After 4 weeks, samples were fixed in 10% formalin for 30 minutes and incubated in .005% crystal violet for 1 hr. Samples were rinsed in water until the washes were clear of stain. Images were acquired using a ChemiDoc XRS+ gel imager (BioRad) and associated software. Colonies were counted using ImageJ.

Orthotopic Breast Tumor Model – All procedures involving animals were approved by the University of York Ethical Review Process and under the authority of a UK Home Office project License. Six week old female $Rag2^{-/-}$, $Il2rg^{-/-}$ mice (Yorkshire Cancer Research Unit, University of York) were selected at random for MDA-MB-231 control or MDA-MB-231-IK injection. A 5×10^5 cell suspension was prepared in 20% v/v matrigel in saline and injected into the left inguinal mammary fat pad of isoflurane anaesthetized mice. A total of 14 and 11 mice were injected with MDA-MB-231 control and MDA-MB-231-IK cells respectively across 4 independent experiments. Tumors did not take in 3 of the control and 2 of the IK expressing mice and were not included in analysis giving n = 11 for MDA-MB-231 control and n = 9 for MDA-MB-231-IK. The length and width of primary tumors was measured

daily with calipers and the tumor volume was calculated as 0.5 x (length x width^2). Mice were euthanized 28 days after injection and tumors and lungs were fixed in 4% paraformaldehyde and frozen.

Statistics – Statistics were analyzed in Prism 5 and significance was determined using a two sample T-test or a one-way ANOVA followed by either a Dunett post test (to compare multiple conditions to a single control) or a Tukey post test (for a comparison of all conditions), alpha = .05. All results are presented as mean with standard deviation from 3 independent experiments unless otherwise noted.

V.4 Results

V.4.1 IK over-expression increases potassium current and hyperpolarizes V_{mem}

Both MCF-10A and MDA-MB-231 cells endogenously express low levels of IK. To modulate IK currents, a combination of genetic engineering and pharmacological approaches were used. A retroviral expression system was used to induce stable over-expression of IK with tagRFP as a marker. MCF-10A and MDA-MB-231 were infected with pMIG-RFP as a control and pMIG-IK and infected cells were

isolated using FACS to sort RFP positive cells. Because of the use of the P2A peptide bond-skip sequence, expression of RFP in pMIG-IK infected cells is expected to correlate with expression of IK. Cells infected with pMIG-IK were sorted a second time selecting for a narrower range of high RFP signal to isolate a more homogenous and highly expressing IK population. These populations are referred to as MCF-10A-IK and MDA-MB-231-IK. Increased mRNA expression was confirmed by RT-PCR (Figure 1A-B).

The electric current density and V_{mem} of individual cells was measured to assess changes in bioelectric properties induced by IK over-expression and activation with 1-EBIO. Electrophysiology recordings were acquired in the cell attached configuration using a perforated patch in order to best maintain the endogenous V_{mem}. In both MCF-10A-IK and MDA-MB-231-IK cells, current density during 1-EBIO treatment was greatly increased as compared to control cells (Figure 1C-D). The reversal potential was near -80 mV, the potassium reversal potential, indicating the current was comprised primarily of potassium flux.

IK over-expression hyperpolarized the V_{mem} of MCF-10A cells from -21 ± 6.3 mV in control cells to -47 ± 14.7 mV in MCF-10A-IK cells (Figure 1E). Application of 1-EBIO did not have a significant effect on MCF-10A control cells (-31 ± 7.4) but did induce a further

hyperpolarization of MCF-10A-IK cells to -69 ± 6.9 mV. Although the membrane potential of control cells was not significantly altered by 1-EBIO, fluctuations in the V_{mem} trace occurred at the time of 1-EBIO application indicating the presence of IK or small conductance calcium-activated potassium channels (SK) on the plasma membrane (data not shown). IK over-expression did not significantly alter the V_{mem} of MDA-MB-231 cells (control -26.3 ± 8.2 mV, MDA-MB-231-IK -33.5 ± 16.5 mV) (Figure 1F). Application of 1-EBIO hyperpolarized the V_{mem} of MDA-MB-231-IK to -73.9 ± -2.8 mV but did not significantly affect control cells (-40.3 ± 17.7 mV). However, as with MCF-10A, fluctuations in the V_{mem} trace occurred with 1-EBIO application indicating active IK or SK channels.

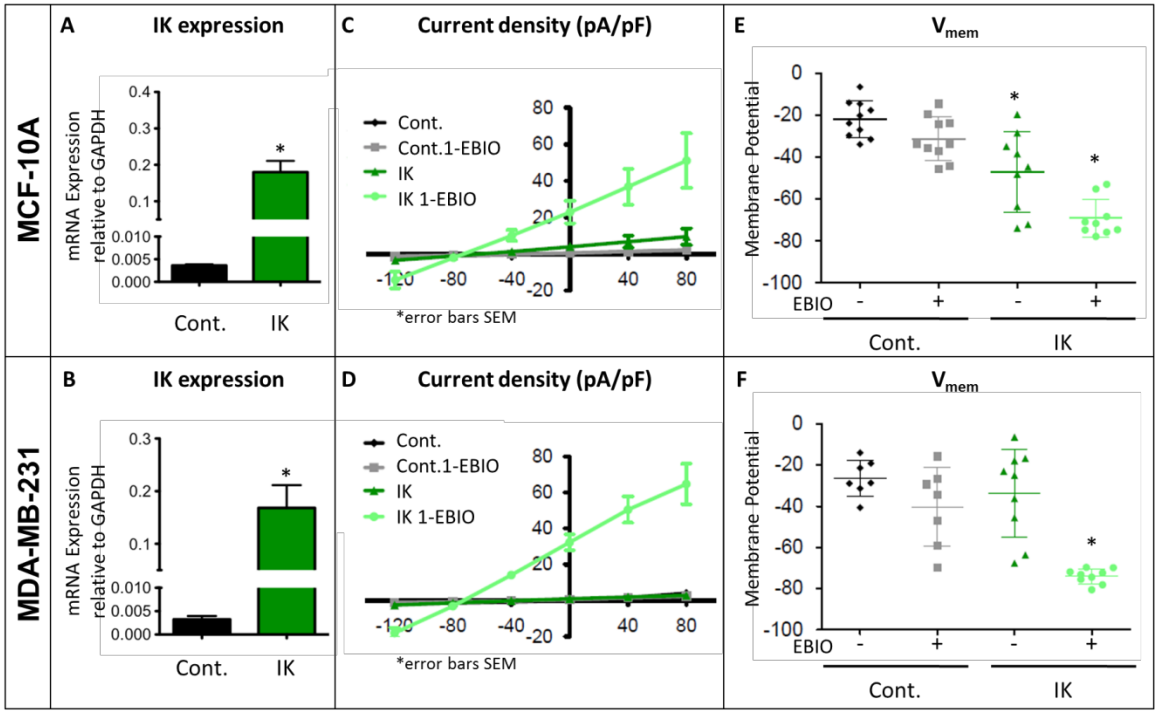

Figure V-1: Functional contribution of IK over-expression to current density and V_{mem}. (**A-B**) IK mRNA expression levels relative to GAPDH in total RNA collected from MCF-10A (A) or MDA-MB-231 (B) infected with pMIG-RFP (Cont.) or pMIG-IK (IK) and selected for RFP fluorescence by FACS. Data are presented as mean with standard deviation of 3 independent replicates, * significantly different from control (2 sample T-test, $p \leq .05$). (**C-D**) Endogenous and 1-EBIO induced current-voltage relationship in control and IK-expressing cells recorded in the cell attached perforated patch configuration from MCF-10A (C) and MDA-MB-231 (D) cells. Data are presented as mean with standard error of the mean from a minimum of 7 cell recordings. **(E-F**) V_{mem} averaged over 20 seconds from recordings of same cells as C and D. Data points represent individual cells, bars show mean with standard deviation, * indicates significantly different than vehicle treated control (One-way ANOVA with Tukey post test, alpha = .05).

V.4.2 MCF-10A Proliferation is Inhibited by 1-EBIO and Cells Accumulate in G2

Over-expression of IK without activation did not affect proliferation of MCF-10A or MDA-MB-231 cells (Figure 2A-B). Activation of IK by 1-EBIO treatment significantly decreased proliferation of both MCF-10A control and IK expressing cells with a larger effect seen in the IK expressing cells. 1-EBIO treatment had no effect on proliferation of MDA-MB-231 control or IK expressing cells. Decreased proliferation could be due to a decrease in the rate of proliferation or an increase in apoptosis and cell death. Cells were cultured for 24 hours in 1-EBIO or DMSO vehicle control and stained with Annexin-V antibody, a marker of apoptosis, and violet dead cell

stain. FACS was used to quantify the percentage of labeled cells. There was no significant difference in the percentage of apoptotic or dead cells across all cell conditions for both MCF-10A and MDA-MB-231 cells (Figure 2C-D). Cell cycle analysis was performed on the same samples by staining with propidium iodide. 1-EBIO treatment increased the percentage of MCF-10A control and IK cells in the G2 phase from 14.80% ± 3.71 in control and 16.08% ± 2.18 in MCF-10A-IK vehicle treated cells to 18.48% ± 3.27 in MCF-10A control and 21.4% ± 5.1 in MCF-10A-IK cells (Figure 2E). No significant differences were found in any of the conditions for MDA-MB-231 cells (Figure 2F).

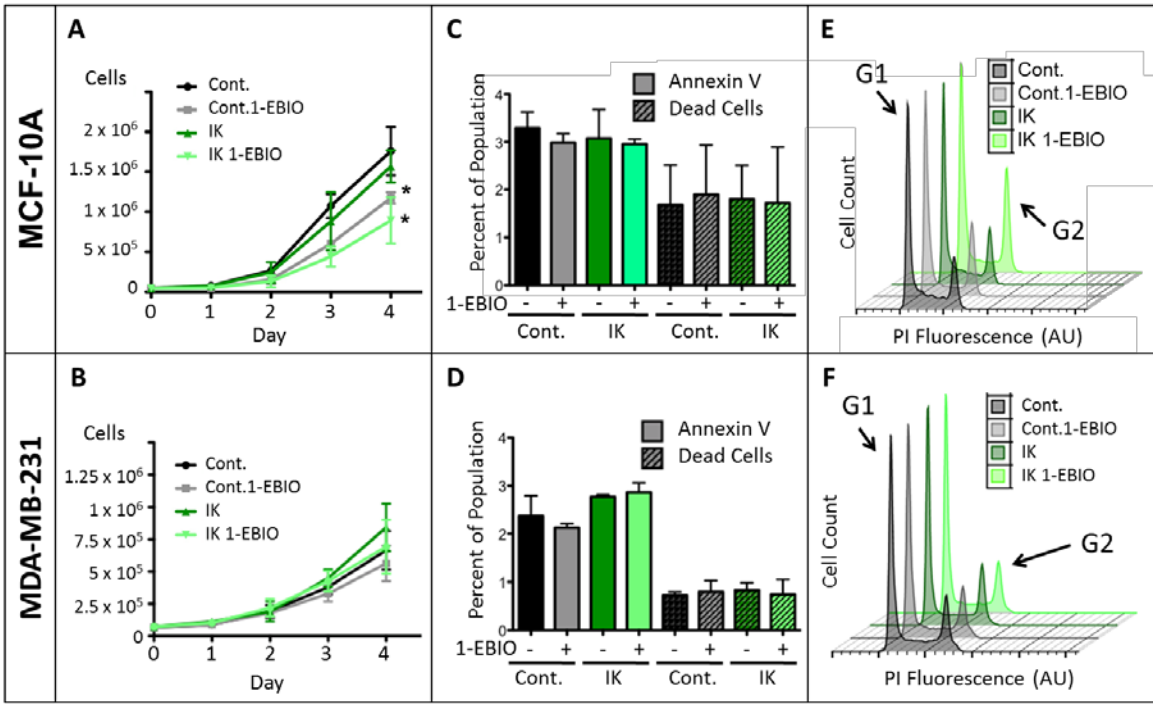

Figure V-2: 1-EBIO Treatment Decreased MCF-10A Proliferation and Increased G2 Phase Accumulation But Had No Effect on MDA-MB-231. (A-B) Control and IK over-expressing MCF-10A (A) and MDA-MB-231 (B) proliferation was quantified over 4 days for cells

treated with vehicle control or 1-EBIO. **(C-D**) Cells were treated with vehicle control or 1-EBIO for 24 hrs, stained with anti-annexin-V antibody and violet dead stain, and analyzed by flow cytometry to quantify the percentage of positively stained cells. Data presented as mean with standard deviation of three independent replicates, * indicates significantly different than vehicle treated control (One-way ANOVA with Tukey post test, alpha = .05). **(E-F)** Plot of cell count verses propidium iodide (PI) fluorescence of same treatment as B-C to analyze cell cycle. Arrow marks fluorescence intensity corresponding to G2 phase. Plot is representative of three independent replicates.

V.4.3 Invasion but not Migration is decreased by expression and activation of IK in MCF-10A cells

Migration was assayed by scraping a confluent layer of serum starved cells and quantifying the decrease in wound surface area over time. Neither MCF-10A nor MDA-MB-231 migration was affected by IK expression or activation (Figure 3A-B).

Matrigel-coated transwell inserts were used to assess invasive capabilities. MDA-MB-231 are much more invasive than MCF-10A and thus a lower cell density and shorter incubation time was used. Activation of IK with 1-EBIO significantly decreased invasion of MCF-10A control and MCF-10A-IK cells with a larger effect observed in MCF-10A-IK (Figure 3C). IK over-expression was sufficient to decrease MCF-10A invasion and caused a similar decrease as 1-EBIO treatment

of MCF-10A control cells. Neither IK over-expression nor activation had a significant effect on MDA-MB-231 cells (Figure 3D).

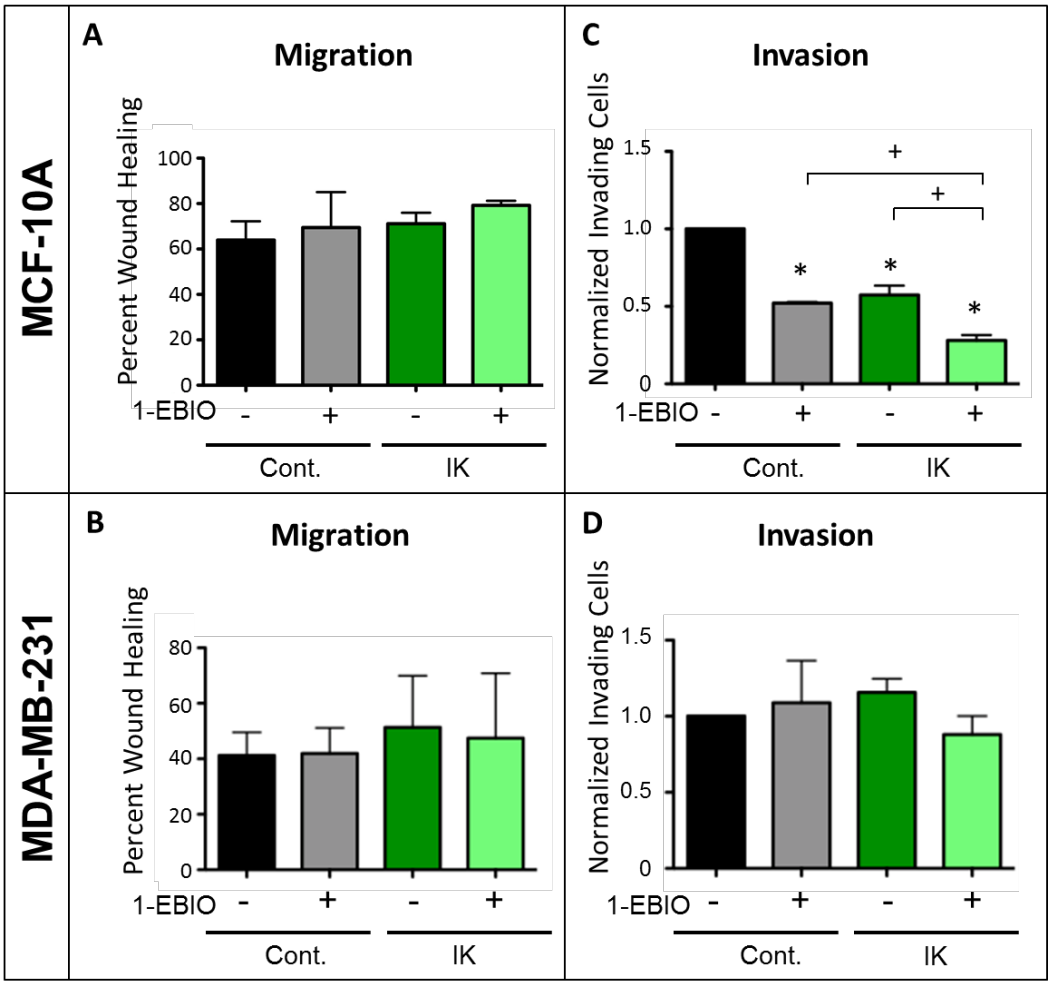

Figure V-3: IK Decreases Invasion of MCF-10A But Not MDA-MB-231 and Does Not Affect Migration. (A-B) Healing of a scratch wound after 12 hrs for MCF-10A (A) and 10 hrs for MDA-MB-231 (B) treated with vehicle control or 1-EBIO. **(C-D)** Invasion through matrigel coated transwell after 24 hrs using horse serum and EGF as a chemoattractant for MCF-10A cells (C) or after 16 hrs using FBS as a chemoattractant for MDA-MB-231 (D). Average number of cells per field of view with 4 fields of view per sample and 4 replicates in each of 3 independent experiments. Data presented as mean with standard deviation of three independent replicates, * indicates significantly

different than vehicle treated control, + indicates significant difference between indicated samples (One-way ANOVA with Tukey post test, alpha = .05).

V.4.4 1-EBIO Treatment Increases MCF-10A Control and MCF-10A-IK Spheroid Sized

MCF-10A and MCF-10A-IK cells were cultured in 3D embedded in matrigel with or without 1-EBIO treatment to interrogate changes in growth inhibition and cell organization. Across all conditions, cells formed sphere-shaped acinar structures with clearly defined borders (Figure 4A). Quantification of spheroid size revealed that 1-EBIO treatment caused a similar increase in size of both cell lines (Figure 4B).

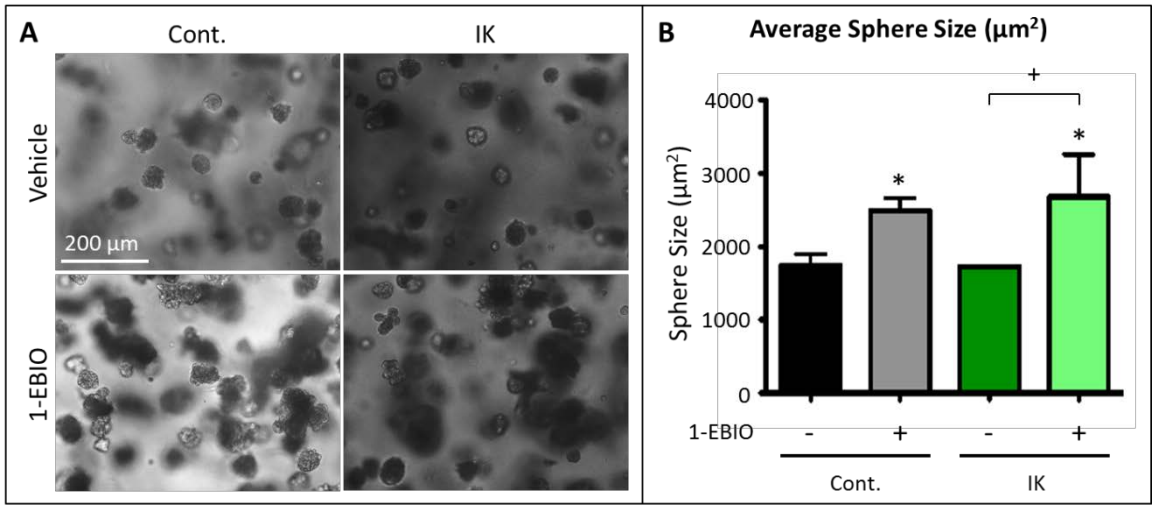

Figure V-4: MCF-10A Spheroid Size Increased by 1-EBIO Treatment. (A) Bright field images of whole mount carmine stained

MCF-10A control and MCF-10A-IK cells cultured in 3D embedded in matrigel for 14 days and treated with vehicle control or 1-EBIO. **(B)** Quantification of average spheroid size from A. Data presented as mean with standard deviation of three independent replicates, * indicates significantly different than vehicle treated control, + indicates significant difference between indicated samples (One-way ANOVA with Tukey post test, alpha = .05).

V.4.5 IK Over-expression and Activation Decreases Colony Formation of MDA-MB-231 Cells

The ability to form colonies in soft agar is used as an *in vitro* measure of transformation and tumor forming ability. MCF-10A is an immortal but not transformed cell line and is unable to form colonies in soft agarose. Inducing expression of oncogenes such as c-MYC or RAS can confer colony forming ability which coincides with tumor formation in mouse xenografts demonstrating the capacity of this assay to assess conversion to a malignant phenotype (Ciardiello et al., 1990). MCF-10A control and MCF-10A-IK cells were not able to form colonies with or without 1-EBIO treatment (data not shown).

MDA-MB-231 cells are highly malignant and therefore readily form colonies. Colony formation was decreased in IK expressing cells and was further decreased by 1-EBIO treatment (Figure 5A-B). 1-EBIO induced a similar decrease in colony formation of control and MDA-MB-231-IK cells.

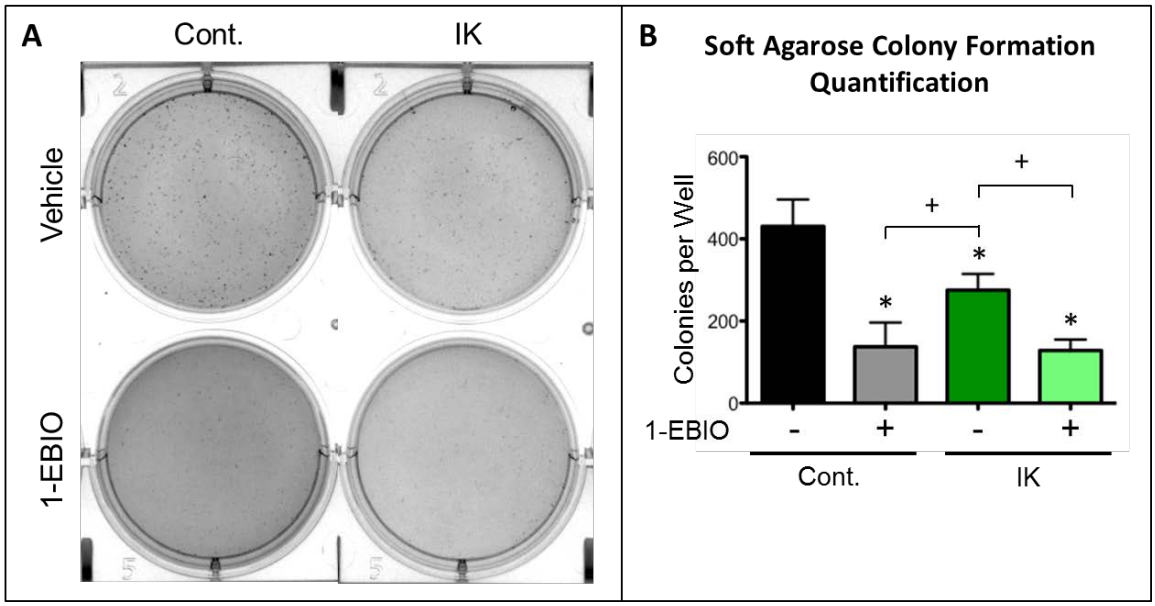

Figure V-5: MDA-MB-231 Soft Agarose Colony Formation Decreased By Both IK Expression and IK Activation. (A) Bright field images of crystal violet stained MDA-MB-231 control and MDA-MB-231-IK cells grown in soft agarose and treated with vehicle control or 1-EBIO for 28 days. **(B)** Quantification of colonies from A. Data presented as mean with standard deviation of three independent replicates, * indicates significantly different than vehicle treated control, + significant difference between indicated samples (One-way ANOVA with Tukey post test, alpha = .05).

V.4.6 IK Expression Increases MDA-MB-231 Primary Tumor Growth

To assess the effect of IK expression on *in vivo* tumor growth and metastasis, MDA-MB-231 control and MDA-MB-231-IK cells were injected into the mammary fat pad of 6 wk old female mice. Caliper

measurements of the size of the primary tumor were used to estimate the tumor volume over 4 wks of tumor growth. Primary tumor growth was increased in MDA-MB-231-IK tumors with a significant increase in size beginning 17 days post cell injection (Figure 6A). Lungs were sectioned and stained with human antigen antibody and the number of metastasizing cells was quantified. There was a greater number of metastasizing cells/mm^2 in MDA-MB-231-IK injected mice than control but this difference was not statistically different (p = .13 by two sample T-test). (Mouse experiments were performed in Will Brackenbury's lab at the University of York (Heslington, UK) by Michaela Nelson and Crystal Frost).

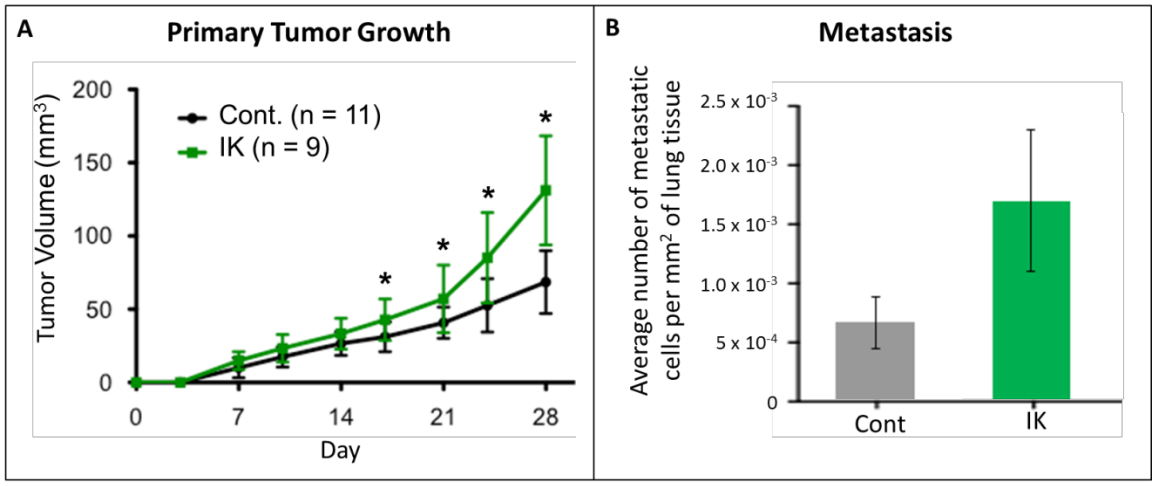

Figure V-6: IK expression increases *in vivo* tumor growth of MDA-MB-231. (A) MDA-MB-231 control (n = 11) and MDA-MB-231-IK (n = 9) cells were injected into the inguinal mammary fat pad of 6 wk old female mice and tumor size was plotted over time. Data presented as mean with standard deviation, samples were significantly different beginning at day 17 and continuing through day 28 (two

sample T-test, $p \leq .05$). **(B)** Lung tissue sections from mice in A were stained with anti-human antigen antibody and the number of positively stained cells was quantified as a measure of metastasis. Data are mean with standard error of the mean of 3 sections per mouse with 4 mice per condition. A two-sample T test gave a p-value of 0.13. Experiments performed and data provided by Michaela Nelson, Crystal Frost and Will Brackenbury (University of York, Heslington, UK).

V.5 Analysis

This study is the first to identify differences in behavioral response to IK activation between tumorigenic and non-tumorigenic cells. Furthermore, there was no significant change in MDA-MB-231 proliferation in response to IK activation, which is in contrast to the previously reported increased proliferation of prostate cancer cell lines. These results suggest important differences exist in the signaling networks downstream of IK activation between healthy and cancerous cells and also within different cancer types.

Functional over-expression of IK was demonstrated in both MCF-10A and MDA-MB-231 by an increase in potassium current and hyperpolarization of V_{mem} with 1-EBIO agonist treatment. 1-EBIO treatment of IK expressing cells had a larger effect on MDA-MB-231 V_{mem} than MCF-10A. Given that the induced IK expression levels were relatively similar, this suggests either a difference in post-translational

regulation, or that compensatory currents such as Cl^- efflux are induced in MCF-10A.

Neither IK over-expression nor activation with 1-EBIO caused a change in MDA-MB-231 proliferation. This is in contrast to increased proliferation seen in prostate cancer cells treated with 1-EBIO suggesting the mechanism downstream of IK activation may not be conserved across cancer types. Proliferation of the non-tumorigenic cell line MCF-10A was decreased by IK activation in both control and IK over-expressing cells but not by IK over-expression alone. There was no change in apoptosis or cell death suggesting the diminished proliferation was due to a decrease in the rate of cell division. Changes in potassium channel activity and V_{mem} are associated with progression through check points of the cell cycle. Activation of IK may prevent depolarization during late G2 and progression to mitosis. MCF-10A control and IK over-expressing cells treated with 1-EBIO had a significant increase in the percentage of cells in G2 while IK over-expression alone had no effect on cell cycle distribution. Thus, accumulation in G2 mirrors the decrease in proliferation suggesting constant IK activation decreases proliferation of MCF-10A by inhibiting progression from G2 to mitosis. It is important to note that 1-EBIO also activates the closely related potassium channel the small conductance calcium-activated potassium channel (SK) and effects

may be partially mediated by SK activation. Further investigation is needed to determine if G2 accumulation is due to hyperpolarization specifically. Cells could be cultured in high potassium media to inhibit the hyperpolarizing effect of IK activation to assess if hyperpolarization is required to decrease proliferation. The different response seen between MDA-MB-231 and MCF-10A cells suggests the cell lines may have different bioelectric profiles that have altered sensitivity to bioelectric events.

Migration was unaffected by IK over-expression and activation in both MCF-10A and MDA-MB-231 cells suggesting IK activity is insufficient to drive migration. Prior studies have reported that IK inhibition decreases migration and have supported a role for activation of IK specifically on the lagging edge. Activation lacking spatial regulation, such as occurs with addition of agonist to the media, may have counteracting effects. The effect of increased IK expression on spatially restricted activation is not known. Activation of IK has been reported to increase intracellular calcium (Lallet-Daher et al., 2009), allowing for the possibility of a positive feed-back loop whereby activation of some channels increases intracellular calcium which activates additional channels. High expression of IK could increase positive feedback mechanisms and cause spatially restricted signals to be propagated to larger portions or the entire cell. Future experiments

could investigate the effect of IK activation exclusively on the lagging edge to determine if spatially restricted activation is sufficient to increase migration.

IK expression and activation decreased invasion through matrigel of MCF-10A but not MDA-MB-231 cells. This effect was most pronounced in IK over-expressing cells treated with agonist and thus the degree to which invasion was inhibited correlated with the level of IK activity. Given that there was no change in MCF10A migration, the decreased invasion is likely related to either an inability to degrade the ECM or dysregulation of volume control preventing volume reduction required to pass through the pores in the membrane. To distinguish these two possibilities, future studies could assess the effect of IK expression and activation on MCF-10A migration across uncoated transwell membranes to specifically isolate the requirement for regulated volume reduction.

The contrasting behavioral response between MCF-10A and MDA-MB-231 suggests there are distinctive downstream signaling mechanisms. Transduction of IK signaling may occur through binding partners and other closely associated proteins that differ between the two cell types. IK signaling is dependent on interactions with beta-1-integrin and TRP member calcium channels in other cell types (Girault et al., 2015; Lallet-Daher et al., 2009). Little is known about variability

of associated proteins and how it affects behavioral response. There are many members within the TRP calcium channel family and unique activation properties may cause IK association with different members to alter calcium entry and downstream signaling. Analysis of behavioral response to IK signaling in additional cell lines and primary cells is needed to determine if the divergent response reported in this study is characteristic of healthy and cancerous cells and if it can be utilized to specifically target one population.

Surprisingly, despite the decreased proliferation in 2D, 3D spheroid structures of MCF-10A control and IK over-expressing cells treated with 1-EBIO were larger in size than untreated controls. Given that potassium current is associated with cell volume decrease, the phenotype is unlikely to be due to an increase of individual cell size and instead is likely due to an increased number of cells per spheroid. In the spheroid assay, healthy cells respond to growth inhibitory signaling and an increase in cell number is indicative of hyperplasia. Characterization of the spheroids to determine if there is increased lumen filling or a loss of apical-basal polarity would provide further evidence of neoplastic phenotypes.

MDA-MB-231 colony formation in soft agarose was decreased by IK over-expression and further decreased by activation with 1-EBIO. Interestingly, 1-EBIO caused a similar decrease of control and IK over-

expressing cells. Electrophysiology demonstrated that IK over-expressing cells have much higher potassium currents in response to 1-EBIO. Thus, this result suggests continuous activation of IK is more detrimental to colony formation than increased potassium current during transient endogenous IK activation. The dramatic decrease in colony formation was not expected given that proliferation, migration, and invasion were all unaffected by IK over-expression and activation. One possible explanation is that decreased colony formation may be an artifact of attachment-free conditions. IK activation is expected to induce cell volume decrease due to the efflux of potassium ions and constant activation by 1-EBIO may have an extreme effect. In attachment conditions, cells may be able to maintain a minimal critical volume by using support from cytoskeleton attachments. However, in the soft agarose assay cells are not able to form any attachments to the surrounding material and may lose the ability to maintain a critical volume.

In support of the initial hypothesis that increased IK activity promotes cancer progression, *in vivo* primary tumor growth of MDA-MB-231 was increased by IK over-expression. Additionally, preliminary results suggest IK over-expression increased the number of cells metastasizing to the lung, although this increase is currently not statistically significant. The *in vivo* data is in contrast to the effect of

IK over-expression on *in vitro* proliferation and aggressive behaviors. While there was no significant effect on MDA-MB-231 proliferation, migration, or invasion, it is interesting to note that there was a trend of MDA-MB-231-IK having the highest value in each assay. It is possible that IK over-expression results in a small increase of each process that is challenging to detect within the inherent variability of the assays. But *in vivo* where the effect of all of these processes is combined during tumor growth, the overall effect is amplified and becomes significant. Alternatively, the opposing *in vitro* and *in vivo* results could reflect a requirement for signaling from the surrounding microenvironment. Growth promoting effects of IK signaling may require highly specialized spatio-temporal activation that is not recapitulated *in vitro*. Signaling may be initiated by interactions with stromal cell types, activation of specific adhesion molecules, or microenvironmental factors such as hypoxia or inflammatory cytokines. Investigation of tumor histology may provide clues as to how IK is promoting tumor growth and metastasis and which microenvironmental factors play a role.

This study investigated the possibility that the cancer associated ion channel IK is sufficient to promote cancer progression. Ion channels are an intriguing potential mechanism of metastasis initiation as they are highly sensitive to microenvironmental factors and

therefore could explain why only a small percentage of syngeneic cells go on to form metastasis. The results of this study support the ability of IK to increase aggression of already transformed cancer cells and possibly to promote over-growth of non-tumorigenic cells. The ability of IK to promote tumor growth and likely metastasis *in vivo* points to the potential of IK signaling inhibitory drugs to decrease cancer progression. Furthermore, the opposing behavioral response between cancerous MDA-MB-231 and non-tumorigenic MCF-10A cell lines suggests there may be unique mechanisms that could be targeted to make drugs cancer-specific to minimize toxic side effects on healthy cells.

Chapter VI: Discussion

The flow of ions as a signaling mechanism, other than calcium ions, is rarely considered outside of excitable cell types. My studies investigating bioelectric signaling in human mesenchymal stem cell (hMSC) differentiation and breast cancer progression support a growing body of work demonstrating the broad impact of bioelectricity on a variety of cell behaviors. The results suggest transduction mechanisms with sophisticated downstream network pathways that enable differential responses depending on the duration and intensity of the bioelectric cue as well as the cell type and environmental factors.

VI.1 Technical Challenges to Studying Bioelectricity

A major challenge in the field of bioelectricity is finding methods that accurately measure ion currents and the membrane potential (V_{mem}). Electrophysiology recordings are considered the gold standard but also suffer from drawbacks particularly for measuring the endogenous V_{mem}. V_{mem} is dependent on intra- and extracellular ion concentrations and thus the choice of bath and electrode solutions effect the measurement. In addition, the bath solution must be free of proteins and thus any ion channels responsive to growth factors, of

which there are many, will have altered activity compared to what occurs *in vivo*. Finally, the process of forming the seal and gaining access to the cell may induce a mechano-sensation response or cause damage to the cell membrane altering V_{mem}. The major benefit of electrophysiology is that it has a very good signal to noise ratio and thus it has remained the most trusted method. To circumvent the deficiencies, bath and electrode solutions are chosen that best replicate endogenous ion concentrations and recordings are taken from many cells. Recordings from cells cultured *in vitro* can also be corroborated with recordings from tissue slices which are likely more reflective of true endogenous V_{mem} because cells maintain cell-cell and cell-ECM connections.

Voltage-sensitive dyes are also used to measure V_{mem}, particularly to assess variability within a population as it is much higher throughput than electrophysiology. However, most of the dyes have a low signal to noise ratio and are difficult to calibrate to enable quantitative measures. Furthermore, the dyes are often responsive to factors unrelated to membrane potential including cell membrane composition, aromatic compounds, and dimethyl sulfoxide (DMSO), a common drug vehicle solvent. More recently voltage-sensitive fluorescent proteins that function via a fluorescence resonance energy transfer (FRET) mechanism have been developed. The proteins contain

two fluorescent domains separated by a voltage-sensitive domain. A change in V_{mem} causes a conformational change in the voltage-sensitive domain and the fluorescent domains to move closer or further from one another altering the FRET signal. The fluorescent protein based systems allows for much longer term measurement than fluorescent dyes or electrophysiology. However, the signal to noise is similar to voltage-sensitive dyes and thus it is challenging to use for small changes in V_{mem} and for quantitative measurement.

An additional challenge to studying V_{mem} is determining methods that reproducibly modulate individual bioelectric characteristics. Altering extracellular ion concentrations, genetically modifying cells to change ion channel expression, and treating cells with ion channel agonists and antagonists can be used individually or in combination to adjust bioelectric properties. Changing extracellular ion concentrations is the simplest method but it is challenging to predict the exact effect on bioelectricity and the artificial environment may have biologically irrelevant effects. Using pharmacological agents to regulate channel activity can be used to induce very specific modulations, as long as expression of the target channel can be verified. Both extracellular ion concentrations and pharmacological agents allow temporal control as the cell media can be exchanged or perfused as desired.

Genetic engineering to alter ion channel expression allows the greatest diversity of bioelectric modulation as well as high specificity. Channel function after over-expression must be confirmed as proper localization may not occur in all cell types and some channels may require additional binding partners to function. Additionally, issues can arise from toxicity either from loss of important housekeeping functions or gain of detrimental ion flows. Most genetic techniques do not allow for temporal regulation unless combined with the use of inhibitors and activators.

IV.2 Isolating signaling from specific bioelectric properties

Ion channel currents are highly interdependent such that a change in one bioelectric property is likely to induce reciprocal effects in other properties. A change in any ion flow will alter V_{mem} and thereby change the driving force on all other ions. The change in V_{mem} may also activate voltage-gated channels inducing large ion flows and changing the relative ion permeability which further alters V_{mem}. Thus, it can be challenging to predict the overall effect of a single bioelectric signal as well as separate the effect of the initial signal from secondary effects.

In particular, it can be challenging to disentangle the role of calcium signaling from calcium independent responses. Multiple studies have shown that a change in V_{mem} is sufficient to alter intracellular calcium concentrations because of the change on the driving force of calcium through open calcium channels (Lallet-Daher et al., 2009; Zhou et al., 2015). Careful study under conditions that regulate calcium flux are then needed to determine whether downstream behavioral responses are dependent on calcium signaling or a separate mechanism related to the initial ion flux. For example, studies could be performed in low calcium media with the expectation that if the downstream effect is calcium-independent low calcium media will cause no change in the cell behavior. It is possible that many downstream responses have been incorrectly attributed to altered calcium flux and that direct mechanisms of sensing the flow of other ions or a change in V_{mem} have been overlooked.

Similarly, it is difficult to separate the effect of individual ion fluxes from the effect of V_{mem}. Attempts can be made to induce additional bioelectric signals that compensate for the altered V_{mem} and return it to the initial level, but such precise control of V_{mem} is challenging and may have unintended repercussions. Furthermore, many bioelectric signaling mechanisms involve highly localized response that may not be targeted by global modulation.

VI.3 The model that V_{mem} acts as a rheostat to instruct differentiation is overly simplistic

Changes in the V_{mem} may act as an instructive regulatory signal. When meta-analysis of V_{mem} from many different cell types revealed a trend wherein less proliferative and more differentiated cells are more hyperpolarized while more proliferative and stem-like cells are depolarized. The trend appears to be consistent across multiple studies, however, care must be taken not to over-interpret comparisons between studies as different recording conditions may alter measurements. This data raised the question of whether V_{mem} plays an instructive role in directing differentiation. A previous study from our group supported the hypothesis that V_{mem} does play an instructive role in differentiation and that exogenous modulation could promote or inhibit differentiation. We were next interested to test the model that V_{mem} instructed differentiation by a rheostat model whereby setting the V_{mem} to a specific range would induce differentiation for a particular cell type. However, the results of interrogating hMSC differentiation by numerous methods of modulating V_{mem} do not support this simplistic mechanism.

The V_{mem} of hMSCs was modulated by altering extracellular ion concentrations, treating cells with channel activators or inhibitors, and/or inducing ion channel over-expression (Chapter 2). Multiple treatments caused decreased osteogenic differentiation, however the treatments included both depolarizing and hyperpolarizing conditions and thus do not support the simple model that hyperpolarization increases and depolarization decreases differentiation. Furthermore, none of the treatments reproducibly increased differentiation. Treatment with the transient receptor potential cation channel subfamily V, member 1 (TRPV1) antagonist capsazepine increased mineralization of primary cells from one donor but not a second donor and did not increase other bone differentiation markers. This response was likely due to a direct effect on intracellular calcium concentration, which is critical to mineralization, and not an overall effect on osteogenic differentiation pathways. The inability to reproducibly increase osteogenic differentiation pathways despite multiple methods of V_{mem} modulation suggests stable alteration of V_{mem} is not sufficient to drive differentiation pathways.

Many of the treatments, including growth in high potassium and GlyR expression, caused a decrease in cell proliferation and cell metabolism. This may suggest that holding V_{mem} to a specific level, either hyperpolarizing or depolarizing, is detrimental to overall cell

health. This may be because holding V_{mem} to a specific level prohibits the fluctuations in V_{mem} need for progression through the cell cycle. Furthermore, it implies the observed decrease in osteogenic differentiation may have been due to a decrease in cell viability and not a direct signaling effect of V_{mem} modulation.

If V_{mem} has an instructive role in differentiation, it is likely far more complex than a simple rheostat model. V_{mem} is known to fluctuate during the cell cycle and it is unknown how cells could distinguish between these shifts and additional V_{mem} signals (Huang and Jan, 2014; Ouadid-Ahidouch et al., 2004a; Urrego et al., 2014). Further characterization of endogenous V_{mem} dynamics during the cell cycle and differentiation is needed to construct a model that more accurately reflects the true complexity of V_{mem} dynamics. Much of the current data on V_{mem} during these processes is undermined by artifacts introduced by the method of measuring V_{mem}. The study reporting that V_{mem} was significantly different between osteogenic and adipogenic differentiated hMSCs utilized a fluorescent dye that is sensitive to V_{mem} but also to the lipid environment (Sundelacruz et al., 2008). The signal from the dye is therefore likely affected by lipid droplets present in adipocytes. Indeed, the reported V_{mem} of differentiated adipocytes was -120.7 mV (± 4.8), well below the reversal potential of any major ion and therefore unlikely to be accurate. Quantification of V_{mem} with an

alternative method, such as electrophysiology, is needed to more accurately measure the V_{mem} of differentiated cell types and to determine if there are significant differences. Electrophysiology also suffers from unintended artifacts including alteration of ion concentrations and growth factor exposure in comparison to native conditions. In order to best characterize V_{mem}, multiple methods of quantification should be used to verify findings. Additionally, measuring V_{mem} from tissue slices will likely more accurately reflect endogenous levels. Tissue slices also allow for direct comparison of multiple cell types recorded in the same conditions, removing extraneous variables induced by *in vitro* culture. Many differentiation processes closely correlate with proliferation and few studies have adequately separated the influence of the cell cycle on V_{mem} to validate differentiation-specific V_{mem} regulation. Better characterization of V_{mem} during differentiation with simultaneous analysis of cell cycle phase is needed in order to distinguish V_{mem} changes that are associated with differentiation verses the fluctuations that occur with the cell cycle.

VI.4 Activity of specific ion channels rather than fluctuations in V_{mem} is more likely to be responsible for cancer progression

Cancer cells are generally more depolarized than their healthy counterparts and it has been suggested that depolarization may be sufficient to promote cancer progression. Increased expression and activity of numerous ion channels is also associated with cancer progression. Paradoxically, some of the cancer associated ion channels are hyperpolarizing and thus would antagonize V_{mem} driven signaling. The results of my studies are more supportive of a role for specific ion channels directing cancer progression than signaling initiated by depolarization of V_{mem}.

Two breast epithelial cell lines were investigated for aggressive phenotypes, the highly metastatic MDA-MB-231 cell line and the non-tumorigenic MCF-10A cell line. Interestingly, despite the polarized behavior of the two cell lines including a mesenchymal vs epithelial phenotype and large difference in invasive capabilities, both were found to have a similar V_{mem}. This finding may indicate that V_{mem} is more indicative of proliferation rate than other characteristics as the proliferation rate of the two cell lines was similar. A previous study reported a 6.3 mV depolarization in the highly metastatic cell line MDA-435-L2 as compared to MCF-10A using microelectrode recordings (Marino et al., 1994). This difference was quite small in relation to V_{mem} variation (reported as roughly 4 mV within single recordings) as well as the dynamic range of V_{mem} which is about 100 mV. Taken

together, these results suggest that if V_{mem} does play a role instructing cancer cell behaviors, the signal must be more complex than simply the average resting V_{mem}.

MCF-10A cells did not gain cancer-associated behaviors in response to alterations in V_{mem}. The morphology of MCF-10A grown embedded in matrigel became more invasive-like in depolarizing high extracellular potassium conditions, but this phenotype could not be replicated by alternative methods of depolarization. In standard conditions, MCF-10A formed round structures with a clear and smooth border. A concentration dependent increase in branching and structures with cell projections occurred with culture in high potassium media suggesting the possibility that depolarization is sufficient to promote invasive behaviors (Chapter 3). However, induced expression of ion channels predicted to also cause depolarization had no effect on morphology, implying that the high potassium phenotype is due to alterations in potassium specifically and not to the global effect of V_{mem} (Chapter 4). Additionally, expression of ion channels expected to alter V_{mem} did not induce changes in cell migration or invasion that corresponded to the expected V_{mem} shift. Expression of one hyperpolarizing channel, the intermediate conductance calcium-activated potassium channel (IK), decreased invasion but other

hyperpolarizing mechanisms including expression of another potassium channel Kir2.1 had no effect (Chapter 5).

Furthermore, hyperpolarization of the highly aggressive MDA-MB-231 had no effect on *in vitro* measures of cell aggression (Chapter 5). Treatment of IK over-expressing MDA-MB-231 with the IK agonist 1-EBIO lead to dramatic and consistent hyperpolarization to -73.9 mV ± 2.8. Interestingly, this had no effect on proliferation, migration, or invasion *in vitro*. This suggests that depolarization is not required for maintenance of aggressive cancer behaviors.

Increasing evidence is emerging linking individual ion channels over-expressed in cancer to downstream behaviors via specific binding partners suggesting the mechanism is dependent on the individual channel and not the net ion flux. The voltage-gated sodium channel (VGSC) $Na_V1.5$ is over-expressed in many cancers and inhibition causes decreased invasion and metastasis (Brackenbury et al., 2007; Fraser et al., 2005). In breast cancer, Nav1.5 activity was required for proton efflux through sodium hydrogen exchanger 1 (NHE1) and inhibition of either channel lead to a similar decrease in invasion with no additive effect (Brisson et al., 2011). Knock down of $Na_V1.5$ results in differential gene expression suggesting it regulates transcription proposed to be via its interaction with the β1 VGSC subunit (Brackenbury and Isom, 2011; House et al., 2010). These studies

point towards the importance of activation of specific interacting partners that may not be recapitulated by increasing sodium flux via alternative channels or perhaps even other VGSC family members.

Alterations in cell behavior in response to modulation of IK activity are dependent on specific calcium channels in prostate cancer and alveolar epithelial cells. In prostate cancer, siRNA knock down of the calcium channel transient receptor potential cation channel subfamily V, member 6 (TRPV6) completely abrogated proliferation induced by IK activation with no additional inhibition caused by co-knockdown of IK (Lallet-Daher et al., 2009). TRPV6 and IK were co-immunoprecipitated demonstrating a close physical interaction. A similar relationship was found between IK and a closely related calcium channel - transient receptor potential cation channel, member 4 (TRPC4) in alveolar epithelial cells (Girault et al., 2015). Both studies support a mechanism whereby IK activation increases calcium entry through a closely associated calcium channel. It is interesting that in both cases IK was primarily dependent on a single calcium channel but that the channel differed in the two cell types. Regulation of the specific IK-associated calcium channel family member may act as an important control mechanism of downstream response. Additionally, in alveolar epithelial cells IK co-immunoprecipitated with beta-1-integrin and endogenous IK activity was dependent on beta-1-integrin

activation. Combined, the results from these studies strongly implicate response from closely localized specific binding partners to the downstream mechanism of IK signaling. The cell response is therefore specific to activation of a particular ion channel and can not be reproduced by exogenous addition of ion current or modulation of V_{mem} through alternative mechanisms.

VI.5 Future Directions

The growing field of bioelectricity has demonstrated that bioelectric signals are an important mechanism by which cells interact with their surroundings and respond with changes in cell behavior, much like signaling from growth factors, the ECM, and mechanical sensation. Traditionally, the roles of signaling mechanisms have been elucidated by modulating the signal and characterizing the change in cell behavior and downstream molecular pathways. However, this approach has been challenging in bioelectricity because it is difficult to predict and induce specific alterations to bioelectric parameters and because bioelectric properties are interdependent and can not be altered in isolation. Thus, the vast majority of studies to date have focused on the role of individual ion channels, which is easier to assess but often does not answer the question of whether the downstream

effect is dependent on the ion flux per se or a non-conducting mechanism of the individual channel.

Due to the difficulty specifically modulating bioelectricity, future studies should focus on characterizing endogenous bioelectric events. A better understanding of bioelectric changes that occur during development, wound healing, and disease will allow for more accurate predictions of potential signaling mechanisms and rational design of experiments to test those predictions. Studies of endogenous signaling should also attempt to characterize multiple parameters simultaneously. The cell cycle is associated with many bioelectric fluctuations and much of the current literature may have attributed bioelectric events to other cell behaviors that are actually dependent on the cell cycle.

Imaging techniques are constantly improving with new fluorescent responsive probes, methods that allow imaging deeper within tissues, and the ability to image live samples for longer time periods. Fluorescent reporters now exist that can indicate the phase of the cell cycle, V_{mem}, intracellular calcium concentration, intracellular sodium concentration, and intracellular pH in live cells. Studies using combinations of reporters over long time periods will be able to specifically link bioelectric events to downstream cell behaviors and distinguish the influence of multiple bioelectric properties by

comparing the responses of many cells. For example, invasion could be assessed with fluorescent reporters of cell cycle phase and V_{mem} to determine whether the depolarization found in aggressive cancers correlates more closely with proliferative cells or with highly invasive cells (Figure 1). An intracellular calcium dye could also be added to further determine how intracellular calcium correlates with V_{mem} and invasion to suggest whether calcium signaling is required as part of the signaling mechanism. In this way, characterization without the need for modulation of bioelectricity would greatly increase our understanding of the specific roles of bioelectric signaling in cell behaviors.

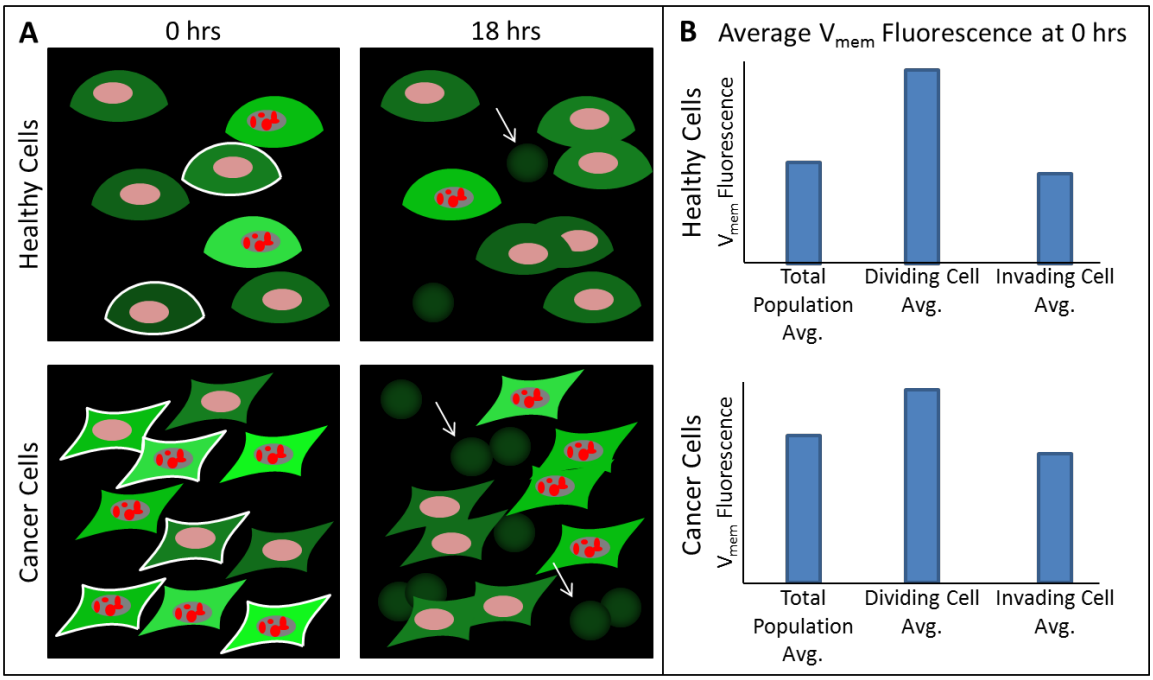

Figure VI-1: Hypothetical experiment characterizing cell proliferation and V_{mem} simultaneously during an invasion assay. Results depict a scenario where depolarization appears to correlate with invasion but individual cell analysis combined with simultaneous analysis of proliferation reveals depolarization is an effect of increased proliferation and does not correlate with invasion. **(A)** Healthy and cancerous cells labeled with V_{mem} sensitive probe (brighter green indicates depolarized) and fluorescent histone tag (red) imaged at 0 hrs and 18 hrs of an invasion assay. Punctate red staining indicates proliferating cells. Arrows mark example invading cells that are no longer in focus. Cells that invaded at 18 hrs are outlined in white at 0 hrs. **(B)** Quantification of average V_{mem} signal at 0 hrs (higher signal indicates depolarization). The total population average V_{mem} is depolarized in cancer as compared to the healthy cells which correlates with increased cancer invasion. Analysis of the average V_{mem} of proliferating cells verses invading cells shows that proliferating cells are depolarized compared to the total population while invading cells are not.

An additional approach that would help elucidate specific aspects of signaling mechanisms is the use of rescue studies. Many studies have characterized the effect of inhibiting and knocking out specific ion channels. But this approach does not provide evidence regarding what aspect of the channel's activity, a conformational change, the increase in a specific ion current, or the effect on V_{mem}, is required for the behavioral response. Studies in which behaviors lost with channel inhibition are attempted to be recovered by expression of first more closely related and then more distantly related channels would help dissect the mechanism. The more limited the ability of other channels to rescue the phenotype the more likely that the mechanism is

dependent on specific protein-protein interactions or localized effects of ion flux. Phenotypes that could be rescued by unrelated channels specific to the same ion or specific to a different ion would suggest the mechanism is dependent on a global change in the specific ion flux or a change in V_{mem} respectively.

VI.6 Final Conclusions

In summary, my studies investigating voltage regulation of stem cell differentiation and cancer progression do not support the sufficiency of stable V_{mem} shifts to instruct cell behaviors associated with differentiation and cancer cell aggression. V_{mem} may act as a regulator of these processes but likely through a more complicated mechanism that possibly involves the timing and amplitude of V_{mem} waves. The ability of over-expression and activation of the cancer-associated ion channel IK to induce changes in cell behaviors while expression of a different potassium channel had no apparent effect possibly points towards the importance of the individual ion channel to downstream signaling. The results of these studies suggest many interesting future research directions to dissect the power of individual bioelectric properties to instruct downstream cell behaviors and determine the molecular mechanisms of action.

Appendix I: Developing a Tissue Engineered Model of Breast Tissue To Investigate the Requirement for Cancer-Stroma Interactions in Bioelectric Signaling.

Ap-I.1 Abstract

Membrane potential (V_{mem}) signaling may require interactions with stromal cell types or signaling mechanisms that are not replicated in simple culture systems. For this reason, interactions with adipocytes and strategies to develop complex engineered tissues that more accurately replicate the *in vivo* environment were investigated. Two methods to create 3D constructs with mature adipocytes were developed, one utilizing differentiation of pre-adipocytes on a scaffold and another using primary adipocytes isolated from adult tissue.

Ap-1.2 Rationale

Many 3D culturing systems have been developed to more accurately reflect the native environment with co-culture of additional cell types and conditions with more similar oxygen and nutrient levels. *In vivo*, mammary epithelial cells are surrounded by primarily fat tissue containing adipocytes and fibroblasts. Cross talk between mammary epithelial cells and other cell types impacts epithelial cell behavior. Thus, accurate replication of these *in vivo* pathways is important to better predicting and understanding epithelial cell behavioral response. Developing methods to co-culture MCF-10A cells

with high density mature adipocytes as is found *in vivo* is challenging. Modifications to current co-culture strategies were investigated for the ability to more accurately replicate epithelial-adipocyte signaling.

A major drawback of the spheroid formation assay used to interrogate mammary epithelial behavior is that it lacks additional cell types found in the mammary gland. Cells have very different behavioral responses to treatments depending on their microenvironment and mammary epithelial response to V_{mem} modulation may differ in the presence of stromal cell types. In some studies investigating the effect of modulating V_{mem} on cell behavior, cells had a different response when interacting only with cells possessing a similar V_{mem} as compared to interacting with cells that had a very different V_{mem} (Blackiston et al., 2015). In most cases, being in contact with cells that had a non-similar V_{mem} caused a more dramatic change in cell behavior.

I wanted to investigate the interdependence of epithelial cell-adipocyte cross talk and V_{mem} signaling. To accomplish that goal, I sought to develop improved tissue engineering strategies that better modeled the *in vivo* mammary gland.

Ap-I.3 Methods

Reagents were purchased from Thermo Fisher Scientific unless otherwise noted.

Adipocyte Cultivation - Pre-adipocytes isolated from human subcutaneous fat were purchased from Lonza and cultured in adipogenic expansion media which consisted of DMEM supplemented with 10% fetal bovine serum (FBS), 0.1 mM non-essential amino acids, 1 ng/mL basic fibroblast growth factor (bFGF), 1 mM sodium pyruvate, 5 μg/mL insulin, 100 U/mL penicillin, and 100 μg/mL streptomycin. Media was changed every 3-4 days and cells were split 1:5 as needed. To induce adipogenic differentiation, cells were placed in adipogenic differentiation media, DMEM supplemented with 10% FBS, 1 mM sodium pyruvate, 5.8 μg/mL insulin, 500 μM 3-isobutyl-1-methyl-xanthine (IBMX), 1 μM dexamethasone, 50 μM indomethacin (Sigma-Aldrich), 100 U/mL penicillin, and 100 μg/mL streptomycin, with media changes every 3-4 days for 3 weeks.

Indirect co-culture - Adipocytes were differentiated on tissue culture plastic. Mammary epithelial cells were added to the top of transwells in 90% matrigel as described previously (Chapter 3) and cultures were maintained for 14 days. Carmine staining, sectioning, and H&E staining was performed as described previously (Chapter 3).

Quantification of Lipid Accumulation - Cells were fixed in 10% formalin for 10 minutes and rinsed in PBS followed by 60% isopropanol. A 210 mg/mL solution of Oil red O in 60% isopropanol 40% PBS was filtered through a 0.2 μm filter and added to the cells. Cells were incubated with shaking for 30 minutes at room temperature. Excess solution was removed and cells were washed in PBS 4 times. Bright field images of oil red O staining were acquired on an Olympus IX71 inverted microscope and Olympus DP70 digital camera with associated software. Oil red O was eluted by adding 100% isopropanol and incubating with shaking for 30 minutes. The solution was transferred to a 96 well plate and the absorbance at 500 nm was read on a SpectraMax5 (Molecular Devices) plate reader.

Fat Tissue Engineering with pre-adipocytes- Porous silk scaffolds were fabricated from 6% aqueous silk solution as previously described (Rockwood et al., 2011). Scaffolds were 4 mm tall and had an 8 mm diameter. The scaffold was seeded with 1 x 10^6 pre-adipocytes in a total volume of 15 μl. For 1 hour, 15 μl of media was added to the scaffold every 15 minutes to keep the scaffold moist while allowing cells to attach. Scaffolds were then placed in 12-well plates with 2 mL of adipogenic expansion media. Twice-seeded scaffolds were seeded a

second time two days later by the same method. Scaffolds were kept in adipogenic expansion media for two weeks and then cultured in adipogenic differentiation media for 3 weeks. Additional cell types were added to scaffolds by making a solution of 2.4 x 10^6 cells/mL mammary epithelial cells with or without 1.2 x 10^6 cells/mL fibroblasts in 90% matrigel and adding 100 μL dropwise to the scaffold giving a final mammary epithelial cell concentration of 1200 cells/mm^3. Scaffolds were incubated at 37° C for 1 hr to allow gelation before adding MCF-10A 3D media supplemented with 5% FBS and 1 mM sodium pyruvate. Scaffolds were cultured for 14 days with media changes every 3 days.

Fat Tissue Engineering with Mature Adult Adipocytes- Fat tissue removed during elective abdominoplasty surgery of a 50 yo female with a BMI of 27 was dissected into small pieces and pulverized in a Ninja blender. Silk scaffolds with a height of 2 mm and 4 mm diameter were placed in a 50 mL falcon tube with 25 mL of the abdominoplasty cell mixture and incubated for 1 hr. Scaffolds were removed from the solution, placed in a 24 well plate, and incubated for an additional 2 hours to allow cells to attach before adding 1 mL of MCF-10A 3D media. Scaffolds were cultured for 1 week before addition of mammary epithelial cell types. Mammary epithelial cells were diluted to 4.8 x 10^6

cells/mL in 90% matrigel and 12.5 μl was added to the scaffold for a final concentration of 1200 cells/mm^3. Scaffolds were incubated for 14 days in MCF-10A 3D media with media changes every 3 days.

Imaging Scaffolds - Scaffolds were cut in half and incubated in PBS containing 0.5 μg/mL DAPI, 0.5 μg/mL Calcein AM, and 2.5% Adipored Assay Reagent (Lonza) for 20 minutes. Scaffolds were placed on a cover slip and images were acquired with a Nikon A1R confocal inverted microscope.

Statistics – Statistics were calculated with Prism 5 using a two-sample T test or one-way ANOVA with Tukey or Dunnett post-test for significance with alpha = .05.

Ap-I.4 Results

Ap-I.4.1 Mammary epithelial cell and adipocyte indirect co-culture

Previously, our group had developed a 3D tri-culture system comprised of mammary epithelial cells, fibroblasts, and immature adipocytes. The cells were mixed together in a matrigel/collagen gel

and seeded onto a porous silk scaffold to provide support. This system provided a simple means to co-culture the major cell types found within breast tissue. However, a drawback of this culture system was a lack of mature adipocytes with significant lipid accumulation. In this system, adipocytes were differentiated from human mesenchymal stem cells (hMSCs) in tissue culture flasks, and then trypsonized to add to the 3D culture. Because mature adipocytes contain large quantities of lipid droplets, the cells floated and were not incorporated into the final scaffold.

Breast cancer is more prevalent in obese individuals but the cause of this correlation is unknown. Previous studies have demonstrated differences in epithelial and adipocyte cell behavior when cells are cultured together suggesting there are important mechanisms of cross talk (Dirat et al., 2011). Given the ease of adipogenic differentiation in 2D, initial studies were performed using indirect co-culture to allow differentiation of adipocytes on tissue culture plastic. Pre-adipocytes were plated on a normal tissue culture plate and grown in expansion media to confluence. Samples were then changed to either differentiation or maintenance media for 2.5 weeks to create mature and immature adipocyte cultures. Breast epithelial cells with or without mammary fibroblasts were seeded in a matrigel collagen mixture in the top chamber of a transwell and placed over the

adipocytes (Figure 1A-B). Samples were collected after an additional 2 weeks of culture. The adipocytes were analyzed for lipid accumulation and the epithelial cells were characterized for changes in morphology. Non-tumorigenic MCF-10A cells did not affect lipid accumulation of mature or immature adipocytes (Figure 1C-D). Highly metastatic MDA-MB-231 cells increased lipid accumulation in both mature and immature adipocytes while non-metastatic tumor forming MCF7 cells increased only immature adipocyte lipid accumulation. The addition of mammary fibroblasts with the mammary epithelial cells had no further effect on lipid accumulation. Carmine staining of whole mount samples and H&E staining of sections did not reveal any changes in epithelial cell morphology for any cell line (Figure 2).

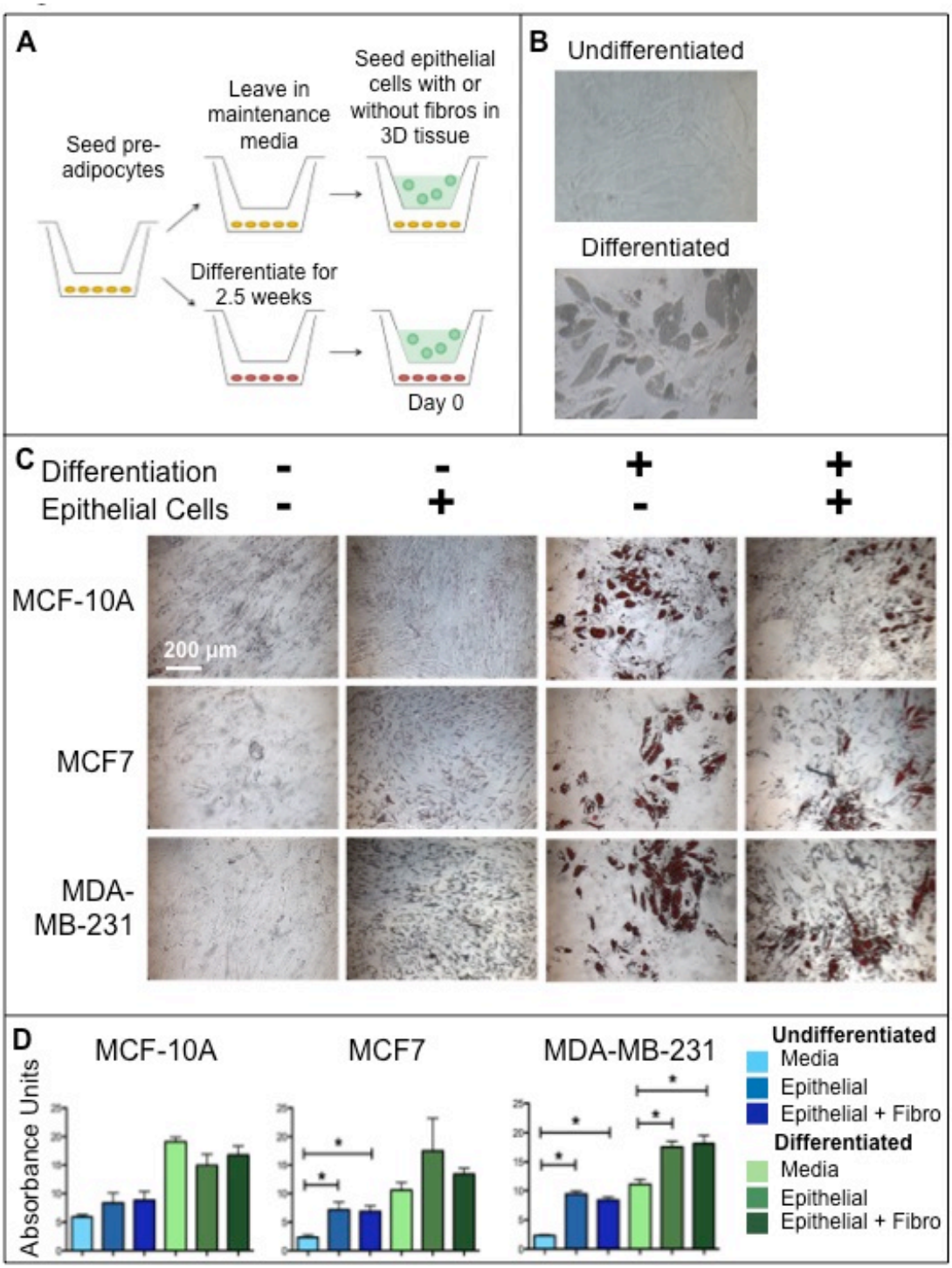

Figure Ap-I.1: Effect of co-culture with mammary epithelial cells on adipocyte maturity. **(A)** Schematic of experimental methods. **(B)** Bright field image of adipocytes cultured in expansion or differentiation media for 2.5 weeks with clear lipid accumulation in

cells cultured in differentiation media. **(C)** Bright field images of oil red O staining of adipocytes grown in indicated conditions. (D) Quantification of oil red O staining from samples in C.

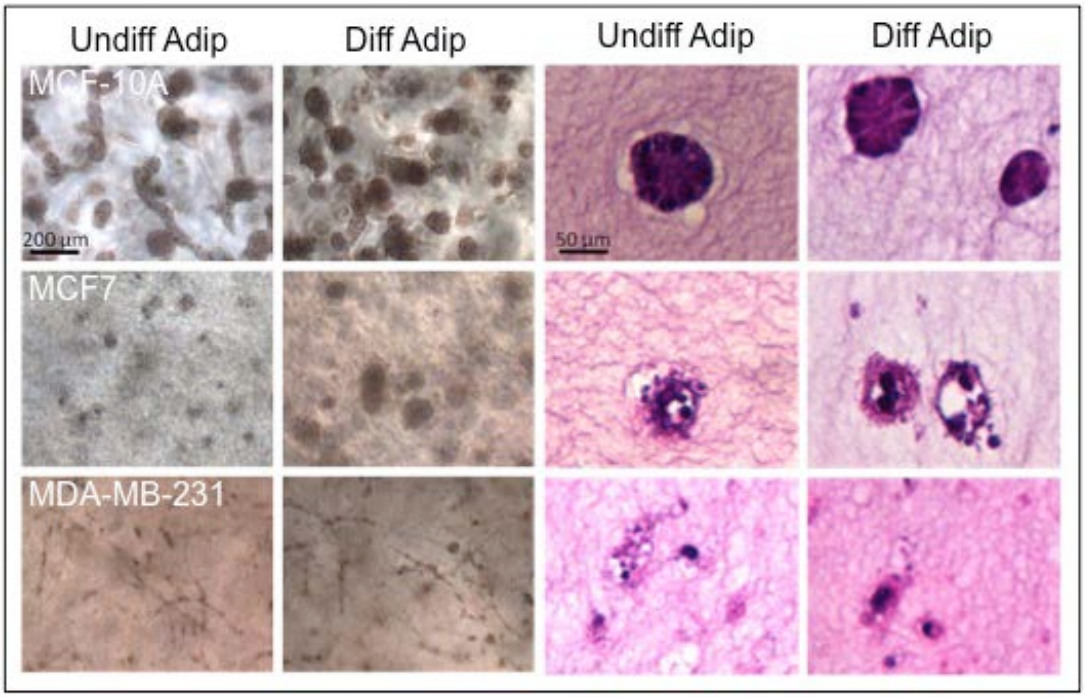

Figure Ap-I.2: Effect of adipocyte co-culture on mammary epithelial cell morphology. Left 2 columns: Bright field images of whole mount carmine stained mammary epithelial cells grown with differentiated or undifferentiated adipocytes. Right 2 columns: H&E staining of same samples showing detailed morphology.

Ap-I.4.2 Improvements to 3D tissue engineered fat tissue

Adipocytes are likely also responsive to 2D verses 3D growth making it important to develop a culture system in which the adipocytes are incorporated into the engineered 3D tissue. Two

methods to create a scaffold with a high density of mature adipocytes were compared. In the first, pre-adipocytes were seeded onto a porous silk scaffold and cultured in expansion media for 2 weeks to allow the cells to grow to a high density on the surface of the scaffold. Seeding the scaffold twice with pre-adipocytes significantly improved cell infiltration into the bulk of the scaffold (Figure 3). After expansion, the media was changed to adipose differentiation media and cells were differentiated for 3 weeks. Samples sacrificed at this time point and stained for lipids contained mature differentiated adipocytes with high lipid droplet accumulation (Figure 3). After differentiation, mammary epithelial cell types were added to the scaffold in matrigel. Scaffolds were cultured for an additional 2 weeks and epithelial cell morphology was assessed by live cell imaging, carmine whole mount staining, and H&E staining of sections (Figure 4). No clear differences in morphology were observed between epithelial cells cultured on empty scaffolds and cells cultured on scaffolds with adipocytes.

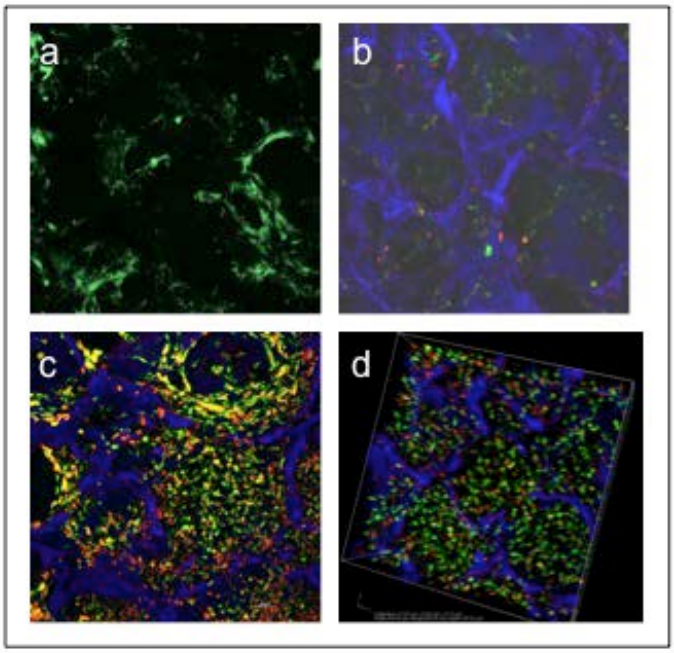

Figure Ap-I.3: Tissue engineered breast tissue models. Live imaging of adipocytes differentiated from pre-adipocytes on a silk scaffold. (a) once seeded scaffold after 2 weeks of expansion stained with only Calcein AM (b) once seeded scaffold after 3 weeks of differentiation (c) twice seeded scaffold after 3 weeks of differentiation (d) 3D projection view of scaffold from c Blue – DAPI, Green – Calcein AM, Red – lipids.

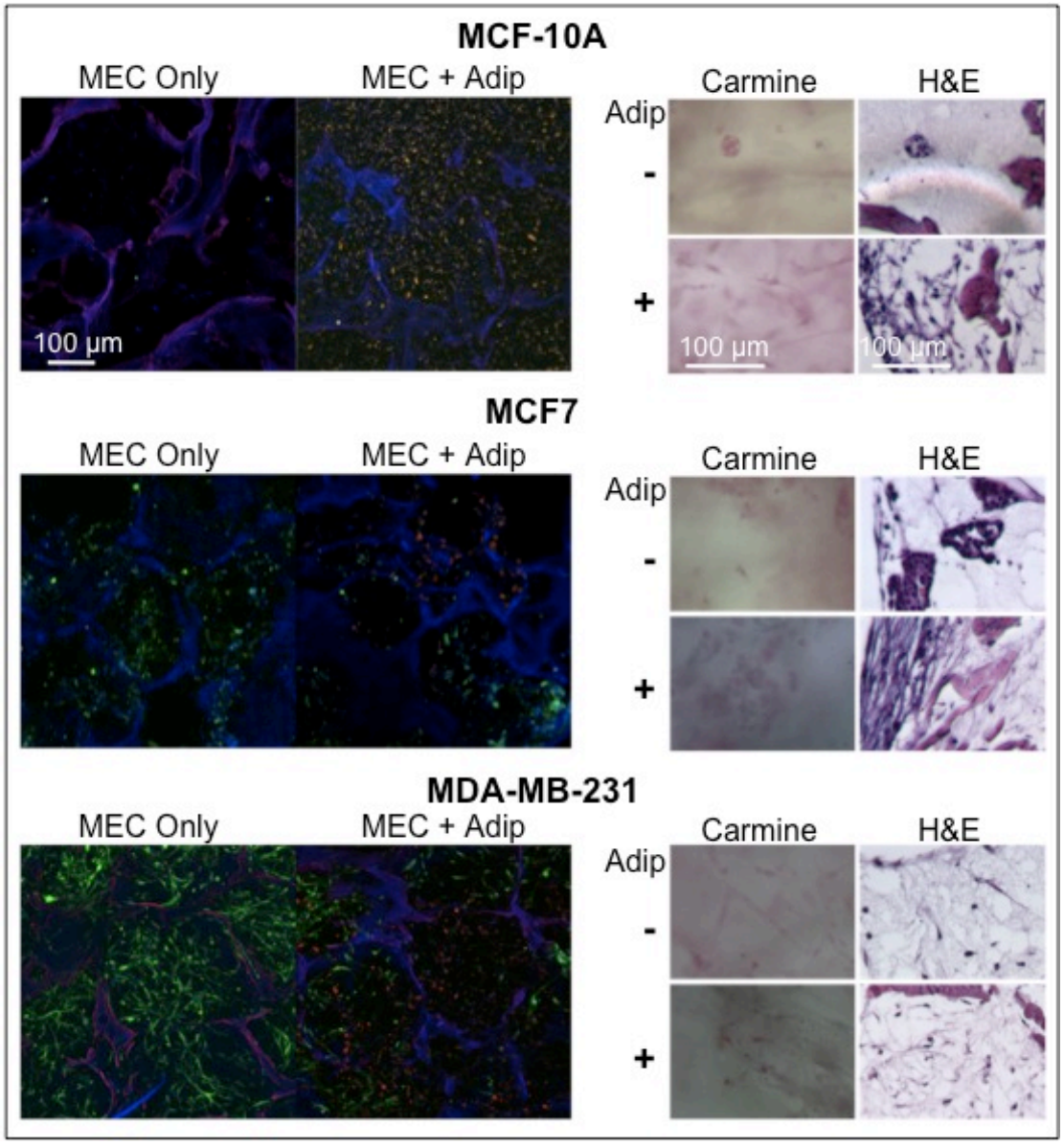

Figure Ap-I.4: Mammary epithelial cells co-cultured with adipocytes on silk scaffold show no change in morphology. Left: Live images of scaffolds with mammary epithelial cells seeded on empty scaffolds or scaffolds with pre-differentiated adipocytes. Blue – DAPI, Green – Calcein AM, Red – lipids. Right: Bright field images of carmine whole mount staining and H&E staining of sections from samples on left.

As an alternative method to create a scaffold with a high density of mature adipocytes, adipocytes were isolated from adult adipose tissue. Tissue was collected from elective abdominoplasty surgery and used to create a dense cell suspension of mature adult adipocytes. Scaffolds were soaked in the solution allowing cells to attach throughout the bulk of the scaffold in high density. Scaffolds were removed from the cell suspension and cultured on low-adhesion plates for 1 week. Dense adipocytes could be found on the outer portions of the scaffold but only sparsely populated the center of the scaffold (Figure 5). MCF-10 cells and/or fibroblasts were added to the scaffold in matrigel. Matrigel was used to hold the cells within the scaffold and also to provide a more ECM-like matrix. No clear differences in morphology were seen in any co-culture condition (Figure 5).

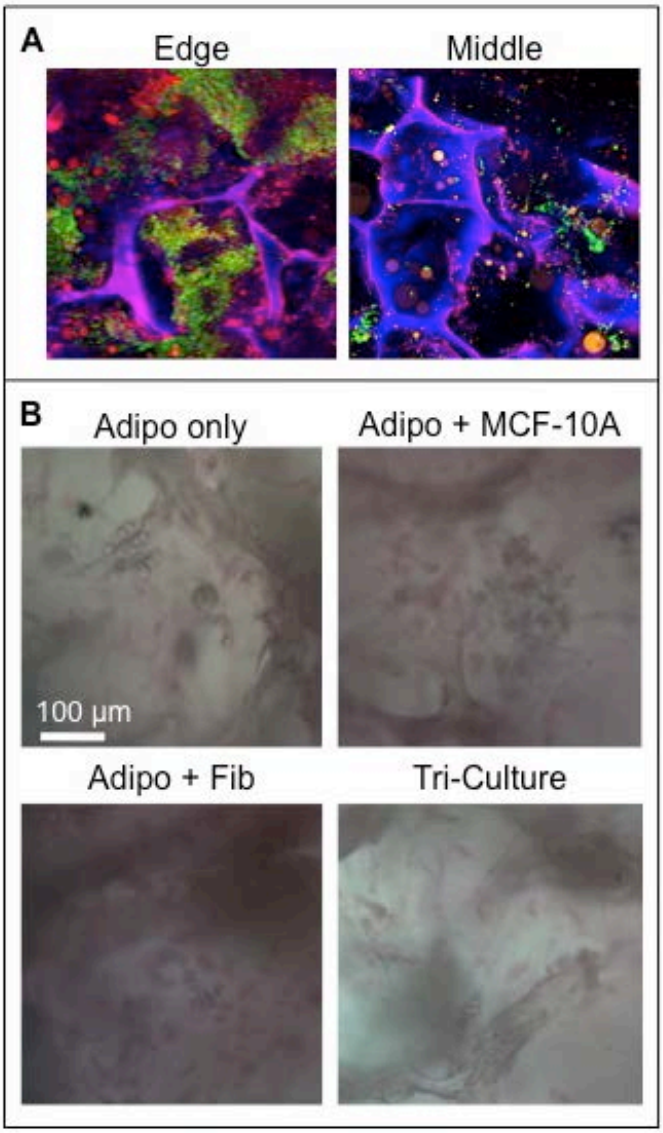

Figure Ap-I.5: Tissue engineered breast tissue model using primary adult adipocytes. (A) Live images of silk scaffold seeded with primary adipocytes isolated from adult fat tissue after 1 week of culture with image of outer edge (left) and center of scaffold (right). Blue – DAPI, Green – Calcein AM, Red – lipids. **(B)** Bright field images of whole mount carmine staining of scaffolds from A seeded with indicated cell types.

Ap-I.5 Discussion

The addition of surrounding cell types found in breast tissue may lead to different responses to V_{mem} modulation. Studies from *Xenopus* suggest differences in V_{mem} between neighboring cells might be more instructive than the absolute V_{mem}. Neurons grafted onto a host had increased extension outgrowth and hyper innervation in host tissue depolarized by activation of chloride channels as compared to control (Blackiston et al., 2015). This result suggests that investigating human cells within a co-culture in which the V_{mem} of only some cell types is modulated may elucidate additional responses.

Co-culture of mammary epithelial cells and adipocytes separated by a transwell membrane lead to changes in adipocyte lipid accumulation demonstrating the existence of signaling pathways between the two cell types. Interestingly, the change in lipid accumulation occurred with cancerous but not healthy epithelial cell co-culture. The epithelial cells appeared unaffected by the presence of adipocytes although more analysis beyond gross morphology is needed.

Towards the goal of a better 3D co-culture system, alterations were made to a previously developed co-culture system to better replicate and understand breast epithelial and adipocyte cell interactions. Two methods were developed that greatly increased the density of adipocytes containing lipid droplets. In the first method,

precursor cells were pre-differentiated on a scaffold while in the second method mature adipocytes were harvested from adult tissue and seeded directly on the scaffolds. Scaffolds pre-seeded with precursor cells had more even seeding and better penetration of cells into the bulk of the scaffold while the scaffolds seeded with primary adipocytes had pockets of denser cell coverage with more lipid accumulation. Alterations to both culture methods, such as increasing the number of cell seedings or enzymatically digesting the adult tissue to create a single cell suspension, could further improve the resulting adipose tissue. The two cell sources each have advantages and drawbacks. The use of pre-adipocytes allows for more control of the environment and differentiation process while isolation from adult tissue provides more authentic mature adipocytes with the option of isolating cells directly from breast tissue as there may be tissue specific differences. Adding mammary epithelial cells to the scaffolds in matrigel proved challenging as the matrigel formed a gel before dispersing throughout the entire scaffold. This lead to pockets of high density mammary epithelial cells but also large areas lacking epithelial cells. Since the adipocytes also did not completely cover the scaffold, mammary epithelial cells were not always in close contact with adipocytes. Further troubleshooting is needed to improve epithelial cell seeding into the bulk of the scaffold. Successful tissue engineering of

constructs with mature adipocytes will allow further interrogation of important cross-talk signaling and microenvironmental factors that drive cancer progression.

APENDIX II: *IN VIVO* BIORESPONSES TO SILK PROTEINS

This chapter was published in Biomaterials with co-authors Fiorenzo G. Omenetto and David L. Kaplan (Thurber et al., 2015). We thank out funding sources the NIH [P41 EB002520, R01 EY020856, R01 DE017207, R01 EB014283] for support of this work, as well as many students and collaborators over the years that have contributed to the work.

Ap-II.1 Abstract

Silks are appealing materials for numerous biomedical applications involving drug delivery, tissue engineering, or implantable devices, because of their tunable mechanical properties and wide range of physical structures. In addition to the functionalities needed for specific clinical applications, a key factor necessary for clinical success for any implanted material is appropriate interactions with the body *in vivo*. This review summarizes our current understanding of the *in vivo* biological responses to silks, including degradation, the immune and inflammatory response, and tissue remodeling with particular attention to vascularization. While we focus in this review on silkworm silk fibroin protein due to the large quantity of *in vivo* data thanks to its widespread use in medical materials and consumer products, spider

silk information is also included if available. Silk proteins are degraded in the body on a time course that is dependent on the method of silk fabrication and can range from hours to years. Silk protein typically induces a mild inflammatory response that decreases within a few weeks of implantation. The response involves recruitment and activation of macrophages and may include activation of a mild foreign body response with the formation of multinuclear giant cells, depending on the material format and location of implantation. The number of immune cells present decreases with time and granulation tissue, if formed, is replaced by endogenous, not fibrous, tissue. Importantly, silk materials have not been demonstrated to induce mineralization, except when used in calcified tissues. Due to its ability to be degraded, silk can be remodeled in the body allowing for vascularization and tissue ingrowth with eventual complete replacement by native tissue. The degree of remodeling, tissue ingrowth, or other specific cell behaviors can be modulated with addition of growth or other signaling factors. Silk can also be combined with numerous other materials including proteins, synthetic polymers, and ceramics to enhance its characteristics for a particular function. Overall, the diverse array of silk materials shows excellent bioresponses *in vivo* with low immunogenicity and the ability to be

remodeled and replaced by native tissue making it suitable for numerous clinical applications.

Ap-II.2 Introduction

Silk has long been used in its native fiber form as a suture material, and more recently is gaining popularity for use in numerous additional applications from tissue engineering to drug delivery to implanted devices. One reason for this widespread appeal is the ability to fabricate silk into a wide range of material formats with tunable mechanical and degradation properties. The natural silk polymer in fiber form has both great strength and elasticity, a combination of properties not matched by current synthetic polymers (Omenetto and Kaplan, 2010). Silk proteins are produced by an enormous variety of insect and spider species including ants, fleas, and crickets (Sutherland et al., 2010). For biomedical applications silk is sourced primarily from the textile industry silkworm *Bombyx mori*, and occasionally spiders. Silk from spiders has superior strength and elasticity but the significantly greater ease of cultivating *B. mori* silk has made it more popular. Most silk suture material is made from *B. mori* silk, but it is important to note that many silk suture materials are not purely silk. Frequently they are coated with waxy materials or

contain contaminants, and thus studies assessing the *in vivo* bioresponse and degradation of silk sutures do not reflect purely silk creating confusion in the literature see Altman et al., 2003 for review.

B. mori silk consists of two main components, fibroin proteins and sericins, a family of glue-like proteins that coat the fibers and hold them together. In its original use as a suture material, silk was typically used in its virgin form. Many patients exhibited a significant inflammatory response and some patients became sensitized leading to severe allergic reactions. While there has been some confusion over time as to the true source of the allergic response, recent careful studies have come to the consensus that the allergic response is elicited by the native combined fibroin-sericin structure, but that either fibroin or sericin alone does not elicit an allergic reaction (Aramwit et al., 2009; Wang et al., 2014). Given that sericin has only recently been exonerated for its role in allergic responses, it has been used in limited *in vivo* studies. While fibroin does not induce an allergic response, as with any biomaterial introduced into the body, it induces a biological response that must be understood to improve its use in clinical applications. The rest of this review will focus on studies utilizing purified fibroin from *B. mori*, referred to simply as ‘silk’, as this has been by far the most commonly used form of silk for biomedical applications.

The key attribute that allows silk to be processed into such a wide variety of materials is its ability to be solubilized in certain high ionic strength or acidic solutions and then remain in solution when exchanged with less harsh solutions. Once solubilized, any one of numerous fabrication methods can be used to form films, gels, solid porous scaffolds, or other materials. Some common fabrication methods include casting and drying for films, sonication to form hydrogels, and lyophilization or salt leaching to form porous solid scaffolds (Figure 1). Next, crystalline beta-sheet formation is induced, usually by either heat or exposure to solvents, which causes the silk material to become water insoluble. Finally, the material must be sterilized prior to implantation. In every method, the mechanical and degradation properties can be modulated by changing the silk processing conditions, silk concentration, and method of inducing β-sheet (crystal) formation. It is important to note that conversely, each step of the processing method affects the final material properties and even small changes in the protocol can greatly alter the material. For example, the method of sterilization can change the molecular weight distribution and degree of beta-sheet formation and therefore change the material stiffness and degradation (Rnjak-Kovacina et al.). For a more thorough review of common processing methods and how the

processing affects the final material properties see (Rockwood et al., 2011).

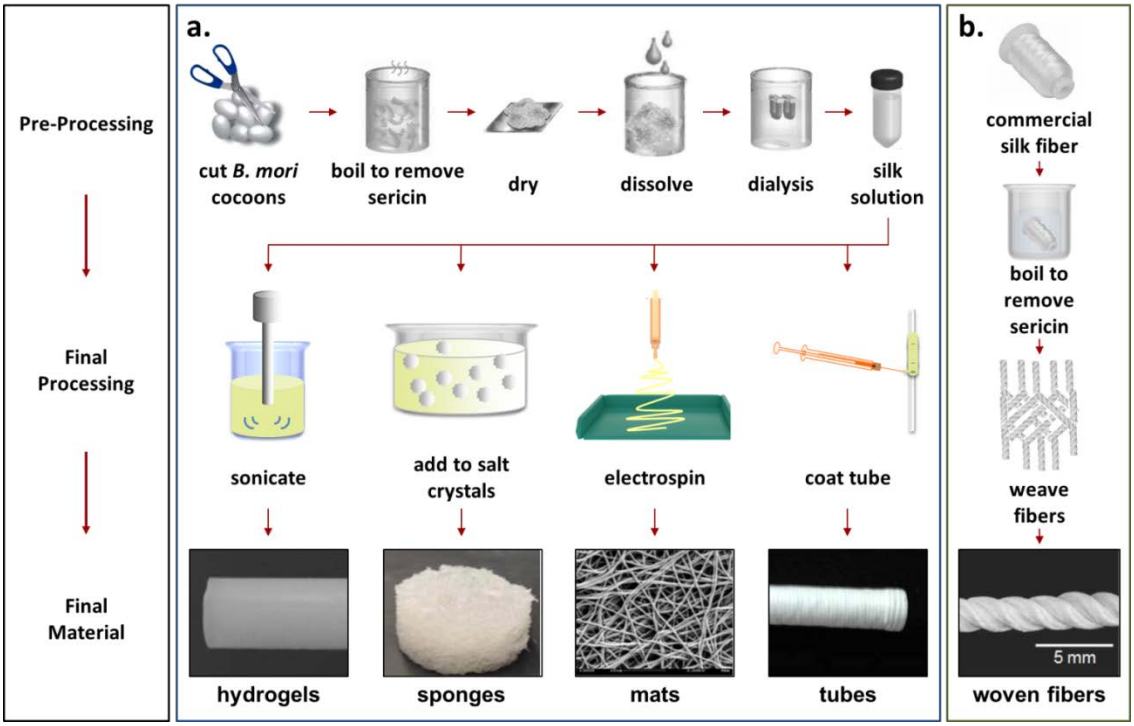

Figure Ap-II.1: Silk Processing. Schematic of common silk material fabrication methods (8-10). Silk materials are made starting from either silk cocoons **(a)** or silk fibers **(b)**, both must be boiled to remove sericin. Cocoons are solubilized while fibers are left intact before final processing to form different silk materials (Altman et al., 2002; Li et al., 2006; Wray et al., 2011).

In order to utilize silk biomaterials in more clinical applications, it is important to understand the biological responses to silk. The goal of this review is to summarize the current understanding of how silk protein-based biomaterials interact with the body *in vivo*. A summary of papers that have characterized the inflammatory response and vascularization of implanted silk materials is provided in table 1. More

extensive reviews on silk sources, silk structure and properties, fabrication of various biomaterial and tissue constructs, and interactions with cells *in vitro* can be found elsewhere (Altman et al., 2003; Omenetto and Kaplan, 2010; Rockwood et al., 2011; Wang et al., 2006).

Table Ap-II.1: Inflammatory response and vascularization *in vivo.* (H = histology, IC = immunohistochemistry, HM = histomorphology)

Silk material and processing	**Response**	**In vivo model and tissue site**	**Time-points, analysis**	**Ref**
INFLAMMATORY RESPONSE				
silk film, HFIP annealed, pre-seeded with rMSCs	mild inflammatory response with layer of macrophages and fibroblasts 3-4 cells thick surrounding implant, no MNGCs	intramuscular implant rats	6 wks H, IC	(Meinel et al., 2005; Navone et al., 2014)
woven silk mesh	macrophages and MNGCs found at interface of silk implant at 7 days, and within bulk of implant at later time points, similar amount of macrophages but more MNGCs as compared to polypropylene	abdominal wall facial repair in rats	1, 2, 4, 12 wk H, IC	(Spelzini et al., 2007)
water or HFIP prepared porous silk scaffold	granulation tissue, MNGCs and macrophages present for both scaffold types at 2	intramuscular and subcutaneous in	2 wk, 2, 6, and 12	(Wang et al., 2008)

	months in lewis rats, fewer macrophages at 6 months for aqueous scaffold, HFIP more resistant to macrophage degradation	Lewis and nude rats	month H, IC and QPCR	
sonicated silk gel	mild inflammatory response with neutrophils and macrophages, response decreasing by 4 wks and not detectable at 12 wks	subcutaneous implantation nude mice	1,2,4,12 wk H	(Etienne et al., 2009)
knitted silk fiber scaffold	mild inflammatory response	subcutaneous implantation in rats	1, 8 wk H	(Seo et al., 2009b)
porous silk scaffold	mild inflammatory response which decreased after day 3, less severe in comparison to PVA scaffold	full thickness skin wound repair in rats	3, 7, 10, 18 day H	(Guan et al., 2010)
98% silk/2% poly(ethylene oxide) porous tube, sonicated and MeOH treated	number of macrophages decreased from 1 to 8 weeks, more macrophages in silk constructs than control collagen or autograft constructs, similar nerve repair in silk and collagen constructs but less than autograft	sciatic nerve repair in rats	1,4, 8 wk H, IC, HM	(Ghaznavi et al., 2011)
porous silk scaffold or cross-linked silk film	inflammatory cells surrounding silk materials, decreased by day 20	buccal mucosa full thickness wound repair in rats	10, 20 day H	(Ge et al., 2012)
porous silk tube gelled with acetic acid, EtOH	macrophage recruitment and functional nerve repair similar to autologous nerve graft	sciatic nerve repair in rats	1, 4 month H, IC,	(Huang et al., 2012)

treated			muscle strength testing	
water or HFIP prepared porous silk scaffold	both scaffolds contained granulation tissue and MNGCs at 4 wks, at 8 weeks foreign body response of water prepared scaffold was diminished while it remained high for HFIP prepared scaffolds	femur defect in rabbits	4, 8 wk H, HM	(Kuboyama et al., 2013)
water or HFIP prepared porous silk scaffold, MeOH treated	lymphocytes, macrophages, and MNGCs found around and within scaffold, no neutrophils, new bone formation in close proximity to MNGCs	tibia and humerous defect in sheep	2 month H	(Uebersax et al., 2013)
electrospun silk sheet treated with MeOH	moderate inflammatory response with MNGCs and M1 macrophages	placed on epicardial surface after myocardial infarction	2, 4, 8 wks H, IC	(Castellano et al., 2014)
sonicated silk gel	mild foreign body response, no neutrophils	injection into cervix of pregnant rats	4 day H	(Critchfield et al., 2014)
lyophilized silk scaffold	foreign body response with similar number of MNGCs at 4 and 8 wks	calvarial defect in rabbit	4, 8 wk H, HM	(Kweon et al., 2014)
braided silk tube	mild inflammatory response to fibroin tube, severe response to fibroin and sericin tube	subcutaneous implantation in mice	10 day H	(Kwon et al., 2014)

HFIP prepared electrospun silk-tropoelastin or silk only scaffold, glutaraldehyde cross-linked, EtOH treated	number of inflammatory cells and inflammatory markers decreased in silk-tropoelastin compared to silk, also less remodeling	subcutaneous implantation in mice	1,2,3, 10, 21 day H, IC	(Liu et al., 2014)
VASCULARIZATION				
porous silk micronet treated with formic acid, pre-seeded with HDMEC, HDMEC and osteoblasts, or no cells	vascular ingrowth into co-culture but not others, in vitro pre-formed vasculature of co-culture integrated with host vasculature	subcutaneous implantation in SCID mice	2 wk H, IC	(Unger et al., 2010)
porous silk micronet treated with formic acid, pre-seeded with osteoblasts	pre-seeded vascularized throughout scaffold, unseeded only vascularized on surface	subcutaneous implantation in SCID mice	2 wk H, IC, HM	(Ghanaati et al., 2011)
silk-RGD porous scaffold MeOH treated, pre-seeded with hMSCs	vascularization improved with larger pore sizes,	calvarial defect in nude mice	8 wk H, HM	(Hofmann et al., 2013)
lyophilized porous silk scaffold with linear channels, autoclaved	channels increased the number of blood vessels and depth of blood vessel growth into the scaffold	subcutaneous implantation in mice	2, 4 wk H, IC	(Rnjak-Kovacina et al., 2014)
porous silk scaffold, loaded with VEGF, BMP-2, or both	vascularization highest in scaffolds with VEGF and lowest in unloaded scaffold	cranial defect in rabbits	4 wk quant. vasc. analysis	(Zhang et al., 2014)

Ap-II.3 Mechanism of Silk Degradation

In the body, silk degradation depends on many factors including the degree of β-sheet formation, the material structure (e.g., gel vs fiber, porosity), and location of implant in the body. For use as a biomaterial, silk fibroin is generally first solubilized in a strong ionic solution, such as 9 M lithium bromide, and then processed to induce β-sheet formation making it water insoluble. Silk primary structure is comprised of repeating hydrophobic bulk domains interspersed by hydrophilic regions (Zhou et al., 2001). Processing of the silk induces the hydrophobic bulk domains to form crystalline β-sheet regions with the degree of β-sheet formation dependent upon the method of processing, thus giving a mechanism to control material properties. For use as a biomaterial, most processing methods induce sufficient β-sheets such that no appreciable silk degradation occurs in water or biological salt solutions (Arai et al., 2004; Numata et al., 2010). However, silk is sensitive to degradation by proteases. *In vitro* studies have demonstrated that many proteases including protease K, collagenase, and alpha-chymotrypsin are able to cleave silk and cause a decrease in the material weight and strength over time (Brown et

al., 2015; Horan et al., 2005; Numata et al., 2010). In contrast, MMPs, including MMP-1 and MMP-2 exhibit lower degradation activity towards insoluble forms of silk compared to soluble silk (Brown et al., 2015). In general, increased β-sheet content has a protective effect on silk degradation, which is likely in part due to the fact that most proteases act outside of the β-sheet regions. Denser structures such as silk fibers or films have longer degradation times suggesting silk is degraded by surface erosion and not bulk degradation (Arai et al., 2004; Brown et al., 2015). Degradation of silk *in vivo* is also dependent on β-sheet content with higher β-sheet scaffolds showing less degradation (Wang et al., 2008). Interestingly, a direct correlation between immune cell invasion into the silk scaffold and degradation was also found. Regions accessible to macrophages showed visible evidence of degradation while cell-free regions did not and scaffolds implanted in immune-compromised nude rats were significantly less degraded than those implanted in Lewis rats (Sengupta et al., 2010). While these results suggest immune cells are primarily responsible for silk degradation *in vivo*, other cell types are also capable of degrading silk.

Ap-II.4 Immune and Inflammatory Responses

The immune response can be broken down into two main components, the innate immune response, which is activated by anything recognized as ‘not-self’, and the adaptive immune response which is activated by specific molecules that were previously recognized as harmful. The adaptive immune response can be severe and it is critical that biomaterials not be targeted by adaptive immune antibodies. Studies have demonstrated that while native fibroin-sericin proteins can activate the adaptive response, purified fibroin does not (Aramwit et al., 2009; Dewair et al., 1985). The innate response, which includes the inflammatory response, can enact a range of symptoms from mild to severe. A mild innate immune response can often be beneficial as it activates many healing processes. However, more severe responses can be detrimental leading to destruction of local tissue or even systemic problems (Murphy et al., 2012).

The innate immune response can be further broken down into the acute and the chronic response. The innate response is typically initiated by macrophages, which are located throughout healthy tissues (Murphy et al., 2012). Macrophages express pattern recognition receptors (PRR) that bind to molecules recognized as being produced generically from pathogens, such as particular sugar or fatty acid structures that are only produced by bacteria or fungi. When a PRR binds a target molecule, it initiates a signaling cascade that leads

to the activation of many pathways including the release of inflammatory cytokines, initiation of phagocytosis, and recruitment of additional immune cells. This response, known as the compliment system, does not involve recognition by specific antibodies. It is activated entirely by receptors that generically recognize 'non-self'. Thus, this system is often activated by non-native implanted materials (Anderson, 2001). Activation of the compliment system leads to the release of cytokines, including interferon-β which activates transcription of the inflammatory cytokines tumor necrosis factor-α, interleukin-1β, and interleukin-6 (Murphy et al., 2012).

In addition to direct interactions between immune cells and silk proteins, another major factor determining the immune response is interactions between immune cells and proteins adsorbed on the implant. Every implanted material will be exposed to extracellular fluid as well as blood proteins due to capillaries or larger vessels damaged during the injection or surgical implantation process. Proteins adsorb rapidly to the exterior of the implant material forming a provisional matrix. The surface chemistry, morphology and structure of the implant will determine the degree and composition of this provisional matrix (Anderson et al., 2008). The proteins that make up the matrix include adhesion proteins and signaling molecules that can allow immune cells to attach and modulate their response. This provisional

matrix is often degraded during the wound healing process and can therefore act as slow release mechanism for inflammatory factors. Thus, the surface chemistry, morphology and structure of an implant play major roles directing the immune response by virtue of the proteins adsorbed to the material.

Indeed, most forms of silk fibroin used in biomedical applications activate the complement system. Silk films, fabricated by hexafluoro-2-propanol (HFIP) induced β-sheet formation, implanted intramuscularly attracted activated macrophages to the implant-tissue interface (Meinel et al., 2005). Silk tubes used for vascular grafts and constructed by winding silk fibers that were then coated in a fibroin solution supported the infiltration of macrophages performing phagocytosis on the fibroin (Enomoto et al., 2010). Similarly, porous scaffolds prepared from silk solution by formic acid evaporation and implanted in a bone defect also supported infiltration of activated macrophages (Ghanaati et al., 2011). Silk-mediated activation of the complementary system is generally short lived and decreases after 14 days. Lyophilized silk sponges implanted subcutaneously had far fewer infiltrating immune cells 4 weeks post implantation as compared to 2 weeks (Rnjak-Kovacina et al., 2014). As a different material format in terms of fabrication method and mechanical properties, silk gels implanted subcutaneously also induced mild compliment system

activation at days 7 and 14 after implantation with the presence of macrophages and neutrophils. But by 4 weeks post implantation the inflammatory response was greatly reduced with far fewer inflammatory cells and no inflammatory cells could be detected 12 weeks after implantation (Etienne et al., 2009).

The inflammatory cytokines, released by the complement response, signal to nearby cells enacting a cascade that leads to local and systemic responses (Murphy et al., 2012). The cytokines act on nearby endothelial cells to slow blood flow and change the expression of adhesion molecules to attract immune cells. Some of the cytokines are also chemokines that create a concentration gradient for neutrophils, macrophages, and leukocytes to follow to the site of the immune response. As increased numbers of immune cells are attracted and activated by interactions with the foreign material, more cytokines are released which can lead to systemic effects including a rise in body temperature and activation of the adaptive immune response. Activation of lower levels of inflammation increase remodeling by inducing vascularization and the release of proteins involved in tissue remodeling and can therefore be beneficial to incorporating and degrading implanted biomaterials as new tissue forms (Mantovani et al., 2013). However, biomaterials must be designed to avoid over-activation of inflammation to the point of releasing inflammatory

signals into the bloodstream and activation of systemic responses, which will lead to rejection of the material and possible severe side effects.

The acute immune response is generally short lived and dissipates after 7-14 days. However, it can go on to activate the chronic innate immune response which can last months or years. The chronic response is characterized by the presence of monocytes, leukocytes, and most notably, foreign body giant cells (FBGC). Multinuclear giant cells (MNGC) are one cell type of the FBGC family and are commonly referred to in the literature. The chronic response is activated by cytokines released during the acute response, especially interleukin-4 (IL-4) and interleukin-13 (IL-13) (Anderson et al., 2008). In addition to direct interactions with the implanted material, whether a chronic response occurs can also be traced back to the composition of the provisional matrix formed around the biomaterial because it also affects cell adhesion and cytokine release. Macrophages already activated by inflammatory signals will then respond to IL-4 and IL-13 by fusing to form multinucleated FBGCs. Both IL-4 and IL-13 have been shown to be secreted in larger quantities by macrophages cultured on electrospun silk scaffolds *in vitro* (Castellano et al., 2014). Not surprisingly therefore, the implantation of silk materials often induces the formation of FBGCs. This has been observed in a wide

range of silk materials implanted in various locations including in scaffolds used to improve healing of bone defects (Ghanaati et al., 2011; Kuboyama et al., 2013), gels injected in the cervix (Critchfield et al., 2014), and macroporous silk constructs implanted in fascial defects (Spelzini et al., 2007).

The role of FBGCs is to destroy pathogens and other harmful materials that are unable to be cleared by phagocytosis. These cells are generally found adjacent to the biomaterial where they release reactive oxygen intermediates and proteases (Murphy et al., 2012). In a full blown foreign body response the biomaterial becomes surrounded by multiple cell layers of FBGCs and activated macrophages. This can lead to the formation of granulation tissue comprised of macrophages, fibroblasts, and new vasculature and is the precursor towards a fibrotic capsule (Anderson et al., 2008). While silk implants have frequently been found to induce the formation of FBGCs, the response generally subsides before the formation of permanent fibrotic tissue. In a study where a silk scaffold was implanted on a heart to aid in cardiac repair after myocardial infarction, fibrosis was seen two weeks after implantation but had disappeared after 8 weeks (Castellano et al., 2014). Some granulation tissue was seen at both time points, but it remained mild as compared to other scaffold materials being tested including poly-lactic acid. Similar results were

found in a study that investigated the biological response to silk scaffolds in a bone defect (Kuboyama et al., 2013). At four weeks post implantation granulation tissue could be seen within the scaffold pores including the presence of FBGCs and lymphocytes. By 8 weeks post implantation the granulation tissue was still present but the number of inflammatory cells had decreased indicating a diminishing foreign body response. To our knowledge, no studies utilizing silk purified of sericin have reported the formation of fibrotic capsules.

The lack of fibrotic encapsulation is a significant improvement over many synthetic polymers including some of the most commonly used polymers in tissue engineering poly lactic acid (PLA), poly glycolic acid (PGA) and their mixture, poly(lactic-co-glycolic acid) (PLGA). These polymers degrade by hydrolysis of the ester bond into lactic and/or glycolic acid monomers and the acidity of the degradation products activates inflammation (Yoon et al., 2008). The severity of the inflammatory response varies greatly and is thought to be directly related to the accumulation of degradation products (Murayama et al., 2002). The severity is also affected by the location in the body of the implant with soft tissue generally having a larger response than bone and cartilage (Athanasiou et al., 1996). Degradation of the polymer has an autocatalytic effect wherein the acidic degradation products cause further increased degradation of remaining polymers. Thus, the

structure of the material and the ability of degradation products to diffuse away from the bulk material greatly affects the inflammatory response (Cao et al., 2006). Numerous studies using PLGA implants have reported fibrous encapsulation, including as early as one week after implantation (Jones, 2008; Kim et al., 2007b; Thevenot et al., 2010). Fibrotic encapsulation decreases vascular growth into scaffolds, and in at least two cases, was sufficiently severe to lead to necrosis of cells growing within the scaffold (Cao et al., 2006; Thevenot et al., 2010). The need to reduce the inflammatory response and avoid fibrotic encapsulation limits the potential structures and, by association, material properties of biomaterials made from these polymers making it unsuitable for many applications.

Looking at natural polymer alternatives to silk, collagen has also been used extensively for tissue engineering. Collagen has very good cell interaction properties with some cell types having higher proliferation on collagen substrates than tissue culture plastic (Chevallay and Herbage, 2000). Collagen from various animal sources is also well tolerated *in vivo* with only a moderate immune response (Lee et al., 2001; Song et al., 2006). Collagen implants activate macrophages and MNGCs are often found surrounding and invading the material (Lyons et al., 2010; Vanluyn et al., 1994). The macrophages are likely involved in remodeling and the number of

immune cells decreases over time (Anselme et al., 1992). However, a major drawback for many clinical applications is that collagen has weak mechanical properties and is degraded very quickly. Collagen scaffolds implanted subcutaneously in rats degraded completely within one month of implantation. The tensile strength of processed collagen is less than 10 MPa, significantly less than the roughly 150 MPa required for tendons and bone (Altman et al., 2003). This makes native collagen on its own unsuitable for any weight bearing applications, or applications requiring that the material remain intact for greater than 15 days. To increase the strength and degradation time, various cross-linking methods have been devised. Depending on the method of crosslinking, the tensile strength can be increased up to 57 MPa (Pins et al., 1997). However, cross-linking changes the biological response *in vivo* often in negative ways. Most methods of cross-linking are associated with mineralization whereby calcium deposits begin forming in the implanted collagen within as little as 7 days and mineralization increases with time (Khor, 1997). While this can be beneficial for bone tissue engineering, it has been a major problem for many clinical uses of collagen, particularly for heart valve and other vascular applications. Interestingly, cross-linking can decrease the immune response possibly because it makes some of the foreign epitopes inaccessible. Thus, while collagen provides a good

substrate for cell adhesion, proliferation, and differentiation, it usually must be combined with additional materials for most applications in order to combat its lack of mechanical strength, rapid degradation, and propensity to be mineralized.

Very few studies have directly compared silk to either natural or synthetic alternatives without the addition of extraneous variables making comparisons of specific aspects of the biological response challenging. However, there are a few direct comparisons worth noting. In a direct comparison of silk, cross-linked collagen, and PLA films implanted intramuscularly in rats, silk induced the smallest inflammatory response (Enomoto et al., 2010). After 6 weeks silk films were surrounded by a layer of fibroblasts and macrophages 3-4 cells thick with macrophages located only adjacent to the film and no MNGCs were present. In contrast, collagen films elicited a slightly stronger inflammatory response with a layer of fibroblasts and macrophages 12-20 cells thick, and PLA had the strongest response with an even thicker layer of fibroblasts and macrophages as well as the presence of MNGCs. Furthermore, the collagen film was nearly completely degraded 6 weeks after implant while both the silk and PLA films remained intact. In a study investigating electrospun sheets made of silk, collagen, or the synthetic polymers Poly (3-hydroxybutyrate) (PHB), poly(caprolactone), polyamide, or PLA,

implanted on the epicardial surface of rats, silk elicited a mild inflammatory response with a less severe granulomatous response than the synthetic polymers with the exception of PHB (Castellano et al., 2014). Collagen had the mildest inflammatory response but had degraded significantly by 8 weeks. Silk and all of the synthetic polymers except PHB elicited a foreign body response with MNGCs but the reaction to silk was the least severe. PHB was the only synthetic polymer with a milder immune response as compared to silk and also had increased vascular ingrowth.

Depending on the material and function of the biomaterial, the foreign body response can be more or less detrimental. Because of the increased release of reactive oxygen intermediates and proteases, the foreign body response creates a harsher environment for the biomaterial to withstand (Anderson et al., 2008). This can lead to premature degradation and device failure in some applications. However, in other applications the degradation can be beneficial as it allows formation of replacement tissue or release of factors embedded in the construct. Silk is primarily degraded via the action of phagocytic cells, especially MNGCs (Wang et al., 2008). Thus, an increased presence of these immune cells increases degradation allowing for more and faster tissue ingrowth. In porous silk scaffolds implanted in bone, immature bone tissue and calcified tissue were found within the

scaffold in close proximity to MNGCs (Uebersax et al., 2013). The pattern of MNGC-mediated degradation followed by extracellular matrix deposition and finally mineralization is the same as for healthy bone remodeling. In another example, a knitted silk tube filled with a porous silk scaffold designed for anterior cruciate ligament regeneration had partially been replaced by native tissue at 24 weeks post implantation allowing it to retain the necessary mechanical strength and also undergo remodeling that is required for long-term functionality (Fan et al., 2009). Much of the degradation of the silk material that allowed for formation of new tissue was likely caused by the activity of FBGCs.

The exact bioresponse to implanted silk materials depends on the interrelated factors of the location of the implant within the body, the material format, and the degradation time. As with most implanted materials, silk implants with longer degradation times or implanted in soft tissues tend to induce a larger response than those with shorter degradation times or located within hard tissues. Unfortunately, despite the extensive number of *in vivo* studies, insufficient data exists to establish more detailed relationships between location of implant, silk format, and degradation time with specific aspects of the inflammatory response. Very few studies have performed more than a minimal analysis of the inflammatory response, and those with

detailed characterization utilize different sets of metrics making aggregation of the findings challenging. More studies are needed that analyze quantifiable metrics over time to give a complete picture of the severity of the response and also the specific cell types and regulatory pathways that are most affected. Only this level of meticulous characterization will allow for future rational design of materials that decrease the inflammatory response or modulate it in ways that are beneficial to the implant function. (Liu et al., 2014) provides an excellent example of the type of studies that are needed. In their work, activation of specific cytokines and the number of invading inflammatory cells was monitored over 3 months post implantation. With this information, one could make modifications to the implant that specifically target the cytokine pathways or specific cell types induced by the original material.

Ap-II.5 Vascular Ingrowth Into Silk Materials

One of the largest challenges facing the field of tissue engineering is the need to develop strategies that increase vascularization to improve oxygen and nutrient diffusion. Passive diffusion is limited to a few hundred microns and any cells further from a blood vessel than the diffusion limit undergo necrosis (Laschke et al.,

2006). This places a severe size limitation on tissue engineered constructs as necrosis increases the inflammatory response and inhibits tissue integration.

The ability of blood vessels to grow within silk scaffolds depends significantly on the silk processing method and scaffold properties such as pore size and pore interconnectivity (Ghanaati et al., 2010; Hofmann et al., 2013). Blood vessels are physically able to grow into silk scaffolds implanted *in vivo* but generally require biological signals to invade beyond the surface and into the bulk of the scaffold. Most silk scaffolds used for tissue engineering are designed to have a high porosity allowing vessels to form without the need to degrade the material. A study of acellular scaffolds implanted subcutaneously in mice found small vessels surrounding and on the periphery of the scaffold within 14 days (Ghanaati et al., 2011). The growth may be induced by the mild inflammatory response to silk. After longer *in vivo* culture periods, there was very little ingrowth of the vessels beyond a few hundred microns of the exterior of the scaffold. However, vascularization was much improved in scaffolds pre-seeded with osteoblasts prior to implantations. This is likely due to vascular endothelial growth factor (VEGF) and other angiogenic factors secreted by the cells.

Unger et al., 2012 further improved vascularization by pre-seeding scaffolds with endothelial cells as well as osteogenic cells that secrete angiogenic factors which lead to the endothelial cells self-organizing into capillary-like structures. Upon implantation, the vessel structures remained intact and became integrated with the host vasculature such that red blood cells were found within vessels composed of the pre-seeded cells. The ability to integrate pre-developed vasculature with host vessels creates important opportunities because, if designed properly, it could allow near immediate blood flow throughout a large construct. Many tissues rely on blood flow not only to avoid necrosis but also for important signaling factors such as those regulating differentiation.

One drawback of pre-vascularized scaffolds is that they require donor cells and long culture times making them unsuitable for many clinical needs. Alternative approaches have been investigated to improve vascular ingrowth from the host by modifying the scaffold structure, or by adding biological signaling molecules. Even highly porous scaffolds limit cell infiltration as demonstrated by the difficulty of evenly seeding scaffolds *in vitro*. To combat this issue, scaffolds have been designed with large, 250-500 micron diameter, arrayed channels to allow cells to quickly infiltrate deep within the scaffold (Wray et al., 2013). *In vivo*, these scaffolds had increased

vascularization by 14 days post implant as compared to scaffolds without channels (Rnjak-Kovacina et al., 2014). Cells also occupied the space within the channels indicating the ability of the host form new tissue within the relatively large open space. Thus, the channels are able to provide increased access to the bulk of the scaffold without detracting from the overall tissue integrity.

Other groups have focused on decorating the scaffold with pro-angiogenic factors, most frequently VEGF. VEGF is released from the scaffold and has a chemoattractant effect on nearby endothelial cells leading to increased vascular ingrowth. VEGF doped silk scaffolds had a significantly increased number of vessels as well as vessel surface area compared to untreated silk in a critically sized calvarial defect in rabbits (Zhang et al., 2013). The VEGF scaffolds also had increased mineralization, likely a direct result of the increased vasculature access.

Ap-II.6 Clinical Application: Small Diameter Vascular Grafts with Improved Patency

Vascular grafts for small vessels (less than 6 mm diameter) must meet a stringent set of requirements in order to maintain long-term functionality. The graft must have sufficient biocompatibility with

the surrounding tissue, flowing blood cells, and adjacent vessels such that it does not induce thrombosis while also having appropriate mechanical strength and elasticity to withstand systolic blood pressure. Autologous vessel transplants have thus far been the most clinically successful treatment. However, many patients requiring a vascular graft suffer from conditions that also cause deterioration of vessel integrity and therefore do not have a suitable donor vessel. For this reason, numerous tissue engineering strategies have been developed. Initially, non-natural polymers including polytetrafluoroethylene (PTFE, Teflon) and poly(ethyleneterephthalate) (PET, Dacron) were chosen. These materials performed well for large vessels but had poor patency for small vessels, often less than 50%. More recently, *in vivo* studies with silk tubular scaffolds have shown improved results as compared to PTFE and PET (see Table 2 for a list of studies characterizing silk vascular grafts *in vivo*).

PTFE and PET grafts in small vessels have a tendency to develop occlusions often due to thrombosis shortly after implant. One cause may be the large difference in mechanical properties between the graft and the adjacent vessel. PTFE and PET have significantly higher tensile strength and elastic modulus as compared to small vessels (Lovett et al., 2010). Silk, with tunable mechanical properties, can be fabricated to have more similar strength and elasticity to the adjacent vessel.

With a smoother gradation between the native vessel and the grafts, there is decreased disruption of the fluid flow through the vessel leading to a lower thrombic response (Lovett et al., 2010). This is supported by *in vivo* studies where PTFE scaffolds often formed occlusions within 24 hours and about half of the grafts failed within 4 weeks. Two groups using different fabrication methods showed that 1-1.5 mm diameter silk grafts implanted in the abdominal aorta of rats had much improved outcomes with 100% patency over 1 month in one study and 85.1% patency after 12 months in the other(Enomoto et al., 2010; Lovett et al., 2010).

In contrast to non-natural polymers, silk can be remodeled allowing cell attachment and infiltration which leads to degradation of the scaffold and replacement by native tissue over time. Endothelial cells begin covering the luminal surface of a silk scaffold within two weeks and cover over 90% of the luminal surface in 12 weeks (Enomoto et al., 2010). Smooth muscle cells also migrate into the scaffold in a similar time frame and form a thickened layer after 12 weeks. Thus, the silk scaffold provided a material in which the cells can self-organize into vessel-like structures. This was in contrast to PTFE scaffolds where neither cell type infiltrated through the graft. Additionally, CD68 (lysosomal/endosomal-associated membrane glycoprotein 4) positive macrophages were found within the silk

scaffold and contained cell structures indicative of phagocytosis, suggesting the cells were degrading the scaffold. Indeed, the silk content of the graft decreased 20% over 12 weeks and 60% at 48 weeks. At the same time, collagen was deposited on the scaffold to replace the lost silk material. The enhanced ability of silk to be remodeled is significant as remodeling of the scaffold towards native tissue decreases the chance of infection, host rejection, and thrombosis thus increasing the long-term patency of the graft.

While silk has made a significant improvement over PTFE and PET, further modifications could be made to improve the mechanical properties, interactions with cells, and overall patency. The best surface for minimizing negative biological responses is the body's natural surface consisting of a layer of endothelial cells. Thus, one way to improve current silk scaffolds is to make modifications that decrease the time until the luminal surface is completely covered by endothelial cells. Recently, groups have investigated the effect of adding biological factors and cell binding sites to stimulate endothelial cell infiltration and proliferation (Schneider et al., 2009). Other groups have added anti-thrombic factors such as heparin to decrease the initial thrombic response following implantation (Seib et al., 2014). Finally, the mechanical properties of the scaffold can be more closely matched to the surrounding vessel by combing silk with other materials (Yagi et

al., 2011). In order to move silk-based constructs into the clinical setting, studies using large animal models are needed to demonstrate efficacy under conditions that more accurately replicate the human body, particularly as it relates to the mechanical stresses induced by blood pressure.

Table Ap-II.2: In vivo studies of silk materials used for vascular grafts. (H = histology, IC = immunohistochemistry)

Silk material and processing	Response	In vivo model and tissue site	Time-points, analysis	Ref
silk formaldehyde cross-linked or collagen glutaraldehyde cross-linked coated commercial knitted polyester graft	100% patency, silk did not induce MNGCs whereas collagen did, silk tubes 85% and 97% cell coverage of luminal surface at 3 and 6 months respectively	abdominal aorta of dogs	3 days, 2 wk, 1, 3, 6 month H	(Huang et al., 2008)
wound silk fibers, coated in fibroin solution, EtOH treated	85% patency after 12 months, nearly complete endothelial cell covering of inner tube surface by 12 wks	abdominal aorta of rats	2, 4, 12, 24, 72 wks H, IC,	(Enomoto et al., 2010)
gel spun silk tube, MeOH treated	patent after 4 wks, interior surface of tube completely covered by endothelial cell layer at 4 wks	abdominal aorta of rats	2, 4 wk H, IC	(Lovett et al., 2010)
braided silk fiber	greater than 80%	abdominal	2, 8	(Yagi

tube coated with fibroin and cross-linked with poly(ethylene glycol diglycidyl ether)	patency at 8 wks, in depth quantitative analysis of tube remodeling and new tissue growth	aorta of rats	wk, H, IC	et al., 2011)
braided silk fiber tube coated with fibroin and EtOH treated	85% patency at 12 months, inner surface of tube mostly covered by endothelial cells at 9 wks	abdominal aorta of rats	9 wk, 12 month H, IC	(Nakazawa et al., 2011)
silk electrospun tube, MeOH treated, 1.5 mm diameter	endothelial, smooth muscle, and macrophage cells found on lumen and within scaffold, 100% patency at 7 days	abdominal aorta of rats	7 day H, IC	(Cattaneo et al., 2013)
silk solution coated silk fiber braided tube, EtOH treated	100 % patency in all grafts, silk tubes near complete coating of lumen by endothelial cells at 3 months while PET tubes had only 50% lumen coverage, silk tubes had significantly improved tissue integration compared to PET	abdominal aorta of rats	2 wk, 3 month H, IC	(Fukayama et al., 2015)

Ap-II.7 Clinical Applications: Ligament Reconstruction

Numerous studies have investigated silk materials as a potential replacement to current clinical tendon and ligament reconstruction strategies. Tendon and ligament injuries including anterior cruciate

ligament (ACL), rotator cuff, and Achilles tendon tears are quite common affecting over 500,000 people per year in the United States alone (Leong et al., 2014). Current clinical methods to repair tendon injuries typically utilize autografts, allografts, xenografts, or suture repair. However, each of these strategies has major drawbacks, including donor site morbidity, risk of disease transmission, and high risk of re-injury, and often does not lead to a complete return to pre-injury strength and range of motion. In the case of ACL repair, current clinical strategies also lead to the development of osteoarthritis. Thus, there is a need for tissue engineering strategies that would allow a complete recovery from injury without increasing the risk of additional health problems. The ideal material would have equivalent mechanical properties to the native tissue, allow remodeling, promote regeneration so that new ECM and tendon tissue could replace the material over time without scar tissue, and have a slow degradation rate in order to maintain the necessary mechanical properties until the replacement tissue could be developed.

In vitro studies (Altman et al., 2002) first demonstrated the feasibility of using silk scaffolds for tendon replacement. A method of weaving silk fibers was developed such that the final mechanical properties of the cord were similar to human ACLs and the scaffolds were shown to support progenitor cell growth and differentiation

towards tendon cell types. Initial studies testing silk scaffolds in *in vivo* models of tendon injuries demonstrated clinical potential for silk scaffolds. In both rabbit and pig models of ACL reconstruction, the silk scaffolds did not rupture and were able to maintain joint stabilization (Fan et al., 2009; Fan et al., 2008). By 6 months post-surgery scaffolds contained fibrous tissue ingrowth and the original silk fibers of the scaffold could still be detected demonstrating a slow degradation profile. However, scaffolds made simply of silk alone were unable to induce complete tendon healing. While the mechanical tensile strength was sufficient to prevent rupture, it was less than 50% compared to the native ACL and decreased over time suggesting the scaffold was degrading more quickly than it was replaced by new tissue (Fan et al., 2008). Tissue ingrowth into the scaffold was incomplete and after 6 months spaces between the silk fibers of the scaffold existed. There was also incomplete formation of the bone-tendon junction, an important indicator of long-term positive clinical outcomes, with the presence of aligned collagen fibers but little to no mineralized fibrocartilage and poor mineralization and graft incorporation into the bone tunnel (Fan et al., 2008).

Following on to these initial studies, many groups have made improvements to silk tendon replacements by incorporating additional materials or pre-seeding the scaffold with tendon cell types. Pre-

seeding scaffolds with mesenchymal stem cells (MSCs) dramatically increased tissue regeneration, collagen deposition and blood vessel growth within a scaffold used for ACL repair (Fan et al., 2008). A similar increase in tissue growth and collagen deposition was seen in silk scaffolds pre-seeded with tendon stem/progenitor cells (TSPCs) used for rotator cuff repair (Shen et al., 2014). The TSPCs also caused a decrease in the inflammatory response with more fibroblasts and less lymphocytes growing within the scaffold as compared to unseeded controls. Pre-seeded scaffolds were better able to maintain mechanical strength, likely because of the increased amount of deposited ECM and organized collagen fibers and decreased inflammatory response (Fan et al., 2009).

While pre-seeding of silk scaffolds has led to improved tendon regeneration, it is not ideal due to long culture times and increased risk of disease transfer, and did little to improve the bone-tendon junction. Thus, other groups have focused on improving the scaffold material. As an alternative means to encourage increased cellularity within the scaffold, silk scaffolds have been coated with a collagen film or filled with collagen sponges. Reconstituted collagen lacks the mechanical properties required for tendons and degrades quickly, but has improved cell attachment, growth, and differentiation compared to silk (Chevallay and Herbage, 2000; Seo et al., 2009a). Thus,

combining the mechanical benefits of silk with the cell compatibility benefits of collagen can make an ideal blend for many tissue engineering applications. Indeed, silk-collagen scaffolds greatly improved tendon reconstruction (Kwon et al., 2014; Seo et al., 2009b; Shen et al., 2014). Silk-collagen scaffolds had significantly increased regenerated tissue and organized collagen fibers compared to silk only scaffolds (Shen et al., 2014). The silk-collagen scaffolds also had increased vasculature at 2 months post surgery, which is an integral aspect of tendon healing and likely contributed greatly to the improved phenotypes seen at later time points. The ligament-bone junction had more fibrocartilage and calcified fibrocartilage compared to silk only scaffolds demonstrating that it more closely resembled the native transition. Interestingly, the silk of silk-collagen scaffolds showed less degradation at 18 months than the silk of silk-only scaffolds. The initial collagen scaffold was degraded quickly suggesting the protective effect on silk degradation may be due to the additional vasculature, cell growth, and provisional matrix provided by incorporation of collagen. The regenerated tendons still lacked the tensile strength of native tendons, but were stronger than silk-only scaffolds (Kwon et al., 2014). As an alternative means to improve the bone-tendon junction of silk scaffolds, tricalcium phosphate (TCP) has been incorporated at the tips of the tendon scaffold (Li et al., 2014a). Addition of TCP

significantly increased fibrous tissue ingrowth surrounding the bone insertion site and Sharpey's fibers could be detected (Li et al., 2014b).

The more recent improved silk scaffolds with additional materials or pre-seeding show clinical promise for improving some of the negative aspects of current clinical strategies (see table 3 for list of studies). Unfortunately, at this time it is difficult to determine how close silk-based approaches are to current clinical standards because none of the *in vivo* studies directly compare tendon reconstruction with silk scaffolds to current clinical methods, and very few of the studies compare the reconstructed tendon to the native tendon. Thus, it is difficult to determine whether any of the newly designed silk scaffolds are likely to improve clinical outcomes. Further studies are needed in large animal models that directly compare silk-based scaffolds with routinely used autograft and allograft methods. Ideally, these studies should investigate both early tissue ingrowth and vasculature as well as long-term development of mature structures, maintenance of mechanical properties, and preservation of surrounding cartilage.

Table Ap-II.3: In vivo studies of silk materials used for tendon and ligament reconstruction. (H = histology, IC = immunohistochemistry, HM = histomorphology, MT = mechanical testing)

Silk material and processing	Response	In vivo model and	Time-poin	Ref

		tissue site	**ts, analysis**	
knitted silk mesh tube filled with porous silk scaffold unseeded or seeded with autologous MSCs	cell ingrowth and ECM deposition minimal in unseeded scaffold, more pronounced in seeded scaffold, tensile strength met requirements but significantly less than reported for native ACL and decreased over time	ACL reconstruction in rabbit	2,4, 6 month H, HM, MT	(Fan et al., 2008)
knitted silk mesh tube filled with porous silk scaffold unseeded or seeded with pig MSCs	significant ECM deposition and cell ingrowth into seeded scaffold with mostly normal insertion site including Sharpey's fibers, little remodeling of unseeded scaffold and less developed insertion site. Seeded scaffold retained tensile strength but only 53% of native ACL.	ACL reconstruction in pig	6 month H, IC, HM, MT	(Fan et al., 2009)
braided silk fiber tube filled with collagen-hyaluronan porous scaffold	silk collagen-HA scaffold had increased remodeling including vascular ingrowth and lower inflammatory response compared to silk only constructs	ACL reconstruction in dogs	6 wk H	(Seo et al., 2009a)
braided silk fiber tube filled with porous collagen scaffold and	seeding greatly enhanced remodeling including more organized	rotator cuff reconstruction in	1,2, 3 month H,	(Shen et al., 2012)

seeded with Tendon stem/progenitor cells	collagen deposition and decreased the immune response	rabbit	IC, HM	
braided silk fiber tube coated in silk/hydroxyapatite solution, MeOH treated	significant ingrowth of fibrous tissue, significant mineralization including within bone tunnel	ACL reconstruction in rabbit	2, 4 month H, IC, HM, MT	(Shi et al., 2013)
braided silk fiber tube filled with porous collagen-chondroitan scaffold	tensile strength 76% of native tissue, significant regenerated tissue with replacement of original collagen scaffold with native collagen bundles but also some fibrosis	achilles reconstruction in rabbit	6 month H, MT	(Kwon et al., 2014)
braided silk fiber tube with tricalcium phosphate polyether ether ketone anchor	substantial tissue ingrowth at junction, bone tunnel contained mineralized as well as unmineralized tissue, Sharpey's fibers present	ACL reconstruction in pig	3 month H	(Li et al., 2014a)
braided silk fiber tube with tricalcium phosphate polyether ether ketone anchor	tensile strength increased with time and similar to autograft studies but less than native ACL, anchor increased silk to bone attachment including regeneration of mineralized tissue and Sharpey's fibers	ACL reconstruction in pig	3, 6 month H, MT	(Li et al., 2014b)
braided silk fiber tube filled with porous collagen scaffold, or braided silk fiber tube alone	silk-collagen constructs had significantly increased remodeling including more and better	ACL reconstruction in rabbit	2,6, 18 month H, IC, HM,	(Shen et al., 2014)

	organized collagen fibrils, silk-collagen had better bone-tendon transition with mineralized fibrocartilage and better preservation of cartilage within the knee joint		QPCR	
interwoven silk and PLGA fiber mesh filled with porous collagen scaffold, seeded with rabbit MSCs	tensile strength increased from 2 to 4 months, seeded samples significantly stronger than unseeded and 58% of native tendon at 4 months more remodeling and collagen deposition in seeded scaffolds	achilles reconstruction in rabbit	2, 4 month H, MT	(Zhang et al., 2015)

Ap-II.8 Clinical Applications: Breast Implants

The ability of silk scaffolds to maintain their shape over long time periods makes them an ideal material for soft tissue reconstruction. Recently, a silk scaffold commercially produced by Allergan was utilized for breast implants in a preliminary clinical trial (De Vita et al., 2014). The number of breast implant surgeries performed annually is increasing for a number of reasons including an increasing number of mastectomies and improved surgical procedures (McGuire et al., 2009). Silicone breast implants have been in use for over two decades but suffer from capsular contraction and rupture

leading to 30-54% re-operation depending on the nature of original surgery (Maxwell et al., 2015). Silicone is not able to be remodeled and it was hypothesized that using a material capable of remodeling such as silk could improve long-term outcomes. The preliminary clinical trial investigated 21 cases of silk implant breast reconstruction, all in oncological patients not treated with radiation (De Vita et al., 2014). Six months after surgery only one implant required re-operation and patient satisfaction was similar to silicone implants. This initial study provides encouraging results for use of silk scaffold breast implants, but further investigation of long-term outcomes, use in more complicated cases, and more in depth analysis of patient response is needed before conclusions can be drawn comparing silk to currently used silicone implants. If silk scaffolds continue to perform well for breast implants, they may also prove useful for other soft tissue applications such as dermal layer skin reconstruction to reduce scarring and abdominal wall reconstruction.

Ap-II.9 Clinical Applications: Skin Graft

Dermal wound healing continues to be a major clinical concern. Whether from major burns, injuries, or diabetic ulcers, improved methods that speed the healing process and cause less scar formation

are needed to decrease the risk of infection, dehydration, and painful scars associated with dermal wounds. The process of dermal wound healing involves first platelet aggregation and inflammation, then the formation of granulation tissue, and finally re-epithelialization and remodeling of newly generated tissue. Clinically, many dressings and grafts have been developed to speed and improve the wound healing process. However, negative outcomes including painful scarring, permanent ulcers, and infections causing serious health problems and possibly death remain problems. Various forms of silk including silk wound dressings and silk graft scaffolds have been tested *in vivo* for their efficacy improving healing and the condition of regenerated skin. Many of these studies have demonstrated improved results over clinically used treatments. In an early study, silk film wound dressings outperformed Duro Active, a dressing commonly used clinically, reducing the healing time of a full thickness skin wound in mice by 7 days (Sugihara et al., 2000). The rate of healing was similar to another clinically used material AlloaskD, which is made from lyophilized porcine dermis and thus suffers from possible disease transmission risks. Similarly, a silk-gelatin electrospun dressing functionalized with astroglaside IV significantly improved healing in a rat full thickness burn model with increased vascularization, collagen deposition, and tissue organization compared to burns treated with

silk-gelatin only dressing and untreated controls (Shan et al., 2015). A major concern for dermal wound treatments is preventing infection as most morbidity associated with skin wounds is caused by infection. (Lan et al., 2014) combined antibiotic loaded gelatin microspheres in silk scaffolds creating a slow drug release wound dressing. The dressings were tested on full thickness burn wounds in rats that had been exposed to *P. aeruginosa* bacteria. The antibiotic-loaded dressings had significantly decreased inflammation and improved healing including faster re-epithelialization as compared to dressings without antibiotic and gauze treated controls.

In addition to wound dressings, other groups have focused on silk-based grafts that remain in the wound and become integrated into the healing tissue. Porous silk scaffolds implanted in a rat full thickness wounds outperformed PVA porous scaffolds with a decreased inflammatory response and improved vascular ingrowth (Guan et al., 2010). Other groups have improved upon this result by functionalizing the silk scaffold with additional factors. Silk combined with alginate, a material purified from algae with excellent hydration properties, improved the healing time in a rat full thickness wound from 12 to 6 days compared to clinically used NuGuoz (Roh et al., 2006). The silk-alginate treated group also had increased collagen deposition. Electropun silk scaffold functionalized by culturing adipose derived

MSCs for 7 days and then decellurizing the scaffold prior to implantation, significantly increased wound healing of a full thickness wound in diabetic mice (Navone et al., 2014). The size of the wound was decreased by 50% at day 10 as compared to silk only or untreated controls. The decellurlazed scaffold had more organized tissue regeneration with a clear epithelial-dermal junction and hair follicles within the wounded area.

These studies demonstrate the ability of xeno-free silk materials to improve skin wound healing, often in direct comparison to current clinical treatments, suggesting these materials are ready to enter clinical testing (see table 4 for list of studies). It is interesting to note that the processing and fabrication methods varied widely for the same application. Many of the materials were designed to improve a specific aspect of healing and could possibly be combined to create an even further improvement.

Table Ap-II.4: In vivo studies of silk materials used for skin grafts and dermal wound dressings. (H = histology, IC = immunohistochemistry)

Silk material and processing	Response	In vivo model and	Time-points,	Ref

		tissue site	**analysis**	
silk film dressing	silk film promoted better healing than clinically used DuoActive and similar healing as AlloaskD	full thickness wound in nude mice	7, 14, 21 day H	(Sugihara et al., 2000)
lyophilized silk-alginate homogenous mixture	silk-alginate blended sponge increased speed of re-epithelialization from 12 to 6 days compared to NuGuaz control, more collagen deposition and higher number of dividing epithelial cells	full thickness wound in rat	3, 7, 10, 14 day H, IC	(Roh et al., 2006)
electrically polarized hydroxyapatite in silk gel fixed with glutaraldehyde and osmium oxide, lyophilized, EtOH treated	scaffolds with polarized hydroxyapatite performed similarly to clinically used IntraSite gel, better than scaffolds with non-polarized hydroxyapatite	full thickness wound in pig	6, 11, 18 day H	(Okabayashi et al., 2009)
lyophilized porous silk scaffold	smaller inflammatory reaction and improved dermis healing compared to PVA scaffold	full thickness wound in rat	3, 7 ,10, 18 day H	(Guan et al., 2010)
lyophilized porous silk scaffold with gentamycin sulfate-impregnated gelatin microspheres, MeOH treated	decreased inflamation and increased vascularization and speed of re-epithelialization compared to non-antibiotic loaded	full thickness burn in rat, bacteria applied to wound 24 hrs after	3,7,10, 14, 21 day H, IC	(Lan et al., 2014)

	and gauze control	burn		
electropsun silk scaffold, EtOH treated, pre-seeded with adipose MSC followed by decellurization	cell seeded and seeded-decellurlarized scaffold increased speed of healing as compared to unseeded silk and untreated controls	full thickness wound in diabetic mice	3, 7 , 10, 14 day wound healing	(Navone et al., 2014)
silk-gelatin electrospun dressing with astragaloside IV	astragaloside infused dressing had improved healing, more organized tissue regeneration, and more vascularization compared to dressing alone and untreated control	full thickness burn in rat	5,10,17,24,31 day H, IC	(Shan et al., 2015)

Ap-II.10 Conclusions

Silk is a versatile natural protein polymer that can be fabricated into many different structures with a wide range of physical properties. Key to its use in clinical application is the favorable short- and long-term biological responses. Silk induces a mild inflammatory response *in vivo*, with recruitment and activation of macrophages, and often a mild foreign body response that includes the formation of MCGCs. The response is affected by the material structure, method of fabrication, and site of implantation within the body. In general, implants with longer degradation times and implanted into soft tissues have a higher

response than materials with shorter degradation times or implanted in hard tissues. Importantly, activation of the immune response does not include activation of the adaptive immune response and thus formation of antibodies towards silk and downstream severe reactions do not occur. The inflammatory and foreign body response tends to peak 1-3 weeks post implantation and then decreases over time with fewer immune cells and less granulation tissue surrounding the implant. A depiction of a typical biological response to silk over time is shown in Figure 2. Activation of the inflammatory response is often beneficial as it leads to increased remodeling and degradation of silk. The enhanced ability to be remodeled at a slow rate is a significant advantage of silk when compared to most synthetic materials and to the rapid degradation of collagens. This feature allows for improved integration with the host tissue and vascular ingrowth, both of which aid in attenuating the foreign body response, preventing fibrous encapsulation, and improving the long-term biocompatibility of the construct. Silk materials also have not been demonstrated to induce mineralization, except when used in calcified tissues. While silk allows for cell attachment, proliferation, and differentiation, some applications require better cell interactions than silk alone can provide. In many of these instances, silk has been combined with additional materials such

as collagen or growth factors, to successfully improve or specifically modulate cell response.

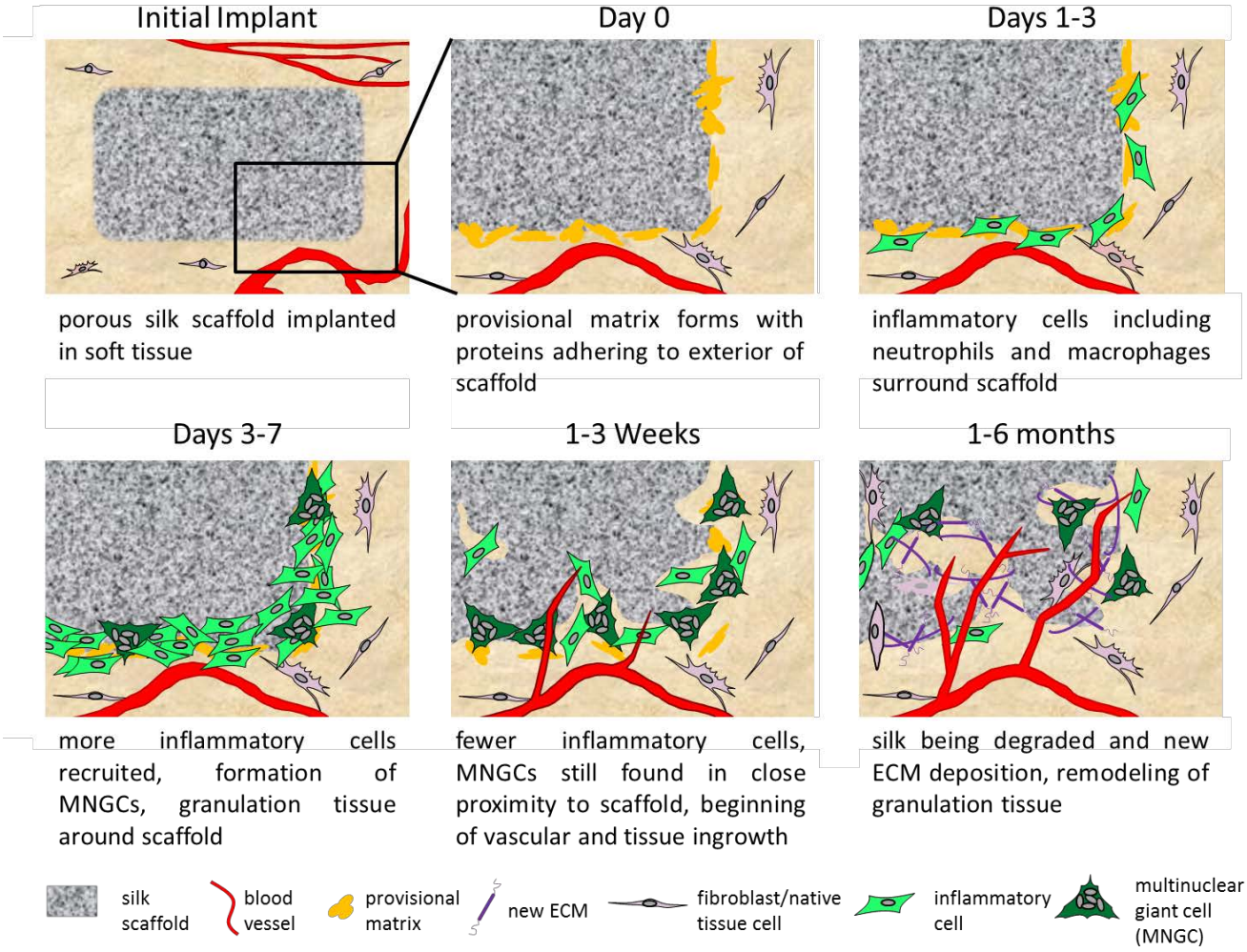

Figure Ap-II.2: Immune response to implanted silk. Overview of immune response to silk materials *in vivo* using a porous silk scaffold as an example.

The combination of versatility and biocompatibility of silk make it a promising material for many clinical applications beyond a suture material. Indeed, it has recently been used in clinical trials including for breast reconstruction and tympanic membrane repair (Lee et al.,

2015; Maxwell et al., 2015). However, in order for silk to be used more extensively, more detailed analysis of its immune response including more extensive characterization of M1 verses M2 macrophage activation, locally released cytokines, and the time course of activation of the foreign body response are needed. This knowledge will allow for better prediction of the specific bioresponse to a silk construct at a given implantation site, which in addition to improving functionality, would also greatly enhance the translational ability for specific purposes. Rational design of constructs, such as incorporation of pharmacological agents, could then be used to augment particular beneficial aspects of the inflammatory response, such as vascular ingrowth, while simultaneously inhibiting other aspects such as MNGC activation. The use of silk as a biomaterial beyond its role as a suture material has been studied for well over a decade and, with extensive *in vitro* characterization and more recently *in vivo* studies, has the potential of becoming a standard clinical treatment for numerous applications.

REFERENCES

Adams, D.S., Levin, M., 2013. Endogenous voltage gradients as mediators of cell-cell communication: strategies for investigating bioelectrical signals during pattern formation. Cell and tissue research 352, 95-122.

Adams, D.S., Masi, A., Levin, M., 2007. H+ pump-dependent changes in membrane voltage are an early mechanism necessary and sufficient to induce Xenopus tail regeneration. Development 134, 1323-1335.

Altman, G.H., Diaz, F., Jakuba, C., Calabro, T., Horan, R.L., Chen, J., Lu, H., Richmond, J., Kaplan, D.L., 2003. Silk-based biomaterials. Biomaterials 24, 401-416.

Altman, G.H., Horan, R.L., Lu, H.H., Moreau, J., Martin, I., Richmond, J.C., Kaplan, D.L., 2002. Silk matrix for tissue engineered anterior cruciate ligaments. Biomaterials 23, 4131-4141.

Anderson, J.M., 2001. Biological responses to materials. Annual Review of Materials Research 31, 81-110.

Anderson, J.M., Rodriguez, A., Chang, D.T., 2008. Foreign body reaction to biomaterials. Seminars in immunology 20, 86-100.

Anselme, K., Petite, H., Herbage, D., 1992. Inhibition of Calcification Invivo by Acyl Azide Cross-Linking of a Collagen-Glycosaminoglycan Sponge. Matrix 12, 264-273.

Arai, T., Freddi, G., Innocenti, R., Tsukada, M., 2004. Biodegradation of Bombyx mori silk fibroin fibers and films. Journal of Applied Polymer Science 91, 2383-2390.

Aramwit, P., Kanokpanont, S., De-Eknamkul, W., Srichana, T., 2009. Monitoring of inflammatory mediators induced by silk sericin. Journal of Bioscience and Bioengineering 107, 556-561.

Athanasiou, K.A., Niederauer, G.G., Agrawal, C.M., 1996. Sterilization, toxicity, biocompatibility and clinical applications of polylactic acid polyglycolic acid copolymers. Biomaterials 17, 93-102.

Beane, W.S., Morokuma, J., Adams, D.S., Levin, M., 2011. A Chemical Genetics Approach Reveals H,K-ATPase-Mediated Membrane Voltage Is Required for Planarian Head Regeneration RID A-5918-2011. Chemistry & biology 18, 77-89.

Ben-Porath, I., Thomson, M.W., Carey, V.J., Ge, R., Bell, G.W., Regev, A., Weinberg, R.A., 2008. An embryonic stem cell-like gene expression signature in poorly differentiated aggressive human tumors. Nat Genet 40, 499-507.
Bennett, E.S., Smith, B.A., Harper, J.M., 2004. Voltage-gated Na+ channels confer invasive properties on human prostate cancer cells. Pflugers Archiv-European Journal of Physiology 447, 908-914.
Berridge, M.J., Lipp, P., Bootman, M.D., 2000. The versatility and universality of calcium signalling. Nature reviews.Molecular cell biology 1, 11-21.
Bizzarri, M., Cucina, A., Biava, P.M., Proietti, S., D'Anselmi, F., Dinicola, S., Pasqualato, A., Lisi, E., 2011. Embryonic Morphogenetic Field Induces Phenotypic Reversion in Cancer Cells. Review Article. Current Pharmaceutical Biotechnology 12, 243-253.
Blackiston, D., Adams, D.S., Lemire, J.M., Lobikin, M., Levin, M., 2011. Transmembrane potential of GlyCl-expressing instructor cells induces a neoplastic-like conversion of melanocytes via a serotonergic pathway RID A-5918-2011. Disease Models & Mechanisms 4, 67-85.
Blackiston, D.J., Anderson, G.M., Rahman, N., Bieck, C., Levin, M., 2015. A novel method for inducing nerve growth via modulation of host resting potential: gap junction-mediated and serotonergic signaling mechanisms. Neurotherapeutics 12, 170-184.
Blackiston, D.J., Levin, M., 2013. Ectopic eyes outside the head in Xenopus tadpoles provide sensory data for light-mediated learning. Journal of Experimental Biology 216, 1031-1040.
Borjesson, S.I., Elinder, F., 2008. Structure, Function, and Modification of the Voltage Sensor in Voltage-Gated Ion Channels. Cell Biochemistry and Biophysics 52, 149-174.
Boyden, E.S., Zhang, F., Bamberg, E., Nagel, G., Deisseroth, K., 2005. Millisecond-timescale, genetically targeted optical control of neural activity. Nature neuroscience 8, 1263-1268.
Brackenbury, W.J., Chioni, A.-M., Diss, J.K.J., Djamgoz, M.B.A., 2007. The neonatal splice variant of Nav1.5 potentiates in vitro invasive behaviour of MDA-MB-231 human breast cancer cells. Breast cancer research and treatment 101, 149-160.
Brackenbury, W.J., Isom, L.L., 2011. Na+ channel beta subunits: overachievers of the ion channel family. Frontiers in Pharmacology 2, 11.
Brinster, R.L., 1974. Effect of Cells Transferred into Mouse Blastocyst on Subsequent Development. Journal of Experimental Medicine 140, 1049-1056.
Brisson, L., Gillet, L., Calaghan, S., Besson, P., Le Guennec, J.Y., Roger, S., Gore, J., 2011. Na(V)1.5 enhances breast cancer cell

invasiveness by increasing NHE1-dependent H+ efflux in caveolae. Oncogene 30, 2070-2076.
Brockes, J.P., 1998. Regeneration and cancer. Biochimica Et Biophysica Acta-Reviews on Cancer 1377, M1-M11.
Brown, J., Lu, C.-L., Coburn, J., Kaplan, D.L., 2015. Impact of silk biomaterial structure on proteolysis. Acta Biomaterialia 11, 212-221.
Cao, Y., Mitchell, G., Messina, A., Price, L., Thompson, E., Penington, A., Morrison, W., O'Connor, A., Stevens, G., Cooper-White, J., 2006. The influence of architecture on degradation and tissue ingrowth into three-dimensional poly(lactic-co-glycolic acid) scaffolds in vitro and in vivo. Biomaterials 27, 2854-2864.
Capecci, J., Forgac, M., 2013. The Function of Vacuolar ATPase (V-ATPase) a Subunit Isoforms in Invasiveness of MCF10a and MCF10CA1a Human Breast Cancer Cells. Journal of Biological Chemistry 288, 32731-32741.
Castellano, D., Blanes, M., Marco, B., Cerrada, I., Ruiz-Sauri, A., Pelacho, B., Arana, M., Montero, J.A., Cambra, V., Prosper, F., Sepulveda, P., 2014. A comparison of electrospun polymers reveals poly(3-hydroxybutyrate) fiber as a superior scaffold for cardiac repair. Stem cells and development 23, 1479-1490.
Cattaneo, I., Figliuzzi, M., Azzollini, N., Catto, V., Fare, S., Tanzi, M.C., Alessandrino, A., Freddi, G., Remuzzi, A., 2013. In vivo regeneration of elastic lamina on fibroin biodegradable vascular scaffold. International Journal of Artificial Organs 36, 166-174.
Chaudhuri, O., Koshy, S.T., da Cunha, C.B., Shin, J.W., Verbeke, C.S., Allison, K.H., Mooney, D.J., 2014. Extracellular matrix stiffness and composition jointly regulate the induction of malignant phenotypes in mammary epithelium. Nature Materials 13, 970-978.
Chevallay, B., Herbage, D., 2000. Collagen-based biomaterials as 3D scaffold for cell cultures: applications for tissue engineering and gene therapy. Medical & biological engineering & computing 38, 211-218.
Ciardiello, F., McGeady, M.L., Kim, N., Basolo, F., Hynes, N., Langton, B.C., Yokozaki, H., Saeki, T., Elliott, J.W., Masui, H., Mendelsohn, J., Soule, H., Russo, J., Salomon, D.S., 1990. TRANSFORMING GROWTH FACTOR-ALPHA EXPRESSION IS ENHANCED IN HUMAN MAMMARY EPITHELIAL-CELLS TRANSFORMED BY AN ACTIVATED C-HA-RAS PROTOONCOGENE BUT NOT BY THE C-NEU PROTOONCOGENE, AND OVEREXPRESSION OF THE TRANSFORMING GROWTH FACTOR-ALPHA COMPLEMENTARY-DNA LEADS TO TRANSFORMATION. Cell Growth & Differentiation 1, 407-420.
Critchfield, A.S., McCabe, R., Klebanov, N., Richey, L., Socrate, S., Norwitz, E.R., Kaplan, D.L., House, M., 2014. Biocompatibility of a sonicated silk gel for cervical injection during pregnancy: in vivo and in

vitro study. Reproductive sciences (Thousand Oaks, Calif.) 21, 1266-1273.
Cullen, P.J., Lockyer, P.J., 2002. Integration of calcium and Ras signalling. Nature reviews.Molecular cell biology 3, 339-348.
Day, M.L., Winston, N., McConnell, J.L., Cook, D., Johnson, M.H., 2001. tiK(+) toK(+): an embryonic clock? Reproduction Fertility and Development 13, 69-79.
De Vita, R., Buccheri, E.M., Pozzi, M., Zoccali, G., 2014. Direct to implant breast reconstruction by using SERI (R), preliminary report. Journal of Experimental & Clinical Cancer Research 33, 78-78.
Debnath, J., Mills, K.R., Collins, N.L., Reginato, M.J., Muthuswamy, S.K., Brugge, J.S., 2002. The role of apoptosis in creating and maintaining luminal space with normal and oncogene-expressing mammary acini. Cell 111, 29-40.
Debnath, J., Muthuswamy, S.K., Brugge, J.S., 2003. Morphogenesis and oncogenesis of MCF-10A mammary epithelial acini grown in three-dimensional basement membrane cultures. Methods 30, 256-268.
Dewair, M., Baur, X., Ziegler, K., 1985. Use of immunoblot technique for detection of human IgE and IgG antibodies to individual silk proteins. The Journal of allergy and clinical immunology 76, 537-542.
Dirat, B., Bochet, L., Dabek, M., Daviaud, D., Dauvillier, S., Majed, B., Wang, Y.Y., Meulle, A., Salles, B., Le Gonidec, S., Garrido, I., Escourrou, G., Valet, P., Muller, C., 2011. Cancer-Associated Adipocytes Exhibit an Activated Phenotype and Contribute to Breast Cancer Invasion. Cancer research 71, 2455-2465.
Enomoto, S., Sumi, M., Kajimoto, K., Nakazawa, Y., Takahashi, R., Takabayashi, C., Asakura, T., Sata, M., 2010. Long-term patency of small-diameter vascular graft made from fibroin, a silk-based biodegradable material. Journal of vascular surgery 51, 155-164.
Etienne, O., Schneider, A., Kluge, J.A., Bellemin-Laponnaz, C., Polidori, C., Leisk, G.G., Kaplan, D.L., Garlick, J.A., Egles, C., 2009. Soft tissue augmentation using silk gels: an in vitro and in vivo study. Journal of periodontology 80, 1852-1858.
Fan, H., Liu, H., Toh, S.L., Goh, J.C., 2009. Anterior cruciate ligament regeneration using mesenchymal stem cells and silk scaffold in large animal model. Biomaterials 30, 4967-4977.
Fan, H., Liu, H., Wong, E.J.W., Toh, S.L., Goh, J.C.H., 2008. In vivo study of anterior cruciate ligament regeneration using mesenchymal stem cells and silk scaffold. Biomaterials 29, 3324-3337.
Ferretti, C., Bruni, L., Dangles-Marie, V., Pecking, A.P., Bellet, D., 2007. Molecular circuits shared by placental and cancer cells, and their implications in the proliferative, invasive and migratory capacities of trophoblasts. Human Reproduction Update 13, 121-141.

Forbes, S.J., Rosenthal, N., 2014. Preparing the ground for tissue regeneration: from mechanism to therapy. Nature medicine 20, 857-869.
Fraser, S.P., Diss, J.K.J., Chioni, A.M., Mycielska, M.E., Pan, H.Y., Yamaci, R.F., Pani, F., Siwy, Z., Krasowska, M., Grzywna, Z., Brackenbury, W.J., Theodorou, D., Koyuturk, M., Kaya, H., Battaloglu, E., De Bella, M.T., Slade, M.J., Tolhurst, R., Palmieri, C., Jiang, J., Latchman, D.S., Coombes, R.C., Djamgoz, M.B.A., 2005. Voltage-gated sodium channel expression and potentiation of human breast cancer metastasis RID C-5994-2008. Clinical Cancer Research 11, 5381-5389.
Fukayama, T., Takagi, K., Tanaka, R., Hatakeyama, Y., Aytemiz, D., Suzuki, Y., Asakura, T., 2015. Biological Reaction to Small-Diameter Vascular Grafts Made of Silk Fibroin Implanted in the Abdominal Aortae of Rats. Annals of Vascular Surgery 29, 341-352.
Furtado, C.M., Marcondes, M.C., Sola-Penna, M., de Souza, M.L.S., Zancan, P., 2012. Clotrimazole Preferentially Inhibits Human Breast Cancer Cell Proliferation, Viability and Glycolysis. Plos One 7, e30462-e30462.
Ge, Z., Yang, Q., Xiang, X., Liu, K.Z., 2012. Assessment of silk fibroin for the repair of buccal mucosa in a rat model. International journal of oral and maxillofacial surgery 41, 673-680.
Ghanaati, S., Orth, C., Unger, R.E., Barbeck, M., Webber, M.J., Motta, A., Migliaresi, C., James Kirkpatrick, C., 2010. Fine-tuning scaffolds for tissue regeneration: effects of formic acid processing on tissue reaction to silk fibroin. Journal of tissue engineering and regenerative medicine 4, 464-472.
Ghanaati, S., Unger, R.E., Webber, M.J., Barbeck, M., Orth, C., Kirkpatrick, J.A., Booms, P., Motta, A., Migliaresi, C., Sader, R.A., Kirkpatrick, C.J., 2011. Scaffold vascularization in vivo driven by primary human osteoblasts in concert with host inflammatory cells. Biomaterials 32, 8150-8160.
Ghaznavi, A.M., Kokai, L.E., Lovett, M.L., Kaplan, D.L., Marra, K.G., 2011. Silk Fibroin Conduits A Cellular and Functional Assessment of Peripheral Nerve Repair. Annals of Plastic Surgery 66, 273-279.
Girault, A., Chebli, J., Prive, A., Trinh, N.T., Maille, E., Grygorczyk, R., Brochiero, E., 2015. Complementary roles of KCa3.1 channels and beta1-integrin during alveolar epithelial repair. Respir Res 16, 100.
Guan, G., Bai, L., Zuo, B., Li, M., Wu, Z., Li, Y., Wang, L., 2010. Promoted dermis healing from full-thickness skin defect by porous silk fibroin scaffolds (PSFSs). Bio-medical materials and engineering 20, 295-308.

Haas, B.R., Sontheimer, H., 2010. Inhibition of the Sodium-Potassium-Chloride Cotransporter Isoform-1 Reduces Glioma Invasion. Cancer research 70, 5597-5606.
Harris, P.J., Speranza, G., Dansky Ullmann, C., 2012. Targeting embryonic signaling pathways in cancer therapy. Expert Opin Ther Targets 16, 131-145.
Hegle, A.P., Marble, D.D., Wilson, G.F., 2006. A voltage-driven switch for ion-independent signaling by ether-a-go-go K+ channels. Proceedings of the National Academy of Sciences of the United States of America 103, 2886-2891.
Hendrix, M.J., Seftor, E.A., Seftor, R.E., Kasemeier-Kulesa, J., Kulesa, P.M., Postovit, L.M., 2007. Reprogramming metastatic tumour cells with embryonic microenvironments. Nat Rev Cancer 7, 246-255.
Hinard, V., Belin, D., Konig, S., Bader, C.R., Bernheim, L., 2008. Initiation of human myoblast differentiation via dephosphorylation of Kir2.1 K+ channels at tyrosine 242. Development 135, 859-867.
Hockaday, D.C., Shen, S., Fiveash, J., Raubitschek, A., Colcher, D., Liu, A., Alvarez, V., Mamelak, A.N., 2005. Imaging glioma extent with I-131-TM-601. Journal of Nuclear Medicine 46, 580-586.
Hoenerhoff, M.J., Chu, I., Barkan, D., Liu, Z.Y., Datta, S., Dimri, G.P., Green, J.E., 2009. BMI1 cooperates with H-RAS to induce an aggressive breast cancer phenotype with brain metastases. Oncogene 28, 3022-3032.
Hofmann, S., Hilbe, M., Fajardo, R.J., Hagenmuller, H., Nuss, K., Arras, M., Muller, R., von Rechenberg, B., Kaplan, D.L., Merkle, H.P., Meinel, L., 2013. Remodeling of tissue-engineered bone structures in vivo. European journal of pharmaceutics and biopharmaceutics : official journal of Arbeitsgemeinschaft fur Pharmazeutische Verfahrenstechnik e.V 85, 119-129.
Horan, R.L., Antle, K., Collette, A.L., Huang, Y.Z., Huang, J., Moreau, J.E., Volloch, V., Kaplan, D.L., Altman, G.H., 2005. In vitro degradation of silk fibroin. Biomaterials 26, 3385-3393.
House, C.D., Vaske, C.J., Schwartz, A.M., Obias, V., Frank, B., Luu, T., Sarvazyan, N., Irby, R., Strausberg, R.L., Hales, T.G., Stuart, J.M., Lee, N.H., 2010. Voltage-Gated Na+ Channel SCN5A Is a Key Regulator of a Gene Transcriptional Network That Controls Colon Cancer Invasion. Cancer research 70, 6957-6967.
Huang, F., Sun, L., Zheng, J., 2008. In Vitro and In Vivo Characterization of a Silk Fibroin-Coated Polyester Vascular Prosthesis. Artificial Organs 32, 932-941.
Huang, G., Yang, D., Sun, C., Huang, J., Chen, K., Zhang, C., Chen, H., Yao, Q., 2014. A quicker degradation rate is yielded by a novel kind of transgenic silk fibroin consisting of shortened silk fibroin heavy

chains fused with matrix metalloproteinase cleavage sites. Journal of Materials Science-Materials in Medicine 25, 1833-1842.
Huang, W., Begum, R., Barber, T., Ibba, V., Tee, N.C.H., Hussain, M., Arastoo, M., Yang, Q., Robson, L.G., Lesage, S., Gheysens, T., Skaer, N.J.V., Knight, D.P., Priestley, J.V., 2012. Regenerative potential of silk conduits in repair of peripheral nerve injury in adult rats. Biomaterials 33, 59-71.
Huang, X., Jan, L.Y., 2014. Targeting potassium channels in cancer. Journal of Cell Biology 206, 151-162.
Huang, Y., Rane, S.G., 1994. Potassium Channel Induction by the Ras/raf Signal-Transduction Cascade. Journal of Biological Chemistry 269, 31183-31189.
Huber, S.M., 2013. Oncochannels. Cell calcium 53, 241-255.
Imokawa, Y., Yoshizato, K., 1997. Expression of Sonic hedgehog gene in regenerating newt limb blastemas recapitulates that in developing limb buds. Proceedings of the National Academy of Sciences of the United States of America 94, 9159-9164.
Jenkins, L.S., Duerstock, B.S., Borgens, R.B., 1996. Reduction of the current of injury leaving the amputation inhibits limb regeneration in the red spotted newt. Developmental biology 178, 251-262.
Jones, K.S., 2008. Effects of biomaterial-induced inflammation on fibrosis and rejection. Seminars in immunology 20, 130-136.
Khor, E., 1997. Methods for the treatment of collagenous tissues for bioprostheses. Biomaterials 18, 95-105.
Kim, D.Y., Carey, B.W., Wang, H.B., Ingano, L.A.M., Binshtok, A.M., Wertz, M.H., Pettingell, W.H., He, P., Lee, V.M.Y., Woolf, C.J., Kovacs, D.M., 2007a. BACE1 regulates voltage-gated sodium channels and neuronal activity. Nature Cell Biology 9, 755-U743.
Kim, M.S., Ahn, H.H., Shin, Y.N., Cho, M.H., Khang, G., Lee, H.B., 2007b. An in vivo study of the host tissue response to subcutaneous implantation of PLGA- and/or porcine small intestinal submucosa-based scaffolds. Biomaterials 28, 5137-5143.
King, R.S., Newmark, P.A., 2012. The cell biology of regeneration. Journal of Cell Biology 196, 553-562.
Kuboyama, N., Kiba, H., Arai, K., Uchida, R., Tanimoto, Y., Bhawal, U.K., Abiko, Y., Miyamoto, S., Knight, D., Asakura, T., Nishiyama, N., 2013. Silk fibroin-based scaffolds for bone regeneration. Journal of biomedical materials research.Part B, Applied biomaterials 101, 295-302.
Kulesa, P.M., Kasemeier-Kulesa, J.C., Teddy, J.M., Margaryan, N.V., Seftor, E.A., Seftor, R.E.B., Hendrix, M.J.C., 2006. Reprogramming metastatic melanoma cells to assume a neural crest cell-like phenotype in an embryonic microenvironment. Proceedings of the

National Academy of Sciences of the United States of America 103, 3752-3757.
Kunzelmann, K., 2005. Ion channels and cancer. Journal of Membrane Biology 205, 159-173.
Kweon, H., Kim, S.-G., Choi, J.-Y., 2014. Inhibition of foreign body giant cell formation by 4-hexylresorcinol through suppression of diacylglycerol kinase delta gene expression. Biomaterials 35, 8576-8584.
Kwon, S.-Y., Chung, J.-W., Park, H.-J., Jiang, Y.-Y., Park, J.-K., Seo, Y.-K., 2014. Silk and collagen scaffolds for tendon reconstruction. Proceedings of the Institution of Mechanical Engineers Part H-Journal of Engineering in Medicine 228, 388-396.
Lallet-Daher, H., Roudbaraki, M., Bavencoffe, A., Mariot, P., Gackiere, F., Bidaux, G., Urbain, R., Gosset, P., Delcourt, P., Fleurisse, L., Slomianny, C., Dewailly, E., Mauroy, B., Bonnal, J.L., Skryma, R., Prevarskaya, N., 2009. Intermediate-conductance Ca2+-activated K+ channels (IKCa1) regulate human prostate cancer cell proliferation through a close control of calcium entry. Oncogene 28, 1792-1806.
Lan, Y., Li, W., Jiao, Y., Guo, R., Zhang, Y., Xue, W., Zhang, Y., 2014. Therapeutic efficacy of antibiotic-loaded gelatin microsphere/silk fibroin scaffolds in infected full-thickness burns. Acta Biomaterialia 10, 3167-3176.
Lang, F., Foller, M., Lang, K.S., Lang, P.A., Ritter, M., Gulbins, E., Vereninov, A., Huber, S.M., 2005. Ion channels in cell proliferation and apoptotic cell death. Journal of Membrane Biology 205, 147-157.
Laschke, M.W., Harder, Y., Amon, M., Martin, I., Farhadi, J., Ring, A., Torio-Padron, N., Schramm, R., Rucker, M., Junker, D., Haufel, J.M., Carvalho, C., Heberer, M., Germann, G., Vollmar, B., Menger, M.D., 2006. Angiogenesis in tissue engineering: breathing life into constructed tissue substitutes. Tissue engineering 12, 2093-2104.
Lee, C.H., Singla, A., Lee, Y., 2001. Biomedical applications of collagen. International journal of pharmaceutics 221, 1-22.
Lee, J.H., Lee, J.S., Kim, D.-K., Park, C.H., Lee, H.R., 2015. Clinical outcomes of silk patch in acute tympanic membrane perforation. Clinical and experimental otorhinolaryngology 8, 117-122.
Lee, S.U., Kang, N.S., Min, Y.K., Kim, S.H., 2010. Camphoric acid stimulates osteoblast differentiation and induces glutamate receptor expression. Amino Acids 38, 85-93.
Leong, N.L., Petrigliano, F.A., McAllister, D.R., 2014. Current tissue engineering strategies in anterior cruciate ligament reconstruction. Journal of Biomedical Materials Research Part a 102, 1614-1624.
Lerchner, W., Xiao, C., Nashmi, R., Slimko, E.M., van Trigt, L., Lester, H.A., Anderson, D.J., 2007. Reversible silencing of neuronal excitability

in behaving mice by a genetically targeted, ivermectin-gated Cl- channel. Neuron 54, 35-49.
Levin, M., 2007. Large-scale biophysics: ion flows and regeneration. Trends in cell biology 17, 261-270.
Levin, M., 2009. Bioelectric mechanisms in regeneration: Unique aspects and future perspectives. Seminars in cell & developmental biology 20, 543-556.
Levin, M., 2012. Molecular bioelectricity in developmental biology: new tools and recent discoveries: control of cell behavior and pattern formation by transmembrane potential gradients. Bioessays 34, 205-217.
Li, C.M., Vepari, C., Jin, H.J., Kim, H.J., Kaplan, D.L., 2006. Electrospun silk-BMP-2 scaffolds for bone tissue engineering. Biomaterials 27, 3115-3124.
Li, X., He, J., Bian, W., Li, Z., Li, D., Snedeker, J.G., 2014a. A novel silk-TCP-PEEK construct for anterior cruciate ligament reconstruction: an off-the shelf alternative to a bone-tendon-bone autograft. Biofabrication 6, 015010-015010.
Li, X., He, J., Bian, W., Li, Z., Zhang, W., Li, D., Snedeker, J.G., 2014b. A novel silk-based artificial ligament and tricalcium phosphate/polyether ether ketone anchor for anterior cruciate ligament reconstruction - Safety and efficacy in a porcine model. Acta Biomaterialia 10, 3696-3704.
Liu, H., Wise, S.G., Rnjak-Kovacina, J., Kaplan, D.L., Bilek, M.M.M., Weiss, A.S., Fei, J., Bao, S., 2014. Biocompatibility of silk-tropoelastin protein polymers. Biomaterials 35, 5138-5147.
Lodish, H., Berk, A., Zipursky, S.L., Matsudaira, P., Baltimore, D., Darnell, J., 2000. Molecular Cell Biology. W.H. Freeman and Company, New York.
Lovett, M., Eng, G., Kluge, J.A., Cannizzaro, C., Vunjak-Novakovic, G., Kaplan, D.L., 2010. Tubular silk scaffolds for small diameter vascular grafts. Organogenesis 6, 217-224.
Lui, V.C.H., Lung, S.S.S., Pu, J.K.S., Hung, K.N., Leung, G.K.K., 2010. Invasion of Human Glioma Cells Is Regulated by Multiple Chloride Channels Including ClC-3. Anticancer Research 30, 4515-4524.
Lyons, F.G., Al-Munajjed, A.A., Kieran, S.M., Toner, M.E., Murphy, C.M., Duffy, G.P., O'Brien, F.J., 2010. The healing of bony defects by cell-free collagen-based scaffolds compared to stem cell-seeded tissue engineered constructs. Biomaterials 31, 9232-9243.
Ma, Y., Zhang, P., Wang, F., Yang, J., Yang, Z., Qin, H., 2010. The relationship between early embryo development and tumourigenesis. J Cell Mol Med 14, 2697-2701.

Mantovani, A., Biswas, S.K., Galdiero, M.R., Sica, A., Locati, M., 2013. Macrophage plasticity and polarization in tissue repair and remodelling. The Journal of pathology 229, 176-185.
Marino, A.A., Iliev, I.G., Schwalke, M.A., Gonzalez, E., Marler, K.C., Flanagan, C.A., 1994. Association between Cell-Membrane Potential and Breast-Cancer. Tumor Biology 15, 82-89.
Maxwell, G.P., Van Natta, B., Bengtson, B.P., Murphy, D.K., 2015. Ten-Year Results From the Natrelle 410 Anatomical Form-Stable Silicone Breast Implant Core Study. Aesthetic Surgery Journal 35, 145-155.
McGuire, K.P., Santillan, A.A., Kaur, P., Meade, T., Parbhoo, J., Mathias, M., Shamehdi, C., Davis, M., Ramos, D., Cox, C.E., 2009. Are Mastectomies on the Rise? A 13-Year Trend Analysis of the Selection of Mastectomy Versus Breast Conservation Therapy in 5865 Patients. Annals of Surgical Oncology 16, 2682-2690.
Meerbrey, K.L., Hu, G.A., Kessler, J.D., Roarty, K., Li, M.Z., Fang, J.E., Herschkowitz, J.I., Burrows, A.E., Ciccia, A., Sun, T.T., Schmitt, E.M., Bernardi, R.J., Fu, X.Y., Bland, C.S., Cooper, T.A., Schiff, R., Rosen, J.M., Westbrook, T.F., Elledge, S.J., 2011. The pINDUCER lentiviral toolkit for inducible RNA interference in vitro and in vivo. Proceedings of the National Academy of Sciences of the United States of America 108, 3665-3670.
Meinel, L., Hofmann, S., Karageorgiou, V., Kirker-Head, C., McCool, J., Gronowicz, G., Zichner, L., Langer, R., Vunjak-Novakovic, G., Kaplan, D.L., 2005. The inflammatory responses to silk films in vitro and in vivo. Biomaterials 26, 147-155.
Murata, Y., Iwasaki, H., Sasaki, M., Inaba, K., Okamura, Y., 2005. Phosphoinositide phosphatase activity coupled to an intrinsic voltage sensor. Nature 435, 1239-1243.
Murayama, Y., Vinuela, F., Tateshima, S., Gonzalez, N.R., Song, J.K., Mahdavieh, H., Iruela-Arispe, L., 2002. Cellular responses of bioabsorbable polymeric material and Guglielmi detachable coil in experimental aneurysms. Stroke 33, 1120-1128.
Murphy, K., Travers, P., Walport, M., Janeway, C., 2012. Janeway's immunobiology. Garland Science, New York.
Nakazawa, Y., Sato, M., Takahashi, R., Aytemiz, D., Takabayashi, C., Tamura, T., Enomoto, S., Sata, M., Asakura, T., 2011. Development of Small-Diameter Vascular Grafts Based on Silk Fibroin Fibers from Bombyx mori for Vascular Regeneration. Journal of Biomaterials Science-Polymer Edition 22, 195-206.
Navone, S.E., Pascucci, L., Dossena, M., Ferri, A., Invernici, G., Acerbi, F., Cristini, S., Bedini, G., Tosetti, V., Ceserani, V., Bonomi, A., Pessina, A., Freddi, G., Alessandrino, A., Ceccarelli, P., Campanella, R., Marfia, G., Alessandri, G., Parati, E.A., 2014. Decellularized silk fibroin

scaffold primed with adipose mesenchymal stromal cells improves wound healing in diabetic mice. Stem Cell Research & Therapy 5, 7-7.
Nelson, M., Yang, M., Dowle, A.A., Thomas, J.R., Brackenbury, W.J., 2015. The sodium channel-blocking antiepileptic drug phenytoin inhibits breast tumour growth and metastasis. Mol Cancer 14, 13.
Numata, K., Cebe, P., Kaplan, D.L., 2010. Mechanism of enzymatic degradation of beta-sheet crystals. Biomaterials 31, 2926-2933.
Okabayashi, R., Nakamura, M., Okabayashi, T., Tanaka, Y., Nagai, A., Yamashita, K., 2009. Efficacy of Polarized Hydroxyapatite and Silk Fibroin Composite Dressing Gel on Epidermal Recovery From Full-Thickness Skin Wounds. Journal of Biomedical Materials Research Part B-Applied Biomaterials 90B, 641-646.
Okada, Y., 2004. Ion channels and transporters involved in cell volume regulation and sensor mechanisms. Cell Biochemistry and Biophysics 41, 233-258.
Omenetto, F.G., Kaplan, D.L., 2010. New opportunities for an ancient material. Science (New York, N.Y.) 329, 528-531.
Onkal, R., Djamgoz, M.B.A., 2009. Molecular pharmacology of voltage-gated sodium channel expression in metastatic disease: Clinical potential of neonatal Nav1.5 in breast cancer. European journal of pharmacology 625, 206-219.
Ouadid-Ahidouch, H., Roudbaraki, M., Ahidouch, A., Delcourt, P., Prevarskaya, N., 2004a. Cell-cycle-dependent expression of the large Ca2+-activated K+ channels in breast cancer cells. Biochemical and biophysical research communications 316, 244-251.
Ouadid-Ahidouch, H., Roudbaraki, M., Delcourt, P., Ahidouch, A., Joury, N., Prevarskaya, N., 2004b. Functional and molecular identification of intermediate-conductance Ca2+-activated K+ channels in breast cancer cells: association with cell cycle progression. American Journal of Physiology-Cell Physiology 287, C125-C134.
Parihar, A.S., Coghlan, M.J., Gopalakrishnan, M., Shieh, C.C., 2003. Effects of intermediate-conductance Ca2+ activated K+-channel modulators on human prostate cancer cell proliferation. European journal of pharmacology 471, 157-164.
Patel, F., Brackenbury, W.J., 2015. Dual roles of voltage-gated sodium channels in development and cancer. Int J Dev Biol.
Pedersen, S.F., Hoffmann, E.K., Novak, I., 2013. Cell volume regulation in epithelial physiology and cancer. Front Physiol 4, 233.
Pfaffl, M.W., 2001. A new mathematical model for relative quantification in real-time RT-PCR. Nucleic Acids Research 29, 6.
Pierce, G.B., Lewis, S.H., Miller, G.J., Moritz, E., Miller, P., 1979. Tumorigenicity of Embryonal Carcinoma as an Assay to Study Control of Malignancy by the Murine Blastocyst. Proceedings of the National Academy of Sciences of the United States of America 76, 6649-6651.

Pietrobon, D., Hess, P., 1990. Novel Mechanism of Voltage-Dependent Gating in L-Type Calcium Channels. Nature 346, 651-655.
Pins, G.D., Christiansen, D.L., Patel, R., Silver, F.H., 1997. Self-assembly of collagen fibers. Influence of fibrillar alignment and decorin on mechanical properties. Biophysical journal 73, 2164-2172.
Press, M.F., Cordoncardo, C., Slamon, D.J., 1990. Expression of the Her-2/neu Protooncogene in Normal Human Adult and Fetal Tissues. Oncogene 5, 953-962.
Prevarskaya, N., Skryma, R., Bidaux, G., Flourakis, M., Shuba, Y., 2007. Ion channels in death and differentiation of prostate cancer cells. Cell death and differentiation 14, 1295-1304.
Rnjak-Kovacina, J., DesRochers, T.M., Fau - Burke, K.A., Burke, K.A., Fau - Kaplan, D.L., Kaplan, D.L., The Effect of Sterilization on Silk Fibroin Biomaterial Properties. LID - 10.1002/mabi.201500013 [doi]. - Macromol Biosci.2015 Mar 11.doi: 10.1002/mabi.201500013.
Rnjak-Kovacina, J., Wray, L.S., Golinski, J.M., Kaplan, D.L., 2014. Arrayed Hollow Channels in Silk-based Scaffolds Provide Functional Outcomes for Engineering Critically-sized Tissue Constructs. Advanced functional materials 24, 2188-2196.
Rockwood, D.N., Preda, R.C., Yucel, T., Wang, X., Lovett, M.L., Kaplan, D.L., 2011. Materials fabrication from Bombyx mori silk fibroin. Nature Protocols 6, 1612-1631.
Roh, D.H., Kang, S.Y., Kim, J.Y., Kwon, Y.B., Kweon, H.Y., Lee, K.G., Park, Y.H., Baek, R.M., Heo, C.Y., Choe, J., Lee, J.H., 2006. Wound healing effect of silk fibroin/alginate-blended sponge in full thickness skin defect of rat. Journal of Materials Science-Materials in Medicine 17, 547-552.
Schneider, A., Wang, X.Y., Kaplan, D.L., Garlick, J.A., Egles, C., 2009. Biofunctionalized electrospun silk mats as a topical bioactive dressing for accelerated wound heating. Acta Biomaterialia 5, 2570-2578.
Schwab, A., Gabriel, K., Finsterwalder, F., Folprecht, G., Greger, R., Kramer, A., Oberleithner, H., 1995. Polarized Ion-Transport during Migration of Transformed Madin-Darby Canine Kidney-Cells. Pflugers Archiv-European Journal of Physiology 430, 802-807.
Schwab, A., Hanley, P., Fabian, A., Stock, C., 2008. Potassium channels keep mobile cells on the go. Physiology 23, 212-220.
Schwab, A., Nechyporuk-Zloy, V., Gassner, B., Schulz, C., Kessler, W., Mally, S., Roemer, M., Stock, C., 2012. Dynamic redistribution of calcium sensitive potassium channels (hKCa3.1) in migrating cells. Journal of cellular physiology 227, 686-696.
Seib, F.P., Herklotz, M., Burke, K.A., Maitz, M.F., Werner, C., Kaplan, D.L., 2014. Multifunctional silk-heparin biomaterials for vascular tissue engineering applications. Biomaterials 35, 83-91.

Seifert, A.W., Kiama, S.G., Seifert, M.G., Goheen, J.R., Palmer, T.M., Maden, M., 2012. Skin shedding and tissue regeneration in African spiny mice (Acomys). Nature 489, 561-+.
Sengupta, S., Park, S.-H., Seok, G.E., Patel, A., Numata, K., Lu, C.-L., Kaplan, D.L., 2010. Quantifying Osteogenic Cell Degradation of Silk Biomaterials. Biomacromolecules 11, 3592-3599.
Sennoune, S.R., Bakunts, K., Martinez, G.M., Chua-Tuan, J.L., Kebir, Y., Attaya, M.N., Martinez-Zaguilan, R., 2004. Vacuolar H+-ATPase in human breast cancer cells with distinct metastatic potential: distribution and functional activity. American Journal of Physiology-Cell Physiology 286, C1443-C1452.
Seo, Y.-K., Yoon, H.-H., Song, K.-Y., Kwon, S.-Y., Lee, H.-S., Park, Y.-S., Park, J.-K., 2009a. Increase in Cell Migration and Angiogenesis in a Composite Silk Scaffold for Tissue-Engineered Ligaments. Journal of Orthopaedic Research 27, 495-503.
Seo, Y.K., Yoon, H.H., Park, Y.S., Song, K.Y., Lee, W.S., Park, J.K., 2009b. Correlation between scaffold in vivo biocompatibility and in vitro cell compatibility using mesenchymal and mononuclear cell cultures. Cell biology and toxicology 25, 513-522.
Shan, Y.-H., Peng, L.-H., Liu, X., Chen, X., Xiong, J., Gao, J.-Q., 2015. Silk fibroin/gelatin electrospun nanofibrous dressing functionalized with astragaloside IV induces healing and anti-scar effects on burn wound. International journal of pharmaceutics 479, 291-301.
Shaw, K.R.M., Wrobel, C.N., Brugge, J.S., 2004. Use of three-dimensional basement membrane cultures to model oncogene-induced changes in mammary epithelial morphogenesis. Journal of Mammary Gland Biology and Neoplasia 9, 297-310.
Shen, W., Chen, J., Yin, Z., Chen, X., Liu, H., Heng, B.C., Chen, W., Ouyang, H.-W., 2012. Allogenous Tendon Stem/Progenitor Cells in Silk Scaffold for Functional Shoulder Repair. Cell transplantation 21, 943-958.
Shen, W., Chen, X., Hu, Y., Yin, Z., Zhu, T., Hu, J., Chen, J., Zheng, Z., Zhang, W., Ran, J., Heng, B.C., Ji, J., Chen, W., Ouyang, H.-W., 2014. Long-term effects of knitted silk-collagen sponge scaffold on anterior cruciate ligament reconstruction and osteoarthritis prevention. Biomaterials 35, 8154-8163.
Shi, P., Teh, T.K.H., Toh, S.L., Goh, J.C.H., 2013. Variation of the effect of calcium phosphate enhancement of implanted silk fibroin ligament bone integration. Biomaterials 34, 5947-5957.
Song, E., Kim, S.Y., Chun, T., Byun, H.J., Lee, Y.M., 2006. Collagen scaffolds derived from a marine source and their biocompatibility. Biomaterials 27, 2951-2961.
Spelzini, F., Konstantinovic, M.L., Guelinckx, I., Verbist, G., Verbeken, E., De Ridder, D., Deprest, J., 2007. Tensile strength and host

response towards silk and type i polypropylene implants used for augmentation of fascial repair in a rat model. Gynecologic and obstetric investigation 63, 155-162.
Sugihara, A., Sugiura, K., Morita, H., Ninagawa, T., Tubouchi, K., Tobe, R., Izumiya, M., Horio, T., Abraham, N.G., Ikehara, S., 2000. Promotive effects of a silk film on epidermal recovery from full-thickness skin wounds. Proceedings of the Society for Experimental Biology and Medicine 225, 58-64.
Sundelacruz, S., Levin, M., Kaplan, D.L., 2008. Membrane Potential Controls Adipogenic and Osteogenic Differentiation of Mesenchymal Stem Cells. Plos One 3, e3737-e3737.
Sutherland, T.D., Young, J.H., Weisman, S., Hayashi, C.Y., Merritt, D.J., 2010. Insect Silk: One Name, Many Materials. Annual Review of Entomology 55, 171-188.
Szaszi, K., Sirokmany, G., Di Ciano-Oliveira, C., Rotstein, O.D., Kapus, A., 2005. Depolarization induces Rho-Rho kinase-mediated myosin light chain phosphorylation in kidney tubular cells. American Journal of Physiology-Cell Physiology 289, C673-C685.
Thevenot, P.T., Nair, A.M., Shen, J., Lotfi, P., Ko, C.-Y., Tang, L., 2010. The effect of incorporation of SDF-1 alpha into PLGA scaffolds on stem cell recruitment and the inflammatory response. Biomaterials 31, 3997-4008.
Thurber, A.E., Omenetto, F.G., Kaplan, D.L., 2015. In vivo bioresponses to silk proteins. Biomaterials 71, 145-157.
Tseng, A.-S., Beane, W.S., Lemire, J.M., Masi, A., Levin, M., 2010. Induction of Vertebrate Regeneration by a Transient Sodium Current RID A-5918-2011. Journal of Neuroscience 30, 13192-13200.
Tsonis, P.A., 1983. Effects of Carcinogens on Regenerating and Non-Regenerating Limbs in Amphibia. Anticancer Research 3, 195-202.
Tsutsui, H., Karasawa, S., Okamura, Y., Miyawaki, A., 2008. Improving membrane voltage measurements using FRET with new fluorescent proteins. Nature Methods 5, 683-685.
Turner, K.L., Sontheimer, H., 2014. KCa3.1 modulates neuroblast migration along the rostral migratory stream (RMS) in vivo. Cereb Cortex 24, 2388-2400.
Uebersax, L., Apfel, T., Nuss, K.M.R., Vogt, R., Kim, H.Y., Meinel, L., Kaplan, D.L., Auer, J.A., Merkle, H.P., von Rechenberg, B., 2013. Biocompatibility and osteoconduction of macroporous silk fibroin implants in cortical defects in sheep. European Journal of Pharmaceutics and Biopharmaceutics 85, 107-118.
Unger, R.E., Ghanaati, S., Orth, C., Sartoris, A., Barbeck, M., Halstenberg, S., Motta, A., Migliaresi, C., Kirkpatrick, C.J., 2010. The rapid anastomosis between prevascularized networks on silk fibroin scaffolds generated in vitro with cocultures of human microvascular

endothelial and osteoblast cells and the host vasculature. Biomaterials 31, 6959-6967.
Urrego, D., Tomczak, A.P., Zahed, F., Stuhmer, W., Pardo, L.A., 2014. Potassium channels in cell cycle and cell proliferation. Philosophical Transactions of the Royal Society B: Biological Sciences 369, 20130094-20130094.
Vandenberg, L.N., Morrie, R.D., Adams, D.S., 2011. V-ATPase-Dependent Ectodermal Voltage and pH Regionalization Are Required for Craniofacial Morphogenesis. Developmental Dynamics 240, 1889-1904.
Vanluyn, M.J.A., Vanwachem, P.B., Leta, R., Blaauw, E.H., Nieuwenhuis, P., 1994. Modulation of the Tissue Reaction to Biomaterials .1. Biocompatibility of Cross-Linked Dermal Sheep Collagens After Macrophage Depletion. Journal of Materials Science-Materials in Medicine 5, 671-678.
Wang, Y., Kim, H.-J., Vunjak-Novakovic, G., Kaplan, D.L., 2006. Stem cell-based tissue engineering with silk biomaterials. Biomaterials 27, 6064-6082.
Wang, Y., Rudym, D.D., Walsh, A., Abrahamsen, L., Kim, H.-J., Kim, H.S., Kirker-Head, C., Kaplan, D.L., 2008. In vivo degradation of three-dimensional silk fibroin scaffolds. Biomaterials 29, 3415-3428.
Wang, Z., Zhang, Y., Zhang, J., Huang, L., Liu, J., Li, Y., Zhang, G., Kundu, S.C., Wang, L., 2014. Exploring natural silk protein sericin for regenerative medicine: an injectable, photoluminescent, cell-adhesive 3D hydrogel. Scientific Reports 4, 7064-7064.
Wonderlin, W.F., Woodfork, K.A., Strobl, J.S., 1995. Changes in Membrane-Potential during the Progression of Mcf-7 Human Mammary-Tumor Cells through the Cell-Cycle. Journal of cellular physiology 165, 177-185.
Wray, L.S., Hu, X., Gallego, J., Georgakoudi, I., Omenetto, F.G., Schmidt, D., Kaplan, D.L., 2011. Effect of processing on silk-based biomaterials: reproducibility and biocompatibility. Journal of biomedical materials research.Part B, Applied biomaterials 99, 89-101.
Wray, L.S., Tsioris, K., Gil, E.S., Omenetto, F.G., Kaplan, D.L., 2013. Microfabricated Porous Silk Scaffolds for Vascularizing Engineered Tissues. Advanced Functional Materials 23, 3404-3412.
Yagi, T., Sato, M., Nakazawa, Y., Tanaka, K., Sata, M., Itoh, K., Takagi, Y., Asakura, T., 2011. Preparation of double-raschel knitted silk vascular grafts and evaluation of short-term function in a rat abdominal aorta. Journal of Artificial Organs 14, 89-99.
Yang, F., Tu, J., Pan, J.Q., Luo, H.L., Liu, Y.H., Wan, J., Zhang, J., Wei, P.F., Jiang, T., Chen, Y.H., Wang, L.P., 2013. Light-controlled inhibition of malignant glioma by opsin gene transfer. Cell Death & Disease 4, 14.

Yang, M., Brackenbury, W.J., 2013. Membrane potential and cancer progression. Front Physiol 4, 185.
Yoon, S.J., Kim, S.H., Ha, H.J., Ko, Y.K., So, J.W., Kim, M.S., Il Yang, Y., Khang, G., Rhee, J.M., Lee, H.B., 2008. Reduction of inflammatory reaction of poly(D,L-lactic-Co-glycolic acid) using demineralized bone particles. Tissue Engineering Part a 14, 539-547.
Zhang, H., Li, H., Yang, L., Deng, Z., Luo, H., Ye, D., Bai, Z., Zhu, L., Ye, W., Wang, L., Chen, L., 2013. The ClC-3 chloride channel associated with microtubules is a target of paclitaxel in its induced-apoptosis. Sci Rep 3, 2615.
Zhang, W., Yang, Y., Zhang, K., Li, Y., Fang, G., 2015. Weft-knitted silk-poly(lactide-co-glycolide) mesh scaffold combined with collagen matrix and seeded with mesenchymal stem cells for rabbit Achilles tendon repair. Connective tissue research 56, 25-34.
Zhang, W., Zhu, C., Wu, Y., Ye, D., Wang, S., Zou, D., Zhang, X., Kaplan, D.L., Jiang, X., 2014. VEGF and BMP-2 promote bone regeneration by facilitating bone marrow stem cell homing and differentiation. European cells & materials 27, 1-11; discussion 11-12.
Zhao, M., Song, B., Pu, J., Wada, T., Reid, B., Tai, G., Wang, F., Guo, A., Walczysko, P., Gu, Y., Sasaki, T., Suzuki, A., Forrester, J.V., Bourne, H.R., Devreotes, P.N., McCaig, C.D., Penninger, J.M., 2006. Electrical signals control wound healing through phosphatidylinositol-3-OH kinase-gamma and PTEN. Nature 442, 457-460.
Zhou, C.Z., Confalonieri, F., Jacquet, M., Perasso, R., Li, Z.G., Janin, J., 2001. Silk fibroin: Structural implications of a remarkable amino acid sequence. Proteins-Structure Function and Genetics 44, 119-122.
Zhou, Y., Wong, C.-O., Cho, K.-j., van der Hoeven, D., Liang, H., Thakur, D.P., Luo, J., Babic, M., Zinsmaier, K.E., Zhu, M.X., Hu, H., Venkatachalam, K., Hancock, J.F., 2015. Membrane potential modulates plasma membrane phospholipid dynamics and K-Ras signaling. Science 349, 873-876.

Licensed content publication	Cell Biochemistry and Biophysics
Licensed content title	Structure, Function, and Modification of the Voltage Sensor in Voltage-Gated Ion Channels
Licensed content author	Sara I. Börjesson
Licensed content date	Jan 1, 2008
Volume number	52
Issue number	3
Type of Use	Thesis/Dissertation
Portion	Figures/tables/illustrations
Number of figures/tables/illustrations	1
Author of this Springer article	No
Order reference number	None
Original figure numbers	Figure 2
Title of your thesis / dissertation	ABILITY OF BIOELECTRIC SIGNALS TO INSTRUCT REGENERATION AND CANCER-ASSOCIATED BEHAVIORS
Expected completion date	Feb 2016
Estimated size(pages)	235
Total	0.00 USD

This is a License Agreement between Amy E Thurber ("You") and Nature Publishing Group ("Nature Publishing Group") provided by Copyright Clearance Center ("CCC"). The license consists of your order details, the terms and conditions provided by Nature Publishing Group, and the payment terms and conditions.

All payments must be made in full to CCC. For payment instructions, please see information listed at the bottom of this form.

License Number	3763300882319
License date	Dec 06, 2015
Licensed content publisher	Nature Publishing Group
Licensed content publication	Nature
Licensed content title	Phosphoinositide phosphatase activity coupled to an intrinsic voltage sensor
Licensed content author	Yoshimichi Murata, Hirohide Iwasaki, Mari Sasaki, Kazuo Inaba and Yasushi Okamura
Licensed content date	May 18, 2005
Volume number	435
Issue number	7046
Type of Use	reuse in a dissertation / thesis
Requestor type	academic/educational
Format	print and electronic
Portion	figures/tables/illustrations
Number of figures/tables/illustrations	1

High-res required	no
Figures	Figure of voltage sensitive domain
Author of this NPG article	no
Your reference number	None
Title of your thesis / dissertation	ABILITY OF BIOELECTRIC SIGNALS TO INSTRUCT REGENERATION AND CANCER-ASSOCIATED BEHAVIORS
Expected completion date	Feb 2016
Estimated size (number of pages)	235
Total	0.00 USD

This is a License Agreement between Amy E Thurber ("You") and Elsevier ("Elsevier") provided by Copyright Clearance Center ("CCC"). The license consists of your order details, the terms and conditions provided by Elsevier, and the payment terms and conditions.

All payments must be made in full to CCC. For payment instructions, please see information listed at the bottom of this form.

Supplier	Elsevier Limited The Boulevard,Langford Lane Kidlington,Oxford,OX5 1GB,UK
Registered Company Number	1982084
Customer name	Amy E Thurber
Customer address	4 Colby St MEDFORD, MA 02155
License number	3763300185431
License date	Dec 06, 2015
Licensed content publisher	Elsevier
Licensed content publication	Biomaterials
Licensed content title	In vivo bioresponses to silk proteins
Licensed content author	Amy E. Thurber,Fiorenzo G. Omenetto,David L. Kaplan
Licensed content date	December 2015
Licensed content volume number	71
Licensed content issue number	n/a
Number of pages	13
Start Page	145
End Page	157
Type of Use	reuse in a thesis/dissertation
Portion	full article
Format	both print and electronic
Are you the author of this Elsevier article?	Yes
Will you be translating?	No
Title of your thesis/dissertation	ABILITY OF BIOELECTRIC SIGNALS TO

	INSTRUCT REGENERATION AND CANCER-ASSOCIATED BEHAVIORS
Expected completion date	Feb 2016
Estimated size (number of pages)	235
Elsevier VAT number	GB 494 6272 12
Permissions price	0.00 USD
VAT/Local Sales Tax	0.00 USD / 0.00 GBP
Total	0.00 USD